The Pennsylvania State University

The Graduate School

College of Earth and Mineral Sciences

ELECTROPHORETIC DEPOSITION:

FUNDAMENTALS, MECHANISMS AND EXAMPLES

WITH AN IN DEPTH EXAMINATION OF THE

ION DEPLETION EFFECT

A Thesis in

Materials Science and Engineering

by

Jonathan J. Van Tassel

Submitted in Partial Fulfillment
of the Requirements
for the Degree of
Doctor of Philosophy

May 2004

The thesis of Jonathan Van Tassel was reviewed and approved* by the following:.

Clive A. Randall
Professor of Material Science
Thesis Advisor
Chair of Committee

James H. Adair
Professor of Materials Science and Engineering

L. Eric Cross
Evan Pugh Professor of Electrical Engineering

Digby D. Macdonald
Distinguished Professor of Materials Science and Engineering

Gary L. Messing
Distinguished Professor and
Head of Materials Science and Engineering

*Signatures are on file in the Graduate School.

ABSTRACT

The research and analysis for this thesis have been directed toward two major goals: to better understand the process of electrophoretic deposition (EPD) and to demonstrate its utility. This is also the order in which these two topics are addressed in the writing of this thesis.

In order to define the limits of the problem, the first chapter is devoted to a description and definition of what is, and is not, EPD. Here EPD is defined as consisting of three steps. The first is the creation of a charge balanced suspension of electrostatically charged particles in a solvent where some mechanism acts to keep the particles from floccing together during the time necessary to perform EPD. The second step is to create and maintain a DC electric field within the bulk of the solvent causing the electrostatically charged particles to move by electrophoresis toward an electrode. The final step is then to induce a change the nature of the suspension next to the electrode so that particles come into contact with each other and form a rigid deposition.

Chapter 2 then gives an outline of the scientific background necessary for understanding each of the three steps defined in Chapter 1. In order to make the complexity of the EPD system intellectually manageable, it is broken down into three components; solvent, particles, and electric field. Even though the scientific literature specifically on EPD is relatively modest, the literature on the binary interactions between each of these components (solvent-electric field, solvent-particle, etc.) is both extensive and elucidating. Previous reviews on EPD have concentrated almost exclusively on solvent-particle interactions. This thesis shows the vital importance of electrochemical reactions at the deposition electrode in understanding the mechanisms of deposition.

This approach also allows the categorization of mechanisms of EPD already demonstrated in the literature as well as the prediction of new mechanisms not previously demonstrated. To do this a list of mechanisms to prevent particles from floccing in the bulk suspension is compared to a list of effects that can be induced in the suspension at the deposition electrode. The list of specific near-electrode effects that can cause particles from specific types of suspensions to floc or coagulate at the electrode then becomes a list of the possible mechanisms of EPD. One of the most interesting of these mechanisms, ion depleted enhanced - automatic leveling deposition, was chosen for in-depth analysis.

The first step in this analysis is to obtain a complete understanding of the suspension from which the particles are to be deposited. This is done in Chapter 3 for alumina powder in ethanol with added HCl. Here it is shown that in the absence of dissolved ions alumina develops a significant positive surface charge in ethanol by the dissociative adsorption of ethanol molecules to the surface and the preferential desorption of ethoxide ions from the surface. The addition of HCl leads to a large rise in surface charge due initially to the reduction in ethoxide activity. After this initial rise the surface charge is set by a competitive adsorption equilibrium of chloride and ethoxide ions to positive surface sites on the powder.

Chapter 4 is then devoted to analyzing the deposition of alumina from this system. The first part of this chapter is detailed analysis of the conduction layer next to the cathode, the deposition electrode for the positively charged particles. The development of ionic and charge gradients, and the inevitability of a transition to convective transport at the electrode is shown for the electrolyte in the absence of particles. It is then shown that the dramatic change in conduction behavior in the presence of particles can be accounted for by the stabilization of an ion depleted, unbalanced charge conduction layer. Extremely high voltage gradients in this layer then exert a strong consolidating force on the positively charged alumina particles, compacting them into a densely packed deposited layer. This high gradient also leads to a strong equilibrating force to maintain a uniform thickness of the compact deposited layer, the automatic leveling effect.

The second objective here has been to demonstrate the potential utility of EPD in addressing current problems in the manufacture of electroceramic devices. This is undertaken in Chapter 5 with a complete description of the process to form suspensions, deposit particles, process these depositions into final form and to characterize the component created. The direct electrostatic deposition of silver/palladium powder is used to demonstrate the ability of EPD to create both very thin layers and very narrow conductor lines that can be measured on the scale of the particles used to create them. The electrophoretic deposition of PZT is used to demonstrate the formation of an intermediate thickness film with well controlled stoichiometry.

In the final chapter the thesis concludes with a discussion of what still needs to be done to advance the understanding and application of EPD.

TABLE OF CONTENTS

LIST OF FIGURES

LIST OF TABLES

ACKNOWLEDGMENTS

It should be obvious that this thesis required far more than just my own personal efforts, and I must express my thanks to all of the authors listed in the references to this thesis. Without their work and the work of others before them, this thesis would be impossible.

The analysis I was able to do during the writing of this thesis is due in large part to the extraordinary patience of two people: Professor David D. Van Tassel, my father, who unfortunately did not live to see the completion of this thesis, and without whom I may not ever have made it into graduate school; and Professor Clive A. Randall, my thesis advisor, who kept faith in the value of this work even in the periods of slowest progress.

Of course, this thesis would not exist at all if it were not for the generous financial support of the member corporations of the Penn State:

Particulate Materials Center

and the

Center for Dielectric Studies

Along with the personal support of Helen L. Van Tassel.

"This whole book is but a draught - nay, but a draught of a draught. Oh, Time, Strength, Cash, and Patience!"

From a letter by Herman Melville to
Evert Duyckinck, December 13, 1850
during the composition of Moby Dick

Introduction to the On-Line Version 2009

When I finished this thesis in early 2004 I regarded it as the best scientific introduction to EPD at the time, and to my knowledge it still is.

However, even though I thought it would be very helpful to people first exploring EPD, I have been slow in posting it to the web. This is due in part to having little time to revisit the thesis, but in larger part due to my dissatisfaction with the completeness of explanation it offered. I continued to see effects in my own work and in the work of others which were not covered by the by the theories presented in the thesis. It gradually became clear to me that to understand the results of the wide variety of experiments that have been reported under the heading of EPD, it is vital to understand the behavior of colloids which are neither fully dispersed nor rigidly deposited.

In my thesis I adopted a fairly strict definition of EPD. This definition requires that the system begin as a stable dispersion of particles which can move independently, and that the end result be a rigid deposit of particles contacting each other at their primary minimum. It was not a conscious decision at the time, but by adopting this definition I was able to avoid making explicit two very significant assumptions.

The first of these assumptions regards dispersion. In the thesis section on dispersion I listed the standard methods for keeping particles far enough apart that they are not pulled together irreversibly by the London-van der Waals force. The implicit assumption was that if the attractive energy between two particles was less than a small multiple of the thermal energy of the solvent, Brownian motion would be sufficient to assure that the particles do not become irreversibly attached to each other, and the particles could therefore be considered to move independently. However, as the volume fraction of particles in suspension rises, the interaction between particles changes from simple two particle interactions to multiparticle interactions where crowding and momentum transfers become significant. At the extreme, particles can pack together to the point that the suspension becomes a pseudoplastic solid. These particles are not deposited, the energy barrier between them is not overcome, and with an adequate volume of solvent they will spontaneously diffuse apart. These particles technically remain dispersed - that is all of the particles are separated by a layer of solvent - even while the dispersion behaves as a solid.

The second implicit assumption is that if the barrier between the particles does not keep them far enough apart, the L-vdW force will inexorably pull the particles into contact at their primary minimum, a contact that is rigid and brittle. However in some cases the interaction between the solvent and the surface is stronger than the attraction between the particles. A layer of solvent then remains between the particles. In this case, even though the particles are bound together by the L-vdW force, the contact between the particles is lubricated. The particles are able to rotate and slide past each other. At high volume fractions they will form a solid capable of large plastic deformation without losing cohesion (i.e. without cracking). At low volume fractions they can form a gel which does not sediment or phase separate but which flows at such a low applied shear force that it can be mistaken for a fully dispersed colloid.

So what is needed to complete the scientific background necessary for understanding EPD? It is the science necessary to describe the behavior of these "Condensed Colloids", colloids with a particulate volume fraction generally greater than 30% and with non-Newtonian shear behavior.

The first step in explaining these colloids is to extend the discussion of the van der Waals forces to include quantitative approximations. A quantitative understanding is vital because the behavior of these colloids depends not just on the nature of these forces but on the ratios of these forces on the angstrom to nanometer scale.

This then leads into a discussion of the solvent/particle interface. The Keesom and Debye vdW forces at a solid interface can alter the structure of a solvent. In polar solvents, this alteration can be so significant that the nanometer of solvent at the interface will have significantly different properties from the bulk solvent. These solvent/solid interactions have been most extensively considered in the literature of wetting, but the focus needed here is primarily on wetting considered on the nanoscopic scale.

The next step is to consider how this altered solvent layer reacts as two particles come together. This should be divided into three cases: when the solvent is completely squeezed out of the contact point, when a monolayer of solvent remains and when the system is stable with a layer several molecules thick. If the solvent is completely removed, the dry contact points between the particles will have mechanical properties approaching those of the material making up the particles. If a monolayer of solvent remains, the

contact point will be much weaker and particles will be better able to roll and possibly slide past each other. If several molecular layers remain between the particles at the contact point, the contact will be lubricated allowing the particles to easily roll and slide past each other while also providing an elastic connection between the particles.

The micromechanics of the contact point between particles then needs to be translated into the mechanical behavior of the colloid. Since the usual objective of EPD is to maximize the consolidation of the particles, we are most interested in the compressive strength of the particulate component of the colloid. However, this property is rarely measured. Shear strength is more easily and far more often measured for colloids, therefore it would be more useful if a connection between shear and compressive strengths could be drawn.

The compliment to the compressive strength of the particulate component of a colloid is the compressive force acting on those particles. In EPD the particles move independently. Their migration in an electric field toward the deposition electrode is well described by straightforward and well-tested electrokinetic theories. In a condensed colloid, the particles by definition do not move independently. Electrokinetic effects chain up to act on multiple particles which also act mechanically on each other. The high viscosity of the condensed colloid will stabilize the solvent against large scale convection. This allows ionic concentration gradients to develop, modifying electric fields and osmotic pressures.

It is because the consolidation of condensed colloids is so fundamentally different from EPD that it should be separated from EPD and referred to as either electrophoretic consolidation (EPC) or simply electrocasting. However, because many processes are a combination of EPD and EPC and because even processes which are purely electrocasting have been identified in the literature as EPD, it is not possible to fully understand EPD without understanding EPC as well.

Finally, there is the subject of drying. It is rare for EPD or EPC to produce a fully dense deposit prior to drying. If a low density, rigid deposition is formed, ≈ 30vol%, it will almost inevitably crack during drying. If a high density, rigid deposit is formed, 40-50vol%, cracking can frequently be avoided. However, the highest density coatings are formed when the particles are not rigidly deposited. It occurs when the particles are

consolidated on the deposition electrode in a solvated pseudoplastic slurry. This condensed colloidal slurry has enough shear strength to allow it to be removed from the deposition apparatus, but the particles are still able to re-arrange during drying, achieving near theoretical maximum random packing density. However, this is not a panacea. If the shear yield strength of the drying deposit is too high in relation to the crack initiation and propagation energy, the coating will achieve high density as a collection of cracked flakes.

EPD and EPC are surprisingly complex phenomena. Understanding all of the phenomena exhibited by experiments in this field requires an understanding of phenomena in a wide variety of scientific subject areas. As time allows, I will elaborate on the topics above and more, both on this site and through additional journal publications. The long term goal is a complete introduction to the relevant existing science. This will firstly promote novel, clearly designed experiments focused on gaps in understanding, and secondly, provide those tasked with developing new EPD/EPC systems a logical basis for designing and improving processes.

Jonathan Van Tassel, 2009

Chapter 1
Electrophoretic Deposition

1.1 What is Electrophoretic Deposition?

Electrophoretic deposition (EPD) is a particulate forming process. It begins with a randomly arranged powder material and then uses an electric field to move the powder particles into a desired arrangement on an electrode surface. This arrangement can be either zero, one, two or three dimensional. A zero dimensional deposition would be a single particle deposited at a single point; one dimensional — a line of particles; two dimensional can be a flat ordered array of particles (**1,2**), or a randomly packed layer of particles coating a flat surface(**3**); three dimensional arrangements can be a cubic close packed array of spheres (**4**) or monolithic objects such as a rocket nose cone or solid electrolyte closed end tubes for electrochemical applications (**5,6**).

There are three basic steps in EPD; formation of a stable suspension of the particles, electrophoretic migration of the particles to the deposition electrode, and deposition of the particles in the desired arrangement on the electrode surface.
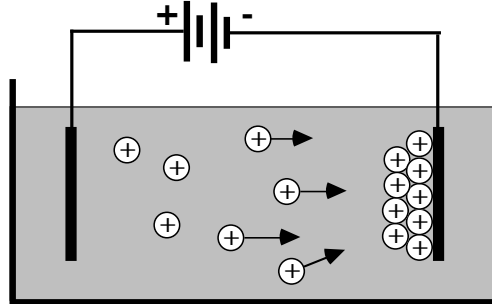
Fig. 1.1 Positively charged particles will migrate to, and deposit on, a negatively charged surface.

The first step is to place the particles into a suspension where each of the particles can move independently. The difficulty is that as long as the dielectric spectrum of the particles is different from that of the solvent there will be a short range attractive London-van der Waals (L-VdW) force between the particles. This will cause any particles that pass within a few tens of nanometers of each other to attract each other and to stick together with an energy usually much greater than the thermal energy of the solvent that might break them apart. Unless there is a stabilizing force to keep the particles apart, then for any reasonable density of particles in the suspension they will quickly begin to stick together in large loose flocs. These flocs can still be deposited electrophoretically but will

result in a low density deposition that can be difficult to dry without cracking. To produce a dense deposition or a deposition with an ordered microstructure this flocculation process in the suspension must be prevented.

There are two methods of stabilizing the suspended particles against flocculation; polymeric and electrostatic. In very simple terms, polymeric stabilization involves coating the particles with a polymer so that the particles cannot approach closely enough to become permanently attached by the L-VdW force. For this to work the polymer coating must have dielectric properties close enough to those of the solvent that there is no attractive force between the polymer coatings. In electrostatic stabilization there is a net charge separation between the surface of the particle and the solvent. The resulting electrostatic attraction between the particle and the solvent creates a layer of higher pressure solvent around the particles. This pressure layer provides a repulsive force as two particles approach one another.

The particles must also have an electrostatic charge so that they can be moved by an electric field. There are three mechanisms for developing this surface charge: selective dissolution of ions from the particle, selective adsorption of ions from the solvent, and dissociative adsorption of molecules from the solvent followed by preferential desorption of one of the dissociated ions.

In the second step a DC electric field is applied to the suspension causing the electrophoretic motion of charged particles toward the oppositely charged electrode. In practical systems this simple picture of the electrophoretic motion is almost always much more complex. There is always Brownian diffusion and sedimentation, and convective transport in the bulk suspension can move particles at a speed orders of magnitude faster than electrophoresis alone. The desired particle motion is usually simple straight line electrophoretic migration of individual charged particles in the applied electric field. However, this migration leads to density gradients in the suspension which result in gravitational convection of the bulk suspension. Further complicating this is electrohydrodynamic convection which can occur on several scales. This will be discussed further in Chapters 2 and 4.

In the final step, deposition, the interparticle repulsion that keeps the particles stably suspended must be overcome. The particles must be brought into contact with each other so that the London-van der Waals and other chemical bonding forces can give the deposition sufficient mechanical strength to be removed from the deposition bath for further processing. However, this step involves more than simply bringing the particles into contact. How the particles are brought into contact and consolidated both before and

after forming a rigid framework of interparticle contacts determines the final structure of the deposition. Although most often a maximum density random packed structure is the desired outcome, random packing is not the desired outcome for forming colloidal crystals, and in other cases the object may be to produce lower density depositions.

EPD is purely a method of moving and arranging particles. To produce a dense, mechanically strong layer or object it must be combined with some other process such as sintering or infiltration of a polymer or metal to eliminate the pores between the particles in the deposition.

1.2 What isn't Electrophoretic Deposition?

To clarify the discussions here, it is useful to draw a clear distinction between EPD and several other similar processes.

The first are the electrochemical processes, including: electrodeposition (**7**), electroforming, electrocoating (**8**), etc. The key word in this case is 'electrochemical'. In these processes a coating is produced by the diffusion and migration of individual ions and molecules dissolved in the solvent to the deposition electrode where they are electrochemically converted to an insoluble form. In the case of electrodeposition and electroforming this reaction is the reduction of metal ions in solution to form the metal. This is a Faradaic process where n x 9.65×10^4 coulombs of current must pass through the cell for each mole of metal deposited, where n is the valence of the metal ions. Another electrochemical process, electrocoating, is best known as the process used for producing the primer coat on automobile bodies. In this case it is a polymer precursor which is deposited by electrochemical polymerization. Electrolysis at the electrode - a metal automobile body - produces radicals which drive the reactions. The great advantage of this process is the high resistivity of the formed coating. A set voltage is applied between the auto body and another electrode in the bath. When the coating reaches the desired thickness virtually all of the voltage drop between the body and the counter electrode will occur across the polymer coating. Uncoated areas will attract charged polymer precursor to the surface until the desired thickness and voltage drop is reached. This allows the creation of a very uniform coating over a complex shape with many internal channels and spaces. In all of these cases a coating or object is produced that is dense and chemically distinct from the phase in solution.

In contrast, if electrochemical processes are necessary for an EPD system at all, their importance is secondary, acting only to reduce the interparticle repulsion in the depositing layer or produce a precipitate to better bond the deposited particles together.

There is no necessary relationship between the current flow and the quantity of powder deposited, and the powder particles deposited are chemically and physically identical to the particles in suspension.

The next set of processes that will be distinguished from EPD in this paper are the electrostatic processes: electrostatic precipitation (ESP), electrostatic spraying (ESS) (**9**), and xerography. These processes are at the other extreme where no chemical reactions occur at all. High resistivity of the fluid in these processes is a requirement to preserve the slight electrostatic charges used to manipulate particles in these processes. This means either dry air or hydrocarbon solvents.

ESP and ESS use sharply pointed corona electrodes to emit electrons at 30 to 100 kV to charge particles in air. ESP is most often used for removing particulates from industrial exhaust gas streams. A precipitator is a large box filled with alternating rows of flat metal sheets and rakes of corona electrodes. A voltage just short of breakdown is applied and electrons emitted by the electrode tips give particles in the gas stream a negative charge. The particles then move in the electric field to deposit in loose, fluffy layers on the metal plates. Periodically the gas flow is cut off and large electromagnetic hammers bang the plates causing the powder to drop off into hoppers below.

In electrostatic spraying a spray gun is used to atomize a powder or paint. In the spray gun is a corona electrode which gives the particles or droplets a negative charge as they exit the spray nozzle. The object to be coated serves as the anode and attracts the charged particles. For liquid paint spraying the advantage of this process is the reduction in overspray that misses the object, saving paint and reducing emissions from small paint shops. In dry powder spraying the electric field is necessary to make the particles stick to the object to be coated. Uncharged particles will not deposit. When the particles are highly resistive they will retain their charge, partially shielding the electric field where they are deposited. This causes additional particles to migrate to and deposit on exposed surfaces yielding a more even coating than possible with simple spraying or dipping. Unfortunately this effect doesn't extend to interior surfaces. Because of the Faraday cage effect, the electric field lines don't extend to interior volumes and particles are not attracted there.

Xerography is an electrostatic process that works in the opposite direction. Here it is the substrate that is given the electrostatic charge. A drum with a thin selenium photoconductive coating is given an electrostatic charge. The drum is then exposed to a pattern of light. Where the drum is illuminated the selenium becomes conductive and the charge is conducted away. The drum then rotates through a dry powder hopper where the

powder adheres to the areas of the drum that remain charged. The drum then passes over a sheet of paper with an electrode on the other side of the paper. This electrode pulls the particles, which now have their own electrostatic charge, off of the drum and onto the paper. The paper then passes through a fuser where the pigment particles are heated to bond them to the paper.

These processes are very similar to EPD in that they are particulate processes that use an electric field to move the particles to a desired location. However, these processes are limited in three important aspects; thickness, density and particle size. Xerographic type processes are limited to a single layer. Electrostatic spraying of dry particles is limited by electric fields in the deposited layer in the case of non-conductive particles and by surface uniformity in the case of conductive particles. The density is limited by the lack of a short range interparticle repulsion. Particles will stick at the first point they contact as they deposit with no lateral movement to improve packing. Finally, the efficiency of the process declines with decreasing particle size, which, along with the difficulty of producing dispersed aerosols of very fine particles, places a practical lower limit on particle size in this process.

EPD, in contrast, uses electrochemical equilibria for particle charging. This allows much better control of particle charge as well as the creation of interparticle stabilization layers. This fundamental difference allows EPD to produce depositions of virtually any thickness or particle size with densities up to 74% for cubic close packed arrays of uniform spherical particles.

1.3 Why EPD?

Just as conceptually EPD falls between electrochemical and electrostatic processes, technologically it falls between thin film deposition processes and traditional particulate processes. It is able to deposit from a monolayer of 10 nm particles (**10**) to centimeter thick sanitaryware (**11**).
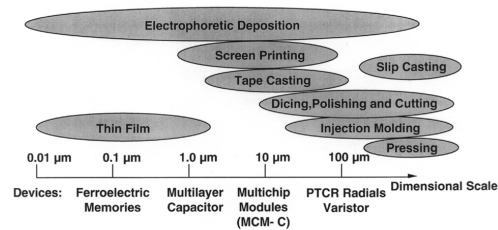
Fig. 1.2 Comparison of processing techniques
over a range of scales

To highlight the advantages of EPD it is useful to focus on one particularly demanding industry, electronic passive component manufacturing. These are components such as capacitors, inductors, resonators, resistors, etc. and the circuitry to interconnect them. Here the primary manufacturing technologies are the traditional particulate methods of tape casting and screen printing. As with any electronics manufacturing technology there is continuous pressure to make these components and circuits smaller, cheaper and lower power in order to pack more and more functionality into smaller packages. Layer and feature sizes in devices traditionally produced by thick film processes, already in the micron range, will need to drop well into the sub-micron range for the next generations of devices.

There are several technologies competing for use in the fabrication of these of these next generation devices. There are still the traditional thick film processes themselves, tape casting, screen printing, and other printing techniques. Although these have been in industrial use for forty years and may be approaching the limits of their applicability, they are still the subject of very considerable industrial research investment. There is also interest in adapting thin film techniques, such as sol-gel coating and the other thin film direct deposition techniques, which must be combined with photolithography for pattern development. Some processes combine screen printing with photolithographic techniques to develop very fine feature sizes.

However, recent advances in the production of high quality sub-micron and nano-sized particles has created an opportunity for another particle processing method, namely electrophoretic deposition.

The primary difference between EPD and traditional thick film particulate methods is the method of particulate consolidation. Tape casting and screen printing use a dispersed 25 to 40 vol.% particulate slip or ink. After the slip is cast or the ink printed, it needs to shrink 20 to 40% to form a good green particulate density of ~60%. Because of the inherent instability of the drying process it can be difficult to produce layers that are only a few particles thick. In EPD the particles come from an essentially random distribution in the suspension and are directly consolidated to ~60% density by the applied electric field. Little shrinkage occurs during drying. This means that even after drying a deposited layer that is only 2-3 particle diameters thick will retain the continuous, flaw free network of interparticle contacts that is necessary to sinter to a continuous layer. This is demonstrated by the 0.6μm silver/palladium layers produced by EPD from 0.3μm powder particles as described in Chapter 5. From this it is clear that EPD has the ability to produce the thinnest possible layers of any technique from a powder of a given particle size.

While much effort is going into reducing the thickness of layers and size of patterns produced by thick film processes, other researchers are attempting to scale up thin film processes. These are the processes used to produce sub-micron or nanometer scale thickness continuous films, such as chemical vapor deposition, molecular beam epitaxy, sputtering, sol-gel coating, and electrochemical deposition. One of the advantages of EPD over these other methods comes from the fact that it is a particulate based method. Stoichiometry can be controlled at the particle production stage, allowing complex oxides to be formed with precisely controlled dopant additions. This is demonstrated by the excellent piezoelectric properties of a $Pb(Zr_{0.52}Ti_{0.48})_{0.976}Nb_{0.024}O_3$ layer formed by EPD, described in Chapter 5.

Sol-gel coating is the only other thin film technique that offers a similar level of control over stoichiometry, however, sol-gel has its own problems of very high shrinkage and a large organic content that must be burned out prior to sintering.

Beyond just stoichiometry however, a particulate based process retains the potential for morphology control that cannot be achieved in any of the thin film processes. Particles can be coated with various materials to create an engineered microstructure, for example: transient liquid phase components to promote sintering, grain boundary pinning additives to prevent exaggerated grain growth, special grain boundary phases to promote or inhibit conduction, and surface dopants that will partially diffuse into the grains during sintering

to provide a compositional gradient from the center of the grains to the grain boundary. This last technique is especially important for forming the core-shell microstructure in barium titanate that is necessary to level its temperature capacitance behavior for capacitor applications.

Finally, there is the most significant advantage of EPD over other thin film processes — cost. The molecular deposition techniques are all slow processes and, with the exception of electrochemical deposition, require expensive high vacuum processing chambers. While sol-gel coating and other simple coating processes require much less expensive equipment to form an initial continuous film, all of the techniques mentioned above rely on a photolithographic process to produce patterns. This introduces additional processing steps that cannot be performed at the speeds currently customary in high volume electronic component manufacturing. In addition, to produce component and circuit patterns most of the material that has been deposited must be washed away. In high volume production this can add up to a considerable expense.

With EPD, a particulate deposition can be made in seconds on an electroded pattern on a carrier. This patterned deposition can then be transferred by standard lamination procedures from the carrier to a multilayer tape lay-up or a wet stack lay-up on a substrate. The carrier with the electrode pattern can be used repeatedly and little material is wasted.

1.4 Overview of Thesis

Chapter 2 is the most general chapter and is mostly devoted to a review of the scientific background necessary to understand EPD. In section 2.7 this information is brought together to create a list of mechanisms of EPD from different types of suspensions. Some of these mechanisms have been demonstrated conclusively either here or in the literature, others are still hypothetical. Finally, there is a brief list of some of the other related effects that can occur when performing EPD. These are based on the experience developed from many hundreds of deposition attempts that were made over the years leading up to this thesis. So as not to try the patience of the reader, only a tiny number of these depositions are analyzed here.

The analysis in Ch. 2 argues that understanding behavior in the electrochemical diffusion layer near the deposition electrode is key for understanding the deposition process. Since it would be difficult to directly measure the properties of the suspended particles in this thin layer, Ch. 3 presents a careful analysis of surface adsorption and charge formation on alumina particles in a simple, well controlled EPD suspension. This

then allows the prediction of the electrochemical behavior of the particles in the vicinity of the electrode.

The conclusions from Ch. 3 are then a critical component for the deposition analysis in Ch. 4. Here the dramatic impact of ions reversibly adsorbed to the particle surfaces is clearly demonstrated. This chapter also offers a conclusive demonstration of the 'Ion Depletion Enhanced Electrostatic' deposition mechanism which is first described in the analysis of Ch. 2.

Chapter 5 is then more practically oriented. Here the deposition of a silver/palladium powder is analyzed and shown to be a case of deposition by direct electrostatic force. This is followed by several demonstrations of how these depositions could be used in electronic device manufacturing. Demonstrations of the deposition, sintering and electronic properties of PZT, barium titanate and titania follow.

Finally, Chapter 6 gives a brief review of some of the most significant findings presented in this thesis. The most significant part of this chapter, however, is a roadmap for future work in EPD. This list breaks down into needs for education to make some of the basic science related to EPD more readily available to the scientific and industrial community, scientific research projects to advance the understanding of EPD, and development projects to help move EPD into commercial applications.

1.5 Summary of New Contributions to the Understanding and Application of EPD

Over the past seventy years there have been more than a thousand articles and patents published related to EPD. Recently the pace of publications has increased as there has been more interest in novel techniques for manipulating sub-micron and nano-scale particles. Excellent reviews covering much of the published literature on EPD have been published by Sarkar and Nicholson (**12**), Gani (**13**), and most recently Boccaccini and Zhitomirsky (**15**). Faced with this large volume of prior art, it is useful to point out some of what in particular is new in this thesis and has not been covered in the prior literature.

What has generally been lacking in this published literature has been a careful analysis of the chemistry, electrochemistry, and electrochemical hydrodynamics of these systems. As mentioned above the primary objective is the electrophoresis and deposition of the particles. The electrochemical effects that occur at the same time are usually ignored and almost never carefully analyzed. Convection driven by any mechanism is almost never mentioned.

This thesis is obviously far too short to cover all of the effects that occur during EPD, but below is a list of some of the novel observations, theories explaining other

observations, and analyses that have been made here while trying to deconvolute this surprisingly complex process.

Categorization of EPD Mechanisms — In Ch. 2 an EPD system is broken into components and the interactions between each of the components is analyzed separately. Finally, a list of the mechanisms for developing stable colloidal suspensions is compared in matrix form to a list of the possible changes that can be induced in a solvent at an electrode. By considering each of the permutations, a list is generated of the suspension stabilization mechanisms and the near electrode effects for each that could lead to the formation of a deposition. This generates what the author believes to be a comprehensive listing of possible mechanisms for EPD. Some of these mechanisms have been conclusively demonstrated before, while others remain speculative. Two of these deposition mechanisms are demonstrated in this thesis. To the author's knowledge this is the first explicit list of EPD mechanisms and is certainly the first list that makes any claim of being comprehensive. This list of mechanisms then clarifies the specific areas of research that would be useful in improving the understanding of EPD for each of these cases. A list of exactly such specific research topics is given in Ch.6.

Surface Chemistry and Surface Charging of Alumina — In Ch. 3 the adsorption isotherm for HCl on alumina in ethanol/water is carefully analyzed. The shape of the isotherm strongly suggests that Cl- ions are adsorbed to surface sites in competition with negatively charged ethoxide ions. For a stable concentration of ethoxide ions to exist at the surface the surface must be acting as a catalyst for the autoprotolysis of the ethanol/water solvent. If this catalysis and competitive adsorption model can be extended to the pure aqueous suspensions most often studied, it could explain some of the seemingly contradictory observations of surface charge and adsorption that have been noted by other authors. (**15**)

Electrohydrodynamic (EHD) Convection — There are two types of EHD convection that are significant in EPD. The first is the boundary layer flow at the surface of a charged particle in an electric field. Some work has been done on this topic, specifically as it relates to clustering of particles at a surface (**1, 2, 16**). In §4.4.6 a qualitative description is offered for how these flows can affect the formation of a thick deposition layer to result in a low density deposition.

This thesis also offers the first discussion of EHD forced convection of the solvent/suspension during EPD. This topic is first introduced qualitatively in §2.2.11 and §2.2.12. A quantitative analysis of convective instability in a specific system is given in Ch. 4. The applied voltage in most EPD cells is well above the 5 to 10 V necessary to induce this type of convection, therefore, this type of convection is likely very common in EPD experiments. Realizing that this convection is happening and analyzing its effects is vital for understanding the formation of the electrochemical gradients necessary for almost all of the mechanisms by which EPD occurs.

Ion Depletion Enhanced Electrostatic Deposition — This is one of the EPD mechanisms first listed in Ch. 2. In Ch. 4 this mechanism is demonstrated through the careful analysis of depositions of alumina from an ethanol/water suspension. It is shown that ionic adsorption/desorption on the surface of the particles being deposited can stabilize the solution against convection that would normally occur. Preventing convection allows an unbalanced charge conduction layer to develop which can have voltage gradients on the order of one million volts per meter. This creates an electrostatic force on the particles which is sufficient to tightly pack the particles at the electrode. This high voltage gradient also provides a strong damping effect against thickness variation, automatically leveling the deposition thickness even with significant electric field non-uniformities in the deposition cell.

Electrostatic Deposition of Metal Powder — In §5.2, an electrostatically stabilized suspension of silver/palladium powder is analyzed and it is shown that the direct electrostatic force of the electric field can reasonably account for the EPD of the powder. It is also shown that this type of deposition of conductive particles can lead to the same type of ramified (branched) growth that can occur in electrodeposition.

Gravitational Convection — Although it is only given brief mention here, §5.2.4, this is the only explicit mention of gravitational convection in EPD that this author is aware of. This is significant given that the majority of EPD studies are performed between vertical electrodes where gravitational convection is almost inevitable.

Symbols used in Chapter 2

<u>Abbreviations</u>
DEBL Diffuse electrostatic boundary layer
EHD   Electrohydrodynamic
EPD   Electrophoretic deposition
RHE   Reversible hydrogen electrode
P-B   Poisson-Boltzmann
P-P   Polymer - Polymer
P-S   Polymer - Solvent

<u>Latin Symbols</u>
A_{131} Hamaker constant for two surfaces 1 separated by a medium 3.
a Particle radius (m)
c Molar concentration of dissolved salt (gram mol equivalent/dm^3)
C_∞ Characteristic ratio for polymer chain flexibility
D Diffusion coefficient (   )
e Elementary charge (1.602E-19 C)
E Electric field (V/m)
E   Reduced electrophoretic mobility (non-dimensional)
F Faraday constant (96,534 C/mol)
F   Force (N)
g Gravitational acceleration (9.8 m/s^2)
h^o Planck constant (6.63x10^{-34}J•s)
h Surface to surface separation distance (m)
h Height in a sedimenting suspension (m)
J_o Flocculation rate (s^{-1})
k Boltzman Constant (1.381x10^{-23} J/K)
k_o Chemical reaction rate constant
K Chemical equilibrium rate constant
l Number of particles in an agglomerate or floc
l_o Length per polymer repeat unit
m Number of particles in an agglomerate or floc
m_o Weight per polymer repeat unit
n Refractive index
n Number of repeat units in a polymer chain
n_i Number density of ion i (m^{-3})
n_{iref} n_i at $\psi = 0$
P Pressure (Pa)
q Surface charge density (C/m^2)
Q Total surface charge on a particle (C)
r Center to center particle separation distance
$\langle r^2 \rangle^{\frac{1}{2}}$ Root mean square (rms) end to end length of a polymer chain
T Temperature (K)

t_c Characteristic time for doublet formation (s)

u_E Particle electrophoretic mobility (μm·cm/V·s)

u Convective velocity (m/s)

u_o Convective velocity (m/s)

y Reduced particle potential at shear layer (non-dimensional)

z Ion valence with sign ±

Greek Symbols

α Transfer coefficient for electrochemical reactions at a surface

α Intermolecular expansion factor for dissolved polymer

ε_o Permittivity of free space (8.854E-12 C^2/J·m)

ε_r Relative dielectric constant

ζ Particle Potential at Shear Layer (mV)

μ Solvent Viscosity (Poise)

η Overpotential necessary to drive electrochemical reactions at a finite rate (V)

κ Inverse Debye length (m^{-1})

$\boldsymbol{\kappa}$ Solvent Conductivity

ν Ion electrophoretic mobility

ν_e Infrared cut-off frequency

ρ_∞ Number density of dissociated molecules of a binary salt in bulk solution (m^{-3})

τ Polymer bond angle

ϕ Electrostatic potential (V)

ϕ^o Standard electrostatic potential relative to RHE (V)

φ Particle volume fraction

Φ Particle interaction energy (kT)

ψ Rational electrostatic potential (V)

Chapter 2

<u>Mechanisms of Deposition</u>

2.1 Introduction

     As was stated in Ch. 1, electrophoretic deposition (EPD) can be broken down into three steps: 1) the formation of a stable, charged suspension; 2) electrophoretic transport of the particles to the deposition electrode; and 3) deposition. The theoretical basis for the first two steps has received considerable attention and these processes are fairly well understood. (**1,2,3**)

     The third step, deposition, has been the subject of far fewer theoretical treatments and is still not well understood. This is in part due to the fact that there is no one single mechanism of deposition and in part due to this being a complex combination of colloidal chemistry and electrochemistry studied primarily by materials scientists. To make the complexity of this system more tractable, this chapter breaks down the system into three basic components. These components are then discussed first as binary interactions of each of the components before putting all three together to describe the various mechanisms of deposition that can occur in particular systems.

     This analysis breaks an EPD system down into three fundamental components: the particles to be deposited, the suspending solvent, and the applied electric field. The binary interactions are then:

    Solvent-Electric Field — An EPD cell is fundamentally a conducting electrochemical cell in which particle deposition occurs. This electrochemical conduction can dramatically change the composition of the solvent and the electric field gradients in the cell.

    Particle-Solvent — A brief discussion of how particles develop an electrostatic charge in a solvent.

    Particle-Electric Field — An electrostatically charged particle will experience a force in an electric field, however, the oppositely charged fluid around the particle will experience an equal and opposite electrostatic force. The particle and the fluid then move in opposite directions. The thickness of the charged layer of solvent around the particle determines its electrophoretic mobility.

    Particle-Particle — Particles in a solvent will inevitably experience a London-Van der Waals (L-VdW) attraction. There must be some mechanism to counteract this attraction to keep the particles from floccing prior to deposition.

These phenomena are then all put together to examine what electrophoretic and electrochemical effects can be combined with which stabilization methods to allow the creation of an adherent deposition of the desired density.

Finally, some of the effects that can occur after deposition will be briefly discussed, both before and after the deposition voltage is turned off, as well as after removal of the deposition from the bath.

2.2 Conduction in a Fluid

The EPD cell is fundamentally an electrochemical cell in which electrophoretic deposition takes place. Understanding how and why particles do or do not form a deposit depends almost entirely on understanding the ionic distribution, and therefore the electric field distribution, in the deposition cell. This not only determines the electrophoretic motion of the particles but the electrohydrodynamic (EHD) convection of the solvent which can move ions and particles at speeds up to four orders of magnitude faster than simple electrophoresis. The following examples will consider a simple parallel plate electrochemical cell.

2.2.1 Non-Conducting System - No Dissolved Ions

The first and simplest case is that of a solvent with no dissolved ions and no electrochemical reactions. Here the solvent will act as a simple dielectric and the potential will change linearly between the electrodes.
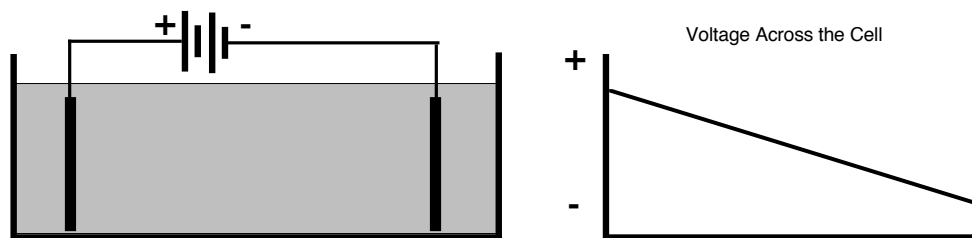
Fig 2.1 Voltage across a cell with no dissolved ions

2.2.2 Non-Conducting System - Dissolved Ions

In the second case the solvent has a concentration of ions but no chemical reactions occur at the electrodes. This case is commonly referred to as that of an ideally polarizable electrode. Ions will migrate toward the oppositely charged electrodes where some may adsorb to the surface of the electrode, reducing the electric field at the surface. Ions that remain dissolved will move toward the electrode until that motion is balanced by concentration diffusion away from the electrode. This charged layer will be referred to here as the Diffuse Electrostatic Boundary Layer (DEBL). In standard terminology (**30**)

the DEBL term used here corresponds to the diffuse portion of the electrical double layer. The electrical double layer refers to an interface between two oppositely charged layers. When the interface is between a solid and liquid this double layer refers to the charge at the surface of the solid and an oppositely charged layer in the solvent. The layer in the solvent may also be broken into two layers, a Stern or compact layer which does not move relative to the surface and a diffuse layer which remains fluid and can move relative to the surface. With the interjection of a Stern layer this interface is sometimes referred to as the triple layer. It is unfortunately very common that the term 'Double Layer' is used to refer to only the diffuse portion of the electrostatic double or triple layer. The term DEBL is used here to clearly identify the nature of the layer referred to and to distinguish it from electrochemical boundary layers which can exist as well.

While the concentration of adsorbed ions on the electrode surface will depend on specific ion-surface interactions, the profile of ions in solution near the surface can be described by combining an equation for the gradient of an electric field as a function of ionic concentration with an equation for the ionic concentration as a function of the electric field. The Poisson equation describes the Laplacian of the electrostatic potential, the gradient of the electric field, as a function of net ionic concentration:

$$\nabla^2 \psi = \nabla E = -\frac{e}{\varepsilon_r \varepsilon_o} \sum_1^N z_j n_j .$$ Poisson Eq.   [2.1]

Where ψ is the rational electrostatic potential, that is the potential relative to a bulk solution potential of zero, E - the electric field, e - the charge of an electron, z_j - the charge on ion j, n_j - the number density of ionic species j, N - the total number of ionic species present, and $\varepsilon_r \varepsilon_o$ -the permittivity of the solvent. The Boltzmann equation then describes the gradient of the ionic concentration as a function of the electric field:

$$\nabla \ln n_j = -\frac{ez_j}{kT} E = -\frac{ez_j}{kT} \nabla \psi$$ Boltzmann Eq.   [2.2]

with the solution

$$n_j = n_{jref} \exp(-ez_j \psi / kT) ,$$ [2.3]

here n_{jref} is the concentration of the ionic species n_j at the reference condition where the electrostatic potential is zero; $\psi = 0$. Putting these equations together forms the Poisson-Boltzmann (P-B) equation which describes the shape of the electric field and distribution of dissolved ions around a charge in a solvent with dissolved ions:

$$\nabla^2 \psi = \nabla E = -\frac{e}{\varepsilon_r \varepsilon_o} \sum_1^N z_j n_{jref} \exp\left(-ez_j \psi / kT\right)$$ [2.4]

Poisson-Boltzmann Equation

If the electrolyte is symmetric, that is where there is an equal number of positive and negative ions in the reference state and the charges on the ions are equal and opposite, +1/-1 or +2/-2, the identity $\sinh p = \left(e^p - e^{-p}\right)/2$ can be used to write the P-B equation as:

$$\nabla^2 \psi = \nabla E = \frac{2ezn_{jref}}{\varepsilon_r \varepsilon_o} \sinh\left(ez\psi/kT\right) \qquad [2.5]$$

If a planar electrode is assumed with a perpendicular vector x, this has the solution (2, §4.7):

$$\Psi(x) = 2\ln\left(\frac{1 + \exp(-\kappa x)\tanh\left(\frac{1}{4}\Psi_s\right)}{1 - \exp(-\kappa x)\tanh\left(\frac{1}{4}\Psi_s\right)}\right) \qquad [2.6]$$

If a planar electrode is assumed with a perpendicular vector x and the sinh function is linearized* assuming a low surface potential ($\psi < 30$ mV) for the electrode relative to the bulk solution , the result is the Debye-Hückel approximation of the P-B equation:

$$\frac{d^2\psi}{dx^2} = \frac{2e^2 z^2 n_{jref}}{\varepsilon_r \varepsilon_o kT}\psi \qquad [2.7]$$

The decay of the potential from a flat charged surface to a neutrally charged solvent can then be described by

$$\psi = \psi_s \exp(-\kappa x) \qquad [2.8]$$

where x is the distance from the surface, ψ_s is the rational electrostatic potential at the surface and κ is the Debye parameter which has the units of m^{-1}.(Eq.s [9] & [10]) The inverse Debye parameter is referred to as the Debye length and is the distance from a flat plate where the voltage will drop by 1/e or 63%. A very frequently used unitless parameter in colloidal electrostatics and electrodynamics is κa, the radius of a particle, a, divided by the Debye length. The resulting parameter gives an index of the thickness of the electrostatic layer around a particle relative to the surface curvature. The thinner the layer relative to particle curvature the more the surface can be approximated by flat plate assumptions (large κa). The thicker the layer relative to particle curvature the better it can be approximated as a point charge (small κa).

$$\kappa = \left[\frac{2e^2 z^2 n_{ref}}{\varepsilon_r \varepsilon_o kT}\right]^{\frac{1}{2}} \qquad \text{Debye Parameter for Symmetric Electrolytes} [2.9]$$

$$\kappa = \left[\frac{\sum_1^N e^2\left(z_j\right)^2 n_{jref}}{\varepsilon_r \varepsilon_o kT}\right]^{\frac{1}{2}} \qquad \text{Generalized Debye Parameter} \qquad [2.10]$$

(* The linearization of the sinh function leads to an overestimation of the potential of ≈ 13% at 25 mV, 40% at 50 mV and 65% at 75 mV, all at 25°C.)
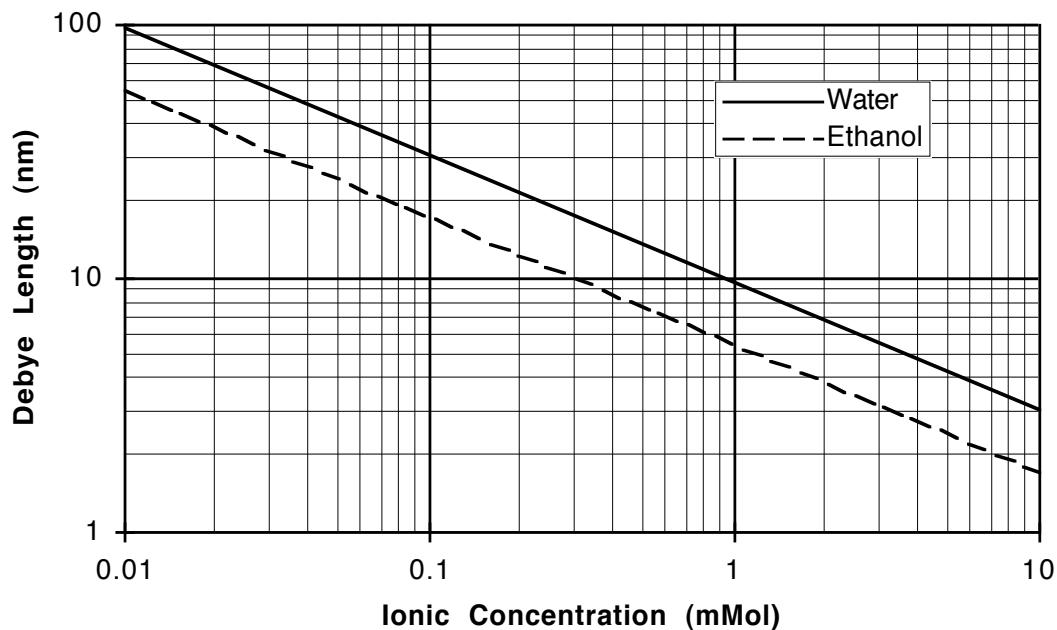
Fig. 2.2 Debye Length for a symmetric 1-1 electrolyte in water and ethanol.
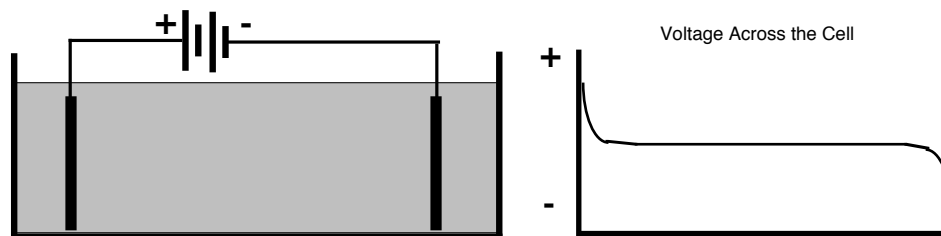
Fig. 2.3 Schematic of voltage distribution across an electrochemical cell with a concentration of ions but with no electrochemical reactions occurring at the electrodes. Almost the entire voltage drop across the cell will be confined to two very thin layers next to the electrodes.

As can be seen from the plot of the Debye length as a function of ionic concentration in Fig. 2.2, this characteristic length is measured on a nanometer scale. Given that the voltage decay is exponential on this scale it can be seen that even at very low ionic strengths almost the entire voltage across the cell will be confined to very thin layers immediately adjacent to the electrode surfaces. This is shown schematically in Fig. 2.3.

So when an electrode is placed into a solvent with dissolved ions, the surface may adsorb some ions with a preference for one polarity or another and thereby develop a surface charge (§ 2.3 below). When a voltage is applied to the electrode, it will attract

positive ions and repel negative ions dissolved in the solvent. The result is that the concentration of positive ions in solution at the surface goes up and that of negative ions goes down. This situation is illustrated in Fig. 2.4. This concentration effect in addition to an electrostatic effect increases the ratio of adsorbed positive ions to negative ions.
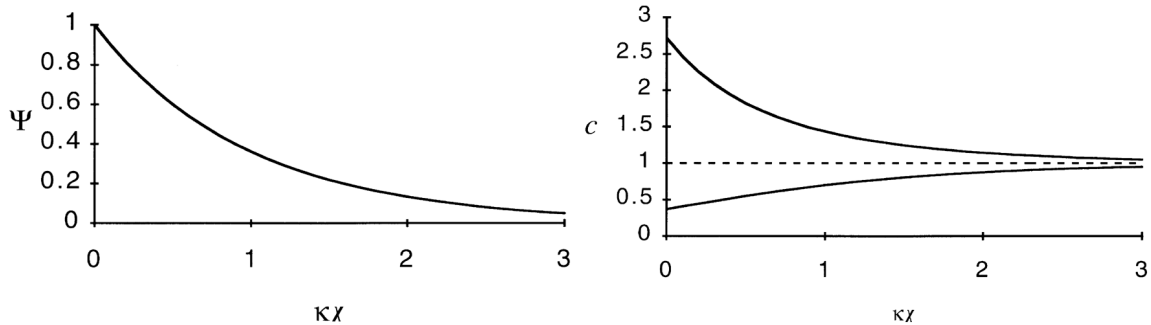
Fig. 2.4 Potential Distribution and Ionic Concentration at an Electrode for a non-dimensional surface potential of 1.0. This corresponds to a potential of 25.7 mV at 298°c. (eq. [6])

If no chemical reactions take place, then when the applied voltage is removed current will flow back out of the electrode as positive ions move away from the surface and the mirror charge within the electrode is reduced. This is the basic principle of electrolytic capacitors or "super capacitors". Very large surface area electrodes are separated by a salt solution. The maximum voltage is kept low to minimize chemical reactions and enormous dielectric polarizations are made possible by the forward and backward motion of positive and negative ions in the salt solution.

2.2.3 Conduction in a Solvent

In the previous section it was assumed that no electrochemical reactions take place at the electrodes, however, in any cell containing a solvent with dissolved ions some conduction will occur.

Solvents, with the exception of liquid metals, are ionic conductors. For conduction to occur ionized atoms or molecules must be oxidized (lose electrons) at the anode and be reduced (gain electrons) at the cathode. Current then is carried by migration of these ions through the solvent. In an electrolytic capacitor the objective is to minimize these reactions since they represent a dielectric loss, and at low voltages some systems can have extremely low currents. Conversely, in electrochemical production processes the objective will be the maximum current at the minimum voltage.

For EPD there must be a significant voltage gradient in the bulk solution for electrophoretic migration of the particles to occur. This means that there must be a

conduction current in amperes usually at least one order of magnitude higher than the conductivity of the cell in seimens. If the conduction current is lower than that, most of the voltage across the system will be concentrated in the thin double layers. There will be little or no voltage gradient in the bulk to drive the particles to the deposition electrode.

Electrolytic conduction can occur by either production or consumption of ions at the electrodes. Ions then move from one electrode to another by a combination of three mechanisms: *Migration* - this is the motion of an ion due to the force caused by its charge in the local electric field; *Diffusion* - net motion of ions due to random motion of individual ions with a concentration gradient of those ions in the solvent; and *Convection* - motion of the solvent and ions together due to either density differences in a gravitational field or net electrostatic charge on a unit of solvent in an electric field. The sum of these components are shown in order as the three terms of the Nernst-Planck equation:

$$i = -F^2 \nabla\phi \sum z_j^2 |v_j| c_j - F \sum z_j D_j \nabla c_j + Fu \sum z_j c_j \qquad \text{[11]}$$
Nernst-Planck Equation for Current Flux

Where i is the current in Amperes, F - the Faraday constant, ϕ - the electrostatic potential, v_j - the mobility of ion j, c_j - the molar concentration of ion j, and D_j - the diffusion coefficient of ion j, and u - the convective velocity of the solution. Although these three components of conduction appear as a simple summation, each of the terms is related to the others by the Poisson equation [2.12], which relates charge concentrations to electric field gradients, and the equation for electrostatic body force, Eq. [2.13], which relates electric field and charge concentration to one of the forces driving convection (the other forces being gravity or mechanical stirring).

$$\nabla^2 \phi = -\frac{F}{\varepsilon_r \varepsilon_o} \sum_1^N z_j c_j \qquad \text{Poisson Eq.} \quad [2.12]$$

$$F = -E \sum_1^N z_j n_j \qquad \text{Electrostatic Body Force} \quad [2.13]$$

To drive the current flow in an electrolytic cell a voltage must be applied between the electrodes. The total voltage across the cell can be broken down into six components: ϕ - electrode potential, η_{sa}, η_{sc} - electrode overpotential at the anode and cathode, η_Ω - ohmic potential, and η_{ca}, η_{cc} - concentration overpotential at the anode and cathode respectively.

$$V = \phi + \eta_{sa} + \eta_{sc} + \eta_\Omega + \eta_{ca} + \eta_{cc} \qquad [2.14]$$

These will be treated in order in the following sections., §2.2.4 to §2.2.7.

2.2.4 Electrode Potential

The electrode potential is the electrostatic potential of a metal electrode in a solution at zero current. This potential is measured relative to a reversible hydrogen electrode. Understanding the nature of this potential provides a basis for understanding the electrode overpotential and boundary layer behavior to be discussed later.

When a metal electrode is immersed into an electrolyte solution electrochemical reactions will begin immediately. A commonly used example is that of a copper electrode in a copper sulfate/water solution. When the copper is immersed in the solution it will immediately begin to dissolve.

$$Cu_m \rightarrow Cu^{2+} + 2e^-$$ [2.15]

This dissolution will generate a current

$$i = zFk_o^f a_m$$ [2.16]

where k_o^f is the dissolution rate constant and a_m is the activity of the metal. Likewise, cupric ions from the solution will precipitate onto the solid metal

$$Cu^{2+} + 2e^- \rightarrow Cu_m$$ [2.17]

Which will generate a current in the opposite direction

$$i = -zFk_o^b a_{Cu^{2+}}$$ [2.18]

If the currents from the dissolution and precipitation reactions are not balanced an electrostatic charge will quickly build up on the electrode, either attracting or repelling cupric ions from the solution. A double layer will form, and the charge on the electrode will increase until the activity of the cupric ions at the surface has reached a value where the net current is balanced:

$$zFk_o^f a_m - zFk_o^b a_{Cu_s^{2+}} = 0$$ [2.19]

where the activity of the cupric ion at the surface, $a_{Cu_s^{2+}}$, is given by the Boltzmann equation;

$$a_{Cu_s^{2+}} = a_{Cu_\infty^{2+}} \exp\left(-\frac{2e}{kT}\psi_o\right)$$ [2.20]

where $a_{Cu_\infty^{2+}}$ is the activity of the cupric ion in the bulk of the solution and ψ_o is the surface potential relative to the bulk of the solution.

It is obvious that equation [15] simplifies to a chemical equilibrium equation

$$K = \frac{a_{Cu_s^{2+}}}{a_m}$$ [2.21]

where K is the ratio of the forward and backward reaction rates. Then using the Boltzmann equation we can solve for the potential necessary to maintain a constant surface activity of the cupric ion for any activity of the ion in the bulk of the solution.

$$\psi_o = \frac{kT}{ze}\left[\ln\left(\frac{a_{Cu^{2+}_\infty}}{a_m}\right) - \ln(K)\right]$$ [2.22]

Because of the difficulty and uncertainty of the measurement of surface potential relative to the bulk solution, electrochemical measurements are almost always measured relative to another electrode. The standard electrode in this scheme is the reversible hydrogen electrode (RHE). This is a platinum surface exposed to both the solution and 1 atmosphere pressure of H_2 gas, usually bubbled across the platinum surface in the solution. This electrode is assigned a potential of zero for a 1 molar activity of the hydronium ion (H_3O^+) in aqueous solution. The standard potential for a copper electrode is then defined as the potential relative to the RHE for copper metal in a solution containing 1 molar activity of Cu^{2+} ions. If the electrode metal is pure copper and is free of adsorbates, then it is assigned an activity of 1. The constant $\ln(K)$ term in equation [22] is combined with the constant term for the offset of the RHE to give the standard electrode potential, ϕ^o, for copper in aqueous solution.

$$\phi = \phi^o + \frac{kT}{z_+ e}\ln\left(\frac{a_{Cu^{2+}_\infty}}{a_m}\right)$$ [2.23]

This is now the well known Nernst equation for equilibrium at a metal electrode. The reason for the above derivation is to illustrate the central nature of the diffuse electrostatic boundary layer in the in the determination of the potential at an electrode.

The one thing that has been skipped in this treatment is the true nature of what is meant by "surface" and "at the surface". Sometimes the surface is simply an exposed layer of atoms of the underlying solid with solvent molecules and ions colliding randomly with that surface. Frequently that surface will attract an ordered layer of solvent molecules and it is only on the other side of this layer that the solvent behaves like a fluid in random motion. The difficulty is that this ordered layer will act as a dielectric — frequently a spontaneously polarized dielectric. This means that the potential measured within the metal of a metal electrode can be very different from the potential one molecular layer away in the solvent. An extreme example of this is the behavior of water at a platinum surface. Molecular dynamic simulations done by Heinsinger (**4**) showed that water molecules will spontaneously orient with the oxygen end toward a crystalline platinum surface. In an uncharged system this spontaneous polarization is sufficient to cause a

potential jump of 1.1 Volts over the 3 Å thick single molecule thick layer of surface water. Thus a metal surface can attract a hydration or solvation sheath just like a metal ion in solution.

This ordered molecular layer at the metal surface, referred to as the Helmholtz layer, will also have a capacitance. In the case of platinum in water the orientation of the molecules at the surface leave this with a relatively low dielectric constant, ≈ 5, but given the thinness of this layer the capacitance will be at least 15 μF/cm^2. Polarization of a second layer of water can then boost the differential capacitance of this layer to more than 40 μF/cm^2. Over a range of voltages this capacitance is close enough to a constant that its effect can simply be incorporated into the constant term of the Nernst equation (**5**). However, for accurate calculation of surface activities, it is the potential on solvent side of this layer that should be used. Therefore here ψ_o will be defined as the potential on the solvent side of this layer with ψ_m being the potential inside the metal, both terms being relative to the solvent potential in the bulk of the solution. So the total potential between the inside of the metal and the solvent will be broken down into two components ψ_m-ψ_o the potential drop from the inside of the metal to the outside of the Helmholtz layer and ψ_o the potential across the diffuse electrostatic boundary layer (DEBL). The terms "at the surface" will mean immediately adjacent to the Helmholtz layer on the solvent side while "on the surface" will mean either in physical contact with the surface or incorporated into the structure of the Helmholtz layer.

2.2.5 Electrode Overpotential

In order to move the system beyond equilibrium and initiate a current flow, a voltage in addition to the equilibrium potential has to be applied. The usual procedure to measure this voltage is to place two electrodes of the same material as close together as possible in the electrochemical bath. A current is then driven between one electrode and a third separate electrode. The voltage difference between the two identical electrodes at various current levels is then recorded as electrode overpotential. The objective in placing the electrodes as close together as possible is to minimize ohmic and concentration voltages between the electrodes. Ideally the overpotential is measured with the exact same conditions prevailing immediately outside the double layers of each of the electrodes.

When this overpotential is applied to an electrode, the change in voltage will cause a change in the activity of ions at the surface. This change can be approximated by the Boltzmann relation. Although this approximation is frequently used without qualification, it should be noted that this equation is an equilibrium equation being applied to a dynamic

system. The diffusion of reactant and product ions in and out of the double layer will change the concentration and potential profile of this layer. Because at medium and high ionic strengths this layer is very thin compared to the speed of diffusion, it has been shown that this has only a minor effect on the double layer profile, (**6**). How well this holds true in very low ionic strength solvents will need to be demonstrated.

So to a first approximation the activity of an ion near the electrode surface will be given by

$$a_s = a_\infty \exp\left(-\frac{ze}{kT}\psi_o\right)$$ [2.24]

However, the reaction rate of an ion at the surface is not linearly related to its activity. The rate of reactions involving electron exchange at an electrode will be a function of the potential across the Helmholtz layer (**5**). The greater the potential drop across the Helmholtz layer the lower the reaction rate. This reaction rate can be written as:

$$k_o^f = B\exp\left(\frac{ze}{kT}\alpha(\psi_m - \psi_o)\right)$$ [2.25]

where B is a theoretical reaction rate at zero potential at the surface, and α is called the transfer coefficient and is a value between 0 and 1, most often it is measured to be 0.5. (z is the charge on the reacting ion assuming that the reaction is between an ion of charge z and a neutrally charged species, i.e. involves a charge transfer of $|z|$ electrons.)

If we now make the simplifying assumptions that both the potential across the Helmholtz layer and across the diffuse double layer are linear functions of the electrode potential, the potential can be written as $\phi + \eta$, the standard potential at a particular molar concentration plus the overpotential. All of the constant terms can now be collected into a catchall term, i_o, called the exchange current. The variable term is then an exponential function of the overpotential times a proportional term, α, the transfer coefficient.

$$i = i_o \exp\left(-\alpha\frac{ze}{kT}\eta\right) \qquad \text{Tafel Equation} \qquad [2.26]$$

Eq. [2.26] is often referred to as the Tafel equation which was determined empirically and is valid in many cases for overpotentials greater that 50-100 mV.

If the reaction is symmetric there will be both a cathodic and an anodic reaction occurring at the same time. The net current in either direction can then be approximated by the so called Butler-Volmer equation:

$$i = i_o\left[\exp\left(\alpha_a\frac{ze}{kT}\eta\right) - \exp\left(-\alpha_c\frac{ze}{kT}\eta\right)\right] \qquad \text{Butler-Volmer Equation} \qquad [2.27]$$

where i is the total current, i_o is the exchange current, α_a, α_c are the anodic and cathodic transfer coefficients, and η is the electrode overpotential.
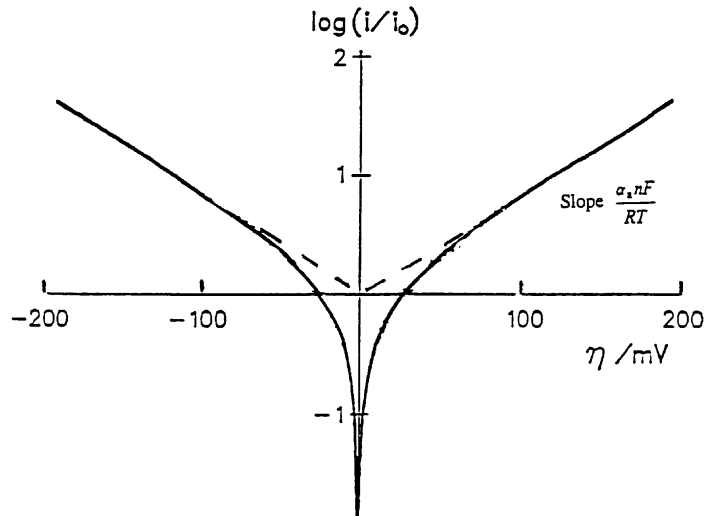
Fig. 2.5 Tafel plot of current-overpotential for a symmetric reaction. (from **7**)

From the perspective of EPD the most important conclusion from this analysis is that, except in very rare coincidences, there will be a double layer at the surface of the deposition electrode. Furthermore, since EPD usually involves the application of tens of volts, not a few hundred millivolts, to a suspension with ionic strengths measured on a fractional millimolar scale, the double layer at the deposition electrode will both be relatively thick, tens of nanometers, and very highly charged. This can lead to a condition where even though the electrode is negatively charged and particles in suspension are positively charged, their interaction will be repulsive and the particles cannot be made to deposit on the electrode. This is a result of the dramatic charge density difference that can exist between the particle and the surface of a conducting electrode (**8**).

On the other hand, a clear understanding of the nature of the electrode DEBL allows its manipulation. By matching the electrode metal, solution composition and applied voltage/current, the electrode diffuse layer can be manipulated or even eliminated, the electrode brought to the potential of zero charge. Thus at one voltage/current particles can be brought to the vicinity of the electrode, allowed to rearrange in a 'floating' layer above the electrode, then the voltage/current changed to allow the particles to contact the electrode and deposit. This understanding will be important for the production of ordered monolayers, deposition on sub micron patterned electrodes, and even controlled single particle depositions.

2.2.6 Ohmic Potential — η_Ω

The Ohmic potential across a cell is due to the intrinsic resistance of the solvent to electrical conduction. This conduction in the solvent will occur by electrophoretic migration of ions under the influence of the external applied electric field. This ionic migration is resisted by random collisions between the ions and other molecules in the solvent. Because the mechanism of resistance is the same as in an electronic conductor there is likewise a linear relationship between electric field and current, which can be written as Ohm's law:

$$i = \kappa \nabla \phi \qquad [2.28]$$

where κ is the conductivity of the solvent. This will apply in areas of the solution where charge is balanced and there are no concentration gradients.

A simple analysis of the conductivity will illustrate most of the significant effects in ohmic conduction. The total current will be the sum of the flux of positive and negative ions:

$$i = z_+ c_+ F u_+ + z_- c_- F u_- \qquad [2.29]$$

where $c_\pm$ is the molar concentration and $u_\pm$ is the velocity of the ions. Since this has been defined to be in a region of charge balance then:

$$z_+ c_+ + z_- c_- = 0 \qquad [2.30]$$

giving:

$$i = z_+ c_+ F\left(u_+ + u_-\right) \qquad [2.31]$$

The velocity of the ions can then given by:

$$u_i = -z_i v_i \nabla \phi \qquad [2.32]$$

where v_i is the electrophoretic mobility of the ion. This mobility in turn can be approximated by:

$$v_i = \frac{D_i z_i e}{kT} \qquad [2.33]$$

where D_i is the diffusion coefficient for ion i. These equations then can be combined to give the final form of this approximate formulation of conductivity in term of the diffusion coefficients of the ions:

$$\kappa = \frac{eF}{kT} \sum D_i z_i^2 c_i \qquad [2.34]$$

The purpose of this analysis is to show the close relationship between migration and diffusion. Electrophoretic migration of ions being simply a type of diffusion in an electric field. In particular migration and diffusion are effects that operate on the same order of magnitude and it is only in special cases where one can be considered without the other.

Of course eq. [2.34] is only a rough approximation of the ionic conductivity of a solution. The actual conductivity will be reduced by interactions between the ions which reduce the mobility of individual ions. Very accurate values for the conductivity of ionic solutions can be calculated using the Fuoss-Onsager equation [2.35]. The values of the various terms in this equation are described more fully in Appendix A.

$$\Lambda = \Lambda_o - S(c\gamma)^{\frac{1}{2}} + E'c\gamma \ln(6E_1'c\gamma) + Lc\gamma - K_A c\gamma f^2 \Lambda \qquad [2.35]$$

2.2.7 Concentration Overpotential — η_c

Also known as concentration polarization — This is the final component of the total cell voltage as given in eq. [2.14]. This potential arises due to ionic concentration gradients in the solution outside of the DEBL's. These gradients are in turn caused by the electrochemical reactions occurring at the electrodes where ions are either produced, consumed or blocked. This can cause either a change in ionic composition or an increase or decrease in ionic strength.

An example of a change in chemical composition is the case of a neutral salt such as KCl in an electrolyzable solvent such as water. When a voltage is applied to the cell K^+ ions will migrate toward the cathode and Cl^- ions toward the anode. K^+ ions approaching the cathode will not react, but will be blocked from further migration by the cathode surface. This will lead to an accumulation of K^+ in the solution near the cathode. Cl^- ions migrating away from the cathode will be replaced by OH^- ions produced by electrolysis of the solvent. Thus the accumulation of K^+ will be electrically balanced by the production of OH^-. K^+ will continue to accumulate until migration toward the cathode in the electric field is balanced by the concentration diffusion away from the cathode. The result is that at the cathode KOH will accumulate at a higher concentration than that of KCl in the starting solution. Likewise at the anode an accumulation of Cl^- ions will be electrically balanced by H_3O^+ ions produced by electrolysis at that electrode.

If this process is continued without convection, eventually the cell will be divided into two regions, one on the cathode side containing KOH and on the anode side HCl. Conduction will occur by migration of OH^- ions away from the cathode and H_3O^+ ions away from the anode. They then meet and neutralize forming water in the middle of the cell. The relative migration of K^+ and Cl^- ions toward the cathode and anode will be balanced by concentration diffusion away from the electrodes. The total number of ions in the cell will have doubled. This division of the cell into purely basic and acidic sides will rarely be seen in practice. These concentration gradients will lead to slight ionic charge imbalances. The electric field will result in an electrostatic body force on these unbalanced

charge regions in the cell. These forces can then initiate convection and convective mixing in the cell.
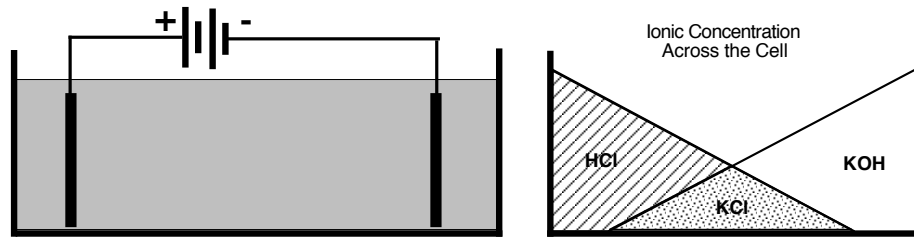
Fig. 2.6 Ionic concentration and composition across the cell.

What is significant here for electrophoretic deposition is that electrochemical reactions can have several effects. It can increase or decrease the ionic concentration at the electrode, in this case increasing the ionic concentration at both electrodes. It can change the ionic composition near the electrode, in this case the hydrogen ion activity (pH), and it can induce EHD convection, changing transport mechanisms in the cell.

2.2.8 Limit Current Behavior

Much larger concentration overpotentials can occur in a different case where an ion is produced at one electrode and consumed by reaction at the opposite electrode. An example of this would be conduction in a Brønsted acid solution where the anion does not participate in the electrochemical reactions. This is the case that will be examined more closely in Ch. 4 where the electrolyte is hydrochloric acid in an ethanol/water solvent. Here the acid dissociates into chloride ions and predominantly hydronium ions. During conduction hydronium ions will be consumed at the cathode, producing H_2 gas and water. On the other side of the cell H_3O^+ ions will be produced by electrolysis of the water in the solvent. Cl^- ions will remain mostly passive in the solvent, primarily just providing charge balance to the H_3O^+ ions.

The first case to consider here is that of equilibrium conduction of a HCl electrolyte in the absence of convection. The following analysis was first published by Levich in 1962 (**9**). In an equilibrium conducting state with no convection, the chloride ions will migrate in the electric field toward the anode. However, since no chloride ions are produced or consumed in the cell, for the concentrations to be in equilibrium the migration in one direction must be balanced by diffusion in the other. So at equilibrium the net motion of the chloride ions will be zero and they will not contribute to conduction in the solution.

$$i_{Cl} = 0 = F^2 z_{Cl}^2 v_{Cl} c_{Cl} \frac{d\phi}{dx} - F D_{Cl} z_{Cl} \frac{dc_{Cl}}{dx} \qquad [2.36]$$

This means that the total current in the cell will be due to migration and diffusion of the H_3O^+ ions.

$$i_{H^+} = -F^2 z_{H^+}^2 v_{H^+} c_{H^+} \frac{d\phi}{dx} - FD_{H^+} z_{H^+} \frac{dc_{H^+}}{dx}$$ [2.37]

Returning to the simple description of ionic mobility:

$$v_i = \frac{D_i z_i e}{kT}$$ [2.38]

allows Eq. [2.36] to be rewritten as

$$\frac{d\phi}{dx} = \frac{kT}{z_{Cl}^2 Fec_{Cl}} \frac{dc_{Cl}}{dx}$$ [2.39]

Eq.s [38] & [39] can now be substituted into Eq. [2.37] to give:

$$i_{H^+} = -F^2 z_{H^+}^2 \frac{D_{H^+} z_{H^+} e}{kT} c_{H^+} \frac{kT}{z_{Cl}^2 Fec_{Cl}} \frac{dc_{Cl}}{dx} - FD_{H^+} z_{H^+} \frac{dc_{H^+}}{dx}$$ [2.40]

Which simplifies to :

$$i_{H^+} = -FD_{H^+} z_{H^+} \left(\frac{z_{H^+}^2}{z_{Cl}^2} \frac{c_{H^+}}{c_{Cl}} \frac{dc_{Cl}}{dx} + \frac{dc_{H^+}}{dx} \right)$$ [2.41]

At this point it is possible to introduce the assumption of quasi-neutrality. Although positive and negative charge are never perfectly balanced in conduction in the presence of a concentration gradient, this assumption is that the quantity of unbalanced charge is negligable in comparison to the total ionic concentration. The validity of this assumption was shown by both Levich and Newmann (**9,7**), and it remains valid down to very low total ionic concentrations. This asumption is expressed mathematically as:

$$c_{H^+} \approx \frac{z_{Cl}}{z_{H^+}} c_{Cl}$$ [2.42]

When this is substituted into Eq. [41] all of the terms involving the concentration or valence of the anion cancel out, and the result is:

$$i_{H^+} = -2FD_{H^+} z_{H^+} \frac{dc_{H^+}}{dx}$$ [2.40]

From this equation it can be seen that the maximum continuous current due to both electrophoretic migration and concentration diffusion is only two times what it would be for diffusion alone in the same gradient.

When this is applied to a simple parallel plate electrochemical cell with a plate separation of d, this equation can be integrated from $x=d$, the anode, to a point x distance from the cathode. This then gives the following formula for the concentration across the cell as a function of the cation concentration at the anode, $c_{H_0^+}$,

$$c_{H^+} = \frac{i}{2FD_{H^+} z_{H^+}} (x - d) + c_{H_0^+}$$ [2.41]

This then shows a simple linear concentration gradient across the cell.

The problem with this equilibrium conduction in a charge balanced solvent is that the limiting current possible in the absence of convection is very low, as is the voltage that will induce this current. If the concentration gradient between the two electrodes is linear then as the voltage is raised there will be a point where at the ionic concentration at the anode will rise to twice the initial average in the cell. This concentration then declines linearly to zero at the cathode. Since negative concentrations are not possible this will be the point at which the cell is conducting the maximum current possible under the above assumptions. This maximum current is given by:

$$i_{\text{lim}} = 2 \frac{FD_{H^+} z_{H^+}}{d} c_{H_0^+}$$

[2.42]

In this treatment the formal charges of the ions have been carried through, even though the stated case of HCl the charges are simply +1/-1. However, by carrying through the charges, the mathematics become valid for a simple salt having any valence combination where an ion of one polarity is produced at one electrode and consumed at the other and opposite ion does not react. The appropriate values for the ion which carries the current can be substituted for the values indicated for the hydronium ion in the above analysis, and the values for the non-reactive ion can be substituded for the chloride ion. This will lead to the same result regardless of the valence of the ions. The current will only be two times the diffusion current for the charge carrying ion in the same concentration gradient.
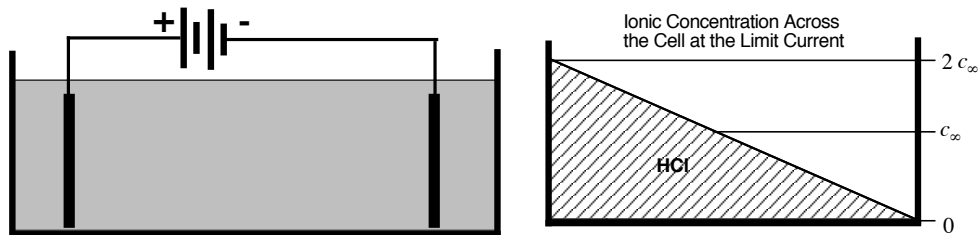
Fig. 2.7 At the limit current the ionic concentration across the cell will decrease linearly across the cell to almost zero at the electrode where the ions are consumed.
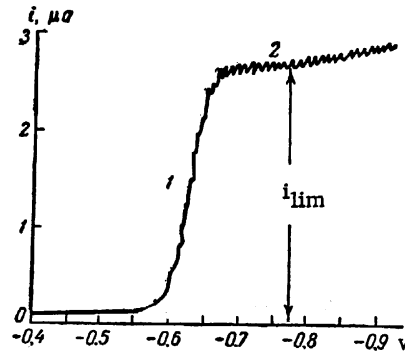
Fig. 2.8 Example limit current behavior (*1*) Ohmic region below the limit current, (*2*) limit current region, additional voltage does not induce significant additional current. (from Levich (**9**)).

Obviously the concentration at the cathode will not go to zero as a current will continue to flow. However, as the concentration approaches zero several other effects become significant, violating the assumptions above.

2.2.9 Beyond the Limit Current

It is useful here to take a qualitative look at an equilibrium approach to this limit current, and analyse what happens when the voltage is raised beyond the point necessary to induce the limiting current.
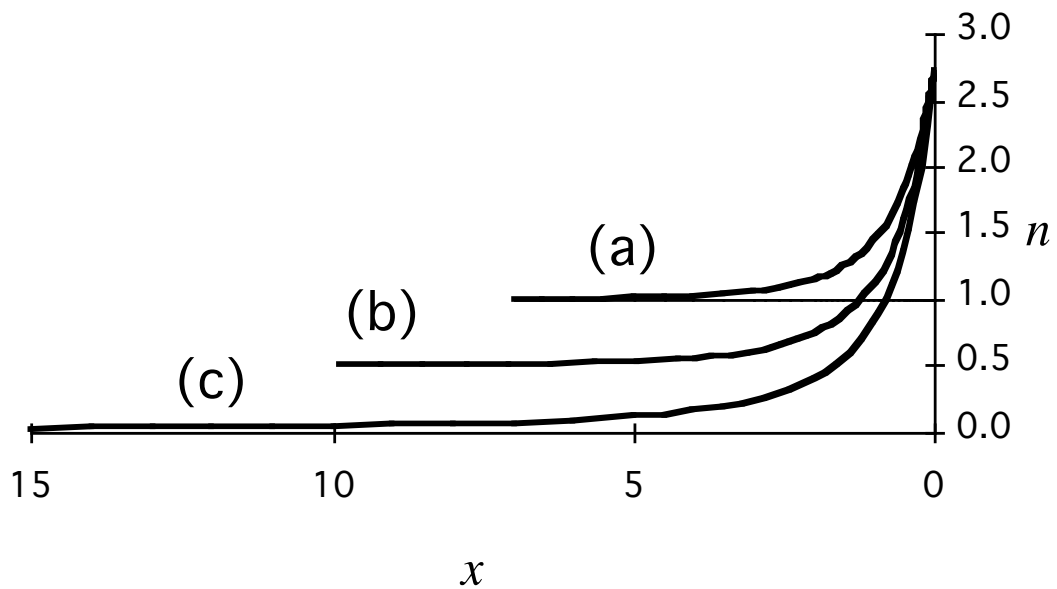
Fig. 2.9 Ionic concentration profiles in the DEBL at an electrode with constant surface activity. (a) initial concentration in the bulk solution, (b) concentration outside the DEBL one half initial concentration, (c) concentration outside the DEBL 0.01 of initial. Potentials calculated using eq.s [6],[3]

Assuming that the equilibrium rational electrode potential of the cathode is negative, the diffuse boundary layer at zero current will as shown by line (a) in Fig. 2.9. When a voltage is applied to induce an equilibrium current of one half the limit current, the concentration across the cell will be as shown by line (b). The concentration outside the cathode DEBL will have dropped by one half. This means that the DEBL thickness will increase by a factor of $\sqrt{2}$. The voltage across the DEBL will have to increase by $kT/_e \ln 2$ just to maintain the same concentration of positive ions at the electrode ($kT/_e = 25.7 mV$ at 25°C). The additional overvoltage necessary to drive the conduction reactions forward will depend on the exchange current for the reduction reaction at this electrode.

Fig. 2.9 (c) shows the situation approaching the limit current. If the concentration outside the boundary layer is now 1% of the initial concentration then the boundary layer thickness will have increased by a factor of 10 and the voltage across the diffuse layer will have to increase by 120 mV just to maintain the equilibrium concentration at the electrode surface. Again there will have to be a significant overvoltage in addition to this to drive the electrochemical reactions at the electrode.

As the cell approaches the theoretical limit current, additional voltage will all be concentrated across the DEBL. With each increase in voltage the concentration outside the DEBL will decrease. This decrease will have very little effect on the concentration gradient in the bulk of the cell and, therefore, very little effect on the total current through the cell. With little change in current there will be little change in the ohmic or concentration potential drop across the cell. This decrease in concentration will, on the other hand, have a large effect on the DEBL. In a non-conducting DEBL concentration diffusion away from the electrode will be balanced by electrophoretic migration toward the electrode. In a conducting DEBL migration must predominate over diffusion for there to be a net current flowing to the electrode. At the innermost edge of the DEBL concentrations are high enough that this is a minor effect. At the outer edge this can become the dominant effect. As the concentration goes down the outer edge of the DEBL will flatten and expand until the concentration gradient reverses. In this outer region both concentration diffusion and migration act to move the positive ions toward the cathode.
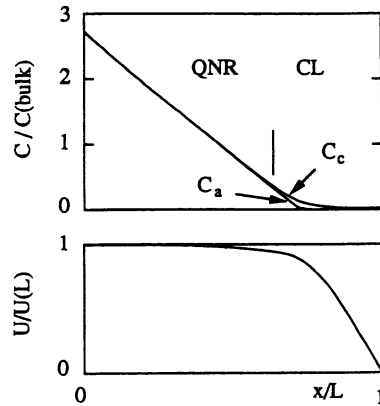
Fig. 2.10 Equilibrium ionic concentration (C) and potential distributiution (U) across the cell at a voltage above that necessary to elicit the limit current in the absence of convection. Electrode boundary layers are not depicted. Cell is divided into the quasi neutral region (QNR) and charged layer (CL). Thickness of the charged layer is exaggerated. (From Chazalviel (**10**))

So, in equilibrium conduction absent convection, at a voltage just beyond the onset of the limit current, the cell can be broken down into four regions: 1) the Anode Boundary Layer - because of the increase in ionic concentration outside this layer, this DEBL will simply get thinner and has little effect on overall cell behavior; 2) the Quasi-Neutral Region - here the ionic concentration can be well described by the analysis of Levich assuming charge balance as discussed above; 3) the Charged Layer - this layer has a very high voltage gradient, 1 to 10 MV/m, a cation concentration gradient declining toward the cathode, a thickness that can be measured on a micron scale, and an almost complete absence of anions; and 4) the Cathode Diffuse Layer - here the voltage gradient is even higher than in the charged layer but the thickness will only be a few tens of nanometers. This difference between this layer and the charged layer is that the cation concentration gradient rises toward the cathode surface in this layer.

2.2.10 Imposition Voltage/Current Above the Limit Current

The prior discussion has focused on equilibrium conduction at each point up to the onset of convection. A more realistic case for EPD is where a current or voltage well beyond the limit current is suddenly imposed on the system. The situation where a voltage greater than that necessary to elicit the limit current will be discussed below. This problem has been analyzed numerically by Chazaviel (**10**). The concentration of the two types of ions was calculated based only on the Nernst-Planck and Poisson equations with no convection. The electrode boundary layers were included in the analysis with the

assumption of an infinite exchange current, therefore the boundary layer voltage was enough to maintain the same surface concentration as at zero current.

When the voltage is first applied to the cell, the instantaneous current will be determined only by the ohmic resistance of the solution, $i = V\kappa$. This current will immediately begin to drop as some of the voltage is taken up by the cathode and anode DEBL capacitances. The current across the cell will still be determined only by the ohmic resistance of the solution but the voltage driving the current will be reduced by the double layer voltages. Once significant electrochemical reactions begin at the electrodes there will begin a depletion of hydronium ions at the cathode and an accumulation of chloride ions at the anode. This situation is shown as the black line in Fig. 2.11.
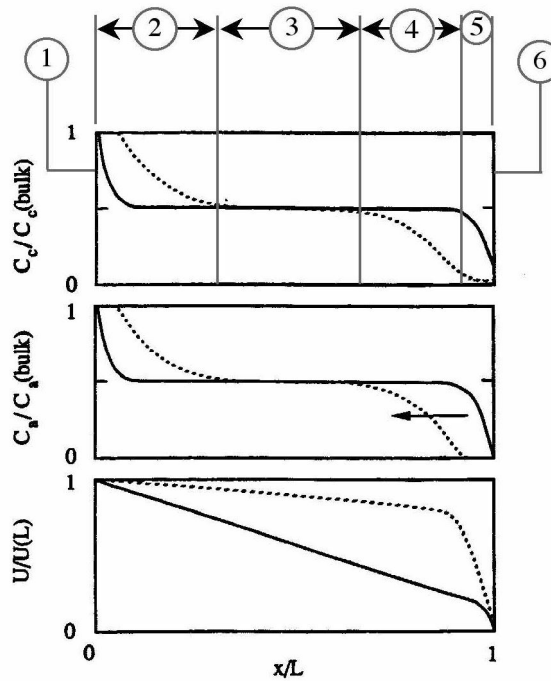
Fig. 2.11 Ionic concentration (C) and potential distributiution (U) across the cell at two times after the imposition of a voltage above that necessary to elecit the limit current . Electrode boundary layers are not depicted. Cell is divided into six layers numbered as identified in text. (Adapted from Chazalviel (**10**))

The accumulation of chloride ions at the anode will increase the solution conductivity in this region but will have little impact on the total voltage across the cell. On the other hand, the depletion region near the cathode will have a dramatic effect on the cell voltage distribution. The concentration gradient region outside of the cathode DEBL will have a lower conductivity than the bulk and therefore will account for a larger and

larger portion of the cell voltage. Likewise, as mentioned previously, as the ionic concentration drops outside the DEBL, the voltage across the DEBL increases as well.
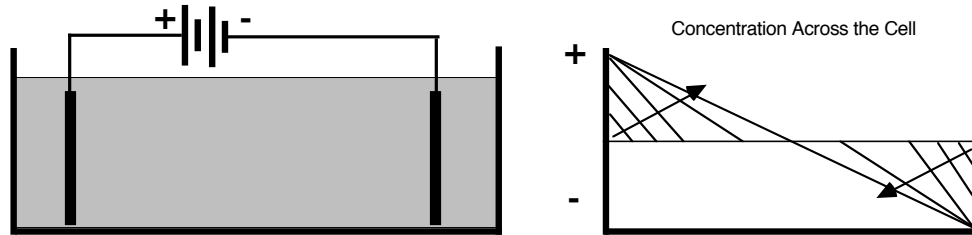
Fig. 2.12 Dropping concentration gradient near the cathode at the initiation of conduction.

This cathode concentration gradient zone will grow as shown in Fig. 2.12. The current will not change dramatically during the growth of this zone therefore the slope of the concentration gradient will remain the same with the width of the zone growing. The solution will remain predominantly charge balanced in this gradient zone until the concentration approaches zero near the boundary layer. The thickness of the gradient region when this will occur can be estimated using Eq. [42] where d will be the thickness of the gradient zone and i_{lim} the current across the cell prior to the formation of the charged layer. Once the gradient layer has reached this thickness the concentration outside the cathode DEBL will drop to the point where this layer will split into two regions. One next to the electrode surface where the concentration of positive ions declines away from the surface, and another much thicker region where the anion concentration rises again moving away from the surface. This second zone is what Chazalviel refers to as the 'charged layer' and the concentration profile of this region is given schematically in Fig. 2.10. In both of these regions there is an almost complete absence of anions.

The resulting concentration and voltage profiles are shown as the dotted line in Fig. 2.11. In this case of non-equilibrium conduction the cell can be separated into six regions of charge/concentration/potential. Going from left to right in Fig. 2.11 these are: 1) the anode boundary layer, 2) the anode gradient layer, 3) the bulk solution, 4) the cathode gradient layer, 5) the charge layer, and 6) the cathode boundary layer. Together the anode and cathode gradient layers and the bulk solution form what Chazalviel has termed the 'Quasi Neutral Region'. At long times these regions will merge into one gradient and the current will reach a minimum which is the limit current for the cell. Any voltage in excess of what is necessary to elicit this very low limit current will be taken up by the very high voltage gradient of the charged layer.

This is a theoretical profile based on the complete absence of convection in the cell. This is actually a very difficult condition to achieve. Chazalviel describes his calculated concentration profile as "unphysical", and Levich in describing the limit current region as shown in region 2 of Fig. 2.8 comments:

> "... a motionless solution can be achieved in practice only in exceptional cases, for example, where the solution is immobilized by the addition of gelatin or agar-agar." (**9**)

To this list could also be added filter material or a porous packing of particulate material. Each of these will act strongly to damp convective motion of the fluid. The necessity for very strong viscous damping of convection in order to see these effects indicates that there must be equally strong forces driving the fluid into convection.

2.2.11 Transition to Convective Transport

In any region where the concentration diffusion and electrophoretic migration are in the same direction there will be a net driving force for convection. A concentration gradient driving diffusion in the same direction as migration will be referred to here as a favorable gradient. So any layer with a favorable gradient will be able to lower its net free energy by bulk motion of the fluid within the layer.

Beyond there just being a driving force for convection, for convection to actually occur the energy released by convection must be greater than the energy consumed by the fluid's viscous resistance to convection. Because the cell is a closed system and will behave as an incompressible fluid, convective transport must occur by circular vortices. That is, motion of fluid in one direction must be balanced by an equal volume moving in the opposite direction. While vortices can and do grow larger that the region they start in, the initial vortex will not be larger that the layer that generates it.

The smaller the vortex, the greater its energy dissipation per unit volume. The energy available to drive the vortex will also be volumetric, going up as the cube of the diameter of the potential vortex. Because of the geometric relationship between energy available and energy dissipation there will likely be a critical thickness of the unstable conduction layers where they will quickly trip into convective motion due to infinitesimal inhomogeneities in conduction or concentration.

Accurate estimates of the critical thicknesses of these layers will rely on future analysis and numerical modeling, however, the stability of each of the six conducting

layers enumerated above and the scale at which they will become unstable to convection can be estimated.

In both the electrode diffuse electrostatic boundary layers the concentration gradients will be unfavorable, so these layers will be highly resistant to convective motion.

The charge layer near the cathode is marked by both a favorable concentration gradient and an electric field on the order of one to ten million volts per meter. Because of the very high energy available in this layer it is likely to break into convective motion when it reaches a thickness of only a few tens of nanometers. The rapidity of the transition of this layer to convective flow explains the difficulty of observing the limit current behavior without some mechanical means of suppressing convection such as gelatin or packed filter material.

The situation is somewhat more complicated for the gradient layers in the quasi-neutral region. Here the concentration of the cation and anion is almost identical with the concentration gradient favorable for one and unfavorable for the other. The key for understanding convectional instability in this region is that the imbalances in the ionic concentration here, while insignificant from a chemical point of view, can have a large electrostatic effect on the conducting fluid. Wherever there is a change in the conductivity of the solution there must be a change in the voltage gradient in order for a uniform current to flow through the cell. However, a change in the voltage gradient implies an accumulation of unbalanced charge. The interaction of this electrostatic charge with the electric field will produce a body force on the solution.

In the cathode gradient layer where the ionic concentration drops, the conductivity drops and there is an increased voltage gradient. This increase in voltage gradient is due to a slight excess positive charge accumulating in the solution at the edge of this layer. There is then a force on this layer toward the cathode due to the local electric field. However, the local electric field will also be a function of the distance between this charged layer and the cathode. If at one point the layer moves closer to the cathode, the potential gradient between this layer and the cathode will increase. The motion of one portion of the fluid toward the cathode will displace fluid, forcing another portion of the charged layer away from the cathode, and decreasing the potential gradient between it and the cathode. Thus the fluid moving toward the cathode experiences an increased force toward the cathode while the fluid moving away experiences a decreased force. This then creates a vortex which will grow progressively mixing the fluid from the gradient layer with the bulk solution and blending out the concentration difference between the gradient layer and the

bulk solution. The scale at which this layer becomes unstable to convection is likely to be measured in tens of microns.

The anode gradient layer will rely on the same effect, however, because of the much lower changes in voltage gradient the forces will be at least an order of magnitude lower than at the cathode. Thus this layer will be unstable at a scale of hundreds of microns to several millimeters.

2.2.12 Convective Transport

As the voltage is raised across a cell there are a series of convective flow patterns that can be expected. These are shown diagramatically in Fig. 2.13. This is assuming a simple rectangular cell with the gravitational vector pointing downward to the bottom of the page.

At the lowest voltage, well below that necessary to induce the limit current, there will be no convection and a uniform concentration gradient will form across the cell. At a slightly higher voltage a single large vortex will form essentially filling the cell. This vortex will usually be initiated by a density gradient in the fluid. The ionic concentration gradient across the cell will make the solvent more dense at the anode and less dense at the cathode. The solvent will then rise at the cathode and fall at the anode, kicking off a circular vortex driven by both gravitational and EHD forces. (Fig. 2.13 a) This bulk vortex will contribute dramatically to ionic transport across the cell and will allow currents much higher than the limit current to be carried across the cell without the need for any other convective motion.

At higher voltages a gradient layer will form at the cathode initiating smaller vortices at the surface. (Fig. 2.13 b) These vortices will be on a scale of a few hundred microns to a few millimeters in size. They may roll across the surface, swept along by the flow of the bulk vortex or can be pinned in place by surface irregularities. These vortices will combine to even further increase ionic transport across the cell. This set of vortices works very effectively to mix the solution across the cell, preventing the formation of large concentration gradients. This allows a current several orders of magnitude higher than the limit current to be carried across the cell.

At even higher voltages this pattern will also become unstable. The gradient layer vortices will not provide sufficient transport to prevent the formation of an unbalanced charge layer at the cathode surface. Once this charge layer reaches the critical thickness it will break into vortices. (Fig. 2.13 c) These vortices will combine and grow outward into the gradient layer. Once these vortices reach a certain size an unbalanced charge layer will

form again, generating new vortices which themselves will grow away from the cathode surface. The surface flow will then be characterized by continuous, chaotic formation and growth of vortices that are ultimately swept away by the bulk vortex.

(a)   **(b)**   **(c)**
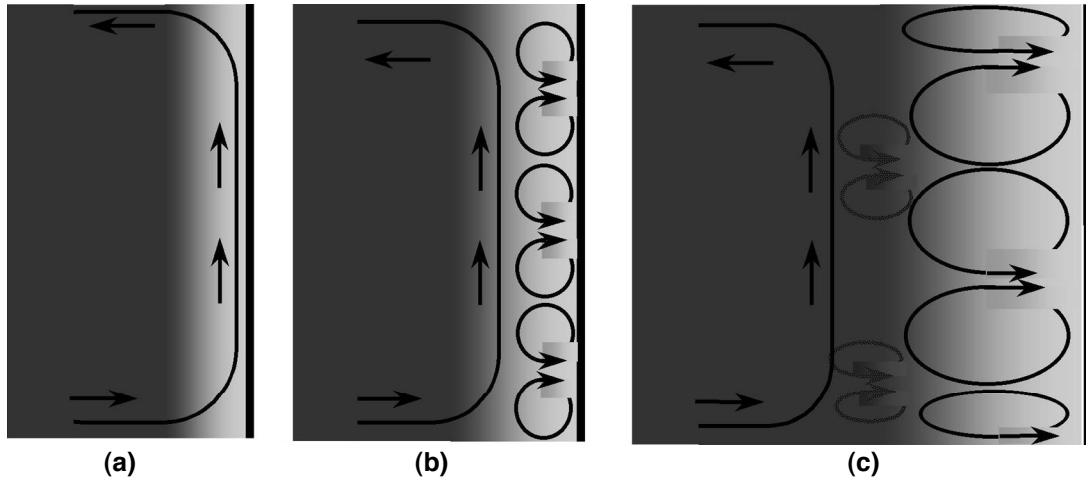
Fig. 2.13 Modes of convection in a simple rectangular cell.

At even higher voltages it is possible for the bulk vortex to split into smaller vortices, but the main effect will be the growth of the chaotic layer near the cathode until it fills the entire cell.

2.2.13 Conduction Summary

There are three main points from the preceding discussion that are particularly relevant for the understanding of EPD

1. There is an equilibrium diffuse electrostatic boundary layer at the surface of the deposition electrode. This boundary layer will change during conduction but only under very special circumstances will it disappear. During conduction this layer will usually have a potential drop an order of magnitude higher than the potential of the particles to be deposited. The potential of the electrode relative to the solvent at equilibrium and during conduction is system dependent and cannot be predicted a priori.

2. At any but the very lowest voltages there will be some level of EHD convection in the cell. This can provide significant mixing in the cell.

3. Where convection is suppressed large voltage and concentration gradients can develop.

2.3 Developing Surface Charge

        The development of a particle surface charge is essential for the process of EPD. Without an electrostatic charge on the particle different from that of the solvent the particles will not move in an applied electric field. Also, obviously, electrostatic stabilization (§ 2.6.2) will not work without an electrostatic charge on the particle. Beyond this, understanding the mechanisms of charge formation will also help in understanding the adsorption of polymers and surfactants to the surface for steric stabilization (§ 2.6.3).

        There are several ways in which particles in solution can develop a surface charge. These are not exclusive and frequently act to oppose one another. What these mechanisms have in common is that they all will involve interactions with ions in solution.

2.3.1 Dissolution/Precipitation

        In this case a pure solid is in equilibrium with dissolved ions of the same material in solution. This is most typically a metal in equilibrium with ions of the same metal in solution. Using the example of copper given above (§ 2.2.4), in pure water copper will dissolve as Cu^{2+} ions leaving behind two electrons. This will continue until the negative charge on the copper particle is sufficient that the concentration of Cu^{2+} ions attracted back to the surface creates an equilibrium between dissolution and precipitation. Likewise, in a strong copper sulfate solution, cupric ions will precipitate onto the copper particles until the particles develop a sufficient positive surface charge to repel the Cu^{2+} ions, reducing the surface concentration to equilibrium again.

        This case of simple dissolution/precipitation requires that the material be a conductor, with electrons moving in and out of the conduction band of the solid, generating a non-localized surface charge.

2.3.2 Selective Dissolution/Precipitation

        This is the typical case for ionic solids where there is a different solubility for each of the ions. The classic example of this is silver iodide where the surface charge can be precisely controlled by the ratio of dissolved silver and iodide ions in solution. One ion will preferentially precipitate and the other dissolve until the accumulated surface charge drives the concentrations at the surface to the equilibrium Ag+/I- ratio. In this case the material does not need to be conductive, and usually is not. The surface charge is due to ions at specific sites of unbalanced charge.
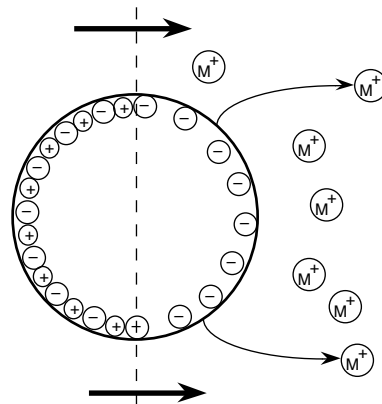
Fig. 2.14 Surface charge created by preferential dissolution.

2.3.3 Selective Adsorption

In this case there is a pre-existing concentration of ions dissolved in the solvent. If one ion has a greater adsorption energy than the oppositely charged ion it will preferentially adsorb to the surface giving the particle the charge of that ion. At very low ionic concentrations in the solvent the surface charge will adjust to bring the ionic concentration ratio at the surface to the ratio of the ionic adsorption energies. However this is a process that also depends on the concentration of adsorption sites available on the surface. As the concentration of ions in solution is raised the number of free adsorptions sites for the preferentially adsorbed ion will go down – the surface will become saturated. This changes the surface ionic equilibrium ratio and causes the surface potential to go down. This supression of surface charge can occur even at very low ionic concentrations in the solvent.
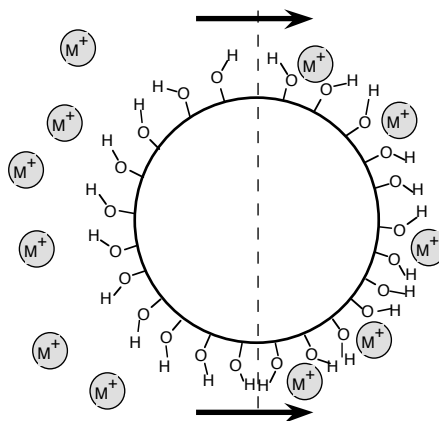
Fig. 2.15 Surface charge created by selective adsorption.

2.3.4 Surface Catalysis

Here there will be a molecular species in solution which is ionizable but is not ionized. This can include molecules of the solvent itself. The ionizable molecule is adsorbed to the particle, dissociated into two ions one of which remains adsorbed and one which returns to solution.

There are two mechanisms by which this dissociation can take place. The first is an interfacial process which is driven by the difference between the solid surface and the solvent. An uncharged molecule or polymer which is soluble in solution adsorbs to the particle surface. The soluble portion of this molecule then redissolves into the solvent either taking a charged entity from the surface or leaving a charged moiety behind. While the most frequent charged entity that is exchanged is a proton in a Brønsted acid/base reaction, the entity can be virtually any charged ion such as Na^+ or SO_4^-.

 The second type of charging catalysis is where the particle surface itself acts as the ionizing catalyst. An example of a non-polar catalyst is the platinum metal surface where H_2 is dissociatively adsorbed as two hydrogen atoms. These atoms are then removed from the surface by water molecules becoming dissolved hydronium ions, leaving behind a negative charge on the platinum. An example of a polar catalytic surface is alumina (Ch. 3) where ethanol molecules are dissociatively adsorbed to negative and positive surface sites as a proton and an ethoxide ion. The ethoxide ion is then more easily desorbed from the surface leaving a slight preponderance of protons and therefore a positive surface charge on the particle. There is little practical difference between interfacial and surface catalysis other than that the surface catalytic effect may more easily be poisoned by strongly adsorbing atoms or molecules occupying the surface catalytic sites.

2.3.5 Special Case - Hydroxide Surface

A very commonly offered example of selective disolution/precipitation surface charging is that of proton exchange with a hydroxide surface. Because of the humid, oxidizing conditions present in most laboratory environments, metals that are not already metal oxides will frequently form an oxide surface. Of these oxides, many will be stable as hydroxides - particularly in aqueous solution. The charging mechanism is then based on the Brønsted acid//base concept. These surface hydroxide groups can act as either proton donors or acceptors. This leads to the familiar 'S-curve' behavior in aqueous suspensions, with the particles positively charged in acidic conditions and negatively charged in basic. This hydroxide surface model is a specific example of the ionizable surface group model of surface charge regulation elaborated by Healy and White in 1978. (**31**)

$$-MO + -M + H_2O \Leftrightarrow 2 -MOH$$
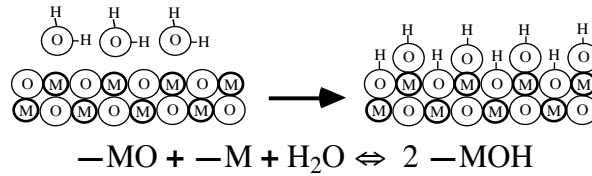
Fig. 2.17 Hydration of a metal oxide surface.
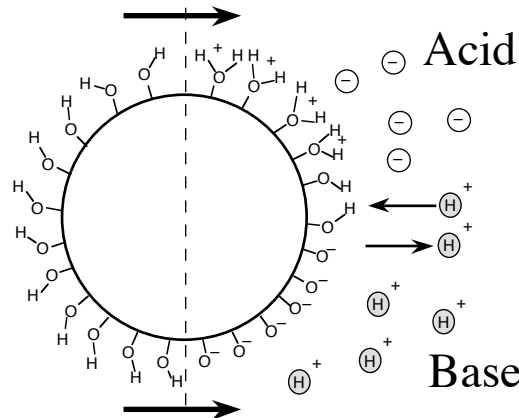
Fig. 2.18 Surface charge regulated by proton acceptance/donation.

However, this case is not as simple as it appears. As pointed out by Hunter (**2**, p 20, p 280) the Nernst equation does not apply in these cases. The surface charge density measured by acid/base titration is orders of magnitude higher than that measured by electrokinetic methods. There must be an additional adsorption/desorption mechanism to reconcile the two measurements.

This same case is analysed for alumina in ethanol/water in Ch. 3. Here it will be shown that surface charging is far more dynamic and complex than the simple adsorption/desorption of protons to and from the surface hydroxide layer. (**11**)

2.3.6 Compensating Effects

As mentioned at the beginning of this section, these effects will often act to counter one another. This is primarily due to action of the DEBL. If the particle begins to develop a positive charge, positive ions will be repelled from the surface while negative ions are attracted to it. The increased concentration of negative ions at the surface increases the likelyhood of their adsorption, decreasing the positive charge. The decreased concentration of positive ions will increase their rate of dissolution from the surface, again reducing positive charge.

A dramatic example of this effect is the etching of polarized ceramics. (**12**) On a single crystal surface in an acidic solution, positively poled surfaces will dissolve at a dramatically higher rate than negatively poled surfaces, with the dissolution of surfaces parallel to the polarization dissolving at an intermediate rate. This can be explained by different surface charges appearing on oppositely polarized surfaces. If the positively polarized surfaces have a more positive surface charge than negatively polarized surfaces, the solution concentration of positively charged metal ions will be much lower at positively polarized surfaces and higher at negatively polarized surfaces. This would result in the rapid dissolution of metal ions from the positively poled surfaces, exposing oxygen ions which are converted to soluble hydroxides. The higher concentration of metal ions at the negativley poled surface would then act to slow the equilibrium dissolution rate of metal ions from this surface. This differential etching strongly suggests that it may be possible to use electrophoretic effects to orient and align electrically polarized particles.

2.4 Electrophoretic Motion of Particles

An isolated particle with a total charge of Q in a solvent will experience a force F due to an externally applied electric field E_∞: $F = QE_\infty$. This force will cause the particle to accelerate until the viscous drag force is equal to the electrostatic force: $F = QE_\infty = 6\pi\mu a u_E$. Where μ is the solvent viscosity; a is the particle radius; and u_E is the velocity of the particle. By substituting in the electrostatic relationship between charge and surface potential, $Q = 4\pi\varepsilon_r\varepsilon_o a\zeta$, we obtain the Hückel formula for the particle velocity in terms of the surface potential at the shear layer, ζ, and which is independent of the particle radius:

$$u_E = \frac{2}{3}\frac{\varepsilon_r\varepsilon_o}{\mu}\zeta E_\infty \qquad \text{Hückel formula for Electrophoresis} \qquad [2.43]$$

where ε_r is the relative dielectric constant of the solvent and ε_o is the current permittivity of our locally observable universe.

However, an electrostatically charged particle in a solvent is rarely isolated. Most often the suspension is charge balanced; there is no net electrostatic charge. This means that for every unit of charge on the particle there will be an opposite unit of charge on an ion in solution. If the only ions in the solvent are the charged ions necessary to balance the charge on the particle surfaces, then the ion clouds around the partilces will be so diffuse that they have little effect on the behavior of the particles, and the Hückel formula will still be valid.

This formula begins to lose its validity as the concentration of independent ions in the solution goes up. Instead of a large diffuse cloud of counterions spread throughout the solvent, the charged surface of the particle will form a polarized layer around itself with one polarity of ion reduced in concentration compared to another. Thus there will be a layer of fluid surrounding the particle that will have a charge equal and opposite that of the particle surface. In this case where an electric field is applied, the particle will experience a force in one direction while the fluid in the layer immediately adjacent to the particle will experience an equal and opposite force. As a result the particle will begin to move in one direction while the fluid boundary layer around it is pumped in the opposite direction.

Smoluchowski analyzed this problem for very thin boundary layers in 1903 (**13**). The resulting formula is very similar to the Hückel formula and is again shown to be independent of the particle radius:

$$u_E = \frac{\varepsilon_r\varepsilon_o}{\mu}\zeta E_\infty \qquad \text{Smoluchowski Formula for Electrophoresis} \qquad [2.44]$$

The formulae are identical with the exception that for the same surface potential the particle in the thick (Hückel) boundary layer case will move 50% faster than the thin (Smoluchowski) case. In the thin boundary layer case the electrohydrodynamic pumping of the charged boundary layer in the direction opposite the motion of the particle adds significantly to the hydrodynamic drag. However, to maintain the same surface potential the net charge, and therefore the electrostatic force, is much higher on the particle in the thin boundary layer case. For example a 300nm diameter Ag/Pd particle with a surface potential of 40mV in acetic acid where the ionic strength is very low (Ch. 4.5), will have a total charge of 47 nC/m^2. For an alumina particle in ethanol (Ch. 3.5) with a surface charge of 42 mV and a 8.6 nm boundary layer thickness, the surface charge density is 1.1 mC/m^2. In the thin boundary layer case the surface charge is more than 20 times higher at the same surface potential. This means that the electrostatic force on the particle in the thin boundary layer case will also be 20 times higher even though the electrophoretic velocities are similar.

The Smoluchowski and Hückel formulae addressed the electrophoretic motion of particles with very thin and very thick boundary layers. In 1931 Henry (**14**) developed a formula for the motion of particles over the entire range of boundary layer thicknesses:

$$u_E = f(\kappa a)\frac{2}{3}\frac{\varepsilon_r \varepsilon_o}{\mu}\zeta E_\infty \qquad \text{Henry Formula for Electrophoresis} \qquad [2.45]$$

The values for the function $f(\kappa a)$ are shown graphically in Fig 2.19 below where κ is the inverse Debye length, a measure of the thickness of the boundary layer. (Eq.s [9] & [10]) This is an analytic solution of the problem, and, as such, Henry had to ignore some effects in order for the problem to remain mathematically tractable. This does not affect the validity of his solution, but restricts it to particles with low surface potentials.
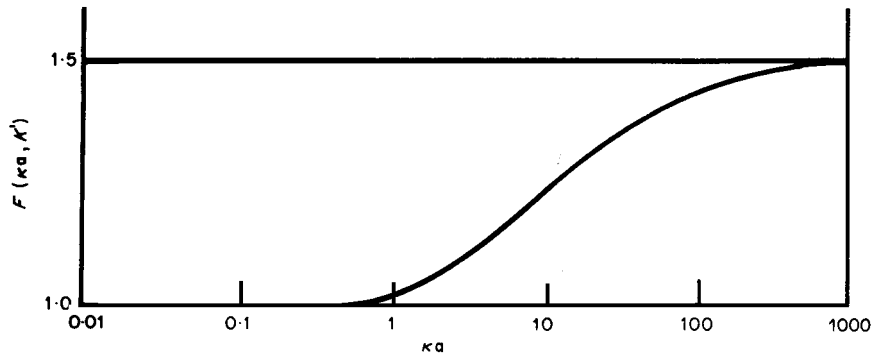
Fig. 2.19 $f(\kappa a)$ of Henry (**14**) from Hunter (**2**).

Two effects that were left out of Henry's treatment were polarization of the boundary layer and ion diffusion into and out of the polarised fluid around the particle. Higher surface potentials mean a higher charge in the boundary layer and therefore a greater ion imbalance. When an external electric field is applied, the particle/boundary layer will polarize with the boundary layer shifting relative to the particle. This eliminates the symmetry of the system on one axis and distorts the external electric field. Furthermore, as it is pumped around the particle, solvent will be entering and leaving the boundary region. The solvent entering the boundary layer around the particle will contain a balance of positive and negative ions and will become part of the charged boundary layer by ionic diffusion in or out of the solvent. Likewise, on the other side of the particle charged solvent will be pumped away from the particle. This solvent will remain charged for the time it takes for oppositely charged ions to interdiffuse and eliminate the imbalance. This electrohydrodynamic pumping of fluid around the particle combined with finite diffusion times will add to the polarization of the particle/boundary layer system.

The complete problem was solved using a computational algorithm by O'Brien and White in 1978 (**15**). Their results for particles in a 1-1 electrolyte, in this case KCl in water, are shown in Fig 19 a) & b). These charts are indexed on the non-dimensional mobility:

$$E = \frac{3\mu e}{2\varepsilon_r \varepsilon_o kT} \cdot u_E \qquad\qquad [2.46]$$

and non-dimensional surface potential:

$$y = \frac{ez\zeta}{kT} \qquad\qquad [2.47]$$
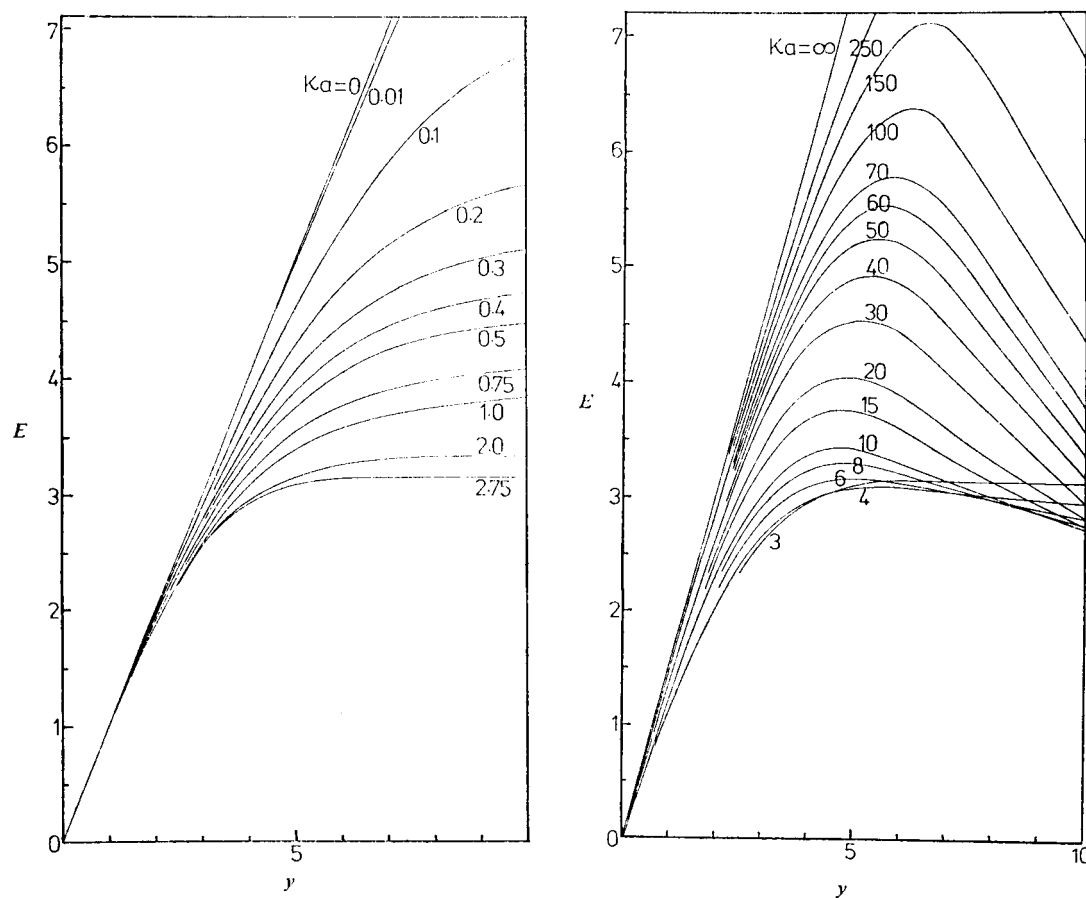
Fig. 2.20 The relationship between non-dimensional surface potential, y, and non-dimensional electrophoretic mobility, E, based on the ionic mobility of KCl in water. From O'Brien and White (**15**)

2.5 Creation of a Stable Suspension of Particles

      The first step in EPD is the creation of a stable, charged suspension of the powder to be deposited, and the first step to be taken here will be to define 'suspension' and 'stability'.

      A suspension most broadly defined is any discrete phase - solid particles, liquid droplets or gas bubbles dispersed in a continuous liquid or gas phase. A suspension is a 0 – 3 composite where the phase suspended is not interconnected in any direction and the suspending phase is continuous in three dimensions and interposed between the each of the units of the suspended phase. A suspension can be anything from soap bubbles floating in air to uranium dioxide precipitates floating in liquid lead oxide. However, to keep the scope of this paper reasonable the suspensions considered here will all consist of solid particles in a liquid at room temperature and pressure.

      Stability in the case of colloidal suspensions is very different from thermodynamic stability. The thermodynamically stable state for most of these suspensions is for the particles to be stuck together and sitting at the bottom of their container underneath the liquid. Stability in the case of suspensions is a relative measure of the resistance of the suspension to achieving this thermodynamic equilibrium. This is a relative measure since a suspension may be stable for only a few minutes or it may be stable for many years, yet either suspension may be stable enough or too stable for a particular purpose.

      The two forces that act against the stability of a suspension are gravity and the van der Waals force (vdW). For particles denser than the suspending solvent gravity will continuously pull the particles toward the bottom of their container. The vdW force will draw particles together and cause them to stick to one another. There are two types of force that can be used to preserve the suspension. One is macroscopic agitation; stirring, shaking, sound waves, etc. The other is the thermal energy of the solvent acting on the microscopic scale where the physical energy of agitation of the solvent molecules can impart kinetic energies on the scale of kT, the Boltzmann constant times the absolute temperature.

Table 2.1 Properties of some materials considered here.

Material	Density	Refractive Index	Dielectric Constant
Quartz (α)	2.65	1.45	3.75
Silica Glass	2.2	1.6	3.8
Mica (Muscovite)		1.6	7.0
Alumina	3.97	1.75	10
Zirconia	5.68	2.15	12.5
Barium Titanate	6.02	2.4	3,000
PZT	8.0	2.5	800
Titania	4.23	2.6	114
Silver 70/Palladium 30	11.0		~
Gold	19.3	3.1	~
Ethanol (20°C)	0.789	1.361	25.3

2.5.1 Gravitational Sedimentation

A spherical particle suspended in a fluid will experience a downward force due to gravity:

$$F_g = \frac{4}{3}\pi a^3 \Delta \rho g \qquad [2.48]$$

where a is the particle radius and $\Delta\rho$ is the particle density minus the density of the fluid. This force will cause the particle to accelerate downward until the gravitational force is balanced by the viscous drag of the fluid. All of the flows that we encounter here will be laminar, so the drag on the particle can be calculated using the Stokes equation: $F_d = 6\pi\mu a u_0$. The particles will reach an equilibrium velocity, u_0, when the forces are equal, Eq (2.1). The equilibrium sedimentation velocities for several materials in ethanol as a function of particle size is shown in Fig. 2.1.

$$u_O = \frac{2a^2 \Delta \rho g}{9\mu} \qquad [2.49]$$
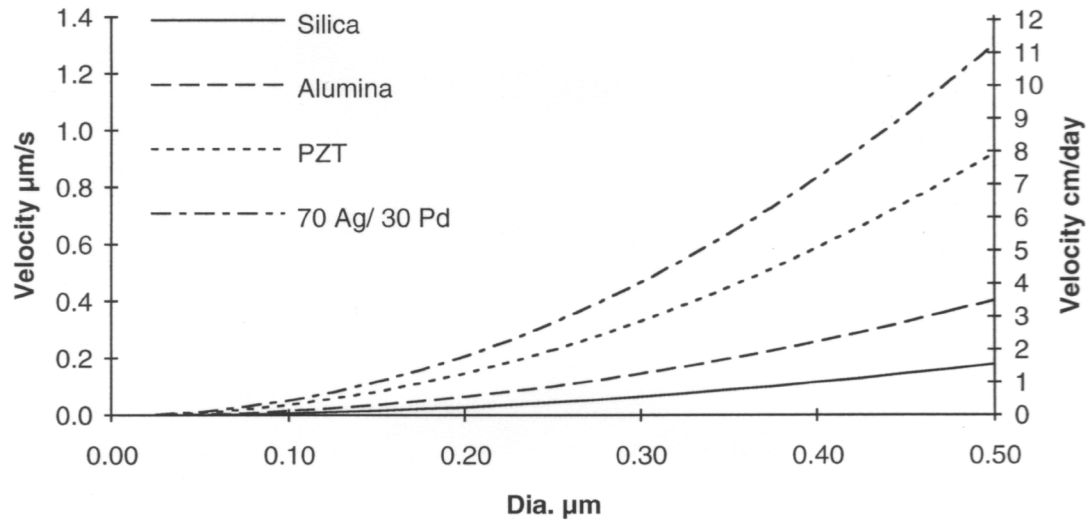
Fig. 2.21 Sedimentation velocity for particles in ethanol.

While the particle falls due to gravity like a macroscopic particle, it will also behave like a very large molecule. That is, it will have an average thermal kinetic energy of $\frac{3}{2}kT$, – the Boltzmann constant times the absolute temperature. A water molecule for example weighing ≈ 3.0 x 10^{-23} g with a kinetic energy of $e_k = \frac{1}{2}mV^2 = \frac{3}{2}kT$ will on average be moving at 520 m/s at room temperature (approximately 1,160 miles per hour). In contrast, a 150 nm diameter alumina particle that weighs 5.65 x 10^{-14} g, will move at an average velocity of 1.5 cm/s (or 0.033 miles per hour).

However, neither a solvent molecule nor the particle can go very far at this speed before hitting other solvent molecules and transferring their momentum to the solvent. This momentum transfer is the definition of viscous drag and, in equilibrium, will conform to the Stokes equation above. So a particle in suspension will pick up a kinetic energy of some small multiple of kT from a collision with a solvent molecule. This momentum will be dissipated by viscous forces on a nanosecond time scale (**1**, §3.2). Thus the particle will have an average velocity of 1.5 cm/s with the direction changing randomly every few nanoseconds. While each impulse and decay is invisible, the result of many submicroscopic motions leads to the visible translation known as Brownian motion. Integrating these random kinetic impulses and viscous damping leads to the Stokes-Einstein equation for particle diffusion:

$$D_O = \frac{kT}{6\pi\mu a} \qquad\qquad [2.50]$$

To form a suspension that is stabilized by this random motion due to thermal energy the flux of particles downward due to gravity must be balanced by the flux of particles upward due to diffusion. If the concentration of particles at height h in a suspension is c_h, then in equilibrium

$$c_h u_0 + D_0 \frac{dc_h}{dh} = 0 . \qquad [2.51]$$

This can be integrated easily to give the equilibrium concentration at a height h in terms of the concentration at the bottom of the container:

$$c_h = c_0 \exp\left(\frac{u_0}{D_0}h\right) = c_0 \exp\left(\frac{-m_p g h}{kT}\right) . \qquad [2.52]$$

The height over which the concentration of an equilibrium suspension will drop by 95% is shown for a few materials in ethanol in Fig. 2.2. For example, for 0.27 μm diameter alumina particles (at the extreme end of the alumina line) given a sediment density of 55% at the bottom of a suspension, the particle concentration will drop by 95% at a little over 100 μm above the sediment and will drop to a few parts per thousand within 0.2 mm of the sedimented layer. It is only for particles well below 100 nm that significant quantities can be held in suspension by Brownian motion.
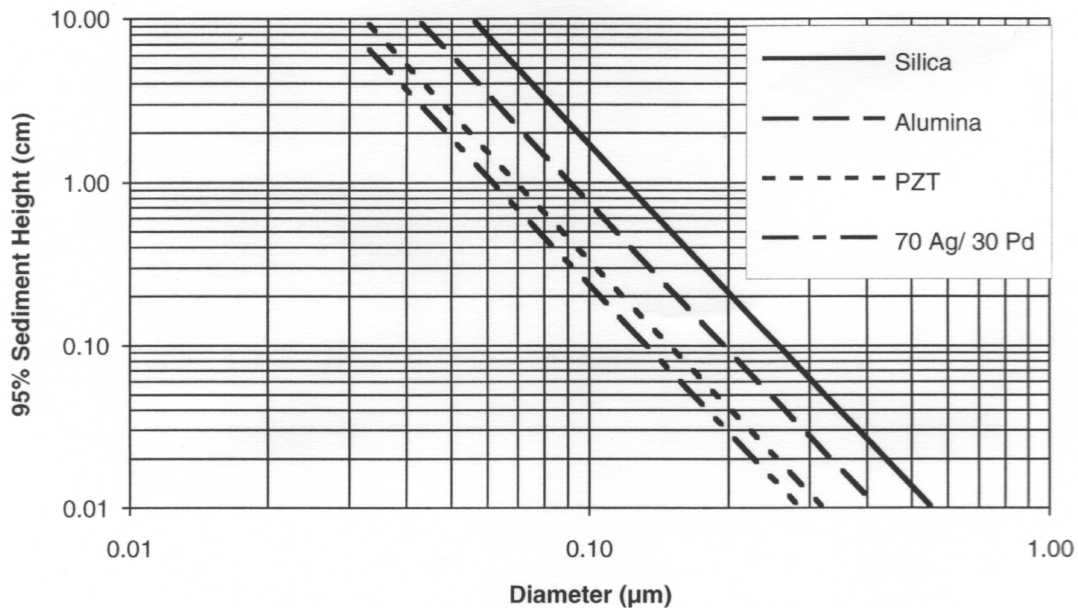
Fig. 2.22 Height over which the density of particles in suspension will drop by 95%, based on the equilibrium between Brownian diffusion and gravitational sedimentation.

There are two non-dimensional numbers that can be used to characterize the sedimentation of a suspension. The number that characterizes how the suspension will sediment is the Péclet number for sedimentation

$$Pe = \frac{u_0}{D_0} H = \frac{\frac{4}{3}\pi r^3 \Delta \rho g}{kT} H,$$ [2.53]

where H is the total depth of the suspension. Large Péclet numbers ($Pe > 1000$) will indicate a suspension dominated by free sedimentation. Auzerais et al. (**16**) calculated the density profiles for the sedimentation of a suspension with $Pe = 8500$ and this is shown in Fig. 2.23. This Péclet number would be equivalent to an alumina powder with a diameter of 0.28 μm in ethanol and a total depth of 10 cm. The second non-dimensional number is the characteristic time for sedimentation, t^*. This is the total height of the suspension divided by the Stokes sedimentation velocity for the particle,

$$t^* = \frac{H}{u_0} = \frac{9\mu}{2a^2 \Delta \rho g} H$$ [2.54]

For the 0.28 μm particle in 10 cm of ethanol mentioned above, this time is ≈ 51 hours.
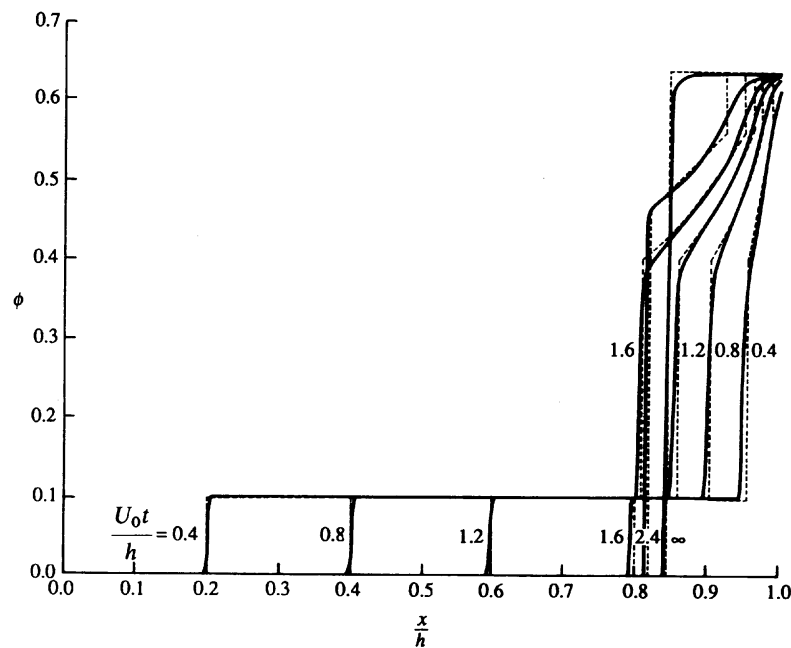
Fig 2.23 Concentration profiles for various times, Pe = 8500, initial volume density 10%, *x/h* relative distance from top of suspension, ϕ particle volume fraction. (from **16**)

In the case illustrated it will take t^* or about two days for the boundary of the clear layer to drop halfway down the container. This is only half the velocity that particles would drop in very dilute suspensions. This is because at finite concentrations there will be a backwash of rising fluid due to displacement by the sedimenting particles and fluid pulled downward by the particles' drag plus near field interactions between the flow fields around the particles. Auzeris et al. developed an emperical estimate for this velocity for

finite density suspensions, U, as a function of the Stokes settling velocity and the particle volume fraction, ϕ,

$$U = U_0(1 - \phi)^{6.55}$$ [2.55]

The conclusion to be drawn from this discussion is that most of the suspensions of sub-micron particles used in EPD are not in fact stable relative to gravitational sedimentation. However for EPD all that is necessary is a quasi-stability for a few minutes to a few hours to perform the depositions. Moreover, if the suspension is stirred periodically then it effectively becomes stable for as long as stirring continues.

2.5.2 Floccing

The next form of stability is preserving the individual particles as entities that can move independently within the suspension. The problem here is the Van der Waals (VdW) forces which will pull particles together if they pass too close to each other. Since the particles approach each other from random directions they will stick together in randomly arranged three dimensional structures or flocs.

Here it is useful to make a distinction between coagulation and flocculation as outlined very clearly by Napper (**17**, p.3). A 'coagulum' in Latin is a curd, as in cheesemaking. This implies a fairly uniform, dense lump. In Latin 'floccus' is a tuft of wool and describes a very loose, low density structure.

Coagulation is a process in which the primary particles will come together in a densly packed clump. This implies that the particles are able to rearrange themselves within the agglomerate. Particles must be able to slide and rotate past on another as they enter the agglomerate to find a well packed position.

In flocculation particles or flocs collide randomly and are frozen into place where they contact. This leads to a low density, fractal structure as shown on several scales in Fig. 2.4 below.
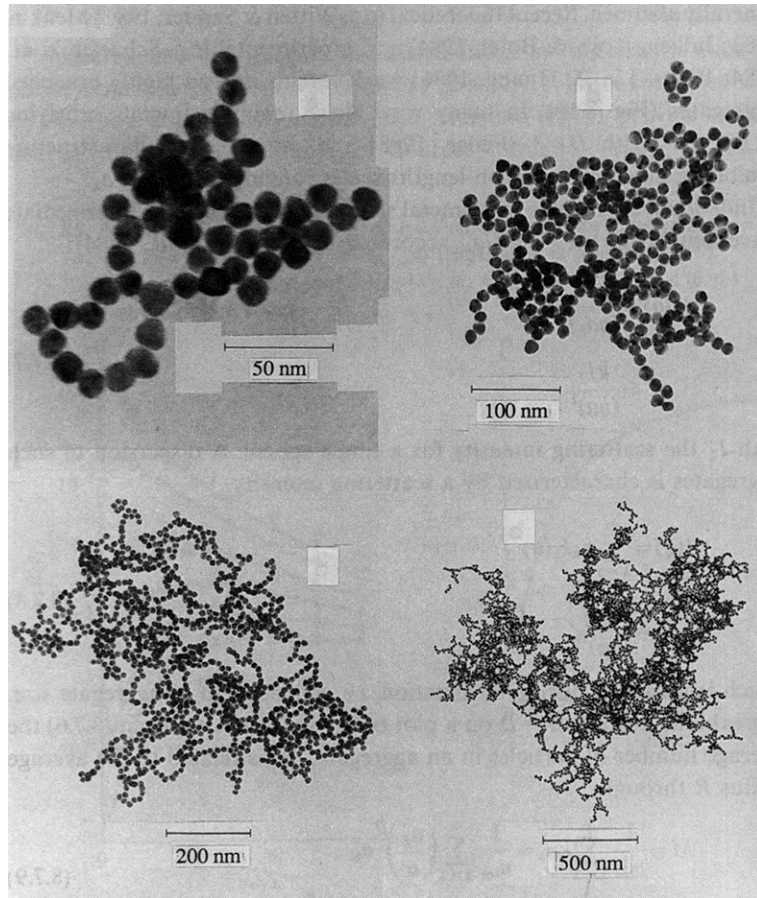
Fig. 2.24 Typical Floc Structures From (**18**) as reproduced in (**2**, p.282)

There are three types of agglomeration of a dispersed phase that lead to three different densities of the agglomerate. The first type is coalescence where the dispersed phase is liquid or gas. When particles touch they flow into each other and the density of the agglomerate is the same as that of the initial particles. The growth rule for this type of agglomerate is simply:

$$l = \left(\frac{a_l}{a_o}\right)^3 \qquad \text{Coalescence growth rule} \qquad [2.56]$$

where a_o is the radius of the initial particles and a_l is the radius of an agglomerate of l particles.

The second type is, as mentioned, coagulation. Here solid particles will be able to move to achieve a uniform packing density that is less than that of the initial primary particles but which does not vary with size. The growth rule for this type of agglomerate is:

$$l = \phi \left(\frac{a_l}{a_o} \right)^3 \qquad \text{Coagulation growth rule} \qquad [2.57]$$

where ϕ is the packing density of the primary particles in the coagulate, usually between 0.6 and 0.7.

Finally there is flocculation, a fractal process. Particles come together randomly and stick at their first point of contact. This is repeated as flocs come together and stick randomly. This repeated collision of larger and larger units in the same manner gives the floc the type of scale independent structure characteristic of a fractal geometry. As small flocs have a lower density than the primary particles, larger flocs will have a lower density than the smaller flocs they are made up of. This leads to a geometric decline in density as the floc grows. This is described by the same formula but where the exponent d is less than 3.

$$l = \left(\frac{a_l}{a_o} \right)^d \qquad \text{Flocculation growth rule} \qquad [2.58]$$

There are two problems with these particulate flocs for EPD. The first is that all of the particles in a floc will behave as one large particle. The density of this composite particle will be much less than that of the individual particles, however, the increased size will lead to a sedimentation rate several orders of magnitude larger than for the separated particles. The second problem occurs during EPD. If the particles are electrostatically charged, these flocs can be attracted to the deposition electrode and can be made to deposit. However, in most cases the deposition forces are not strong enough to break the floc structure, and their low density structure will be preserved in the deposition. In the usual case where maximum random packing of the particles is the desired outcome, this is an undesirable outcome.

2.5.3 van der Waals Force

The van der Waals force is made up of three components. The first component is the permanent dipole-permanent dipole or Keesom force. The second is the permanent dipole-induced dipole or Debye interaction. These first two forces are generally ignored in the colloidal literature as particles are almost always assumed to be isotropic. There are, however, many cases where these forces will have a significant effect. Crystalline particles can have different surface charge on different facets, thereby adding a dipolar component to their interaction. (Although this is generally masked for larger particles by the electrostatic double layer.) The dipoles of magnetic particles will certainly interact.

Further, both of these dipoles can be induced in suspended particles with the application of sufficient external fields.

The third force is the dispersion or London force. It is a quantum mechanical force resulting from the exchange of virtual photons between virtual resonant dipoles created in a material on the atomic, molecular and crystal structure level. To obtain the total interaction force, the electromagnetic resonant response of the material is integrated over the electromagnetic spectrum from the infrared through the visible into the ultraviolet. In the vast majority of colloidal suspensions this is the only one of the van der Waals forces that is significant. Since the following analysis will all be based on the assumption of the particles being isotropic spheres, this is the only force that will be considered here.

There are various different formulas for calculating the London-Van der Waals (L-VdW) interaction force between two bodies, depending on their geometry. Each of these formulas is the product of two terms, one is a geometric term which depends only on the shape and separation distance of the interacting bodies, and the second is the Hamaker Constant, which is a function of the electromagnetic properties of the materials that are interacting and of the medium separating them. The formula below from Israelachvili (**3**) can be used to give an accurate estimate of the Hamaker constant for two bodies of material 1 separated by a solvent 3 (A_{131}). The largest part of this force comes from the second term (>98%), which depends on the relative refractive indices, n, of the materials. The greater the difference between the refractive index of the solvent and the suspended particles, the greater the attraction between the particles.

$$A_{131} = \frac{3}{4} kT \left(\frac{\varepsilon_1 - \varepsilon_3}{\varepsilon_1 + \varepsilon_3} \right)^2 + \frac{3h^\circ \nu_e}{16\sqrt{2}} \frac{\left(n_1^2 - n_3^2 \right)^2}{\left(n_1^2 + n_3^2 \right)^{3/2}} \qquad \text{Hamaker Constant Est.} \qquad [2.59]$$

The refractive index of the material is used in this formula is a measure of the polarizability of the material. The more polarizable the material the stronger the L-VdW attraction. The difference in refractive index between the particles and the solvent surrounding them is significant because there is also a L-VdW attraction between the solvent and the particles. If the dielectric spectrum of the solvent is the same as that of the particles then the particle-solvent attraction will be the same as the particle-particle attraction. This means that there will be no net particle-particle attraction in that solvent.

Fig. 2.5 below shows the dramatic increase in the attraction energy going from low refractive index materials that have been the subject of a many EPD studies (Al_2O_3, SiO_2), to some typical electroceramic materials, to metals.
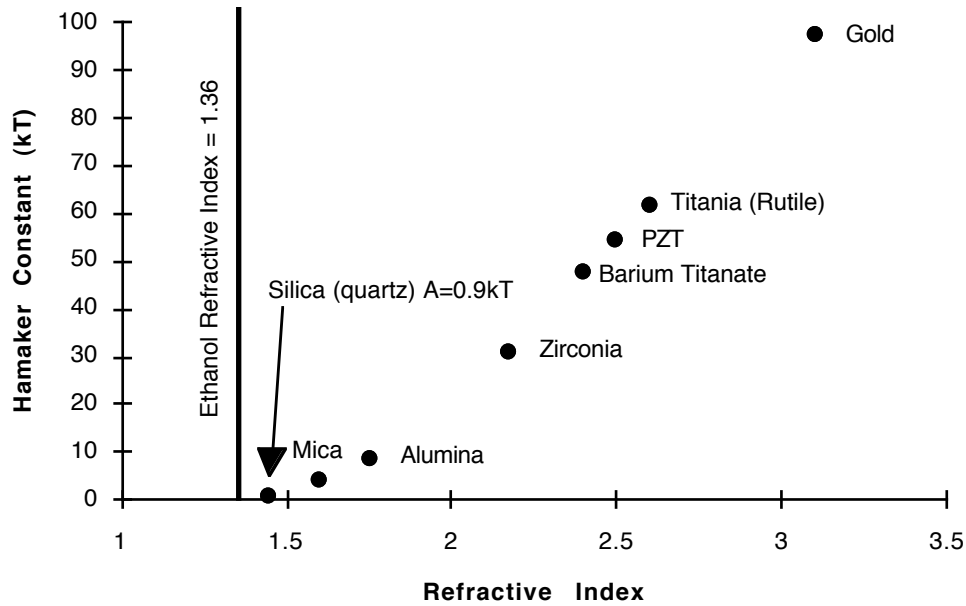
Fig.2.25 Hamaker Constant (A_{131}) vs. Refractive Index for various materials in ethanol.

To get the interaction energy the Hamaker constant is multiplied by a geometric term which accounts for relative proximity of the material in the two bodies being considered. It is essentially a volume integral of material divided by the square of the separtation distance. The formula below is for two equal diameter spheres. It has the standard terms for the decrease in the force with separation distance. This does not include a retardation term which accounts for the decrease in the force as the higher frequency interactions fall out of phase with increasing separation. The values calculated in figures 2.26 and 2.27 include an estimation of this retardation effect as presented in (**1**).

$$\Phi = -A_{131}\frac{1}{6}\left(\frac{2a^2}{r^2-4a^2} + \frac{2a^2}{r^2} + \ln\frac{r^2-4a^2}{r^2}\right) \qquad [2.60]$$

Van der Waals Attraction Energy Between Two Particles of Radius *a*

The L-VdW force is usually thought of as a short range force and this is valid for most colloidal systems that have been studied quantitatively. These are water-hydrocarbon mixtures, spherical polystyrene and silica particles in water, and the crossed cylindrical mica sheets used by Israelachvili.(**3**) The interaction enegy for two 270 nm diameter silica particles in ethanol will only be less than -5 kT energy units within 5 nm of the surface. For alumina particles of the same size this -5 kT distance increases to 8 nm in ethanol.

Moving to materials with a higher refractive index, the distance jumps by more than a factor of two, such as the value of 20 nm for PZT. The extreme would be gold or other similar metals where this -5 kT distance would be 23 nm or 17% of the particle radius. This illustrates why far more work and care are required to generate stable suspensions of these highly polarizable materials.
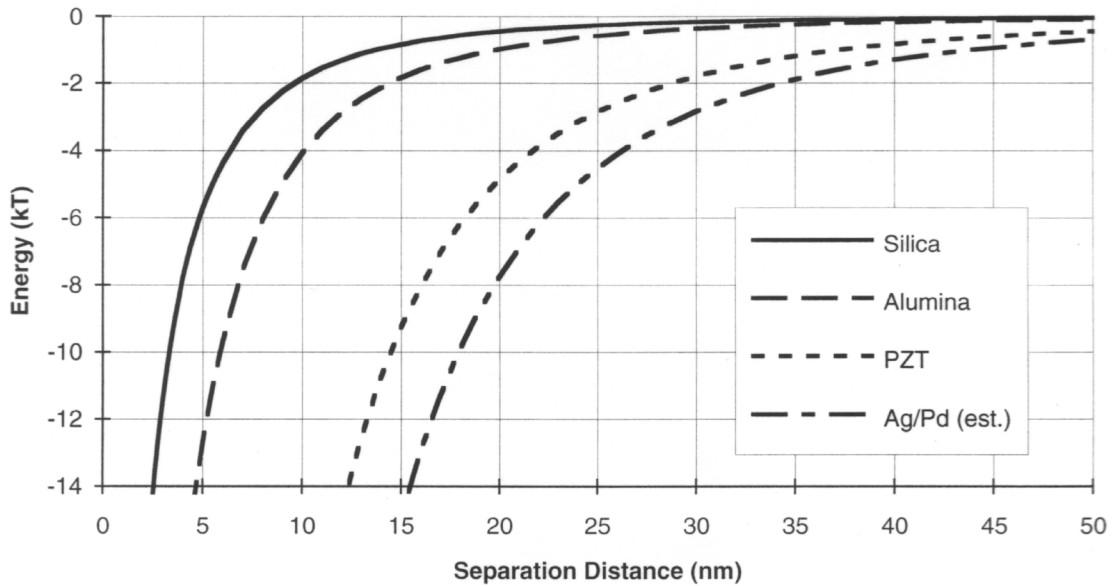
Fig 2.26 Retarded L-VdW energy-distance profiles for two 270 nm dia. spheres in ethanol.
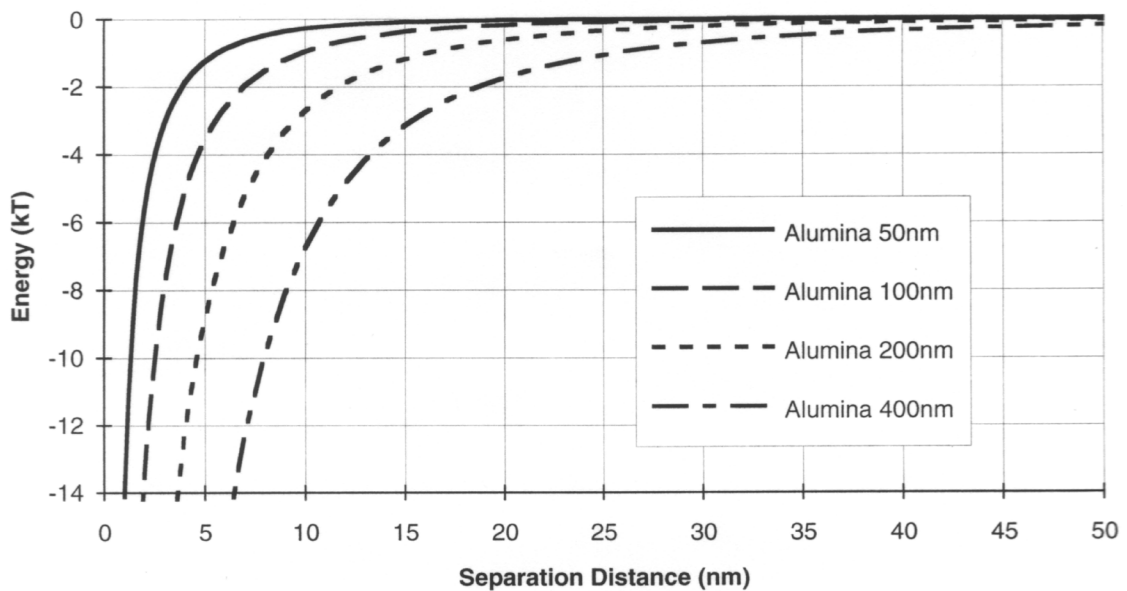
Fig. 2.27 L-VdW energy distance profiles for spherical alumina particles of different diameters in ethanol.

2.6 Stabilization

There are three main categories of stabilization for a particulate suspension: kinetic, electrostatic, and polymeric. These are all simply ways of keeping particles apart on the time scale of interest. Kinetic stabilization is simply to make the suspension sufficiently dilute that Brownian diffusion does not bring the particles into contact at a significant rate. Electrostatic stabilization uses the attraction between fixed charges on the surface of the particles and counter ions in solution to create a pressure layer around the particles which serves as an additional energy barrier keeping the particles apart. Finally in polymeric stabilization the particles are coated with a polymer layer which is thick enough to keep the particles from approaching within range of the L-VdW force, and itself has an insignificant L-VdW interaction in the solvent.

2.6.1 Kinetic Stabilization

Kinetic stabilization relies on the spacing between particles being large relative to the diffusion rate of the particles and the time period of interest. This can either be the time necessary to perform EPD or the sedimentation time for individual particles.

The theory for the rapid coagulation of particles was first developed by Smoluchowski in 1916 (**19**). The assumptions for this most basic theory are: the particles move only by Brownian diffusion, there is no particle interaction until two particles touch, and when two particles do touch they are irreversibly attached. This was conceptually modeled by assuming a stationary particle in a suspension where each mobile particle in the suspension disappears when it comes into contact with the stationary particle. This allows the instantaneous doublet formation rate to be calculated without the consideration of the effects of triplets, quadruplets, et ceterae.

Mathematically this was modelled as a suspension with a concentration of particles per unit volume, n. Within this suspension there is a sphere of radius, R, two times the particle radius, within which the particle concentration is zero. The rate of diffusion of particles through this surface is then the rate at which interparticle contacts would occur. This is then generalized for the entire suspension by using a diffusion coefficient for mutual diffusion of particles. For symmetric particles this is simply two times the single particle diffusion rate. Finally this is integrated for the time probability of an inter-particle contact over the number of particles per unit volume.

$$J_{\mathrm{o}} = \frac{\mathrm{d}n_o}{\mathrm{d}t} = \frac{8kTn^2}{3\mu} = n\frac{2\phi kT}{\pi\mu a^3} \qquad\qquad [2.61]$$

where n is the number density of particles and ϕ is the particle volume fraction.

This expression for the flux of single particles dissapearing from the suspension can then be integrated to give the particle concentration at a given time based on the initial particle density, n_o:

$$n_t = \frac{n_o}{1 + t / t_c} \qquad [2.62]$$

where t_c is the characteristic time for doublet formation:

$$t_c = \frac{3}{4} \frac{\mu}{n_o kT} = \frac{\pi \mu a^3}{\phi_o kT} . \qquad [2.63]$$

This is the time in which one half of all single particles will turn to doublets, assuming that only doublets are formed. Of course, doublets, triplets and large flocs cannot be ignored in real systems, but this approach does give an accurate estimate of coagulation rates in the initial stages of coagulation and in very dilute suspensions.

One of the key points highlighted by these formulas is the linear dependence of the coagulation rate on the number of particles per unit volume. This means that the volume fraction must go down as the cube of the particle diameter. Fig. 2.8 below shows the characteristic time for doublet formation in ethanol, $\mu=1.07$cP, at 25°C. A 1 vol.% suspension of 4 μm particles will have a characteristic time of ten minutes. For a suspension of 0.4 μm particles to have the same characteristic time the volume fraction must drop by 10^3 to 10 parts per thousand. For 40 nm particles this drops again to the usually impractical volume fraction of 10 parts per billion.

From this analysis it is clear that there is a window of particle size and volume fraction where a suspension will be stable for long enough to perform EPD, even though there is no force slowing or preventing the particles from coming into contact. The lower limit of particle size will be set by the flocculation rate, the upper limit by sedimentation rate, and the volume fraction by the time it takes to go from turning off the high energy agitation necessary to disperse the particles to the end of deposition.
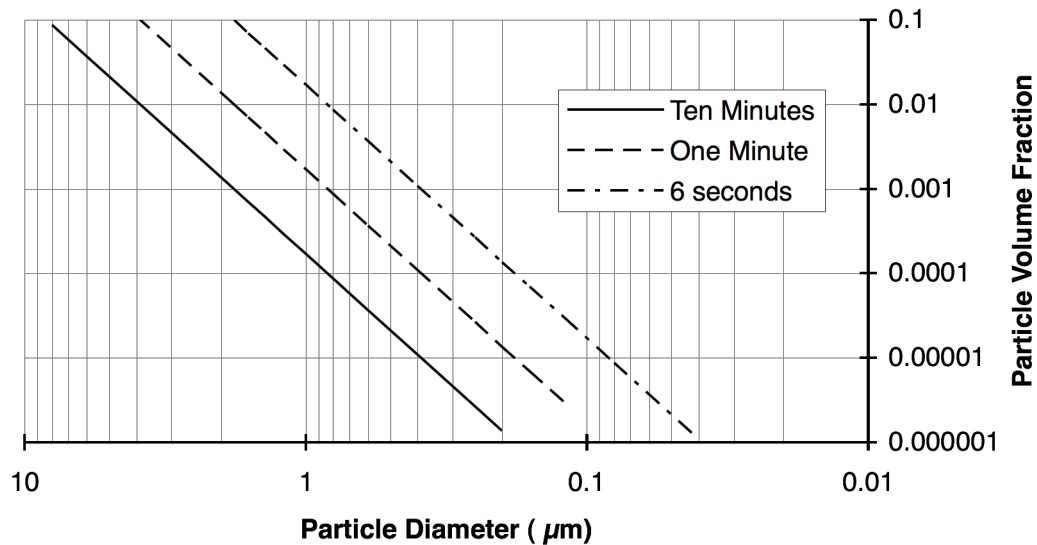
Fig. 2.28 Particle volume fraction as a function of particle diameter for three characteristic times of doublet formation.

Another phenomenon that can be mentioned here is that of a kinetically stable flocced suspension. That is a suspension which consists of flocs but where the flocs are neither growing nor sedimenting significantly on the time scale necessary for EPD. From the treatment above, for a 0.5 vol.% suspension of 0.25 μm diameter particles, the characteristic doublet formation time is only 0.32 seconds. This is approximately the time it will take for one half of the single particles to form doublets. At longer times these doublets will then more slowly combine to form quadruplets, then again more slowly forming octuplets, etc.

Smoluchowski was able to extend his theory for the coagulation of individual particles to multiple particles on the basis of two assumptions. The first was that the hydrodynamic radius of a floc would be the same as the effective capture radius for the floc. Since the diffusion coefficient for a particle is inversely proportional to the hydrodynamic radius, this allowed the statement that $D_l a_l = D_1 a_1$; that is the product of the diffusion coefficient and the capture radius of a floc made up of l particles is the same as the product of the diffusion coefficient and capture radius of a single particle. The great advantage of this assumption is that it is both reasonable and eliminates the need to have any knowledge of the density or geometry of the flocs. A lower density floc will have a larger area for collision and capture of other particles/flocs, but this will be proportionally compensated by the reduction in the floc's diffusion velocity.

While this first assumption cancels the floc density from the equations for the colision of flocs of the same size, it is not eliminated from the calculation for the relative diffusional motion of different sized flocs. This necessitates the second critical assumption, that most of the collisions occur between flocs of similar size such that:

$$a_l + a_m \left(\frac{1}{a_l} + \frac{1}{a_m} \right) = 4 , \qquad [2.64]$$

where a_l, a_m are the hydrodynamic and capture radii of two colliding agglomerates, l & m. This allows the generalization that $D_{lm}a_{lm} = 2D_l a_l$; where D_{lm} is the relative diffusion rate of a floc containing l particles to a floc of m particles. This equation would, of course, be exact for flocs of the same size: $D_{ll} = 2D_l$.

These assumptions then allowed the analytic solution of the conservation equations for number density of independently moving particles/flocs containing l particles, n_l. The sum of all of the independent particles/flocs as a function of time is found to be

$$\sum_{l=1}^{\infty} n_l = \frac{n_o}{1 + t/t_c} . \qquad [2.65]$$

This is the same as equation [62] above with the same t_c. It is only the meaning that is changed.

From this equation it is possible to make an estimate of the time it takes to form 5 μm and 10 μm flocs. Using an intermediate value for the fractal dimension of 2.25,

$$l = \left(\frac{a_l}{a} \right)^{2.25} \qquad [2.66]$$

a suspension with a starting particle size of 0.25 μm will generate 5 and 10 μm flocs containing 800 and 4,000 primary particles respectively. To reach this state from an initial primary particle dispersion would take about 5 minutes for 5 μm flocs and 20 minutes for 10 μm flocs. To go from an average floc size of 5 μm to 10 μm takes 15 minutes. For the number density of flocs to drop in half again will take a further 30 minutes.

These flocs, of course, will be sedimenting out of the suspension. However, because of their very low density the sedimentation velocity is still low on the time scales here. For the 5 μm flocs in this example the particle density within the floc will be only 10 vol. %. If these particles are alumina in ethanol, this will yield a barely noticable sedimentation rate of 0.25 mm/minute. Ten micron flocs will be only 6% dense, but because of their larger size will have the more noticable sedimentation rate of 0.6 mm/minute. However, even this sedimentation would be invisible with even the slightest agitation.

Thus we have the situation where even though the particles are 'rapidly' flocculating, because of the very low solids loading frequently used in EPD a kinetically quasi-stable suspension of flocs can be formed. A mechanically dispersed suspension of individual particles will become substantially flocced within seconds of the ending of high energy agitation of the suspension. With a solids loading of a few volume percent or more these flocs will rapidly consume the entire volume of the suspension forming a gel or pseudoplastic paste which would be useless for EPD. Below one volume percent these flocs can reach a state of relatively slow growth and sedimentation. These flocs can easily be deposited electrophoretically. The increased density at the deposition electrode will bring the flocs together in a low density sediment structure.

2.6.2 Electrostatic Stabilization

In the absence of an externally applied voltage, if a surface is charged in a solution then for each unit of charge on the surface there is an opposite charge dissolved in solution. The opposite charges will attract, and the ions in solution will migrate toward the surface until electrophoretic migration is matched by diffusion away from the elevated concentration near the surface. This results in a concentration gradient of ions near the surface governed by the Poisson-Boltzmann equation [4] as described before for electrode surfaces.

This diffuse portion of the electrostatic layer at the surface will have a higher hydrostatic pressure than the surrounding fluid. This can be thought of in two ways. One way is to regard this higher pressure layer as a Maxwell force due to the electrostatic attraction between the charged particle surface and the charged solution in the DEBL. Alternatively this can be regarded as the increased osmotic pressure due to the higher ionic concentration in this layer. Both approaches are merely looking at different sides of the P-B equation.
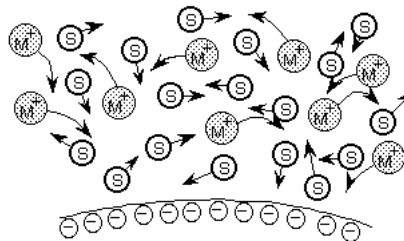
Fig. 2.29 The electrostatic attraction between the counter ions and surface leads to a higher hydrostatic pressure at the charged surface.

So a particle with an electrostatic surface charge will surround itself with a layer with a higher hydrostatic pressure than the bulk of the solvent. As one particle approaches another these higher pressure layers will act as bumpers holding the particles apart. This is the primary mechanism of electrostatic stabilization. Actual electrostatic repulsion between like charges only occurs when the separation between particles is much less than the thickness of the DEBL between the particles. This is usually only significant in suspensions with very low ionic strengths and therefore very thick boundary layers (small κa).

Estimating Electrostatic Repulsion

There are two commonly used approximation methods for calculating the force between electrostatically charged particles: the Derjaguin and the Linear Superposition approximations. Both make different simplifying approximations for the ionic distribution between two spheres, making them valid for different particle separations and diffuse layer thicknesses. Both, however, rely on the same linearization of the P-B equation [2.7] which is the basis of the Debye-Hückel approximation. This means that even in the proper range of diffuse layer thicknesses and particle separations these formulas will only provide good quantitative estimates for relatively low surface potential (< 25 mV).

There are two radial components in the problem of approaching spheres which have prevented the creation of a closed form solution of the interparticle force even with the linearizaton of the P-B equation. The first is the curvature of the particles themselves. Moving away from a curved surface the volume gradient dV/dr increases. It is only for very thin diffuse layers (high κa) that the surface can be treated as a flat plate. This is the particle radial component. The second significant component is the central plane radial component. To calculate the forces between two particles the hydrostatic pressure is integrated over the central plane separating the particles. When particles approach solvent with the dissolved counter ions is squeezed out from between the particles. This causes charge imbalance in the region of closest approach of the particles. This can lead to both a classical electrostatic like-charge repulsion between the surfaces as well as a strong radial electrostatic field in the central plane between the particles, changing the counter ion distribution and therefore the osmotic pressure distribution.

The Derjaguin approximation is based on an accurate solution of the linearized P-B equation between two flat plates. In exchange for this accurate solution of the P-B equation this approximation ignores both of the radial components. Because of this, it is only valid for thin boundary layers and small particle separations. Furthermore, because it ignores the central plane radial component this estimation method does not work well for

most separation distances at constant surface charge conditions. The exception is for very thin diffuse layers ($\kappa a > 30$) with a particle separation distance greater than κ^{-1}.

The Linear Superposition Approximation replaces the accurate solution for the linearized P-B equation in the Derjaguin formulation with an accurate solution for the diffuse layer around a sphere and estimates the interaction force by summing the ionic concentrations where the diffuse layers overlap. Because this formulation includes the contribution from the particle radial component it will generate accurate estimates for thick diffuse layers and large particle separations. Unfortuantely, at particle separation distances of less than $2\kappa^{-1}$ superposition becomes a very inaccurate method of estimating the counter ion distribution and significantly overestimates the interparticle force.

Electrostatic Interaction Energy Approximation Formulae

- Derjaguin Approximation Interaction Potential Energy - Constant Potential

$$\Phi = 2\pi\varepsilon_r\varepsilon_o\psi_o{}^2 a\ln\left(1+e^{-\kappa h}\right) \qquad [2.67]$$

- Derjaguin Approximation Interaction Potential Energy - Constant Charge

$$\Phi = 2\pi\frac{q^2}{\varepsilon_r\varepsilon_o} a\ln\left(1-e^{-\kappa h}\right) \qquad [2.68]$$

- Linear Superposition

$$\Phi = 4\pi\varepsilon_r\varepsilon_o\frac{a^2}{h+2a}\psi_o{}^2 e^{-\kappa h} \qquad [2.69]$$

- Thin Double Layer Linear Superposition

$$\Phi = 32\pi\varepsilon_r\varepsilon_o\left(\frac{kT}{ze}\right)^2 a\gamma^2 e^{-\kappa h} \quad ; \quad \gamma = \tanh\left(\frac{ze\psi_o}{4kT}\right) \qquad [2.70]$$

(From (**1**))

In 1982 Glendinning and Russel (**20**) used a combined analytic/numeric scheme to generate accurate solutions for two spheres as a function of diffuse layer thickness and separation distance. They used a solution of the linearized P-B equation in the form of the product of a Bessel equation and a Legendre polynomial expansion. They were then able to use a coordinate translation to put a second sphere into the coordinate system of the first. The result, when truncated, was a system of linear equations which could be solved numerically.

They then compared the results of this calculation to the values of the Derjaguin and linear superposition approximations to generate charts of the percentage deviations between the estimation methods and the accurate solution. From these deviation charts

they created the validity maps in Fig 2.30 below. The regions marked Derjaguin and LSA are where each of the interparticle force approximations are within 10% of the accurate solution. The regions marked 'exact' are where only the accurate solution will generate quantitatively meaningful results. Because the Glendinning and Russel solution is again based on the linearized P-B equation the location of these 10% lines is independent of surface potential with the limitation that they are only valid themselves for low surface potentials (< 25 mV).
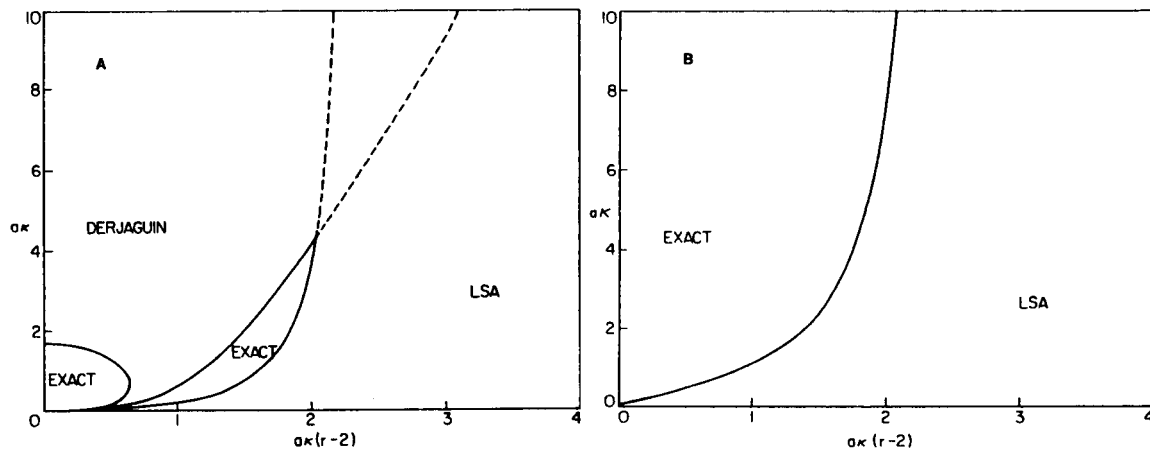
Fig. 2.30 Regions where the Derjaguin and Linear Superposition (LSA) Approximations are within 10% of the exact solution. Regions marked EXACT are where neither approximation is valid.
Horizontal axis is particle surface separation distance in multiples of Debye length, κ^{-1}.
(A) Constant surface potential conditions; (B) Constant surface charge conditions.

More recently Sader, et al. (**32**) presented a much improved set of approximation formulas which retain a fairly simple form while having a much increased range of applicability. This author will, and the reader is encouraged to, use the formulae presented in this reference in future calculations.

Although not discussed in depth here, there are two cases of the interaction of dissimilarly charged surfaces that should be mentioned here. (**8**) The first is the approach of two surfaces having constant surface potentials of the same polarity but different magnitudes. At long range there will be a repulsive electrostatic force between the particles, but at short range, to maintain constant surface potentials relative to the bulk of the solution, the sign of the surface charge on the surface with the lower potential will switch polarity creating an attractive electrostatic force between the surfaces. The second situation is that of two surfaces with constant surface charge of opposite polarity but with a large difference in surface charge density on each surface. At large separations the force between the particles will be attractive due to the opposite charges on each surface. At

short separation distances, less than the Debye length, the surface with a lower charge density will displace more charges from the diffuse layer of the surface with higher charge density than it brings due to charges on its surface. There is still an electrostatic attraction between the high charge density surface and counter ions dissolved in the solution, and therefore, an electrostatic force to keep a layer of solvent between the surfaces. This means that even if two surfaces are oppositely charged, if the charge density is significantly different there can be a short range repulsive force between the surfaces. This is one reason why particles with a steady positive charge can fail to deposit on a negatively charged electrode in spite of what would seem to be an inevitable electrostatic attraction.

2.6.3 Polymeric Stabilization

There are far too many possible types of interactions between particles, polymers and solvent to offer even a brief overview here. For example, Napper (**17**, p. 17) lists fourteen types of interaction for colloidal suspensions with non-ionic polymers. These fourteen could be further sub-divided by types of non-ionic polymers and added to by consideration of ionic polymers. What will be presented here are only a few cases which may be suitable for EPD, within the categories of steric, depletion and electrosteric stabilization.

Soluble Polymer in Solution — Understanding of polymer-steric stabilization requires first understanding the interaction of polymer and solvent. The most critical factor here is the solubility of the polymer in the solvent.

In free space the L-VdW force will always be attractive. This means that in free space polymer will stick to polymer, particle to particle and polymer to particle. Thus in free space, including in almost all gasses, steric stabilization is not possible. The critical role of solvent is in eliminating the *net* polymer-polymer (P-P) VdW attraction. Since the VdW is a fundamental property that cannot be eliminated, the attraction between the solvent and polymer should be at least as strong as the P-P interaction so that there is no net preference between a P-P and a polymer-solvent (P-S) interaction. In this case with no energetically favorable position, the polymer will diffuse by entropic/Brownian/osmotic forces until it is uniformly distributed throughout the solvent. In short — the polymer must be soluble in the solvent.

The next question is how the polymer will behave in solution. Here it is the simplest and most illuminating to analyse the case of a simple straight chain polymer. If

this polymer were completely straight rod its length would be simply $l_o \frac{M}{m_o} Sin\left(\frac{\tau}{2}\right)$;

where l_o is the length per bond in the chain, M is the molecular weight, m_o is the molecular weight per chain bond, and τ is the bond angle in the chain. However, these molecules are flexible and Brownian motion will cause them to take the form of a tangle approximating a random walk. If each of the chain bonds of the polymer were perfectly flexible this would give a root-mean-square end-to-end distance $\langle r^2 \rangle^{\frac{1}{2}}$ of $\left[nl_o^2\right]^{\frac{1}{2}}$, where n is the number of repeat units in the chain. Of course, while the polymer is not stiff it is not completely flexible either. It is only over 4 to 10 bonds that the polymer will be completely flexible. Thus there is another factor added to the equation called the characteristic ratio, C_∞, which accounts for this lack of flexibility. The larger the value the less flexible the polymer chain. Some experimentally determined values for the characteristic ratio are given in Table 2.2

Table 2.2 Values of the Characteristic Ratio (from (2&3)).

Polymer	$\underline{C_\infty}$
Poly-oxyethylene	3.9 - 4.0
Poly-dimethylsiloxane	5.2 - 6.4
Poly-12-hydroxystearic Acid	6.1
Poly-methylene	6.9
Poly-oxymethylene	8.5
Poly-styrene	9.5 - 10.0

Finally, there is the intermolecular expansion factor, α, which is a function of the P-S/P-P interaction energy ratio. In treating the polymer configuration as a random walk it was assumed that each segment of the chain is a volumeless line. A real polymer will, of course, have a volume, but the solvent surrounding the polymer will also have a volume. If the P-S/P-P interaction energy ratio is exactly one, then the polymer will in fact behave as a volumeless chain. This condition, where $\alpha = 1$, is referred to as the theta, θ, state and the solvent that produces this state as a θ-solvent. If the solvent is better than a θ-solvent, P-S interactions are energetically favored over P-P interactions. This causes the polymer to expand beyond a purely random walk ($\alpha > 1$). Values of α are generally between 1.0 and 1.5. Values of a less than one would occur in a worse than θ solvent and results in a contraction of the polymer chain, however, this is rarely seen since if P-P interactions are

favored, the polymer molecules will rapidly floc together and can no longer be considered dissolved in the solvent.

Thus we obtain a rough but useful model of the length of a dissolved polymer molecule:

$$\left\langle r^2 \right\rangle^{\frac{1}{2}} = \left[\alpha C_\infty n l_o^2 \right]^{\frac{1}{2}} \tag{2.71}$$
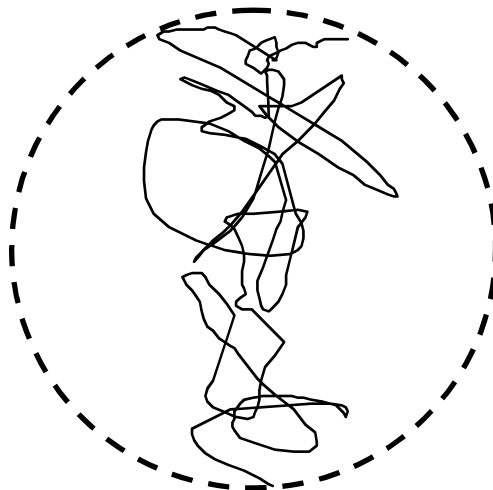
Fig. 2.31 Polymer random walk will not have a spherical shape, however, due to rotational motion a completely unconstrained polymer can be considered to occupy a spherical space.

Although the polymer is almost never spherical at any single moment in time, bacause it can rotate freely in the solvent the above rms end-to-end length can be used to define a spherical volume for the polymer. Anytime this sphere is compressed, such as by the surfaces of two approaching particles, the number of configurations available to the polymer is reduced and the total energy of the system is increased. As particles approach more closely solvent is forced out from the loops of the polymer increasing the energy further.

In the classic physical sense the steric force is the repulsion which prevents one atom from interpenetrating another and is based on the Pauli exclusion principle. In colloidal science the steric repulsion force is primarily an entropic/osmotic pressure force. Only when the polymer is fully compressed does the repulsion become steric in the classical sense. A soluble polymer will act as a linear spring extended by osmotic/entropic forces. This polymer-steric repulsion has a much different force-distance curve than the classic steric repulsion force and is able to act over the much longer distances necessary to keep particles out of range of their mutual VdW attraction.

Polymer at a Solid Surface — When a solid surface is introduced to the polymer solution the polymer can exhibit a range of adsorptions from zero to very strong.

Homopolymer   Block Co-Polymer   Terminally Anchored Polymer
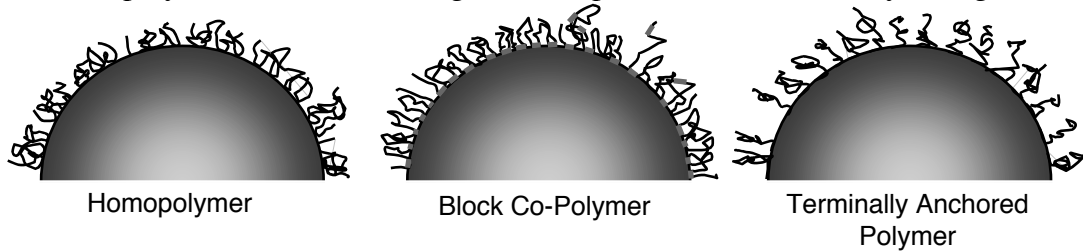
Fig. 2.32 Behavior of Various Polymers at a Surface

In the case of non-adsorbing polymer the polymer molecules near the surface will try to retain their time averaged spherical shape. This means that immediately adjacent to the surface there will be a layer of about $\frac{1}{4}\langle r^2 \rangle^{\frac{1}{2}}$ thick which will have a significantly lower average concentration of polymer chain segments than the bulk solution. In a good solvent for the polymer, i. e. a negative free energy of dissolution, this depleted layer will have a higher energy than the bulk solution. From the standpoint of osmotic pressure, the lower concentration of dissolved polymer at the surface than in the bulk means that the hydrostatic pressure in this surface layer is lower than in the bulk.
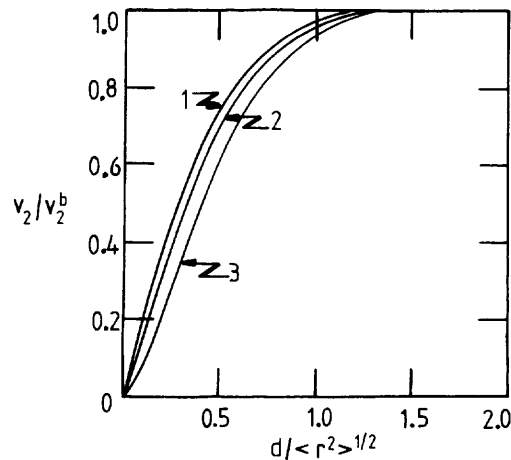
Fig. 2.33 Density of dissolved polymer near a surface. $1.0 \equiv$ density in solution. (1) poly(oyxethylene) MW. 400, (2) poly(oyxethylene) MW. 4,000, (3) random flight chain of 4,000 bonds. Napper (**17**, p. 387)

A polymer made up of the same repeat unit, a homopolymer, can also weakly adsorb to the surface. If this polymer adsorbs too strongly it will collapse entirely onto the surface. If the polymer is only weakly adsorbed then segments will be dynamically adsorbing and desorbing to the surface. This leaves loops of the polymer extending out into the solvent.

There are also polymers that have specific adsorbing groups. These can be either terminally anchored polymers or block co-polymers. These have groups that will attach to

the solid surface either because they are insoluble in the solvent or due to specific adsorption interactions. Terminally anchored polymers at low coverage will extend out into the solvent by the same rms. distance, $\langle r^2 \rangle^{\frac{1}{2}}$, as the polymer in free solution. As the coverage increases the polymer tails will extend much further away from the surface as the scaling law exponent of number of repeat units changes from 1/2 to almost 1 as the polymers crowd each other laterally, forcing each other out into straighter and straighter lines. The extension of block co-polymers is more complex but follows the general rules with increased coverage leading to a thicker layer.

Finally there are the polyelectrolytes. These polymers have ionic groups along their length. These ionic groups will create a strong self repulsion extending the molecules well beyond the $\langle r^2 \rangle^{\frac{1}{2}}$ of an uncharged polymer. This molecule can adsorb to charged or ionizable sites on the surface. The coverage and extension of these charged polymers into the solvent is a complex function of site density on the surface, and, in the solvent, the polymer concentration, chemical activities, and the ionic strength.

Polymer Between Two Surfaces — For two surfaces approaching in a solution of completely dissolved polymer there is first a repulsive force as polymer molecules are compressed between the surfaces. Then as polymer molecules are forced out of the gap an 'attractive' force as solvent diffuses out into the bulk solution. When the gap between surfaces approaches the size of the dissolved polymer, the polymer is compressed, increasing the osmotic pressure between the surfaces and driving polymer out of the gap between the surfaces into the bulk solution. When the surfaces get close enough, so much polymer is forced out of the gap that the concentration drops below the bulk and the osmotic pressure in the bulk is higher than between the surfaces. This causes a 'suction' between the surfaces pulling them together. This final stage can also be considered as an overlap of the depleted layers described in Fig. 2.33 above.

Figure 2.34 below shows the equilibrium energy of approach of two 155nm particles calculated by Feigin and Napper (**21**) for three polymer concentrations. The particles will experience no net force until the surfaces approach to less than $2\langle r^2 \rangle^{\frac{1}{2}}$ of the dissolved polymer. At this point the number of possible conformations for the polymer chains begins to be constricted. The concentration of polymer segments per unit volume goes up and therefore the osmotic pressure in the gap rises. This rise continues until at about $\langle r^2 \rangle^{\frac{1}{2}}$ the increased concentration of polymer in the gap causes polymer to diffuse out of the gap faster than it is compressed and the pressure begins to decline again. At

about [ ] the concentration of polymer has dropped to the same as in the bulk and

there is no net force between the surfaces. Below [ ] the polymer concentration drops

below the bulk and the osmotic pressure drops below that of the bulk. The surfaces experience a "suction" force which can cause the particles to floc together independent of the van der Waals force.
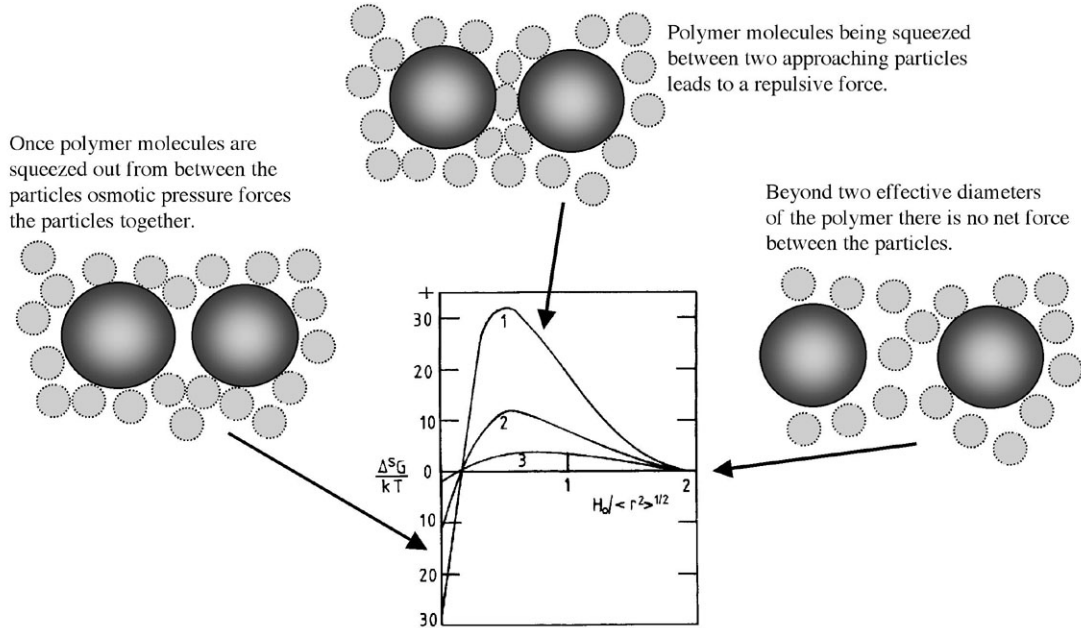
Fig. 2.34 Interaction energy chart for depletion stabilization. (adapted from Napper **17**, p. 387)

In the cases where the polymer is adsorbed to the surfaces the behavior is initially the same. As the surfaces approach to less than two times the thickness of the soluble portion of the adsobed polymer layers, these layers are compressed driving out solvent and increasing pressure between the surfaces. As long as the polymer remains adsorbed, the force between the surfaces is uniformly repulsive.

However, for different types of molecules varying adhesion can lead to different long term behavior. A homopolymer coating which is only weakly adsorbed will diffuse out from between the two surfaces, in the same manner as the non-adsorbed polymer but more slowly. This also applies to terminally anchored chains at less than complete coverage where the chains can be forced across the surface away from particle contact points. For block co-polymers, also at less than full coverage, an adsorbing block one one surface can desorb and adsorb to the opposite surface creating a bridge holding the surfaces together. Thus adsorbed polymers can have a time dependent hysteretic effects on the forces between particles.

2.7 Application to EPD

What makes suspension development for EPD unique is that whatever mechanism is used to keep the particles separate in the suspension, something must change to allow the particles to be bound together at the deposition electrode. Therefore the suspension must be designed for stability or quasi-stability in the bulk and instability at the deposition electrode. Therefore, before discussing deposition methods, it will be useful to list briefly some of the differences that can exist between the bulk solution and the immediate vicinity of the deposition electrode.

1. Density – With electrophoresis particles will accumulate at the deposition electrode causing the particle volume fraction and number density to go up by an order of magnitude or more. Frequently, this alone can change the stability of the system.

2. Electrostatic and Electrohydrodynamic (EHD) Forces – In the bulk, charged particles will move by electrophoresis toward the oppositely charged electrode with an EHD flow around the particles going the opposite direction. When the particle motion stops either at the electrode or against other particles stopped by the electrode the balance of the electrostatic and EHD forces will change.

3. Electrosedimentation – In EPD particles can rarely be considered alone. The force on a particle will include the sum of the forces on the particles behind it relative to the deposition electrode. This is the same as for gravitational sedimentation where the force on a layer is the sum of the forces on all of the layers above it.

4. Electrochemical Gradients – It is important to recognize that EPD is always an electrodynamic process. Current must flow through the deposition cell, which means that electrochemical reactions will be occuring at each of the electrodes. This leads to the formation of an electrode boundary layer that can have either an increased or decreased ionic strength, changed acid/base equilibrium, as well as a change in the ionic species present.

It is these differences at the deposition electrode that must be managed and used to take freely moving particles from the bulk suspension and bind them together in a rigid mass with the desired thickness, density and adhesion.

2.7.1 Deposition from Electrostatically Stabilized Suspensions

  The question then becomes how these near electrode effects can be used to convert freely moving particles in the suspension to mutually adherent components of a stable, rigid deposition. To answer this, each of the above enumerated effects will be considered in turn as they relate to an electrostatically stabilized suspension.

  Density — Increased density alone will be a relatively ineffective means of depositing particles. Electrophoresis can raise the density of particles by one or two orders of magnitude at the electrode, however, density alone does not change the stabilizing force between the particles. Only for suspensions with little or no stabilizing force where particles are already floccing in the bulk suspension will the increase in density lead to the formation of a deposit. Moreover, in this case since the particles will ultimately come into contact due to the random Brownian motion superimposed on their electrophoretic velocity, the deposition will likely be a very weak, low density structure with a very low average number of interparticle contact points.

  Electrostatic Force —The externally applied electric fields commonly used in EPD range from a few volts to several hundred volts per centimeter. This electric field causes the electrophoretic motion of the particles toward the deposition electrode, however, in most cases where there is a sufficient electrostatic repulsion to stabilize the particles from floccing in suspension, the electrostatic force due to the average electric field is insufficient to overcome the interparticle repulsion.

  Figure 2.35 below gives the total interaction energy for alumina particles in ethanol at one condition where EPD was successfully performed. The ionic concentration of the suspension was 0.4 millimolar and particle zeta potential was 42mV. The interaction energy was calculated using the Derjaguin approximation for constant potential and the Van der Waals interaction calculated using Eq. [60]. This gives an energy barrier to flocculation of 53 kT units; a maximum interparticle repulsion force of 13.4 picoNewtons at a 7 nm separation; and a total charge on one particle of 0.29 femtoCoulombs (10^{-15}). To produce an electrostatic force on a single particle equal to the maximum repulsive force would require an imposed electrostatic field of 460 V/cm. Given that the average applied electric field is only $\approx$ 10 V/cm, it is clear that more than simple electrostatic force must be involved here. (More details of this type of deposition are given in Ch. 4.)
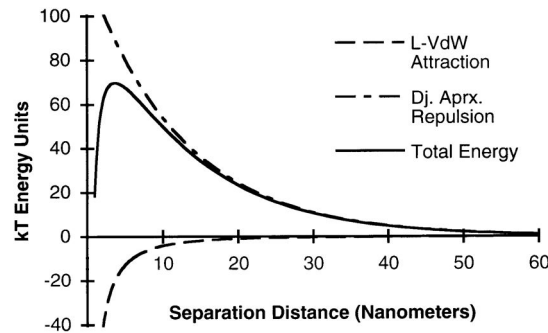
Fig. 2.35 Energy potential of two approaching 270nm dia. alumina particles
with a Debye length of 12.5 nm and surface potential of 51 mV.

However, this does not mean that electrostatic force cannot be used to drive
deposition from a stable suspension. Table 2.3 below shows the calculated surface
potential necessary to create an energy barrier of 15 kT between two 270 nm dia. alumina
spheres in ethanol. This is an energy barrier sufficient to provide long term stability
against flocculation in the bulk suspension. The voltage fields necessary to overcome the
interparticle repulsion at these conditions are given in the last column. These voltage
gradients are not unreasonable and are frequently used in very low conductivity
suspensions. In higher conductivity suspensions continuous use of these voltages would
lead to vigorous convection and heating of the suspension, however, this would not
preclude their use in brief pulses.

Table 2.3

Surface potential necessary to provide a 15 kT electrostatic energy barrier to flocculation for two
270 nm diameter alumina particles in ethanol at several ionic strengths; maximum repulsive force
between the particles (picoNewtons); separation distance at which maximum force occurs
(nanometers); total surface charge for one particle (attoCoulombs); and electric field necessary to
produce a force on the charged particle equal to maximum interparticle repulsion force.

κa	κ^{-1} (nm)	mMol	mV for 15kT	pN	@ nm	attoC ($\times 10^{-18}$)	V/cm
4	34.0	0.026	26	1.27	23	51	250
6	22.5	0.059	28	1.84	18	77	240
8	16.9	0.105	30	2.45	15	108	230
10	13.5	0.165	32	3.13	13	142	220
12	11.3	0.235	33	3.5	11	172	200
16	8.4	0.42	36	4.8	9	250	190
20	6.7	0.66	39	6.2	8	340	180

This deterministic approach, however, ignores Brownian motion. The most likely
scenario for the formation of a deposition is that the electrostatic force will reduce the

effective interparticle force to a certain point and then this final energy barrier is overcome by thermal motion of the particle. The superposition of the Brownian motion on the electrophoretic motion of the particle introduces a time/probability function to the problem of particle contact. This can affect the density of the deposition, with faster deposition rates leaving less time for particle re-arrangement in the depositing layer and thus lower deposition densities.

Electrohydrodynamic (EHD) Forces — Given that there is a net charge balance in the suspension, there will be a net electrostatic force balance due to the applied electric field as well. In the suspension this means that as particles are pulled toward the deposition electrode, the charged solvent around them is pushed in the opposite direction. The effect of this EHD flow in the opposite direction on electrophoresis of a single particle is discussed in § 2.4. There have been some studies on EHD flows around single or paired particles in the vicinity of an electrode (**22,23**). These show the mechanism by which particles at less than a single layer coverage can be made to aggregate into one dimensional colloidal crystal arrays on an electrode. However, how these EHD flows affect the approach of a particle to an existing layer of particles, how they affect particle re-arrangement prior to deposition, and finally their effect on the deposition of has not been determined. Some specualtion on this topic is presented in Ch. 4.

Electrosedimentary Force — That the electrostatic force on a single particle alone was insufficient to cause deposition became apparent very early on in the compilation of the theory electrostatic repulsion (**24**). A simple solution to this inconsistency was proposed by Hamaker and Verwey in 1940 (**25**). Rather than the electrostatic force on a single particle this deposition mechanism relies on the force on a layer of undeposited particles to provide the force necessary to overcome the repulsion on the innermost layer. Because this mimics gravitational sedimentation with electrostatic force replacing gravity, this is referred to as electrosedimentary deposition. Below is the original chart from Hamaker and Verwey showing the effect of a superposition of the linear compaction force on the interparticle energy barrier.
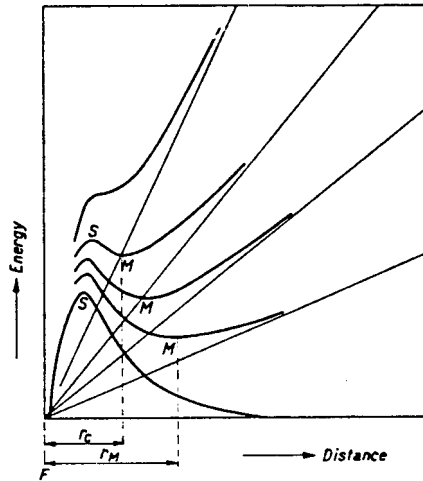
Fig. 2.36 Superposition of an electrostatic compaction force on the
interparticle energy barrier, from Hamaker and Verwey, 1940 (**25**)

Electrochemical Changes — Finally, there are the electrochemical changes that can
occur due to conduction at the deposition electrode. These changes can go in any
direction, either an increase or decrease in ionic strength, proton activity or a change in
ionic composition.

— *Ion Depletion Enhanced Electrostatic* — The first electrochemical change is the
decrease of the ionic strength in the deposition layer. If an ion in solution is consumed at
the deposition electrode there will be a decrease in the total ionic concentration at that
electrode due to the outward migration of the counter ion. This is source of the limit
current behavior discussed in Section 2.2. The important difference between the formation
of this charge depleted layer in a solution and during EPD is the presence of the growing
deposit on the electrode surface. The ion depleted layer is very unstable and in the free
solution quickly transitions to convective flow. This improves mass transport of ions and
eliminates the charge depleted region. However, the presence of an electrophoretically
deposited layer of particles on the electrode can act as a strong damper to the initiation of
convective flow as will be shown in Ch. 4. This damping allows the charge depleted layer
to grow, and voltage gradients can rise to levels on the order of 10,000 V/cm. If the
particles retain their surface charge, the electrostatic force on the particles is both sufficient
to overcome interparticle repulsion and to provide a significant compressive force to
compact the deposition.

— *Salting Out* — In some cases the exact opposite will occur and electrochemical reactions at the deposition electrode will lead to an increase in the ionic strength of the solution at the electrode. This can occur when the current through an electrode-solvent interface is due to electrolysis of the solvent or dissolution of the electrode material. This is illustrated in the left part of the diagram in Fig. 2.11.

This increase in ionic strength in the vicinity of the electrode will reduce the thickness of the diffuse layer around the particles. This can reduce or eliminate the electrostatic stabilizing force around the particles allowing them to deposit. This flocculation by increased ionic (salt) concentration is commonly referred to as 'salting out'.

What will be critical for this type of deposition is the ratio of the growth of the ion enriched layer to the growth of the deposition layer. If the ion enriched layer grows faster than the deposition layer particles can be destabilized and begin to floc before entering the deposition. If the ion enriched layer grows slowly through a dense suspension of particles held in place by electrophoresis, the gradual thinning of the repulsion layers around the particles should allow the layer to gradually compact as the particles move toward each other resulting in a fairly dense deposition. If particles arrive at the deposition electrode much faster than the growth of the ion enriched layer then deposition may occur by electrosedimentation and the growth of the ion enriched layer will be irrelevant.

— *Charge Reduction/Neutralization* — The final case where electrochemical reactions at the deposition electrode cause electrostatically stabilized particles to deposit is where the ionic strength changes relatively little but there are critical changes in the composition. This can occur when the electrochemical reactions produce ions of opposite charge to the particle surfaces, which then adsorb to the particles eliminating the surface charge. Conversely, if the particle surface charge is produced by the equilibrium adsorption of one ionic species, if that species is consumed at the electrode the concentration near the electrode will drop, causing desorption of the charging species from the particle surface. This again reduces the particle surface charge and therefore the electrostatic stabilizing force, allowing the particles to deposit.

2.7.2 Deposition from Polymerically Stabilized Suspensions

One of the great attractions of steric stabilization for the creation of colloidal suspensions is the ability to create dispersions which are thermodynamically stable. At all distances the force between particles are repulsive. Even particles that are brought into intimate contact, such as by drying, will spontaneously redisperse with the addition of solvent.

This is, of course, not the behavior we need for EPD. Deposited particles must adhere to each other so that the deposition will remain after the deposition voltage is turned off and the deposition is removed from the deposition bath. To do this the soluble polymer must either be removed from the contact points between the particles so they can adhere due to VdW forces, or the polymer must itself become a binder holding the particles together. There are three ways that this destabilization can take place: squeezing out of the polymer from particle contact points, bridging flocculation between particles, and a change in the solubility of the polymer. The first two rely only on the electrostatic and electrosedimentary forces slowly pulling the particles together. Change in solubility will depend on electrochemical changes in the depositing layer.

The simplest polymer to squeeze out, naturally, is the non-adsorbed polymer used in depletion stabilization. The combination of viscous and depletion stabilization in the bulk can be used to create exactly the sort of slowly floccing suspension which is stable long enough to perform EPD but where the stabilizing force can easily be overcome in the depositing layer. This is particularly true for the viscous component of stabilization. Viscous forces will preferentially damp the Brownian motion of one particle toward another. With a steady unidirectional force the additional viscosity of the dissolved polymer will only slow the final approach of one particle to another without creating a repulsive energy barrier.

The greatest advantage of this stabilization scheme is that it does not require any specific interaction with the particle surface. There is no need to find a match between the adsorbing groups of a polymer and the particle surface. One polymer/solvent pair could potentially stabilize many types of particles. Furthermore, none of the active surface sites on the particle will be covered by adsorbed polymer. So if particles only develop a modest surface charge it will not be reduced or eliminated by polymer adsorption.

This appears to be the mechanism used by Bouyer, et al. (**26**) to stabilize their suspensions of silicon carbide for deposition. They added $AlCl_3$ to their suspension to create a positive surface charge on the particles by preferential adsorption of Al^{+3} ions. However, the charge was too low to significantly stabilize the suspension. They then added 2 wt. % polyvinylbutyral (PVB) which significantly improved the stability of their suspension without any indication of significant adsorption to the particle surfaces.

Unfortunately, the authors did not report the molecular weight of their polymer, so it is not possible to say for certain, but depletion stabilization seems the most reasonable explaination of their reported data. While they had difficulties in deposition due to electrochemical reactions at the deposition electrode, there was no indication that the stabilization scheme created any difficulty in producing adherent depositions of the particles.

This squeezing out process can also work with either weakly adherent homopolymer or terminally anchored polymer stabilized suspensions at less than complete coverage. In these cases the diffusion outward will be driven by the same osmotic forces as drive out the non-adsorbed polymer. The homopolymer is by its nature constantly desorbing and re-adsorbing loops onto the surface . The homopolymer can effectively 'roll' across the surface away from particle contacts points. At less than complete adsorption the anchor group on terminally anchored polymer chains can 'walk' from site to site across the surface.

The drawback with using this scheme of stabilization/destabilization the very slow speed at which this squeezing out of adsorbed polymer can occur.

> "... a distinctive feature of polymer interactions — one that has often been noted by experimentalists — is the extreme sluggishness with which equilibrium is attained once polymer molecules are confined within a narrow space ... Most of these processes involve the concerted motions of many entangled molecules which may require many hours or days even though the rate of similar molecular motions of isolated coils in the bulk may take less than 10^{-6} sec."
>
> Israelachvili (**3**, p. 303)

For block co-polymers at less than full coverage the polymer can be used to make the particles adhere to one another. A block co-polymer will likely adhere too well to the surface to be squeezed away from the particle contact points. However, not all of the adsorbing groups on the polymer chain will necessarily be adsorbed or remain adsorbed to the particle surface. If another particle which has free surface area is brought within the polymer's effective radius some of these free groups will adsorb to the other particle. One polymer molecule then has groups adsorbed to both particles and forms a bridge between them. This is very attractive because this type of polymer bonding between particles in a deposition would create a green body which would be much stronger and more damage resistant than a compact held together only by VdW forces. It would also do this with relatively little polymer that would not close off the porosity in the deposition.

However, it is not known whether block co-polymer stabilization will work for EPD. At low surface coverages this bridging flocculation will be the only interaction

between the particles and there will be no stabilizing mechanism preventing flocculation prior to deposition. At full coverage the interaction between particles will be purely repulsive, the dispersed condition will be thermodynamically stable, and it will be impossible to electrophoretically deposit the particles. It is not obvious whether there is a transition region where there can be a repulsive interaction in the bulk with bridging flocculation occuring an electrophoretically formed compact.

Finally, there are changes in the chemistry of the solvent in the deposition layer that can be used to cause the polymer to either desorb from the particle surface or to cause the polymer to collapse into a much more compact configuration allowing particles to approach within range of their L-VdW attraction. Using chemical changes to manipulate the stability of a suspension will most like require that the stabilizing element be a polyelectrolytic polymer. Non-ionic polymers which adsorb by combining soluble and insoluble segments can be manipulated by composition or temperature changes in the solvent but will be relatively unaffected by changes in ionic strength or ionic composition. Ionic polymers, on the other hand, have the potential to be changed from adsorbing to non-adsorbing and from soluble to insoluble by changes in the ionic composition of the solvent around them.

Table 2.4 Mechanisms of Electrophoretic Deposition

Stabilization Type	Deposition Mechanism	Examples
Kinetic/Density	Densification	R. Bagwell - $BaTiO_3$ (Unpublished)
Electrostatic	Electrostatic Force	Here - PZT, Ag/Pd
"	Electrosedimentary	Here - Alumina
"	Ion Depletion Augmented Electrostatic	Here- Alumina Sarkar & Nicholson-Alumina
"	Salting Out	Overbeek - MgO (**27**)
"	Charge Reduction/ Neutralization	*Unknown*
Polymer Depletion	Squeezing Out	Bouyer & Foissy - SiC (**26**)
Homopolymer	Squeezing Out	*Unknown*
Terminally Anchored at less than full coverage	Squeezing Out	*Unknown*
Block Co-Polymer at less than full coverage	Bridging Flocculation	*Unknown*
Homo-, Terminal-, or Block Polymer	Desorption of Neutral Polymer	*Unknown*
Terminal polymer, Block or Simple Polyelectrolyte	Desorption of Charged Polymer	H. Saita, (Unpublished) Polyethyleneimine (PEI)
Polyelectrolyte Electrosteric	Polymer Neutralization	PEI

2.8 Post-Deposition Effects

      The floccing of particles at a deposition electrode to form an adherent coating is not the end of the evolution of the deposition. There are several changes that can occur in the deposited layer — while the deposition voltage/current is still applied, — when the voltage/current is turned off, — and when the deposition is removed from the deposition bath for further processing.

2.8.1 Electrosedimentary Collapse

      When particles are deposited from an electrostatically stabilized suspension with a low interparticle repulsion energy they can form a very soft, low density deposition. As the deposition grows the electrosedimentary force from the accumulating outer layers will increase the pressure on the loosely flocced inner layers. At some point this pressure will exceed the shear strength of the inner layers. This can trigger a collapse in one area of the deposition, transferring additional stress to the areas around it. This can cause an avalanching collapse of the deposition inner layer with the layer temporarily fluidizing then resetting in a denser confuguration. The extent of the densification will be limited by the viscosity of the solvent which must be forced out of the consolidating deposition before it rigidifies again.

      This is the same behavior that is seen in natural sediments consolidated by gravity. The consolidating sediment behaves as a pseudoplastic solid, compressing elastically to a critical stress at which point the structure breaks and the sediment densifies plastically until it reaches a new stable equilibrium. The sediment compacts through a series of these discrete events, with density increasing non-linearly with distance from the surface. (**28**)

      In the case of EPD this behavior manifests itself as a deposition which, when first pulled out of the deposition bath, has a surface marked by plateaus and flat bottomed craters. If the deposition remains adherent and does not crack as it dries, the thicker areas will be consolidated by drying so that the final layer has a uniform thickness. This is because the deposition rate over the electrode area will remain essentially constant, therefore the amount of powder per unit area will be constant as well. Drying (§ 2.8.6 below) is a much stronger force than electrosedimentary compaction and so will compact the deposition to a uniform density. However, density gradients in the deposition layer will lead to a strong curling force during drying. If the deposition is on a flexible substrate it will curl up and if the deposition cracks it will curl up away from the substrate.

2.8.2 Ion Depletion Enhanced Compaction

       In some depositions where an ion depletion layer forms, it is possible for this layer to grow more slowly than the growth of the deposition. This is shown very clearly in Ch. 4. This means that outer portions of the deposition will only be exposed to the average electric field of the deposition bath while the inner portions of the deposition are consolidated by the very high fields in the ion depletion region. This can lead to a deposition with a bi-modal density distribution which can lead to a strong tendency to curl up from the substrate during drying or sintering.

2.8.3 Convective Lumping, Cratering & Flaking

       While the presence of a deposition on a surface can retard the initiation of EHD convection, at some voltage-thickness level the driving force for convection will exceed the damping of the deposition and relativley large scale convection will begin through the deposited layer. Given that the velocity of this convection will be orders of magnitude higher than the electrophoretic velocity of the particles, particle transport will now be almost exclusively by convection. Where a convective flow enters a deposition layer particles will be deposited by filtration of the flow, leading to a lump on the surface. Flows out of the deposition away from the electrode will carry particles away from the deposition surface and stop the growth of the deposition in this area. This outward flow can also erode the existing deposition leaving craters that extend down to the electrode surface. Another phenomenon which has frequently been observed here is the flaking off of portions of a dense deposition formed prior to the initiation of convection. Where the convection flows inward the flow will press the deposition more firmly onto the electrode. Where this convective flow moves away from the electrode the hydrostatic pressure necessary to force the flow through the deposited layer can grow to the point that it will pop flakes of the deposition off the electrode.

2.8.4 Electrolytic Gas Termination

       This effect occurs while the deposition current-voltage is still applied but acts very quickly to terminate the deposition process. In a conductive EPD bath the reactions at the electrodes frequently produce a gas. In low conductivity solutions the amount of gas produced is small enough that it is able to dissolve in the solution and diffuse away from the electrode surface without forming bubbles. However, as a deposition builds up on an electrode surface the diffusion path will get longer and longer. At some point the gas concentration in solution at the electrode will reach a critical point and a gas bubble will

form. The bubble will spread along the electrode/deposition interface stopping conduction in that area. This increases the current density in the areas where there is still liquid contact with the electrode, increasing the generation of gas in these areas. Since these areas are also likely to be close to the critical concentration of dissolved gas, they will form gas bubbles as well, decreasing the conductive area further. Thus the electrode/deposition interface will flood with gas at an exponential rate until conduction and therefore deposition are terminated.

2.8.5 Electrostatic Pop-Off

In the case where the ion depletion effect is used for deposition or for consolidating a deposition, a significant unbalanced electrostatic charge can build up. This can cause flakes of a deposition to pop off when the voltage is turned off. This is especially noticeable when the deposition is transferred to clear solvent for rinsing of the deposition. Flakes popping off of the deposition electrode can be seen to move several millimeters away from the deposition electrode in a fraction of a second.

2.8.6 Repulsive Decomposition

If particles are electrostatically stabilized in the bulk suspension, after the deposition current is turned off the same repulsive force will exist between the particles in the deposition. If the particle diffuse layer thicknesses approach the scale of the pores in the deposition this can create a higher osmotic pressure inside the deposited layer.

If the deposition is dense, with a high average number of interparticle contacts, then the L-VdW forces will be sufficient to hold the deposition together. If the deposition is slightly less dense, the internal pressure can be sufficient to break flocs off of the outer surface of the deposition. Rinsing in pure solvent will maximize the osmotic pressure differential within the deopsition. It was observed that an alumina deposition when rinsed briefly in pure ethanol would lose very little mass. However, if the deposition was held vertically without motion in the ethanol a small but continuous cascade of alumina flocs was seen to flow down off of the surface as the surface slowly decomposed due to the internal osmotic pressure.

2.8.7 Drying and Sintering

The final stage of the process is drying the solvent from the deposition. Even though the particles can be well packed by the EPD process, some particle re-arrangement

and a slight additional densification is possible. The following example illustrates the relative magnitudes of the forces generated by EPD and drying respectively.

A 7μm deposition of Al_2O_3, powder was made from ethanol using a constant current . During the course of the deposition the voltage across the cell increased from 20 to 64 volts. If we assume that this entire additional 44 volt field drop occurs across the deposited layer we can calculate a pressure due to electric field $P = \varepsilon_r \varepsilon_o \dfrac{V^2}{d^2}$. For a voltage drop of 44V across a 7μm deposition layer the Maxwell pressure is ≈ 8 kPa. This is an oversimplification of what is occurring in the deposition layer, but gives an idea of the relative forces involved.

During drying, a capillary tension is created in the particle compact as the solvent/vapor interface moves into the pores in the final phase of drying. (**32,33**) The capillary tension is a function of the surface energies of the solvent/vapor and solvent/particle interfaces and pore diameter in the compact. This capillary pressure can be estimated by

$$P = \gamma_{LV} \cos(\theta) \frac{S_V}{V_{P_V}} \qquad\qquad [2.72]$$

Given: γ_{LV} surface energy of ethanol = 2.197 N/m, θ liquid/solid contact angle $\approx 40°$, S_V the surface area/unit volume calculated using; powder surface area = $9.9 m^2$/g, α-alumina theoretical density 4 g/cc, deposition packing density 60%, and V_{P_V} the volume fraction porosity, the estimated capillary tension is $\approx {}^-100$MPa. As can be seen from the formula above, the most significant variable affecting the drying stresses is the surface to volume ratio, which is inversely related to the particle size. While the liquid-vapor surface energy would be eliminated by supercritical drying which can eliminate the drying stresses, at normal pressures and temperatures it is difficult to have a significant impact on this variable. Frequently something that reduces this energy will also reduce the wetting angle, negating the effect. However, each step going from micron to sub-micron to nano scale powders involves an order of magnitude increase in the capillary tension.

A dense electrophoretically deposited layer will behave as a brittle solid, with the probability of cracking during drying a function of defect size and volume under stress. Remarkably enough, despite the order of magnitude higher stress during drying compared to deposition of the sub-micron scale Al_2O_3 powder in the above example, cracking is not a problem on continuous deposited layers up to 0.1 mm dried on a flat, rigid substrate. Cracking in thinner coatings is usually an indication of a low density deposition and can be eliminated by improving the stability of the deposition suspension. In moving to nano-

scale particles, the drying stresses will jump another order of magnitude. However, given that one of the primary reasons for depositing nano-particulate materials will be to form layer thicknesses in the low sub-micron region, these stresses should not be a problem so long as dense, uniform, and defect free particulate depositions can be formed.

Constrained sintering is a problem very similar to constrained drying. The film is constrained in the two in-plane dimensions and sintering shrinkage can only occur in the thickness direction. However, these sintering stresses are an order of magnitude lower than the drying stresses (**29**). If the deposition is not cracked by drying stresses it will likely remain intact through sintering as well.

2.9 Summary

EPD is not simple, and to look at it from any one point of view will miss many important aspects of the process. This chapter is intended to be an introduction to the four areas of science that bear on aspects of EPD: electrochemistry, colloidal chemistry, surface chemistry and electrohydrodynamics. Space and time are too limited to discuss fully how each of these fields relate to EPD, and, in general, most of the relations between these fields of study and EPD awaits future study and analysis. However, just by considering each of these aspects of the operation of an EPD cell, a list of near-electrode effects was generated. This list was then compared with a list of means by which a colloid suspension can be stabilized. The result is a matrix of stabilization mechanisms vs. near electrode effects. From this matrix a list of combinations that may lead to deposition of the particles on or next to the deposition electrode was compiled.

This list, to the current knowledge of the author, is the first comprehensive list of mechanisms of EPD ever compiled. Some of the mechanisms are speculative and there are no clear demonstrations of deposition by that mechanism in the literature reviewed for this thesis. Other mechanisms have been established in previous work.

The next two chapters here will be devoted to clearly demonstrating one of the most interesting of these mechanisms, ion depletion enhanced electrostatic deposition. A vital part of demonstrating this clearly is developing an accurate, quantitative description of the surface and colloidal chemistry of the deposition suspension. This is done in Ch. 3. This information is then used to complete a quantitative analysis of a series of depositions in Ch. 4. This chapter then clearly demonstrates the formation and stabilization of an ion depleted conduction layer and its role in the EPD of alumina particles. Future studies can then be devoted to attempting to demonstrate clearly each of the other mechanisms to fill out this table.

Symbols used in Chapter 3

Fundamental constants

e	Elementary charge (1.602E-19 C)
k	Boltzman Constant (1.381E-23 J/K)
ε_o	Permitivitty of free space (8.854E-12 C^2/J·m)

General symbols

a	Particle radius (m)
a_O	Geometric mean distance of closest approach of ions in solution (nm)
E	Reduced electrophoretic mobility (non-dimensional)
EtO⁻	Ethoxide ion
HEtO	Ethanol molecule
K_S	Solvent autoprotolysis equilibrium constant
$pa_{H+}*$	-Log$_{10}$ $a_{H+}*$ where $a_{H+}* \equiv \frac{[H_+]}{[H_+^\circ]}$ at infinite dilution in the solvent.
pHi	Indicated pH (pH meter display)
pH*	Operational pH (equal to $pa_{H+}*$ in dilute solutions.)
q	Surface charge density (C/m^2)
Ss	Surface adsorption site
T	Temperature (K)
u_E	Particle electrophoretic mobility (μm·cm/V·s)
z	Ion valence
f_-	Activity coefficient for negative ion at particle surface
f_+	Activity coefficient for positive ion at particle surface
$f_\pm$	Activity coefficient for ions in bulk solution
δ	Conversion constant between pHi and pH* for a given solvent and reference electrode combination.
ε_r	Relative dielectric constant
η	Solvent Viscosity (Poise)
κ	Inverse Debye length (m^{-1})
ρ_∞	Density of dissociated molecules of a binary salt in bulk solution (m^{-3})
ζ	Particle Potential at Shear Layer (mV)
$\tilde{\zeta}$	Reduced particle potential at shear layer (non-dimensional)
$[x]$	Molar concentration of chemical species x
$[x^\circ]$	Standard concentration of chemical species x (usually 1 molar)

Conductivity

Λ	Molar conductivity (μS·dm^3/cm·Mol)
Λ_O	Molar limit conductivity (μS·dm^3/cm·Mol)
c	Molar concentration of dissolved salt (Mol/dm^3)
α	Dissociated fraction of dissolved salt
K_A	Association constant for oppositely charged ions in solution

Electroacoustics

δ	Pressure wave decay parameter for acoustophoresis
ω	Measurement frequency in acoustophoresis (s^{-1})
ρ	Solvent density in acoustophoresis

Chapter 3

Surface Chemistry and Surface Charge Formation
for an Alumina Powder in Ethanol

3.1 Introduction

As has been mentioned in previous chapters, there have been relatively few studies that have attempted to analyze the deposition process in a quantitative manner. This due in large part to the complex, dynamic and non-equilibrium electrochemical environment near the deposition electrode. References (**1-3**) are some of the most notable exceptions to this rule.

To venture a quantitative analysis of a particular deposition requires a quantitative knowledge of the interaction between the particles, the suspending solvent and the ions dissolved in that solvent. Therefore, the objective of this chapter is to develop a model of the surface chemical reactions on the depositing powder sufficient to predict its behavior in the unique chemical environment near the deposition electrode. This means developing mathematical models of the particle adsorption isotherms for individual ions, independent of the activity of their co-ions. These adsorption isotherms are then critical for the deposition analysis presented in Ch.4.

The alumina-ethanol system analyzed here was chosen for simplicity, stability and the level of information available in the literature on the system components. Alumina was chosen as the powder component for its low solubility and our own experiments showing that it could be washed easily to remove surface contaminants. Ethanol was chosen as a readily available, non-toxic solvent. Because ethanol is very hydrophilic, making and maintaining completely anhydrous ethanol is quite difficult. Therefore, ethanol with a known water content was used. Hydrochloric acid is a simple acid that is almost fully dissociated in low concentrations in ethanol, has been shown to raise the surface potential of alumina in ethanol, and has been used previously for EPD. (**4**)

3.2 Materials

Alumina - The powder used in this study is AKP-50, Sumitomo Chemical Co., Osaka, Japan. For particle size measurement the powder was dispersed in water using an ultrasonic horn, and size was measured by laser light scattering (Mastersizer, Malvern Instruments Ltd., Worcestershire, UK). The particle size distribution was bi-modal with 90 vol.% having an average size of 0.27μm and 10% an average 3μm. 10 vol.% of the powder was less than 130 nm. Surface area as measured by single point BET (Monosorb, Quantachrome Corp., Boynton Beach, Florida) is 10.0m^2/g. The powder is 100% α-phase by X-ray diffraction. The particles have an axisymmetric but angular morphology.

Ethanol - The ethanol used in this study is from Pharmco, Inc., Brookfield, Connecticut. The as-received water content is 0.045 wt.% as determined by Karl Fischer titration. The conductivity of the ethanol prior to water addition is less than 0.1 μS/cm. Deionized water, conductivity $\approx 0.5\,\mu$S/cm, was added to adjust the water content to 0.5 wt.%. The density of this mixture is 0.7866 g/cc by linear interpolation of literature data at 100% and 95% ethanol. This gives a 0.218 molar water concentration. The conductivity measured at the beginning of each of the titrations was less than 0.1 μS/cm.

It should be noted that the water content of the ethanol is very significant for the measurements made here. Small quantities of water will affect both the mobility of H$^+$ ions as well as level of association between the positive and negative ion.

In the pure solvent the ion is able to hop from molecule to molecule, passing through the solvent much more quickly than ordinary ionic migration. This is referred to as either anomalous proton conduction or the Grotthus mechanism. However if there is water present the proton can jump to a water molecule:

$$C_2H_5OH_2{}^+ + H_2O \Leftrightarrow C_2H_5OH + H_3O^+$$
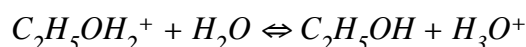
De Lisi et al. have calculated the free energy of this reaction to be -14.01 kJ/mol. (**10**) Because of the strong forward bias of this reaction, protons will be trapped by water molecules in the ethanol and have to migrate through the solvent as hydronium ions significantly reducing the H$^+$ mobility. This is shown in Fig 1 from where the molar limit conductivity for HCl in ethanol drops by nearly fifty percent with the addition of the first 1 % of water added to the ethanol.
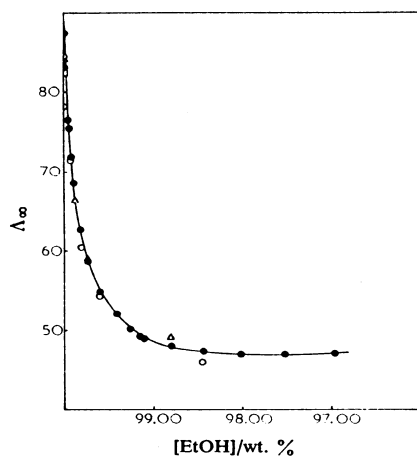
Fig. 3.1 Molar limit conductivity of HCl as a function of ethanol concentration with water. (**10**)
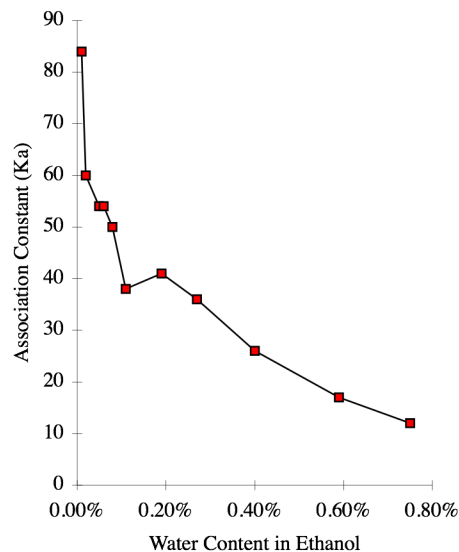
Fig. 3.2 Association constant of H$^+$ and Cl$^-$ in ethanol as a function of water content. (**10**)

The second chart is a graph of data also from De Lisi et al. for the association constant between the positive ion and the chloride ion in solution as a function of water content:

$$Cl^- + H_3O^+ \Leftrightarrow Cl^- \bullet H_3O^+ \quad \text{or} \quad Cl^- + H_2EtO^+ \Leftrightarrow Cl^- \bullet H_2EtO^+$$
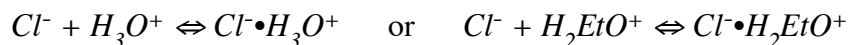
When the positive and negative ions are associated there will be no net migration in an electric field, therefore associated ions will not show up in a conductivity measurement.

The effect of these small quantities of water on the dielectric constant of the medium is small, therefore, this dramatic effect would not be predicted by a solvation model that considers the solvent as a continuous dielectric medium. A reasonable explanation is that water makes a solvation shell around the ions which has an effective dielectric constant much higher than the bulk of the solvent. The water molecules are attracted to the vicinity of the ions both by their higher dipole moment and by the break in the ethanol structure caused by the ions.

HCl - Hydrochloric acid was titrated from 0.103 and 0.0103 wt.% solutions in ethanol prepared by dilution of a 37 wt.% HCl/water azeotropic solution (Fisher Chemical Co., Pittsburgh, Pennsylvania) into ethanol. The HCl content was verified by pH titration in water against the KOH standard solution below. Water contents as calculated from

component compositions were 0.11 and 0.05 wt. % for the 0.1 and 0.01 wt. % solutions respectively.

KOH - 0.098 molar potassium hydroxide standard solution in ethanol (J. T. Baker Co., Phillipsburg, NJ.) was used for titration both in as-received form and diluted by a factor of ten using as-received ethanol above. Density of the 0.098 molar solution at 25.0°C was measured as 0.7887 g/cc. Water content was 0.45 wt.% as determined by Karl Fisher Titration. This equals a 0.197 molar water concentration.

3.3 Experimental Methods

3.3.1 Washing and Hydration of Powder Surface

To prevent the introduction of unknown ionizable compounds into the system, the alumina powder was washed thoroughly prior to use. 150 g of powder was placed into a 0.5 liter HDPE bottle and filled with de-ionized (D.I.) water. The bottle was heated to $\approx$60°C in a commercial microwave and shaken for $\approx$ 1 minute. The powder was allowed to sediment out for varying lengths of time, usually overnight. The conductivity of the supernatant was measured, the supernatant poured off, and the bottle refilled with D.I. water. This procedure was repeated until the room temperature conductivity of the supernatant was equal to or less than the conductivity of the D.I. wash water ($\approx$0.5 μS/cm). For the powder used in this study this required nine rinsing cycles.

To verify that the powder lost when pouring off the supernatants did not affect the specific surface area, the surface area was re-measured after washing and was found to be unchanged at 10.0 m^2/g.

Thermal gravimetric analysis (TGA) of the powder after exposure to liquid water showed a discrete weight loss as it was heated from 220° to 260°C in flowing dry air. The magnitude of this weight loss increased with time held in room temperature water and did not reach a saturation value over three days. (Fig. 3.3) However, by holding the powder in water at 80°C, it was found that the weight loss reached a maximum value of 0.20% in two days. (Fig. 3.3) Powder held for three days showed a slightly lower weight loss. No additional runs were made to determine if this is a real effect or due to experimental error.
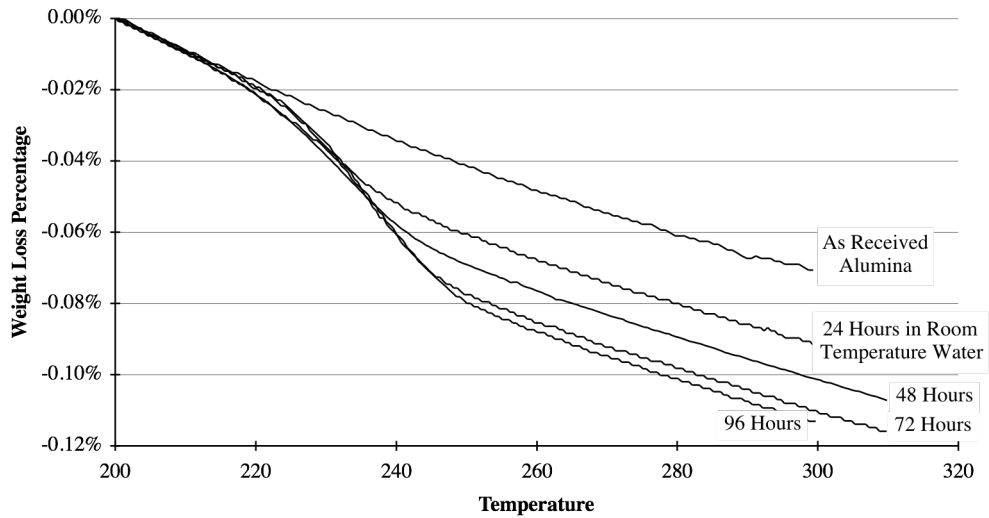
Fig. 3.3 Weight loss for alumina powder as a function of temperature for powders held in water at room temperature for 0, 1, 2, 3, and 4 days, all weights normalized to 0 at 200°C.
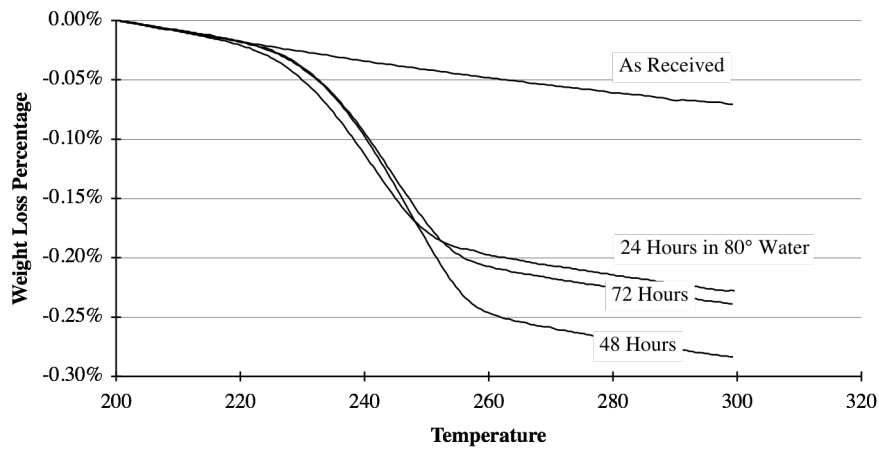
Fig. 3.4 Weight loss for alumina powder as a function of temperature for powders held in water at 80°C for 0, 1, 2, and 3 days, all weights normalized to 0 at 200°C.

It has been reported previously that the point of zero charge of α-alumina powders in room temperature water can drift over several days from a pH of 6.7 to 9.2. (**5**) Water has been shown to actually reverse the charge on very well dried α-alumina in longer chain alcohols. (**6**) To standardize the alumina surface all powder was equilibrated in 80°C water for two days after washing.

3.3.2 Conductivity Measurements

Conductivity was measured using a rectangular parallel plate conductivity probe having a cell constant of 0.22. The plates were of polished platinum 2.6 mm apart. The voltage across the conductivity probe was measured using a voltage divider circuit. A sine wave input signal of ≈ 1V rms was provided by an HP 33120A signal generator. The voltage across the conductivity probe was reduced to ≈ 0.5 V rms using a resistance decade box. The total input voltage and voltage across the decade box were measured using an HP 54645A oscilloscope and used to calculate the resistance across the conductivity probe.

A simple equivalent circuit for the for the conductivity measurement setup used is shown in Fig. 3.4. V_i is the test signal input; R_r is the reference resistance which must be close to the R_{cp}, the resistance of the conductivity probe, in order to generate accurate results; C_{cp} is the capacitance of the test cell, which is a constant as long as the test cell geometry and the solvent remain the same; C_{sc} and $R_{cp\ lim}$ are the space charge capacitance and limiting resistance. The voltage output, V_o, is measured with the oscilloscope which has an input capacitance, C_o, of 13 pF and an input resistance, R_o, of 1.00 MΩ. The behavior of the conductivity probe in regions where significant space charge accumulates is considerably more complex than is suggested by this simple parallel capacitor/resistor, however, in the range where charge only begins to accumulate this is a reasonable approximation.
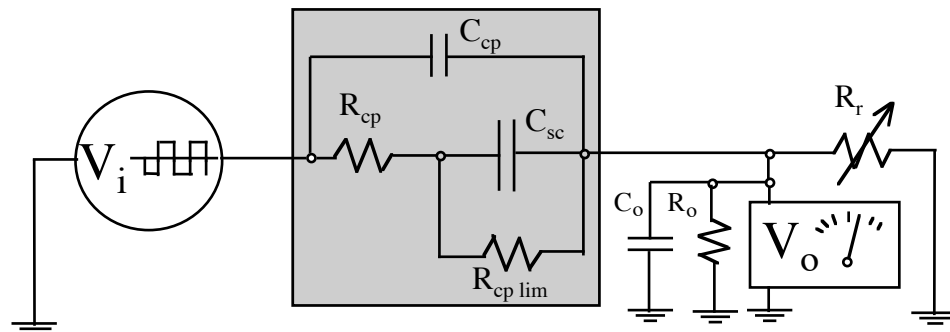
Fig. 3.4 Equivalent circuit for conductivity measurement setup. The area in the gray box is a simplified equivalent circuit for the conductivity probe.

Frequency was adjusted as a function of conductivity from 20 Hz to 20 kHz to remain between double layer capacitance effects in the conductivity cell and capacitance effects in the measuring circuit. At low frequencies the voltage across the conductivity probe includes components due to both the resistance of the fluid and space charge build up at the electrodes. As the frequency is raised the voltage alternates faster than the space

charge can form, and the voltage across the cell will be due only to the resistance of the fluid. At higher frequencies the resonance of the input capacitance of the oscilloscope will begin to short circuit the oscilloscope. Therefore the measurement procedure is to scan a set of frequencies, each time adjusting the reference resistance to divide the signal voltage evenly between the conductivity cell and the measurement circuit. The resistance of the conductivity cell is then calculated at each frequency assuming that $C_o = 0$. The minimum calculated resistance is then taken as the resistance value for the conductivity probe.

$$R_{cp} = \left[\left(R_r \right)^{-1} + \left(R_o \right)^{-1} \right]^{-1} \frac{V_i - V_o}{V_o} \qquad \text{Conductivity Probe Resistance Calc.}$$

Calibration of the test cell and determination of absolute accuracy of the measurement procedure was performed by comparison of measurements to previously published data. Calibration was performed by titration of KCl into water using as a standard the equation of Lind, et al. (**7**) This was verified and measurement accuracy estimated by titration of LiCl into ethanol compared to the data of Graham, et al. (**8,9**) and HCl into ethanol containing 0.5 wt.% water compared to the data of De Lisi et al. (**10**) Measurement accuracy was within ±1% over the range from $4\,\mu$S/cm to 120μS/cm and within ±2% from 1 to $4\,\mu$S/cm. Percentage accuracy declined rapidly below $1\,\mu$S/cm, however, absolute accuracy above $0.3\,\mu$S/cm is estimated to be within $\pm0.05\mu$S/cm.

The conductivity test cell was held in the suspension with the plates aligned vertically. The bottom edge of the cell, 5.9 mm wide, was open so that powder sedimenting out of the suspension would not accumulate in the test cell. The surface conductivity of the powder can be significantly higher than that of the bulk solution. If sedimented powder is allowed to accumulate between the plates, the higher conductivity of the sediment will short circuit the cell. A small hole in the top of one side of the cell allowed for free circulation of suspension through the cell.

3.3.3 Titration Procedure

Conductumetric and pH titrations were performed in a jacketed beaker maintained at 25 ± 0.02°C by a circulating isothermal bath. Titrants were added manually by weight. Where alumina was added, it was first held in a drying oven at 135°C for at least 2 hours to standardize the quantity of adsorbed water. In all cases alumina was added to yield an approximately 1 vol.% suspension.

The solution was mixed using a magnetic stirrer. The powder was sufficiently flocced from the washing process that it rapidly sedimented out at all conditions when the stirrer was turned off. Conductivity measurements made with the powder held in

suspension by stirring and in the quiescent supernatant after sedimentation were identical within the measurement error of the apparatus and technique.

3.3.4 Electrophoretic Mobility

Mobility was measured using a Delsa 440 laser Doppler velocimeter (Beckman Coulter, Inc., Fullerton, California). This instrument measures particle velocity in suspension within a rectangular capillary. An electric field of 57 V/cm is applied across the capillary for 2.5 seconds, turned off for 2 sec., and a reverse field is applied for 2.5 seconds. This is repeated 12 times and the results are averaged. Reversing the field is intended to minimize the electrochemical boundary layer formation at the electrodes. If the velocity measured in each polarization direction was not the same, the measurement was rejected.

To separate the electro-osmotic flow of the fluid in the capillary from the electrophoretic motion of the particles, particle velocity was measured at nine points across the capillary, the results fitted to a parabola, and the particle velocities at the theoretical stationary levels calculated from the parabola. For all of the data points reported here the r^2 fit of the parabola was better than 98%.
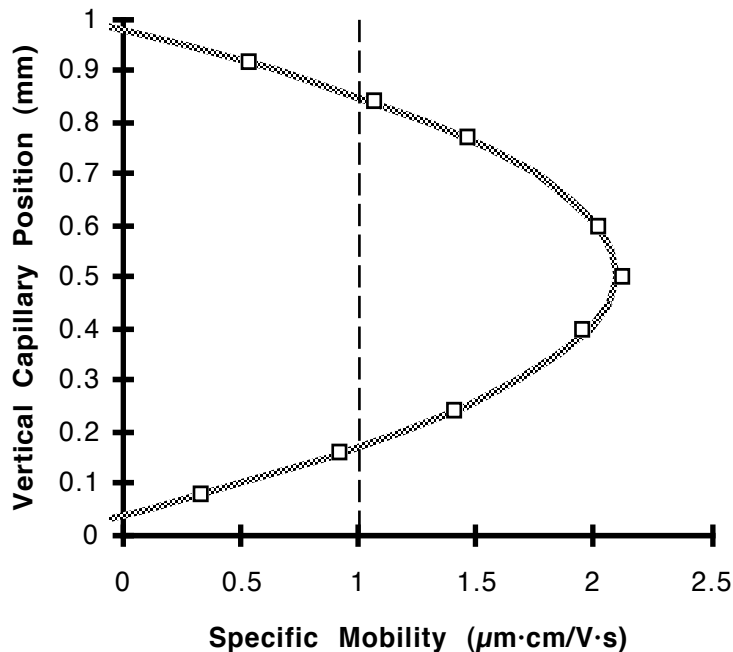
Fig. 3.5 Specific mobility vs. vertical position in measurement capillary. Squares are data points, gray line is parabola fitted by least squares. Vertical dashed line intersects parabola at theoretical stationary layers. This is the data for one of two measurements made for the 1.23 μS/cm case in table 3.1. Cell center calculated to be at 0.51 mm, r^2 fit for parabola 0.999, specific mobility 1.00 μm·cm/V·s.

For a significant signal to be generated by the instrument the laser must be able to propagate across the capillary with only modest scattering. This requires that the sample have a volume density of particles in suspension of 0.01% vs. 1% in the standard working suspensions used here. To prepare samples for measurement a 1% suspension was prepared in a centrifuge tube. HCl solution was added, the suspension mixed, and conductivity was measured to determine the ionic strength in the solvent. The suspension was centrifuged at 3,600 m/s^2 for 3 minutes. This usually left enough particles suspended in the supernatant for an electrophoretic measurement. If there were too few particles in the supernatant, some of the clear supernatant was drawn into a syringe, the remaining material was resuspended and a small amount was drawn into the same syringe and mixed. Volume density was judged visually.

We were only able to produce credible measurements using this instrument for very stable suspensions that were also stabilized against floccing to the quartz capillary wall. Although there was no attempt to quantify the surface charge on the capillary walls, in all of the measurements where a stable, symmetric, parabolic electroosmotic flow developed the flow indicated that there was a significant positive charge on both the capillary walls and the particles. Without this stability, the horizontal capillary is susceptible to sedimentation of particles onto the bottom surface. This gives the bottom a different surface charge from the top and prevents the development of a symmetric parabolic flow. As a result we were unable to make any valid measurements in suspensions with added KOH.

3.3.5 Electroacoustic Measurement

These measurements were made using an ElectroAcoustic Spectrometer DT-1200 with automatic titrator (Dispersion Technology, Inc., Mt. Kisco, New York). This instrument uses a piezoelectric actuator to apply a 1 MHz acoustic signal to a particulate suspension. Because of the density difference between the particles and solvent, there will be a relative motion between the two in the acoustic wave. This relative motion polarizes the electrostatic double layer around the particles. This polarization is detected as a current at an electrode on the face of the acoustic actuator.

To prepare the suspensions for electroacoustic measurement the alumina powder was placed in a 135°C oven for 2 hours to standardize the adsorbed water. This was added to the 99.5/0.5 wt.% ethanol/water solvent to produce a 1.00 vol. % alumina suspension. The mixture was placed on a vibratory mill for ≈ 6 hours with 2mm spherical alumina milling media. The HCl titration was performed the next day and the KOH titration was

performed on a portion of the same suspension one day later. The suspension was very stable and the initial zeta potential reading for each titration was within ±1 mV.

The instrument was calibrated with a 10 vol. % silica Ludox suspension with a zeta potential of -38 mV in water measured independently with an optical zeta potential instrument. Readings were made in a partially covered beaker rapidly and continuously stirred with a magnetic stir bar at ambient temperature, 25° ± 3°C. An automatic titrator was used to inject fixed volumes of titrant. In the titration with HCl, the suspension was allowed to equilibrate for 5 minutes after each injection of HCl solution before two zeta potential readings were made, each 40 seconds apart. In the KOH titration the equilibration time was reduced to two minutes.

3.3.6 pH

The pH numbers reported here are the direct numerical reading measured using a Fisher Accumet 20 pH meter (Fisher Scientific, Pittsburgh, Pennsylvania). An Accumet combination probe was used consisting of a general purpose glass sensing membrane and a Ag/AgCl reference electrode with a porous plug junction. The meter was calibrated using aqueous standard buffers at pH 4.00, 7.00, and 10.00. This direct readout of the pH meter in ethanolic solutions using a probe calibrated in aqueous standard solutions will be referred to here as the 'Indicated pH' or pHi.

In ethanolic solutions with a conductivity of $\approx 1\mu$S/cm or less, pHi readings were not stable. Above this conductivity and below readings of $\approx$ pHi 9, stable reproducible readings were produced within three minutes of immersion in the ethanol while stirring. When the probe was replaced in the aqueous standard it returned within one minute to the standard value. Above readings of $\approx$ pHi 9 there was considerable drift in the readings and when the probe was returned to an aqueous standard up to 20 minutes could elapse before the probe returned to the correct reading for the standard.

To verify the validity of this measurement a titration was performed in the 99.5/0.5 wt. % ethanol/water solvent used in this study. A forward titration was performed with HCl, and a reverse titration performed using NH_4OH. The concentration of protonated ions was calculated as the sum of moles of HCl added minus the number of moles of NH_4OH added where this yielded a positive number. Where this yielded a negative number, indicating a preponderance of ethoxide/hydroxide ions, the concentration of protonated ions was calculated by dividing the equilibrium constant for the autoprotolysis reaction in this solvent by the absolute value of this number. A constant pK_s of 13 was determined by iteration to achieve the best fit of a straight line connecting the pHi readings in the acidic and basic solvent. This is shown in Fig. 3.6.

$$HEtO + H_2O \Leftrightarrow EtO^- + H_3O^+$$

$or \quad 2HEtO \Leftrightarrow EtO^- + H_2EtO^+ \quad$ Autoprotolysis Reactions in Ethanol/Water

$or \quad 2H_2O \Leftrightarrow OH^- + H_3O^+$
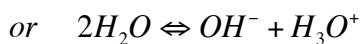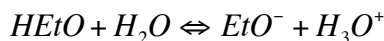
$$K_s = \left[H_2EtO^+ + H_3O^+ \right] \bullet \left[EtO^- + OH^- \right] \bullet f_\pm^2$$

Autoprotolysis Equilibrium in Ethanol/Water
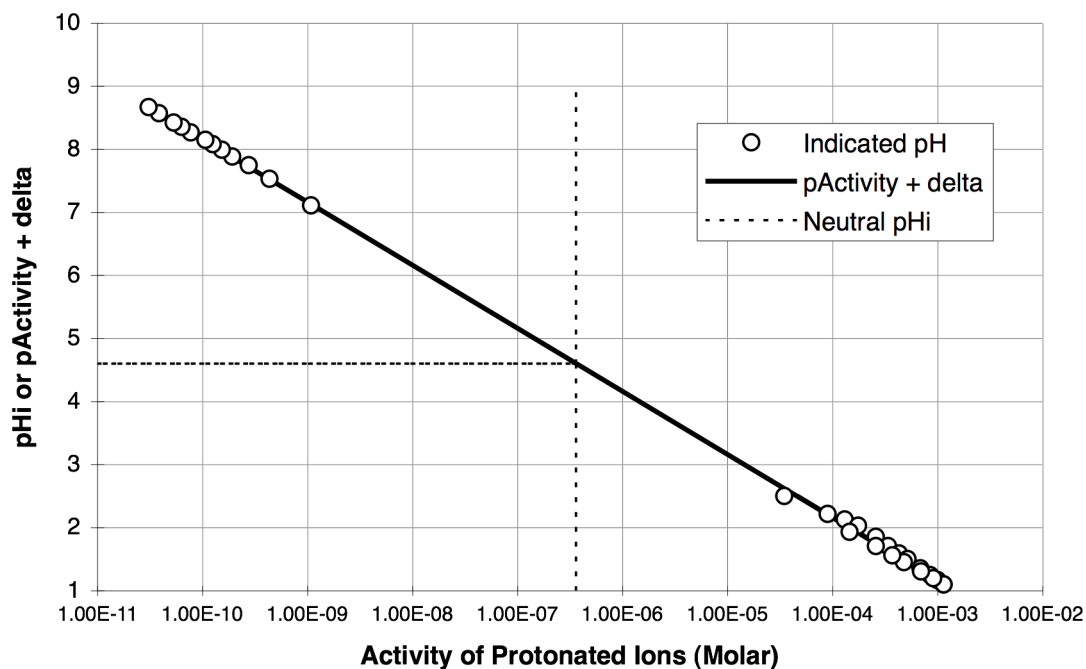
Fig. 3.6 pHi titration in 99.5/0.5 wt. % ethanol/water; forward titration with HCl, reverse titration with NH$_4$OH. Activity of H$^+$ ions (a_{H+}*) calculated using an autoprotolysis constant of 1.3e-13. Circles indicate pHi readings, the solid black line is the -Log$_{10}$ a_{H+}* + δ, where δ is -1.84. Neutral pHi is 4.6.

To further verify these measurements the pa_{H+}* was calculated where a_{H+}* is the activity of the protonated ions in the solvent where activity is equal to concentration at infinite dilution. This activity was calculated as the product of the concentration of protonated ions in the solvent and the activity correction factor, $f_\pm$, calculated using the Debye-Hückel formula [7] below. At the low ionic concentrations used here the pa_{H+}* scale will be essentially congruent with the pH*, or operational pH scale for this solvent. To convert from the operational pH (pH*) to the indicated pH (pHi) requires the addition of a correction factor δ. This factor compensates for the liquid junction potential between aqueous reference electrode and the ethanol/water solvent as well as the medium activity effect for the transference of the positive ion from water to the ethanol/water solvent. A δ

of -1.84 produced the very good fit shown in Fig. 3.6 where the circles are the pHi readings and the straight line is the calculated $pa_{H+}* + \delta$. This titration and activity fitting demonstrate that pHi readings can be reproducible and can be interpreted quantitatively.

A summary of the relevant proton exchange reactions in ethanol with very low concentrations of water ($<1\%$) is as follows:

Proton Distribution (**10**):
$$C_2H_5OH_2{}^+ + H_2O \Leftrightarrow C_2H_5OH + H_3O^+ \qquad\qquad K_+ = 285$$
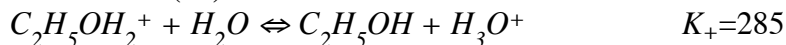
Ethoxide/Hydroxide Equilibrium (**18**):
$$C_2H_5OH + OH^- \Leftrightarrow C_2H_5O^- + H_2O \qquad\qquad K_- = 2$$
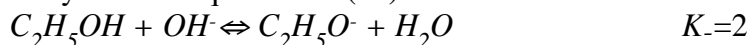
Pure Ethanol Autoprotolysis (**17**):
$$2\,C_2H_5OH \Leftrightarrow C_2H_5OH_2{}^+ + C_2H_5O^- \qquad\qquad pK_{SEtO} = 19$$
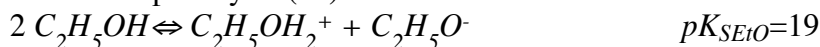
Pure Water Autoprotolysis (**17**):
$$2\,H_2O \Leftrightarrow H_3O^+ + OH^- \qquad\qquad pK_{SW} = 14$$

Autoprotolysis of combined solvent (0.995/0.005 wt. ethanol/water):
$$C_2H_5OH + H_2O \Leftrightarrow C_2H_5O^- + H_3O^+$$
$$and \quad 2C_2H_5OH \Leftrightarrow C_2H_5O^- + C_2H_5OH_2{}^+ \qquad pK_S = 13$$
$$and \quad 2H_2O \Leftrightarrow OH^- + H_3O^+$$
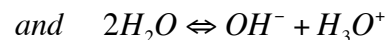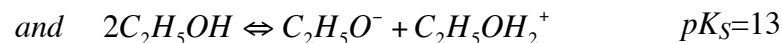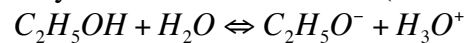
3.4 Surface Charge Development of Alumina in Ethanol

3.4.1 Surface Charge with the Addition of HCl

3.4.1.1 Zeta Potential

Mobilities measured by electrophoresis are given in table 1 below. Without an independent mobility standard in ethanol the accuracy of the measurements could not be estimated, however, when a symmetric electroosmotic flow profile was established in the measurement capillary, reproducibility was within ±5%.

The conductivity was measured using a commercial parallel plate conductivity cell with a cell constant of 0.107cm^{-1}. The edges of the cell were open and, therefore, due to edge effects there is a great deal of uncertainty in the conductivity measurements below $4 \mu \text{S/cm}$. Above this the estimated accuracy is ±10%. The first point represents only the washed alumina in ethanol with no added HCl and no conductivity measurement was made. Previous measurements of this concentration of alumina in ethanol have shown conductivity less than $0.05 \mu \text{S/cm}$.

The molar ionic concentration in the bulk solution was then calculated with the Fuoss and Onsager equation (**11**) using values for HCl in 99.5wt.% ethanol linearly interpolated from the data of DeLisi, et al. (**10**) taken at 99.60 and 99.41 wt.% ethanol: $\Lambda_O = 53.40$, $a_O = 3.64$ and $K_A = 21$.

The bulk molar ionic strength was then used to calculate the Debye length, κ^{-1} eq. [3.1]. The relative double layer thickness, κa, was calculated using the average particle radius of 150nm. The non-dimensional reduced mobility **E** was calculated from the electrophoretic mobility, u_E eq. [3.2]. These values were then used to find the reduced potential, $\tilde{\zeta}$, graphically from the charts for a 1:1 electrolyte published by O'Brien and White. (**12**) The zeta potential was then calculated in millivolts using eq. [3.3]. (Definitions of the terms used in these and all subsequent equations can be found at the head of the chapter.)

$$\kappa = \left[\frac{2e^2 \rho_\infty z^2}{\varepsilon_o \varepsilon_r kT} \right]^{\frac{1}{2}}$$ [3.1]

$$\mathbf{E} = \frac{3\eta e}{2\varepsilon_r \varepsilon_o kT} \cdot u_E$$ [3.2]

$$\tilde{\zeta} = \frac{ez\zeta}{kT}$$ [3.3]

Table 3.1

Calculation of zeta potential from electrophoretic mobility.

Conductivity (μS/cm)	Bulk Molarity (mMol)	Debye Length	κa	Mobility (μm·cm/V·s)	Reduced Mobility	Reduced Potential	Zeta Potential
< 0.1			< 1	0.81	2.27	2.36	61 mV
0.46	0.009	58.5 nm	2.6	1.00	2.80	3.55	91 mV
1.23	0.023	36.0 nm	4.2	1.00	2.80	3.38	87 mV
4.91	0.095	17.7 nm	8.5	0.88	2.46	2.28	59 mV
12.02	0.242	11.1 nm	13.5	0.84	2.35	1.97	51 mV
19.81	0.400	8.6 nm	17.4	0.74	2.07	1.65	42 mV

Zeta potential was also measured using an electroacoustic instrument that measures the colloid vibration current and calculates the particle zeta potential based on a thin double layer assumption. The inputs to this instrument are the suspension volume fraction, solvent and particle densities, and average particle size. The instrument controls an automatic titrator and its output is the volume of an HCl solution titrated into the suspension and the calculated zeta potential.

The quantity of acid titrated into the suspension was first converted into bulk concentration of HCl by interpolation of the raw adsorption data as shown in the section on acid adsorption below. Using the resulting zeta potential vs. bulk ionic strength a chloride adsorption isotherm was calculated and used to recalculate the bulk ionic strength from the quantity of acid titrated in. This data was then used as the bulk free molarity of HCl on the horizontal axis in Fig. 1.

Concurrent with the calculation of bulk ionic strength, the zeta potential must be adjusted for double layer thickness effects. The zeta potential reported by the instrument is calculated based on a thin boundary layer assumption (**13**) and significantly underestimates the actual zeta potential for the range of double layer thicknesses considered here ($\kappa a \approx 1$ to 20). Sawatzky and Babchin (**14**) have developed theory for arbitrary double layer thickness. A key component of this theory is a function, not reproduced here, $f_1(\kappa a, a/\delta)$ which gives the ratio of the actual dynamic electrophoretic mobility to the mobility calculated assuming a thin double layer. The parameter δ, eq. [3.4], is a characteristic distance related to the distance over which the pressure waves generated by an oscillating particle decay. As the parameter $a/\delta \rightarrow 0$ the function f_1 goes to the function $f(\kappa a)$ of Henry (**15**) for calculating the DC electrophoretic mobility of particles with intermediate thickness double layers. The electroacoustic measurements used here were performed at a frequency of 1 MHz, which for ethanol will give a value for δ of 1.65 μm. Using the average particle radius, a, of 0.15μm and evaluating f_1 at its limits shows that the error in using the adjustment factor of Henry over the more complex formulation of Sawatzky and

Babchin is everywhere less than 10%. Therefore the adjustment of zeta potential values was done using values for the Henry formula interpolated from tabulated values. The resulting values are shown in Fig. 3.7, showing the agreement between the different zeta potential measurement methods.

$$\delta = \left(\frac{2\eta}{\rho\omega} \right)^{\frac{1}{2}}$$ [3.4]
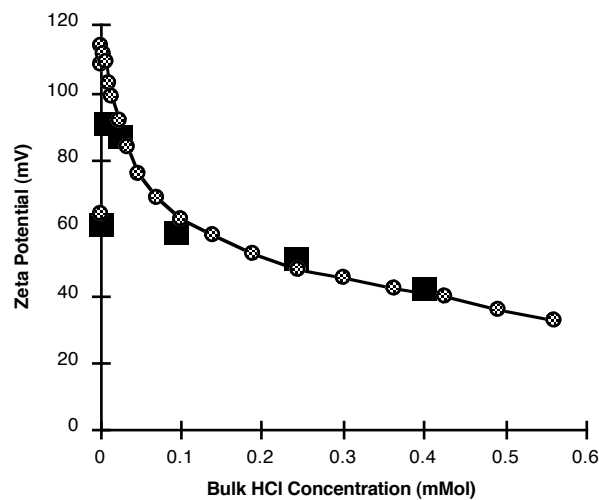
Fig. 3.7 Solid squares are zeta potentials calculated from electrophoretic mobility, circles are calculated from electroacoustic current using thin boundary layer theory and adjusted using the correction factor of Henry·
(**12**)

When this data is replotted as a function of $-\log_{10}$ of the concentration of HCl in the bulk solution it appears reasonable that for bulk molar concentrations of HCl greater than 10μMol the zeta potential can be modeled as a straight line. Since the deviation between the straight line model and the data is less than the expected error in measuring and calculating the zeta potential ($\approx$10%), values from the straight line approximation will be used in the subsequent calculations.
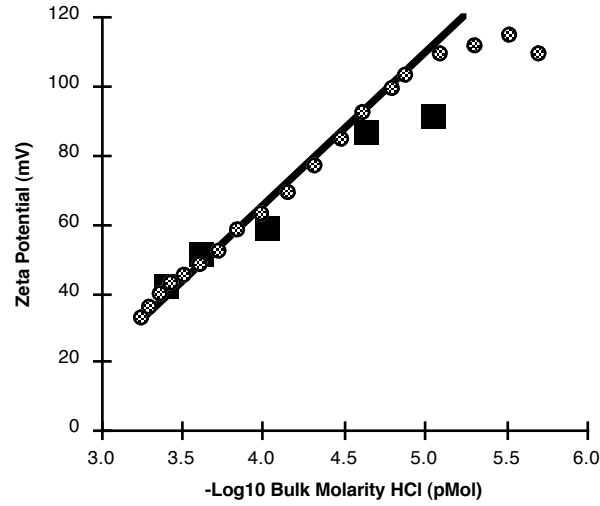
Fig. 3.8 Solid squares are zeta potentials calculated from electrophoretic mobility, circles are calculated from electroacoustic current using thin boundary layer theory and adjusted using the correction factor of Henry (**12**).

3.4.1.2 Surface Charge

Given the surface potential and the bulk ionic strength of the solvent, the surface charge density can be calculated. Loeb, et al. (**16**) used a numerical algorithm to calculate the surface charge density of a spherical colloid particle for a range of potentials and double layer thicknesses. They also presented an empirical formula, eq. [3.5], that can be used to estimate the results of their numerical calculations for surface charge density in a 1-1 electrolyte system to within 1% for the range of potential and double layer thickness values being considered here. We have used this equation to calculate the particle surface charge density, q, in milliCoulombs/meter^2 for the zeta potentials shown in Fig. 3.8 above. The results are shown in the graph in Fig. 3.9. These values were calculated using the linear zeta potential approximation except for the three data points below 10μMol HCl which diverge from the linear model. These points were calculated directly from the adjusted electroacoustic data and are shown as circles on the graph in Fig. 3.9.

$$q = \frac{\varepsilon_o \varepsilon_r kT}{e} \kappa \left(2\sinh\left(\tfrac{1}{2}\tilde{\xi}\right) + \frac{4}{\kappa a}\tanh\left(\tfrac{1}{4}\tilde{\xi}\right) \right)$$ [3.5]
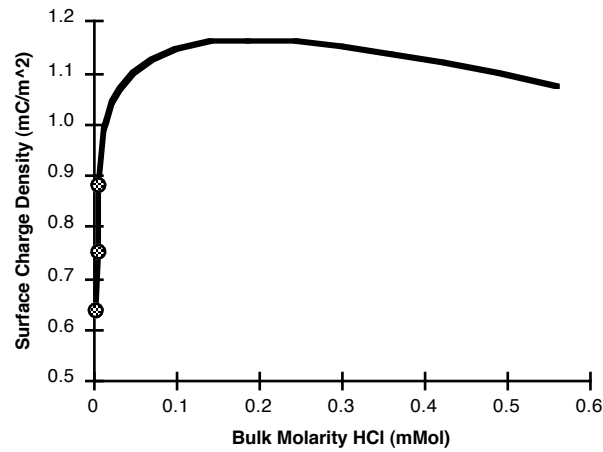
Figure 3.9 Surface charge density milliCoulombs/m^2. Circles are data points for bulk molarity less than 10μMol that do not correspond to the linear approximation shown in figure 2.

3.4.1.3 Acid Adsorption

Adsorption of HCl to the powder surface was determined using conductivity measurements. HCl was titrated into the 99.5/0.5 wt. % ethanol/water solvent mixture without alumina. This conductivity as a function of HCl addition is shown as round points in Fig. 4. The line labeled (1) superimposed on these points is the predicted conductivity/concentration curve using the Fuoss and Onsager (**11**) equation for an associated electrolyte, eq. [3.6] (see also Appendix A). It is calculated using values for HCl in 99.5wt.% ethanol linearly interpolated from the data of DeLisi, et al. (**10**) taken at 99.60 and 99.41 wt.% ethanol: $\Lambda_O = 53.40$, $a_O = 3.64$Å and $K_A = 21$.

$$\Lambda = \Lambda_o - S(c\gamma)^{\frac{1}{2}} + E'c\gamma \ln(6E_1'c\gamma) + Lc\gamma - K_A c\gamma f^2 \Lambda \qquad [3.6]$$

The square data points are for the same conditions with the addition of 1 vol% alumina powder. The molarity of HCl in the solution is calculated from the conductivity. The difference between the HCl in solution and the total HCl titrated is taken to be the surface adsorption of the powder.
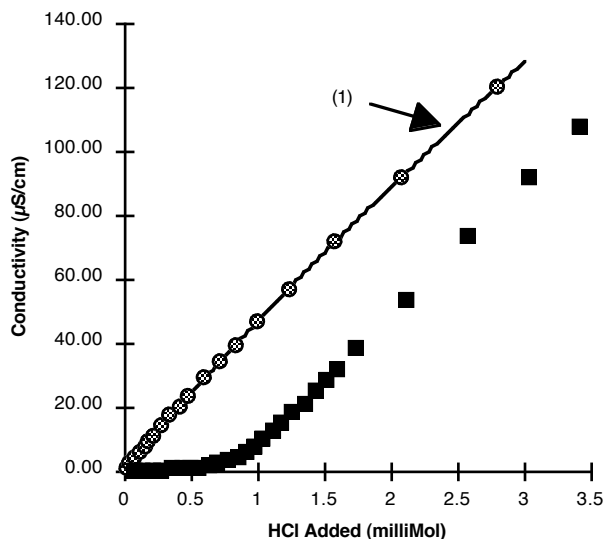
Figure 3.10 Solution conductivity with and without alumina
powder present. Line labeled (1) is Fuoss and Onsager (**11**)
equation plotted based on data from DeLisi and Goffredi (**10**).

3.4.1.4 Reversibility of Adsorption

 Although the disappearance of HCl from solution in the presence of alumina can be
measured accurately by conductometry, the question remains whether this is by surface
adsorption or by an irreversible chemical reaction either changing the composition of the
surface or converting the HCl to non-ionizing species in solution.

 The reversibility of the adsorption was tested by pHi titration as shown in Fig. 3.11.
HCl was titrated into ethanol with and without alumina. pHi readings were unstable until a
concentration of HCl in solution of 0.02 mMol was reached (Conductivity $\approx 1\,\mu$S/cm).
Above that the difference between the HCl titrated with and without alumina at equal pHi
readings confirms the adsorption of HCl as determined by conductivity. Back titration of
the solutions with KOH then shows the buffering of the pHi change in the alumina
suspension due to the adsorbed HCl.

 As a further check for other chemical reactions, the supernatants of alumina
suspensions were checked by plasma spectroscopy for dissolved species containing
aluminum. Suspensions of alumina in ethanol were prepared in ethanol alone, ethanol with
up to 0.5 mMol KOH, and ethanol with up to 2.5 mMol added HCl. Supernatant was
removed from the samples two hours, one day and ten days after preparation for analysis.
No aluminum was detected in the solvent from any of the samples above a 90% confidence
level minimum detection limit of 0.05 mMol aluminum. This indicates that the adsorption

does not involve reactions leading to a significant dissolution of aluminum from the surface.
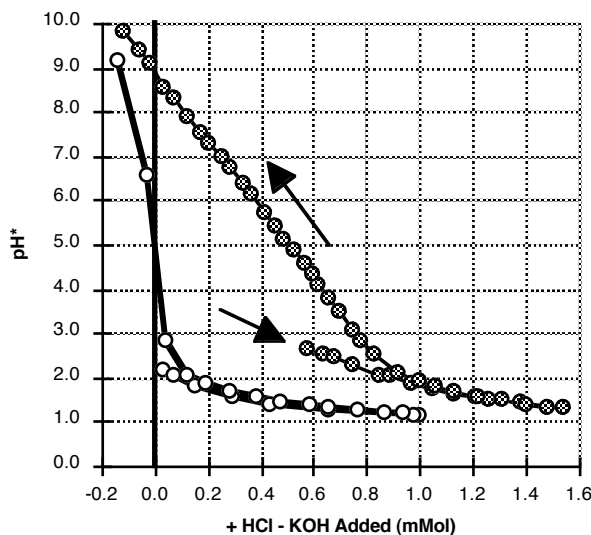
Fig. 3.11 Indicated pH, pHi, in ethanol + 0.5 wt. % water. Forward titration with HCl, back titrated with KOH. Open circles ethanol only, filled circles ethanol plus 1 vol. % alumina powder, surface area ≈320m²/liter.

3.4.1.5 Notes on Concepts and Terminology

Before beginning further analysis of the data it will be useful to define some of the basic concepts used here regarding the surface, diffuse layer and solution chemistry in an ethanol-water solvent.

The particle is presumed to have a fixed number of surface sites which are either unoccupied, occupied by a proton, or occupied by a proton and negative ion. There are no assumptions about the nature of the bonding nor the invocation of an electrostatically bonded Stern or Helmholtz layer. All ions that are not adsorbed to a surface site are presumed to be in solution and outside the shear plane. Thus the terms 'on the surface' or 'adsorbed to the surface' imply ions that are rigidly attached to the particle surface and are inside the shear plane for electrophoretic measurement. The term 'at the surface' is then used to imply activities and potentials immediately adjacent to the surface but still dissolved and moving freely in the solvent, therefore outside the shear plane. As a result, the zeta potential, the potential measured at the shear surface, will be assumed to be equal to the surface potential.

The standard continuum assumptions are made, first that the surface charge is continuous across the surface and second that the solvent is a continuous dielectric medium

with the ions behaving as point charges. The second assumption seems reasonable given that at the maximum ionic strength where we have measured a zeta potential in this study the Debye length is 7.3 nm, about twenty times the 3.65 Å distance of closest approach of oppositely charged ions in solution determined by conductometry. The assumption that is likely to be violated first is that of a uniform, continuous surface charge. For the measurements with HCl the calculated surface charge of ≈ 1 mC/m^2 translates to one positive charge per 160 nm^2 or a uniformly distributed charge-charge separation distance of 13 nm. This is close to two times the Debye length mentioned above.

Notation in square brackets indicates either volume concentration in Mol/m^3 (milliMolar) or surface concentration in Mol/m^2. Activity of ions in the bulk solution is calculated as the product of the concentration and the Debye-Hückel mean molar activity correction factor, $f_\pm$, calculated using eq. [3.7]. Where the concentration is multiplied by an activity correction factor it is implicitly divided by the standard concentration to give a unitless activity. It is assumed that where the solution is charge balanced the activity correction factors for the positive and negative ions are equal. Where the solution is not charge balanced, such as in the particles electrostatic boundary layer, the activity correction factors for positive and negative ions, $f_+ f_-$, cannot be asumed to be equal, however, there will be no attempt to calculate either these correction factors or the surface ionic concentrations. Only the product of the two, the surface activity, will be calculated from the bulk activity using the Boltzmann relation, eq. [3.11].

$$-\ln f_\pm = \frac{\kappa e^2}{8\pi\varepsilon_o\varepsilon_r kT\left(1+\kappa a_o\right)} \qquad [3.7]$$

Finally, a note on the behavior of acids and bases in ethanol-water solvents. In the case of a Brønsted acid, the proton will have a greater affinity for water molecules in the solvent. Based on the equilibrium constant calculated in (**10**), in a 99.5/0.5 wt. % ethanol/water solvent mixture the protonated species will be 70 wt. % H_3O^+ and 30 wt. % H_2EtO^+. For a Brønsted base such as KOH in the same solvent mixture the negative ions will be greater than 99.9 wt. % ethoxide and the balance hydroxide, based on the equilibrium constant in (**18**). In the following discussion references to hydronium and ethoxide ions will implicitly include equilibrium concentrations of the ethoxonium and hydroxide ions, respectively.

3.4.1.6 Modeling Adsorption and Surface Charge with HCl

When the alumina powder is first put into the ethanol it develops a significant surface charge. The hypothesis for the development of this charge is that sites on the

alumina surface acts as a Lewis base, an electron donor. Ethanol molecules are adsorbed to these sites by their polar hydroxyl group.
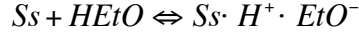
$$Ss + HEtO \Leftrightarrow Ss \cdot H^+ \cdot EtO^-$$

There is then a equilibrium dissolution of ethoxide ions from the surface leaving protonated surface sites and a positive surface charge. The equilibrium for this reaction is given in eq. [3.8].

$$Ss \cdot H^+ \cdot EtO^- \Leftrightarrow Ss \cdot H^+ + EtO_S^-$$

$$\mathbf{K}_1 = \frac{[Ss \cdot H^+] \, f_- [EtO_S^-]}{[Ss \cdot H^+ \cdot EtO^-]} \qquad [3.8]$$

As HCl is added to the suspension there is a very rapid rise in the surface charge and zeta potential. This is likely due to a sharp reduction of ethoxide concentration in the bulk of the solvent due to reaction with the added HCl.

$$EtO_B^- + H_B^+ \Leftrightarrow HEtO$$
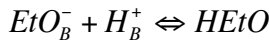
As shown in §3.3.6 the $-\log_{10}$ of the equilibrium constant for this reaction, pK_S, is 13 for the 99.5/0.5 ethanol/water misture used here.

Simultaneously there is an adsorption of chloride ions to the surface by substitution of chloride for the ethoxide ions at the surface. Surface charge now becomes principally a function of the equilibrium dissolution of chloride ions from the surface.

$$Ss \cdot H^+ \cdot Cl^- \Leftrightarrow Ss \cdot H^+ + Cl_S^-$$

$$\mathbf{K}_2 = \frac{[Ss \cdot H^+] \, f_- [Cl_S^-]}{[Ss \cdot H^+ \cdot Cl^-]} \qquad [3.9]$$

Equations [8] & [9] can be combined to yield eq. [10], showing that the adsorption of chloride can be modeled as a substitution of a chloride ion for an ethoxide ion on the surface, with the adsorption ratio determined by the ratio of dissolved chloride to ethoxide at the surface.

$$\frac{[Ss \cdot H^+ \cdot Cl^-]}{[Ss \cdot H^+ \cdot EtO^-]} = \frac{\mathbf{K}_1}{\mathbf{K}_2} \frac{f_- [Cl_S^-]}{f_- [EtO_S^-]} \qquad [3.10]$$

From conductivity measurements we know the bulk activity of the chloride ion, and with the zeta potential, the surface activity of chloride can be calculated using the Boltzman relationship and the bulk activity coefficient.

$$f_-\left[Cl_S^-\right] = f_\pm\left[Cl_B^-\right]\exp\left(\frac{e\zeta}{kT}\right)$$
[3.11]

Then it will be assumed *a posteriori* that the surface ethoxide concentration can be estimated as a constant multiplied by an exponential of the zeta potential.

$$f_-\left[EtO_S^-\right] = K_{EtO}\exp\left(\frac{e\zeta}{2kT}\right)$$
[3.12]

Substituting [3.11] and [3.12] into [3.10] we generate an equilibrium equation in which the ratio of chloride to ethoxide adsorbed to the surface is a function of a constant and a lumped parameter which is the bulk chloride concentration times an exponential of the zeta potential, as shown in eq. [3.13].

$$\frac{\left[Ss\cdot H^+\cdot Cl^-\right]}{\left[Ss\cdot H^+\cdot EtO^-\right]f_\pm\left[Cl_B^-\right]\exp\left(\frac{e\zeta}{2kT}\right)} = \frac{K_1}{K_2 K_{EtO}}$$
[3.13]

To simplify the following equations all of the constants will be collected into one lumped parameter and a simplified expression for the chloride dependence is given, eq.s [3.14] and [3.15] respectively. Note that the function $f(Cl)$ depends on both the bulk chloride concentration and the zeta potential.

$$K_L = \frac{K_1}{K_2 K_{EtO}}$$
[3.14]

$$f(Cl) = \left[Cl_B^-\right]\exp\left(\frac{e\zeta}{2kT}\right)$$
[3.15]

Assuming that there are a fixed number of surface sites and that these can be broken down into sites occupied by an ethanol molecule, HCl, a proton or unoccupied, the total surface site concentration is given by eq. [3.16].

$$\left[Ss_{Tot}\right] = \left[Ss\cdot H^+\cdot EtO^-\right] + \left[Ss\cdot H^+\cdot Cl^-\right] + \left[Ss\cdot H^+\right] + \left[Ss\right]$$
[3.16]

A further approximation can be made assuming that the number of surface sites that are only occupied by a proton or are unoccupied are small relative to the total number of surface sites. With these approximations eq.s [3.14], [3.15], [3.16] can be substituted into

eq. [3.13] and algebraically manipulated to obtain an equation in the form of a Langmuir adsorption isotherm, eq. [3.17].

$$\left[Ss\cdot H^+\cdot Cl^- \right] = Ss_{Tot} \frac{\mathbf{K}_L f(\mathrm{Cl})}{1 + \mathbf{K}_L f(\mathrm{Cl})} \qquad [3.17]$$

By plotting the inverse of this equation, which is linear, eq. [3.18], the values for the total number of surface sites and the lumped equilibrium parameter $\mathbf{K}_L$ can be estimated by a least squares fitting. This is plotted in Fig. 3.12(a) for data points taken at conductivities above 2 μS/cm (≈ 0.04 mMol bulk molar concentration). The resulting values are $Ss_{Tot} = 3.48$ μMol/m^2 and $\mathbf{K}_L = 7.7$. The direct form of the equation, eq. [3.17], is plotted using these parameters and is shown in Fig. 3.12(b). The actual adsorption data points are superimposed on this curve showing the level of fit.

$$\left[Ss\cdot H^+\cdot Cl^- \right]^{-1} = Ss_{Tot}^{\;-1} + \left(\mathbf{K}_L Ss_{Tot} f(\mathrm{Cl}) \right)^{-1} \qquad [3.18]$$
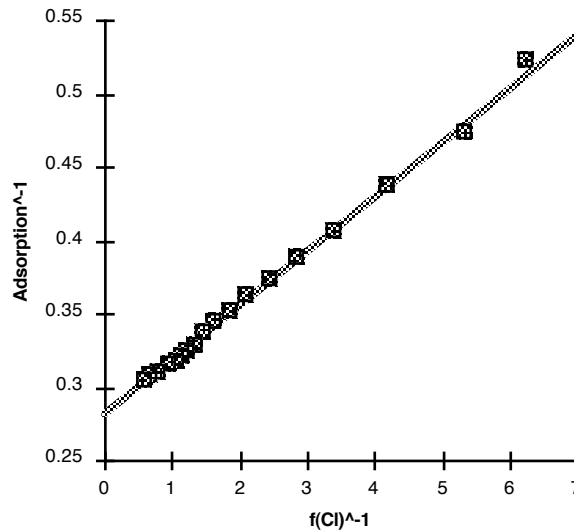
Fig. 3.12(a) Inverse of surface adsorption data for bulk molar HCl concentrations above 0.04 mMol plotted as a function of inverse of eq. [3.15]. Straight line fitted by least squares.
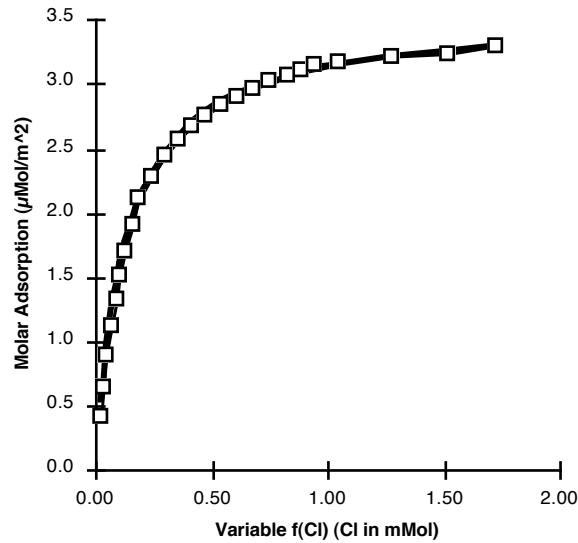
Fig. 3.12(b) Surface adsorption data plotted as a function of Eq. [3.14] superimposed on a fitted plot of the adsorption isotherm, Eq. [3.17].

Having developed an equation which accurately describes the chloride adsorption, it is now necessary to review the assumptions that were made in the derivation.

The assumption that the number of surface sites occupied only by a proton is small relative to the total number of surface sites does appear reasonable. The maximum surface charge density measured here is 1.14 mCoulombs/m^2 or 11.8 nanoMol/m^2. This is 0.34% of the total number of surface sites estimated by the chloride adsorption isotherm.

The assumption that the number of unoccupied surface sites is small is more difficult to address as there is no direct measurement of empty surface sites. However, if the equilibrium constant for the dissolution of an ethanol molecule from a surface site, eq. [19], is significantly larger than the equilibrium constant for the removal of a proton from a surface site by either an ethanol or water molecule, eq. [3.20], it can be shown that the concentration of empty surface sites will not affect the results derived here.

$$Ss \cdot H^+ \cdot EtO^- \Leftrightarrow Ss + HEtO \qquad [3.19]$$

$$Ss \cdot H^+ + H_2O \Leftrightarrow Ss + H_3O^+ \qquad [3.20]$$

The assumption that there are a fixed number of surface sites is supported by the excellent fit of the adsorption data to a standard isotherm model.

It was also assumed that there is an equilibrium between the surface charge, free chloride ion concentration at the surface, and the total adsorbed chloride. If this is true the value of K_2 calculated from eq. [3.9] should be a constant over the range where there is a significant level of chloride adsorbed to the surface.

$$\mathbf{K}_2 = \frac{\left[Ss \cdot H^+\right] f_-\left[Cl_S^-\right]}{\left[Ss \cdot H^+ \cdot Cl^-\right]} \qquad [9]$$

As can be seen from the plot in Fig. 3.13, the calculated value of $\mathbf{K}_2$ varies by $\approx$ $\pm 10\%$, however, although the denominator is known to within a percent over most of the range, the numerator is the product of two values that are an exponential function of the zeta potential. This makes the calculated value of this function very sensitive to the magnitude of the zeta potential. A change of 5% in the value of the zeta potential at 100 mV leads to a 30% change in the calculated value of $\mathbf{K}_2$. This sensitivity to a $\pm 5\%$ change in the zeta potential is also plotted in Fig. 3.13. While the data does not conclusively prove that $\mathbf{K}_2$ is a constant, this assumption seems reasonable and is well within the limits of measurement error for the data used here.
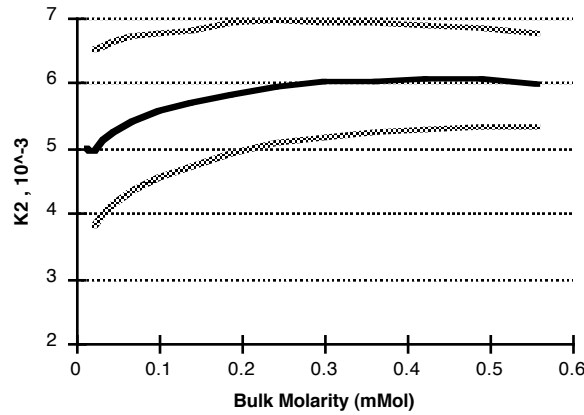
Fig. 3.13 Plot of $\mathbf{K}_2$ from Eq. [9]. Quantities are in Moles or Mol/m^2, as appropriate. Gray lines show the sensitivity of the calculation to a $\pm 5\%$ change in zeta potential.

Justification of the next two assumptions is somewhat more involved, and they will be treated together. The first is that there is an equilibrium between surface adsorbed ethanol, protonated surface sites and dissolved ethoxide ions at the surface eq. [3.8]. The second is that the concentration of the ethoxide ion at the surface changes in proportion to the square root of the Boltzmann relation of the zeta potential eq. [3.12].

$$\mathbf{K}_1 = \frac{\left[Ss \cdot H^+\right] f_-\left[EtO_S^-\right]}{\left[Ss \cdot H^+ \cdot EtO^-\right]} \qquad [3.8]$$

$$f_-\left[EtO_S^-\right] = K_{EtO} \exp\left(\frac{e\zeta}{2kT}\right) \qquad [3.12]$$

One way of testing these assumptions is to substitute eq. [3.12] into eq. [3.8] and calculate the value K_1/K_{EtO} to see how closely this approximates a constant over the range of HCl concentrations used here. The result of this calculation as shown in Fig. 3.14 is within ±8% of a constant. As with K_2 above, this is a very sensitive function of zeta potential and the assumption that the value K_1/K_{EtO} is a constant does not appear unreasonable.
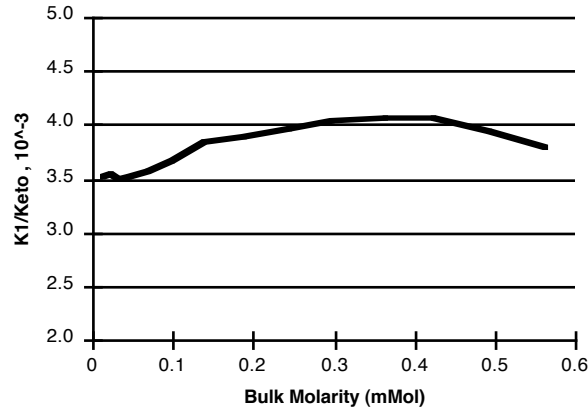
Fig. 3.14 Plot of K_1/K_{EtO} from equations [8] & [12]. Variation around the average value is ±8%.

Although a theoretical justification can be made for why the surface concentration of the ethoxide ion should be approximated by eq. [3.12], the best test of this assumption is to return to eq. [3.10], substitute eq. [3.8] for the surface ethoxide concentration, and recalculate the adsorption isotherm. Although there is insufficient data to estimate the absolute ethoxide concentration at the surface, and therefore a value for K_1, the adsorption can be plotted as a function of the surface chloride concentration divided by the ethoxide concentration over K_1. To do this, eq. [3.18] is replotted replacing f(Cl) with f'(Cl) below where f'(Cl) is given by eq. [3.21] and plotted in Fig. 3.15. The fit to a straight line is slightly worse than shown in Fig. 3.12, particularly at the extrema, however, the assumption embodied in eq. [3.12] has been eliminated and it has been shown that surface charge and the adsorption of HCl to the surface can be modeled using only the very basic equations [3.8], [3.9] and [3.16].

$$f'(Cl) = \frac{f_{\pm}\left[Cl_B^-\right]\exp\left(\frac{e\zeta}{kT}\right)}{\left(f_-\left[EtO_S^-\right]\middle/\mathbf{K}_1\right)}$$

[3.21]

$$= \frac{\left[Ss\cdot H^+\right] \times f_{\pm}\left[Cl_B^-\right]\exp\left(\frac{e\zeta}{kT}\right)}{\left[Ss_{Tot}\right]-\left[Ss\cdot H^+\cdot Cl^-\right]}$$
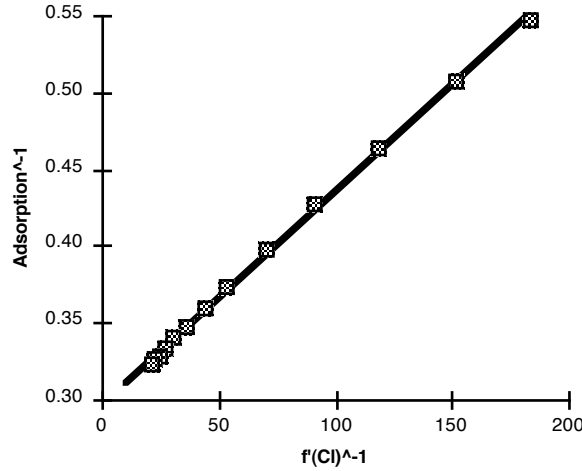
Fig. 3.15 Inverse of surface adsorption data for bulk molar HCl concentrations above 0.04 mMol plotted as a function of inverse of Eq. [321]. Straight line fitted by least squares.

The one significant reaction that has not yet entered into the discussion is the autoprotolysis equilibrium for ethanol, eq. [3.22]. This controls the ethoxide ion concentration given the concentration of the protonated species and vice versa. If the surface proton activity is calculated from the bulk concentration and zeta potential using the Boltzmann relation, eq. [3.23], this activity would be expected rise by four orders of magnitude over the measurement range, as plotted in Fig. 3.16. If the autoprotolysis equilibrium eq. [3.22] is valid at the surface, then the activity of the ethoxide ion at the surface would be expected to decline proportionally by four orders of magnitude.

$$HEtO \Leftrightarrow EtO_B^- + H_B^+$$
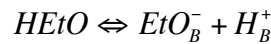
$$\mathbf{K_S} = \frac{f_{\pm}^2\left[H^+\right]\left[EtO^-\right]}{\left[HEtO\right]}$$

[3.22]

$$f_+\left[H_S^+\right] = f_{\pm}\left[H_B^+\right]\exp\left(\frac{-e\zeta}{kT}\right)$$

[3.23]
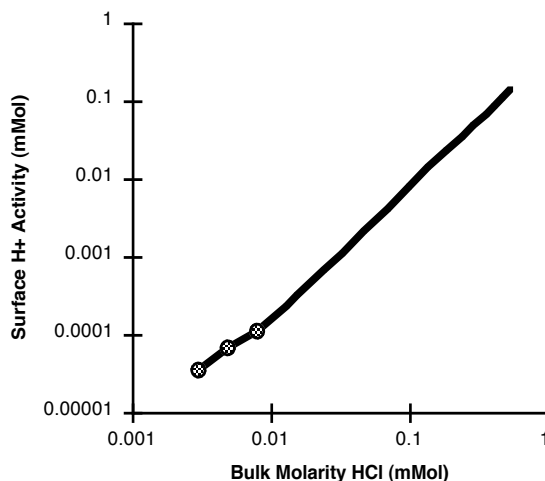
Fig. 3.16 Log/Log plot of surface activity of H+ ion calculated from bulk concentration using the Boltzmann relation.

That, however, contradicts the model developed above where the ethoxide concentration at the surface is set by a surface equilibrium reaction. When the relative change in ethoxide concentration is plotted using equations [3.8] & [3.16] in Fig. 3.17, the ethoxide concentration is seen to change by only one order of magnitude. Even further, over the range of bulk HCl concentrations from 0.01 to 0.56 milliMolar, the predicted concentration of the proton at the surface is seen in Fig. 3.16 to increase by a factor of more than one thousand while the relative ethoxide concentration as shown in Fig. 3.17 declines by less than a factor of 7.

$$\frac{f_-\left[EtO_S^-\right]}{\mathbf{K}_1} = \frac{\left[Ss_{Tot}\right] - \left[Ss \cdot H^+ \cdot Cl^-\right]}{\left[Ss \cdot H^+\right]} \qquad [3.8, 3.16]$$
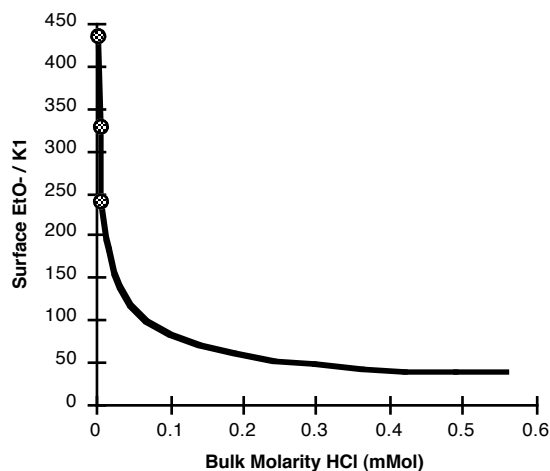
Fig. 3.17 Relative surface activity of EtO⁻ ion calculated from surface equilibrium equations [3.8], [3.16].

This contradiction only exists if the autoprotolysis equilibrium constant is taken to be constant. If this constant is higher at the surface than in the bulk by three orders of magnitude or more, then this contradiction disappears. In other words, our model of surface adsorption and charge formations remains consistent if the surface also acts to catalyze the autoprotolysis reaction of ethanol.

This is not a large jump to make given that the first step of the catalysis reaction has already been proposed as the charging mechanism for the alumina surface in the pure solvent. As proposed above, an ethanol molecule adsorbs to the surface and desorbs as an ethoxide ion leaving a proton on the surface. This gives the particles their positive surface charge. The next step would be for some of the protons on the surface to desorb as either a hydronium or protonated ethanol ion. These two ions would then diffuse outward a finite distance from the surface and react in solution, re-forming a neutral ethanol molecule. The voltage gradient in the double layer around the particle would accelerate the outward diffusion of the positive ions while retarding the outward diffusion of the ethoxide ions. The outward flux of positive ions from the surface would balance the inward flux of positive ions being consumed by reaction with ethoxide near the surface. The result is that the particle would be able to maintain a layer containing a significant concentration of ethoxide ions even when the bulk solution has a significant proton activity, and therefore an effectively zero concentration of ethoxide.

3.4.2 Behavior with Added KOH

Having examined the behavior with the addition of a simple acid, the next step is the addition of a simple base. Potassium hydroxide was chosen because it was readily available in a low water content ethanol solution. As was mentioned above, potassium hydroxide will react with ethanol, and in a 99.5/0.5 wt. % ethanol/water solvent it will convert to more than 99% potassium ethoxide. (**18**)

3.4.2.1 Conductivity

In order to measure ionic strengths in solution it is necessary to know the conductivity function for KOH in this concentration of ethanol. Lacking literature data, our first step was to measure the molar conductivity and fit this to the Fuoss & Onsager equation [3.6]. The curve was fitted to data points taken between concentrations of 1 and 6 milliMolar which lie in the most accurate measurement range for our system. An iterative fitting algorithm was used which converged unambiguously to the following values: Molar limit conductivity, $\Lambda_O = 40.75$; ionic distance of closest approach, $a_O = 3.50$; and ionic

association constant, $K_A = 0$. The result is plotted in Fig. 3.18 below along with the data points below 1 milliMolar not used in the fitting.
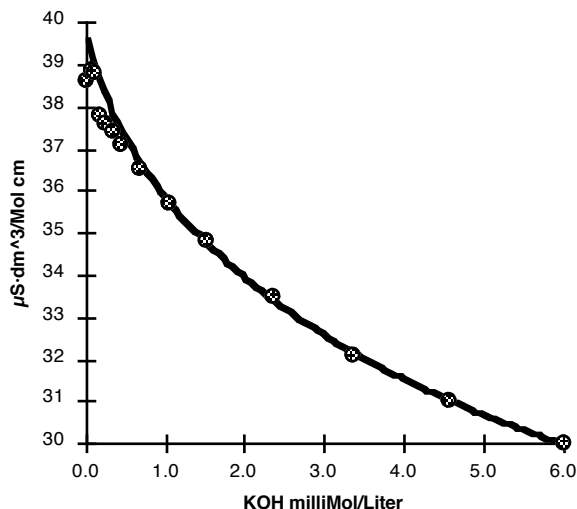
Fig. 3.18 Molar conductivity of KOH in 99.5/0.5 wt. % ethanol/water solvent. Circles are measured data points. Curve is Fuoss and Onsager equation fitted to data points between 1 and 6 milliMolar.

3.4.2.2 Adsorption

Adsorption data was obtained by measuring conductivity changes as KOH was titrated into a stirred 1 vol. % suspension of alumina powder. Concentration of KOH in solution was determined from conductivity measurements using the Fuoss-Onsager equation with the parameters fitted above. The difference between the KOH in solution and the total KOH added was taken as the powder surface adsorption.

Fig. 3.19 shows the molar conductivity as a function of the total KOH addition to the alumina suspension. This highlights the counterintuitive behavior of adsorption below an addition of 0.4 milliMolar. In this initial region the more KOH that is adsorbed the larger the proportion of additional KOH that will be adsorbed. This is exactly the opposite of what would be expected from a normal adsorption isotherm, and can be explained by first understanding the surface charging of the particles.
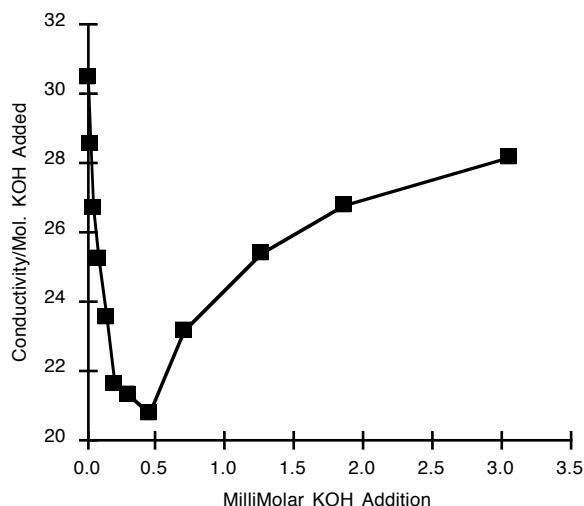
Fig. 3.19 Conductivity per molar addition of KOH to a 1 vol. % alumina suspension.

3.4.2.3 Zeta Potential

As a result of the low surface potentials and consequently low stabilities of alumina suspensions with added KOH, zeta potentials were measured only electroacoustically. Electroacoustic measurements were made in a continuously stirred suspension of 1 vol. % alumina powder. An automatic titrator was used to inject a solution of 0.1 molar KOH in 12 μl increments. An unadjusted zeta potential of 44.6 mV was measured before the titrator tip was inserted into the solution.

The bulk ionic strength was used to calculate the Debye length and Henry correction factor for the zeta potential as in the measurements with HCl above. The corrected zeta potential values as a function of bulk KOH concentration are shown in Fig. 3.20. At a bulk molar concentration of approximately 0.2 milliMolar the indicated zeta potential dropped below zero and went to -1.4 mV at the maximum KOH concentration measured.
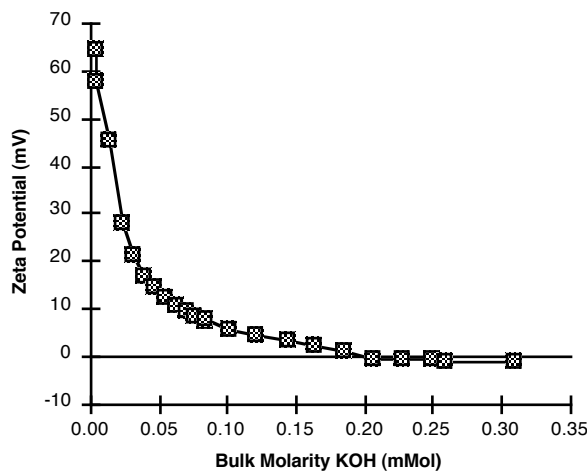
Fig. 3.20 Zeta Potential as a function of molarity of KOH in bulk solution.

3.4.2.4 Surface Charge

With the zeta potential and the bulk ionic strength, the surface charge density can be calculated using eq. [3.5]. The results are shown in Fig. 3.21. The zeta potential is again assumed to be the same as the surface potential.
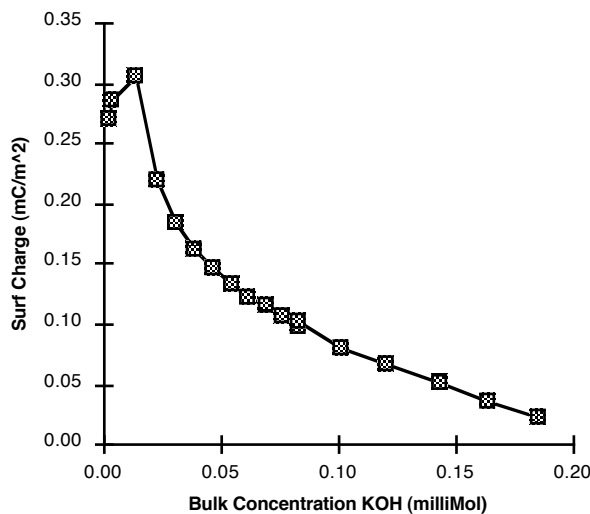
Fig. 3.21 Surface charge density in milliCoulombs per square meter.

3.4.2.5 Modeling Surface Charge with KOH

Returning to the model for surface charge of alumina in pure ethanol above, ethanol molecules adsorbed to the surface dissociate, and ethoxide ions desorb from the surface leaving a positive surface charge. Knowing the bulk ethoxide activity and zeta

potential, the surface ethoxide activity can be calculated using the Boltzmann relation, eq. [3.11]. With this it is now possible to plot K_1 from eq. [3.8], and this is shown in Fig. 3.22.

$$Ss \cdot H^+ \cdot EtO^- \Leftrightarrow Ss \cdot H^+ + EtO_S^-$$

$$K_1 = \frac{[Ss \cdot H^+] \, f_-[EtO_S^-]}{[Ss \cdot H^+ \cdot EtO^-]}$$
[3.8]
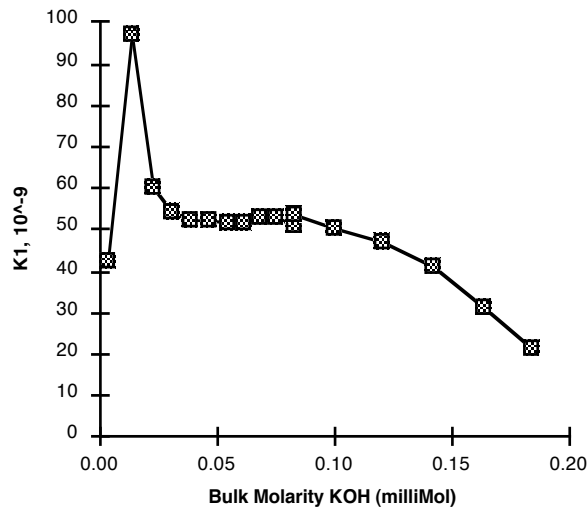
Fig. 3.22 Plot of K_1 from Eq. [3.8]. Quantities are in Moles or Mol/m^2, as appropriate.

Looking at this plot more closely, it can be seen that if the first three points at the lowest KOH concentrations and the last four points at the highest KOH concentrations can be neglected, then the remaining data points are well within 5% of a constant, as shown in Fig. 3.23. Moreover, there are very reasonable bases for believing that these points at the extremes can be neglected.
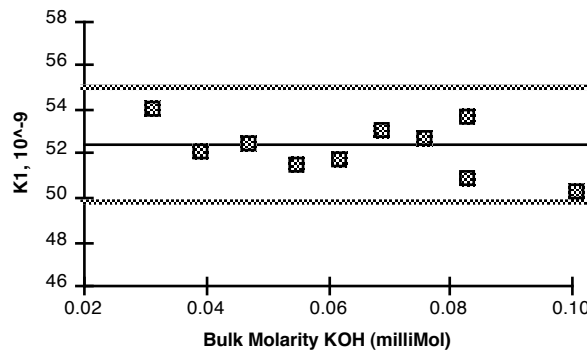
Fig. 3.23 Plot of K_1 from Eq. [3.8]. Range of zeta potentials from 21 to 5.7 mV, bulk conductivities from 1.3 to 4.1 μS/cm. Dashed line is average value of 5.25E-8. Gray lines indicate ± 5% from average.

The first three points in Fig. 3.22 have a relatively high degree of uncertainty both because of uncertainty of the exact quantity titrated in the initial injections of KOH titrant and the uncertainty of the interpolation of free molarity from adsorption data taken in a region where the conductivity is less that 1 μS/cm. Furthermore, if the hypothesis that the surface catalyzes the autoprotolysis of ethanol is correct, then at low ionic strengths in the bulk, the ionic strength at the surface cannot be calculated from the bulk. This adds an additional uncertainty to the surface charge density calculation which depends on knowing the ionic strength near the surface.

The final four data points plotted in Fig. 3.22 represent data points where the measured zeta potential is less than 5 mV. There are two easily identifiable sources of error in surface potential measurement at values this low; floccing of the particles, and the nature of the surface charge. DLVO calculations indicate that the interparticle repulsion goes to zero at a bulk molarity of 0.06. Therefore as zeta potential continues to drop and ionic strength to rise with further additions of KOH, it is reasonable to expect that floccing of the particles would cause the measured zeta potential to deviate from the actual value beyond this point. Furthermore, at the highest ionic strength/ lowest zeta potential point in Fig. 3.23, the uniform surface charge assumption implicit in the calculations performed here becomes questionable. At this point the zeta potential is 5.7mV and the bulk ionic strength 0.10 mMol, this gives a surface charge density of 8.1×10^{-5} C/m^2 and a Debye length of 17nm. If the charge sites are uniformly distributed across the surface, this gives a charge-charge separation distance of 46 nm, almost three times the Debye length.

So if the hypothesis is that the equilibrium of eq. [3.8] describes the particle surface charge, the test of this hypothesis is whether the value of $\mathbf{K}_1$ calculated from measured data is a constant. Given the above arguments, the range of data that supports the contention that $\mathbf{K}_1$ is a constant, as shown in Fig. 3.23, is actually better than might be expected.

3.4.2.6 Adsorption of KOH

As can be seen from Fig. 3.19 above, the marginal adsorption of KOH increases with increasing KOH concentration. This is only possible if adsorption is mediated by the positive K$^+$ ion. With the initial small additions of KOH, the positive surface potential repels the positive ions and little adsorption occurs. As more KOH is added, the surface potential drops and the surface concentration of K$^+$ rises many times faster than the concentration in the bulk. This leads to the inverse marginal adsorption behavior in the region where the particles have a positive and declining surface charge, illustrated in Fig. 3.19.

Without making any assumptions about the nature of the surface adsorption site for the potassium ion, the adsorption can be written as an equilibrium with a generic surface site Ss' as shown in eq. [3.24].

$$Ss' + K_S^+ \Leftrightarrow Ss' \cdot K^+$$

$$\mathbf{K}_K = \frac{[Ss \cdot K^+]}{[Ss'] f_+ [K_S^+]} \tag{3.24}$$

This can be rewritten in the form of a standard Langmuir adsorption isotherm, eq. [3.25].

$$[Ss \cdot K^+] = Ss_{Tot} \frac{\mathbf{K}_K f_+ [K_S^+]}{1 + \mathbf{K}_K f_+ [K_S^+]} \tag{3.25}$$

As above in the case of Cl⁻ adsorption, the inverse of eq. [3.25] is plotted and a straight line is fitted to the data by least squares. The result is a total surface adsorption of 2.4 μMol/m² and an adsorption equilibrium constant $\mathbf{K}_K$ of 1.8 with quantities in millimolar or millimoles/m².
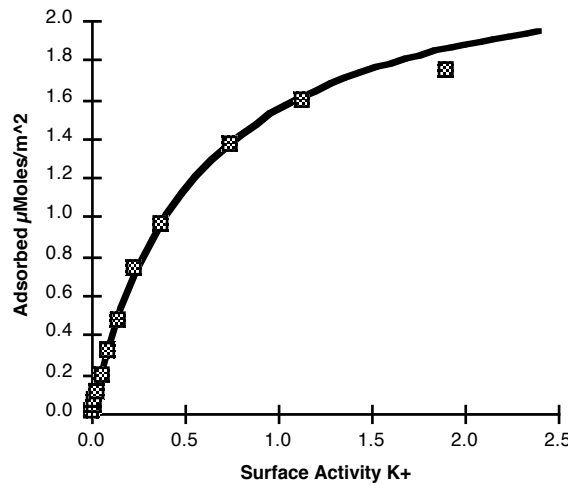
Fig. 3.24 Surface adsorption as a function of surface K⁺ activity.

What is interesting about this adsorption isotherm is that it appears to be a function only of the surface activity of the positively charged potassium ion, yet has no effect on the surface charge density. Over the concentration range shown in Fig. 3.23 where surface charge appears to be only a function of ethoxide concentration, the adsorption of K⁺ goes up from 2% to 60% (0.047 to 1.4 μMol/m²) of total surface sites, and the surface activity goes up by a factor of 70, from 0.011 to 0.75 mMolar. From this it is clear that the adsorption of K⁺ must be by some charge neutral mechanism. The adsorption of a K⁺ ion must either be accompanied by the adsorption of a negative ion or the desorption of a

positive ion and must occur in such a manner that it does not affect the ethoxide adsorption equilibrium.

One possible explanation for the absence of an effect of the K^+ adsorption on surface charge would be that the K^+ could only stably adsorb along with a negative ethoxide or hydroxide ion, eq. [3.26].

$$Ss' + K_S^+ + EtO_S^- \Leftrightarrow Ss' \cdot K^+ \cdot EtO^- \qquad [3.26]$$
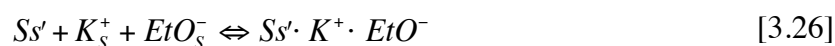
However this implies a dependency of adsorption on the ethoxide activity at the surface which is not supported by the data.

Another charge neutral mechanism would be the substitution of a potassium ion for the proton from a surface adsorbed ethanol molecule.

$$Ss \cdot H^+ \cdot EtO^- + K_S^+ \Leftrightarrow Ss \cdot K^+ \cdot EtO^- + H_S^+ \qquad [3.27]$$
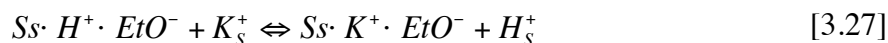
An argument against this mechanism would be that there should be an effect of the activity of the proton in the solution at the surface. This means that the adsorption should be a function of both the K^+ activity and the inverse of the ethoxide activity, but here again there is no indication of an ethoxide dependency in the data.

However, if we accept the hypothesis that the surface acts as a catalyst to dissociate ethanol molecules into adsorbed protons and ethoxide ions, then the adsorbed proton concentration will be a function of ethanol activity, which is effectively constant. This mechanism can then fulfill the two seemingly contradictory conditions that: 1) adsorption is only a function of activity of the positive potassium ion, and 2) the adsorption of the K^+ ion have no effect on the surface charge, which remains only a function of the ethoxide activity.

A second possible argument against this adsorption mechanism is that the number of sites does not match the number of sites determined by Cl^- adsorption. The total K^+ adsorption is 2.4 μMol/m^2 vs. a Cl^- adsorption of 3.5 μMol/m^2. This can potentially be explained by the size difference of the proton and the K^+ ion. An adsorption site density of 3.5μMol/m^2 would give a site-site spacing of 7.4 Å assuming a uniform hexagonal spacing of sites across the surface. Given that the sites are likely not uniformly spaced, it seems reasonable that there would be sites that would not fit the 3.0 to 3.3 Å diameter K^+ ion.

An implication of this adsorption mechanism and the lack of an effect of K^+ adsorption on the surface charge is that the positive and negative surface adsorption sites are separate sites and do not interact. There has to be a significant physical separation between positive and negative sites for the substitution of the much larger potassium ion to have no effect on the ethoxide adsorption. This in turn implies that surface adsorbed ethanol is completely dissociated into ethoxide and a proton adsorbed to different sites.

This again supports the picture of the alumina surface as a catalyst for the autoprotolysis of the ethanol-water solvent.

3.4.3 Conclusions Regarding Alumina Surface Charging

The picture of the behavior of the alumina surface in ethanol that emerges from the data above is as follows.

When the alumina powder is put into ethanol it adsorbs a coating of ethanol molecules. This is a dissociative adsorption process where a proton is adsorbed to a Lewis base site and an ethoxide ion is adsorbed to an adjacent Lewis acid site. Of the two ions, the ethoxide ion is more readily dissolved from the surface. This leaves behind a net positive charge on the particles in pure ethanol.

When alumina is put into ethanol it will adsorb a coating of ethanol dissociating it into an ethoxide ion adsorbed to a positive site and a proton adsorbed to a negative site.

The negative ethoxide ion is more likely to be desorbed from the surface, leaving the surface with a net positive charge.

7.4Å
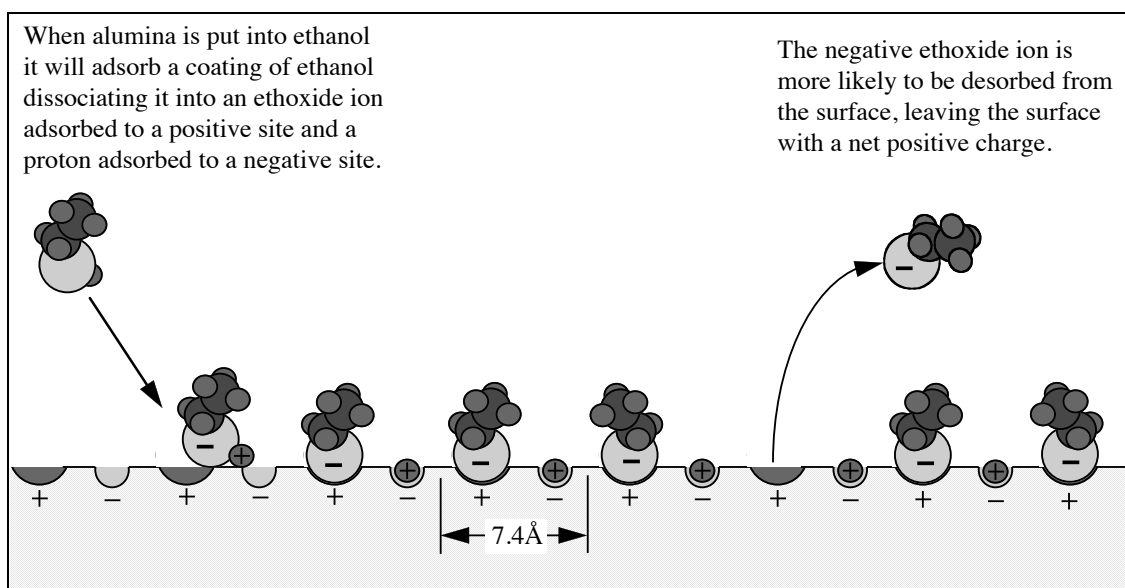
Fig. 3.25 Development of surface charge in pure ethanol.

The dissociated ethanol will also desorb from the surface as negative ethoxide ions and protons in the form of hydronium or protonated ethanol ions. The alumina surface therefore acts as a catalyst for the autoprotolysis reaction of ethanol, eq. [3.22]. (Hydroxide and protonated ethanol molecules exist but solvent ions will primarily be hydronium and ethoxide.)

$$HEtO + H_2O \Leftrightarrow EtO^- + H_3O^+ \qquad\qquad [3.22]$$

As the two types of ion diffuse outward from the surface they will recombine to form neutral ethanol molecules until at some distance from the particle they reach the equilibrium prevailing in the bulk solution. The effect of this is that the particle surrounds

itself with its own ionic atmosphere. At the particle surface there can be significant concentrations of ethoxide ions even when they are virtually non-existent in the bulk solution. This behavior is critical in understanding the surface adsorption and surface charging of the alumina powder.

When HCl is titrated into the suspension the activity of the ethoxide in the bulk drops effectively to zero due to reaction with the acid. This reduces but does not eliminate the ethoxide in solution at the surface. The reduction of ethoxide in solution at the surface does mean that more ethoxide desorbs from the surface and the net positive charge on the surface increases.

When HCl (really hydronium chloride) is added the chloride ion will substitute for an ethoxide ion on the surface and the hydronium ion will react with an ethoxide ion to form neutral water and ethanol molecules.

More ethoxide ions will now be desorbed due to their lower concentration in solution and chloride ions will desorb more easily due to their lower adsorption energy leading to a rapid rise in surface potential.

Fig. 3.26 Surface charge formation in ethanol/water with added HCl.

The Cl⁻ ions are adsorbed at the same Lewis acid sites as the ethoxide ions on the surface. This leads to a competitive adsorption process where the ratio of Cl⁻ to EtO⁻ adsorbed to a fixed number of sites on the surface is determined by the activity ratios of the two ions in solution at the surface.

The adsorption energy of the Cl⁻ ion to these sites is lower than that of the EtO⁻ ion. Therefore the number of unoccupied sites, which determines surface charge, will be higher at a given concentration of Cl⁻ compared to the EtO⁻ ion. The positive charge increases with the reduction of ethoxide and the substitution of Cl⁻ on the surface sites until the concentration of Cl⁻ at the surface is sufficient to begin to suppress the desorption of Cl⁻ from the surface.

The strongest base in ethanol is the ethoxide ion. Any stronger base will react with the ethanol solvent to form ethoxide ions. In the titration of potassium hydroxide/ethoxide,

the increased concentration of ethoxide in solution suppressed the dissociation of ethoxide from the surface, rapidly eliminating the net positive charge on the particle surface. However, despite a significant concentration of free ethoxide in the solvent, the desorption of protons from the surface never significantly exceeded the desorption of ethoxide and no net negative charge formed within the probable margin of error of the measurements made here. Thus it appears unlikely that in the absence of specific adsorption this hydrated alumina will develop a negative surface charge in this solvent.

If this model of surface chemistry, adsorption and charge formation can be extended to pure aqueous solutions, it would explain two frequently observed experimental phenomena. The first is the large difference between the surface charge density determined by titration and that determined by electrokinetic measurements. (**18**) This is explained here by the very large ratio between the number of active surface sites and the number of unoccupied sites necessary to generate the kinetically observed surface charge. The second is the nature of the surface charge. The second is the measured force between two approaching charged surfaces. It has been observed that the force falls between that predicted by a constant surface charge and a constant surface potential model. (**20**) If the surface charge was independent of ionic composition of the bulk solution then constant surface charge behavior would be expected. If the surface charge was only a function of the ionic composition of the bulk solution then the constant surface potential model would be correct. In the theory put forward here the surface charge is set in part by the activity of the solvent at the surface, which is a constant, and in part by ionic activities at the surface, which is a function of surface potential and composition of the bulk solvent. This leads to a behavior which will be in between constant charge and constant potential.

The objective of this chapter is to better understand the surface chemical behavior of an oxide powder in a particular system for electrophoretic deposition, with the ultimate goal of being able to quantitatively predict adsorption and surface charge in an arbitrary chemical environment. Based on the formulas and quantities developed here, it is possible to make quantitative estimates of the particle-electrode double layer interaction for many conditions during electrophoretic deposition, and at least qualitatively describe the interactions at all times and positions in the depositing layer. With a modest amount of additional work this information could be adapted for computational modeling of the deposition process. In the following chapter the surface adsorption quantities developed here are a vital component of an analytic description of the ionic flux at the deposition electrode. The data in this chapter provides a foundation for a very compelling analytic demonstration in Ch. 4 of the existence, nature and scale of what is referred to here as the Ion Depletion Augmented Electrostatic deposition mechanism.

Symbols used in Chapter 4

Abbreviations

DEBL — Diffuse electrostatic boundary layer

EHD — Electrohydrodynamic

EPD — Electrophoretic Deposition

Symbols

a	Particle radius (m)
c_o	Ionic concentration in bulk solution (Mol/m^3 or milliMolar)
c	Ionic concentration (Mol/m^3 or milliMolar)
d	Distance between parallel electrodes (m)
D_{Cl}	Chloride ion diffusion coefficient (m^2/s)
D_H	Hydrogen ion diffusion coefficient (m^2/s)
E	Electric field (V/m)
F	Faraday Constant
$\boldsymbol{F}$	Force (N)
I	Current Density (A/m^2)
J	Ionic flux (Mol/s•m^2)
k	Boltzmann Constant
q	Solution net specific electrostatic charge (C/m^3)
T	Temperature (K)
u_{Cl^-}	Chloride ion electrophoretic mobility (m/s)
u_∞	Particle velocity (m/s)
x	Distance parallel to electric field (m)
ε	Relative dielectic constant
ε_o	Permittivity constant
κ^{-1}	Debye length (m)
κa	Diffuse layer thickness index
$\boldsymbol{\kappa}$	Conductivity (μS/cm)
Λ	Molar conductivity (cm^2/Ω•Mol)
μ	Solvent viscosity (cP or mPa•s)
$\boldsymbol{\nu}_{Cl}$	Chloride ion mobility (m^2/V•s)
$\boldsymbol{\nu}_H$	Hydrogen ion mobility (m^2/V•s)
ϕ	Electrostatic potential (V)

Chapter 4
Electrophoretic Deposition of an Electrostatically Stabilized
Alumina Powder Suspension

4.1 Introduction

        Having developed in Ch. 3 a fairly complete picture of the solution and surface chemistry of alumina in ethanol, this chapter now undertakes an analysis of the electrophoretic deposition (EPD) of alumina particles from these suspensions.

        The chapter begins with the description of a simple EPD experiment in which a series of twenty one deposition trials were performed on a suspension of alumina particles in ethanol with increasing quantities of added HCl. Of these twenty one trials, three trials showing different types of behavior were chosen for detailed analysis.

        Unfortunately, even the simplest EPD experiment is a complicated event. To break this process down into components the explanation will follow the same 4-C pattern used in Ch. 2: chemistry, conduction, convection, and colloid. Chemistry — what ions are created or consumed at the electrodes during conduction. Conduction — what ionic concentration and voltage gradients form in the solution due to diffusion and migration of ions between the electrodes. Convection — some of the gradients that develop are unsustainable in a conducting liquid medium and additional ionic transport must be provided by electrically driven convection (electrohydrodynamic or EHD convection). Colloid — only after describing behavior of the solvent alone are the effects of the suspended particles introduced.

        A large portion of this chapter is devoted to analysis of conduction in the solvent in the absence of particles. It is only after understanding the behavior of the solvent in conduction without particles is it possible to understand the effects of particles on the system. The apparently contradictory result of this analysis is that, while particle electrophoresis has a negligible effect on conduction, it has a decisive effect on ionic transport. Secondly, once the particle electrophoresis is stopped at the deposition electrode, the physical effect of an accumulation of solid, non-conducting particles is again negligible compared to the ionic buffering effect of particle surface adsorption. Only once the complex interactions of conduction in a colloid suspension are understood and how voltage and concentration gradients are suppressed or stabilized at the deposition electrode, does it become possible to describe how stably suspended particles can be deposited and consolidated to form a dense deposition.

Of the many effects and concepts discussed in this chapter, the concept of primary importance is that of 'Ion Depletion Enhanced' electrostatic deposition. This is one of the most important practical mechanisms for EPD both because it is one of the few mechanisms that can produce a dense deposition prior to drying and because it has an effective, inherent automatic leveling effect. This means that uniformly packed, uniform thickness depositions can be reliably and repeatably produced even without perfect conditions of electric field or suspension density. The information in this chapter should allow the careful reader to direct research on deposition systems to try to induce this effect, to recognize this mechanism of deposition when it occurs, and to optimize conditions when this mechanism of deposition is used.

4.2 Procedure

4.2.1 Suspension Preparation

The Al_2O_3 powder was washed and hydrated as detailed in Ch. 3. Prior to mixing the Al_2O_3 powder was placed in a 135°C drying oven for at least 1 hour to remove excess condensed moisture. 7.988 g of this powder was added to 155.42 g of 99.5/0.5 wt. % ethanol/water in a HDPE bottle. This yields a 1.01 vol. % suspension of alumina particles based on an α-alumina density of 3.97 g/cc. 1 mm diameter alumina milling media was added to $\approx$ 50 vol. % of the mixture (filling the bottle to 1 cm below the surface of the ethanol-alumina suspension). This bottle was placed on a vibratory mill for 20 hours to de-agglomerate the alumina particles. The suspension was then poured into another HDPE bottle through a sieve to remove the milling media prior to deposition trials. There was no evidence of remaining alumina sediment.

4.2.2 Deposition Device

(a)   (b)
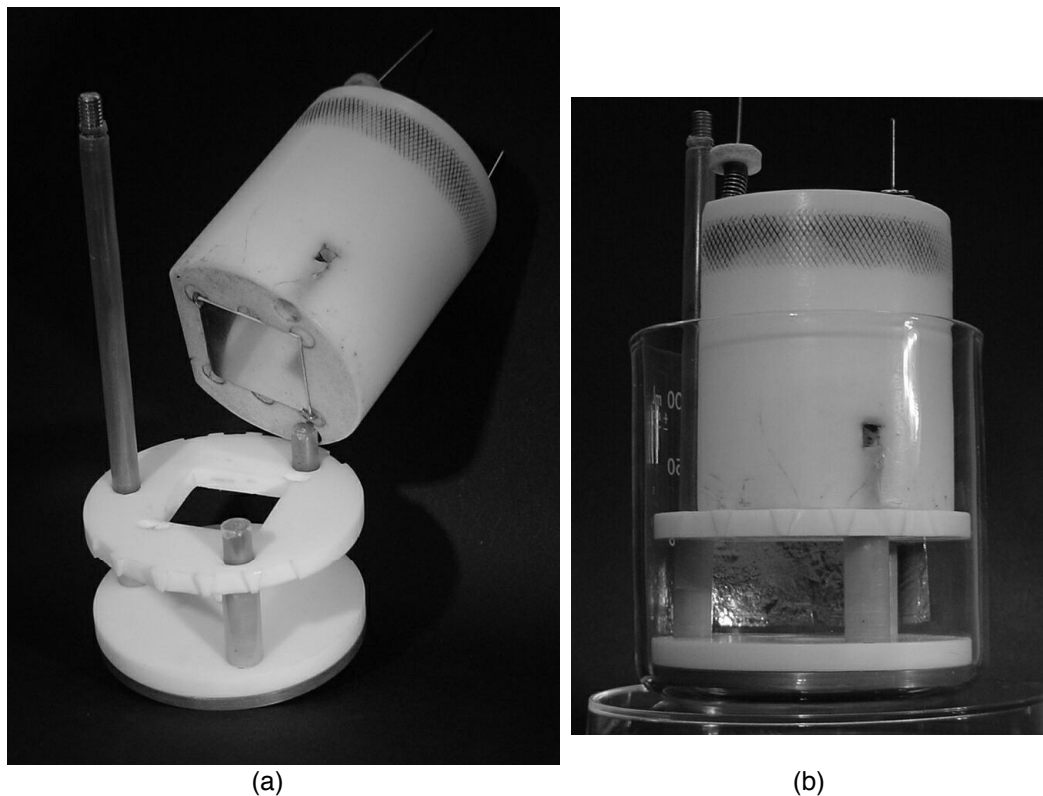
Fig. 4.1 Deposition Cell; (a) Device with holder block (upper) lifted from stand and masking disk (lower). Reflective square on the bottom of the holding block is the deposition electrode. (b) Assembled deposition device. One counter electrode is removed for clarity, second counter electrode is visible behind device stand.

The deposition trials were performed using a deposition device designed to be immersed in suspension in a 250 ml, 6.2 cm inside diameter Pyrex beaker. The deposition electrode is a 25.4 x 25.4 x 0.5 mm alumina circuit substrate with a sintered platinum coating on one side which was polished to a mirror finish. The deposition substrate is clipped to a PTFE holder block by two spring loaded stainless steel hooks which also serve to provide electrical connection to the platinum surface. The holder block is placed onto a 5 mm thick PTFE masking disk with a square cut out which exposes a 5.2 cm^2 area of the deposition electrode. The mask disk is mounted horizontally on three posts above a cylindrical volume 1.5 cm high and 6 cm in diameter. The counter electrodes are two platinum foils which each cover one quadrant of the sides of this cylindrical volume.

During a deposition trial particles will move away from the counter electrodes. This creates an area of lower density fluid at the surface of the electrodes. The cell is designed so that this lower density, particle depleted fluid can rise to the surface of the suspension well above the electrophoresis zone. Undepleted fluid from below the surface

of the suspension can then flow back down into the electrophoresis zone in the two quadrants not covered by the counter electrodes, replacing the depleted fluid. This flow pattern prevents gravitational convection or particle depleted solvent from the anode from affecting the deposition behavior at the cathode. In the center of the cylindrical volume the electrophoretic motion of the particles will become vertical, moving into the square mask cut-out toward the deposition electrode. Constant voltage/current is provided by a Keithly 2410 power supply which also provided voltage/current measurements.

4.2.3 Conductivity Measurement

Conductivity was measured using a voltage divider circuit with a 0.5 V oscillating current at the conductivity probe. Oscillation frequency ranged from 100 Hz at the lowest conductivity to 2 kHz at the highest. The conductivity probe was a shiny platinum parallel plate design with a cell constant of 0.107 cm^{-1} (Orion Research, Inc., Beverly, MA). Accuracy is estimated to be the larger of $\pm$ 0.2 μS/cm or $\pm$ 3%.

4.2.4 Deposition Procedure

The following is the step by step procedure for each deposition trial:

- 1 wt. % HCl solution in ethanol, if any, is added using a transfer pipette. The quantity is determined by the weigh of the pipette before and after the acid solution is added.
- Suspension is stirred for at least 30 sec. to assure suspension uniformity, regardless of whether acid solution is added.
- Measure Conductivity.
- Deposition substrate is mounted on holding block and holding block placed on deposition device in the suspension.
- The power supply is turned on for approximately 1 sec. at 20 V and the current is recorded. The power supply is then switched to constant current mode and this current is entered.
- The power supply is then turned on for 120 sec. at constant current and the voltage recorded manually every 15 sec.
- The mounting block and deposition substrate are then removed from the suspension and observed for deposition. The deposition substrate is removed from the mounting block with tweezers for rinsing. The deposition is exposed to air for approximately 30 sec. during this step. Although some evaporation occurs, no area of the deposition or substrate becomes dry prior to rinsing.

- The deposition substrate is rinsed in clear, as-received ethanol.
- The deposition is then allowed to dry and the weight is measured.
- The deposition substrate is then cleaned and the procedure is repeated.

The procedure for determining the set point for the constant current deposition trials proved to be a useful shortcut for determining a current which generates a uniform electric field at different conductivities. The relationship between conductivity and current setting is shown in Fig. 4.2.
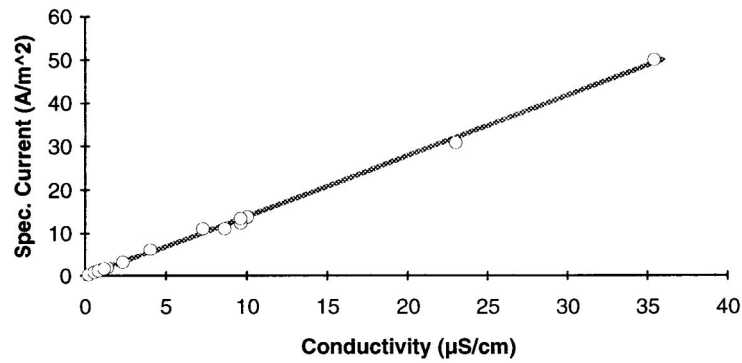
Fig. 4.2 Relation between current set point and conductivity.

4.3 Data

This chapter will analyze a series of twenty one deposition trials performed on a single alumina suspension with increasing additions of HCl. As shown in Fig. 4.3 these depositions can be separated into three groups: depositions that occurred with no added acid, trials with small amounts of added acid where no depositions occurred, and trials at higher conductivities marked by significant voltage rises and dense deposition layers.
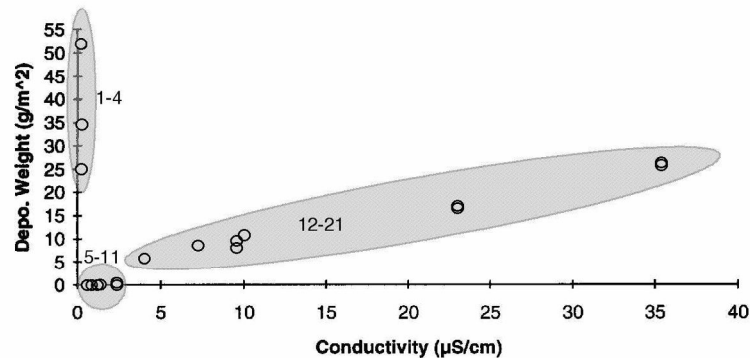
Fig. 4.3 Relationship between conductivity and deposition weight. Deposition trials can be separated into three groups.

Deposition Trials 1-4 — The first four deposition trials were performed on the as-prepared suspension containing only ethanol solution and alumina powder. Measured conductivity was $0.2 \, \mu$S/cm. The current setting for deposition was 32.7 mA/m^2.

Although depositions resulted from these trials, the results were very non-uniform. The voltage rises during deposition were 0.5, 2.0, 0.8 and 0.7 V. The first trial resulted in a thick, fluffy deposition covering most of the center of the electrode. The deposited area had irregular edges. Near the boundaries of the masked area there was no deposition. The unrinsed average deposition weight was 24 g/m^2. The second deposition covered the entire deposition area, however the entire deposition was removed by rinsing. During rinsing a distinct flow pattern was observable. The third deposition was very thick and appeared uniform prior to rinsing, however rinsing revealed a distinct flow pattern. Weight after rinsing was 53 g/m^2. The final deposition in this set again yielded a fairly uniform, low density deposition. When the deposition was removed from the holder block and held at an angle the surface of the deposition was observed to flow off. The deposition weight without rinsing was 34 g/m^2.

Deposition Trials 5-11 — Deposition trials in this set were conducted with progressively higher additions of HCl yielded no significant deposition. The first five trials in this set covered a conductivity range from 0.6 to 1.2 μS/cm and showed voltage rises from 0.2 to 0.7 V. The final two deposition trials were conducted at a conductivity of 2.3 μS/cm and showed voltage rises of 1.0 and 1.1 V. A very small deposition of particles was observed as a slight fogging of the reflective platinum surface. The deposition weight of 0.6 g/m^2 is only slightly above the estimated accuracy of the scale used here of ±0.2 g/m^2 , however this deposition appears to correspond to a uniform, well packed monolayer of particles. The final deposition trial of this set, #11, was chosen for detailed analysis in the following sections. The data for this trial is given in Table 4.1 and the voltage rise is shown in Fig. 4.5.

Depositions 12-21 — This set of trials was marked by significant voltage rises during deposition, an overlayer of particles which rinse off the substrate, and a uniform, dense deposition layer which does not rinse off. Conductivities range from 4.4 to 35.4 μS/cm. Voltage rises increased with conductivity from 2.0 to 18.9 V. Deposition weights also increased with conductivity from 5.8 to 26.1 g/m^2.

Depositions in this set were rinsed by dipping the substrate into the rinse ethanol and moving it back and forth at several tens of centimeters per second until no further alumina was seen to rinse off. The remaining deposited layers did not show evidence of any large scale convection patterns.

Two depositions in particular, #'s 16 and 20, were chosen from this set for detailed analysis. The data from these depositions are listed in Table 4.1 and their voltage rise profiles are shown in Fig. 4.5.
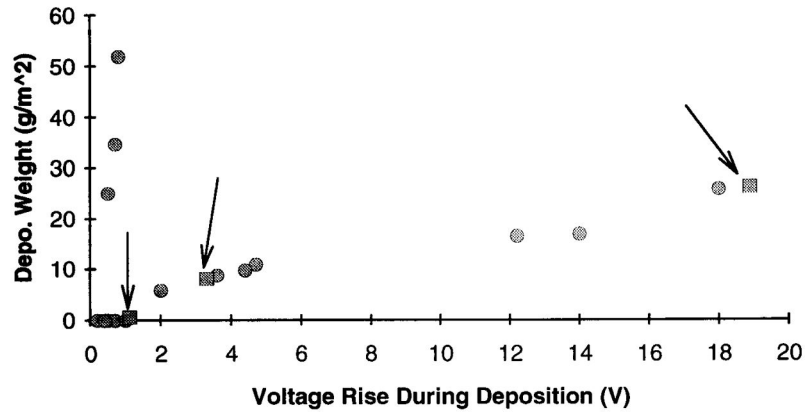
Fig. 4.4 Relationship between voltage rise and deposition weight. Deposition trial #'s 11, 16 & 20 are square markers indicated by arrows.

Table 4.1 Deposition Data

	Trial 11	Trial 16	Trial 20
Conductivity	2.31 μS/cm	9.58 μS/cm	35.4 μS/cm
Current density (*I*)	0.32 A/m^2	1.25 A/m^2	5.0 A/m^2
Total current	38.3 C/m^2	150 C/m^2	600 C/m^2
Voltage rise	1.0 V	3.3 V	18.9 V
Deposition weight	0.6 g/m^2	8.1 g/m^2	26.1 g/m^2
Deposit specific current	66 C/g	18 C/g	23 C/g
Deposition thickness at 60 vol. % density	0.24 μm	3.4 μm	11.0 μm
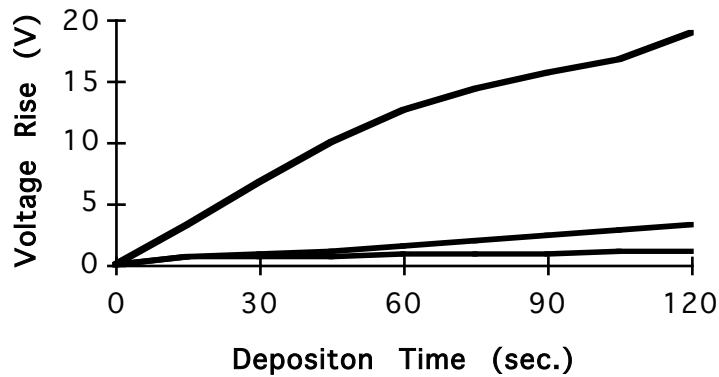
Fig. 4.5 Voltage rises in deposition trial #'s 11, 16 & 20 .

Data from Prior Experiments — Two facts used here result from prior experience with depositions of this type. The first is the density of the deposited layer. Density of the deposited layers was not measured in this experiment, however, previous measurements have shown that these types of depositions, marked by a rise of several volts during deposition and which cannot be removed even by vigorous agitation during rinsing, have a density between 50 and 65%. Based on this, a density estimate of 60 vol. % is used here. A lower actual density will not significantly affect the conclusions reached here.

The second fact used here is the location of the excess voltage that arises during deposition. Experiments using a platinum wire as a voltage probe have shown that the voltage rise during deposition is almost completely accounted for by a potential difference across the deposited layer. For example, a constant current deposition with an initial potential of 20 V shows a rise in voltage to 40 V over the course of the deposition. The final voltage breakdown will be approximately: 20 V due to resistance of the solution; 1 V to drive convection in solution due to concentration gradients, this is sometimes referred to a concentration potential; and 19 V across the deposited layer. The wire probe can be pressed against the deposited layer, and, as long as the deposited particles are not scraped away, a 19 V potential difference will be measured between the deposition electrode and the solvent side of the deposition. This was confirmed by the voltage measurements of Sarkar and Nicholson (**1**).

4.4 Analysis

     The quantitative analysis of any of the mechanisms of EPD is not a simple prospect. Many reactions happen at one time in a very small space where particles, ions and solvent are all in relative motion due to diffusional gradients and electrostatic forces on several scales. Equilibrium is the exception — not the rule. Furthermore, of the various mechanisms of deposition the one featured here, Ion Depletion Enhanced Electrostatic, is likely the most complex and least intuitive.

     To handle the complexity of this process a description is built up step-by-step with each step adding an element of complexity to make the description more complete. Before beginning on the EPD process a foundation for this step-by-step buildup is given in § 4.4.1. Using the data and analysis from Ch. 3, a complete, quantitative description is given of the three suspensions to be focused on here. The first step in understanding the EPD process, § 4.4.2, is a description of the electrochemical reactions involved in conduction in the solvent, ignoring all other effects. The next step, § 4.4.3, adds a significant level of complexity by analyzing the transport of ions through the solvent at the deposition electrode in the absence of convection. This analysis is then the basis for the next step, § 4.4.4, describing the initiation of convection in the solvent. It is only after this basic picture of conduction and convection in the solvent is drawn up that particles are first introduced. In § 4.4.5 it is shown that even though the particles do not contribute significantly to the conductivity of the solution, they have a dramatic impact on ionic transport and convection. Finally this is brought together in § 4.4.6 for a complete explanation of the deposition experiment.

4.4.1 Suspension Description

     Molar Conductivity, Ionic Mobility & Diffusion — Using the Fuoss-Onsager equation as detailed in Ch. 3, from the conductivity it is possible to iteratively solve for the molar conductivity and ionic concentration in the solution. These are shown in Table 4.2. The molar limit conductivity for HCl in this ethanol/water mixture is 53.4 S•cm^2/Mol. This conductivity is the sum of the conductivity due to the mobility of the chloride and hydrogen ions in solution.

$$\Lambda^{\circ}_{HCl} = \lambda^{\circ}_{Cl^{-}} + \lambda^{\circ}_{H^{+}} \qquad\qquad [4.1]$$

Grahm et al. (**2**) measured the molar limit conductance for the chloride ion in anhydrous ethanol as 21.9 S•cm^2/mol. The mobility of the chloride ion will be relatively unaffected by water content therefore this can be taken as an estimate for the limit conductance of chloride in this solvent as well. This gives a molar limit conductance for the proton of

31.5 S•cm^2/mol. Since ionic strength effects will affect both positive and negative ions equally, this ratio is used to divide the molar conductivity at each concentration between chloride and proton components. This molar conductivity is converted to an ionic mobility by dividing by the Faraday constant:

$$\nu_i = \frac{\lambda_i}{F} \qquad\qquad [4.2]$$

The Einstein relation is then used to estimate the diffusion coefficients, D_i, from the ionic mobilities:

$$D_i = \frac{kT}{z_i e}\nu_i \stackrel{or}{=} \frac{RT}{z_i F}\nu_i \qquad\qquad [4.3]$$

These values are listed in Table 4.2 for the three deposition conditions to be analyzed here.

Table 4.2 Ionic Properties of Solution

	Trial 11	Trial 16	Trial 20
Conductivity	2.31 μS/cm	9.58 μS/cm	35.4 μS/cm
Molar conductivity (Λ)	51.3 cm^2/Ω•Mol	49.9 cm^2/Ω•Mol	47.1 cm^2/Ω•Mol
Bulk HCl Concentration (milliMolar or Mol/m^3)	0.045 mMolar	0.192 mMolar	0.751 mMolar
Chloride ion mobility (ν_{Cl})	2.19x10^{-8} m^2/V•s	2.13x10^{-8} m^2/V•s	2.01x10^{-8} m^2/V•s
Chloride ion diffusion coefficient (D_{Cl})	5.62x10^{-10} m^2/s	5.42x10^{-10} m^2/s	5.16x10^{-10} m^2/s
Hydrogen ion mobility (ν_H)	3.13x10^{-8} m^2/V•s	3.04x10^{-8} m^2/V•s	2.87x10^{-8} m^2/V•s
Hydrogen ion diffusion coefficient (D_H)	8.03x10^{-10} m^2/s	7.81x10^{-10} m^2/s	7.37x10^{-10} m^2/s

Mobility, Electrostatic Stability & Surface adsorption of particles — Table 4.3 gives some of the colloidal and electrochemical properties of the suspensions in the three deposition trials to be analyzed in detail. The diffuse layer thickness index is calculated using the average particle radius of 135 nm. For trials # 11 and 16 the mobility was interpolated from data collected in Ch. 3. For trial # 20 the mobility was extrapolated using the straight line fit shown in Fig. 3.8. Surface potential and particle charge were calculated using the procedure of § 3.4.1. The particle charge is calculated by multiplying the surface charge density with the surface area of an average size 270 nm dia. particle. The surface adsorbed quantity of HCl is calculated using Eq. [3.17].

Table 4.3 Surface and Colloid Properties

	Trial 11	Trial 16	Trial 20
Debye length (κ^{-1})	26 nm	12.5 nm	6.3 nm
Diffuse layer thickness index (κa)	5.24	10.8	21.4
Electrophoretic mobility	0.97 μm•cm/V•s	0.85 μm•cm/V•s	0.47 μm•cm/V•s
Surface potential	79 mV	51 mV	26 mV
Average Particle Electrostatic Charge	2.52x10^{-16} C	2.64x10^{-16} C	2.40x10^{-16} C
Surface adsorbed HCl	21.4 μMol/g	27.5 μMol/g	31.6 μMol/g

From the data above it is possible to estimate the interaction potential of two average diameter spherical particles. These are shown in Fig. 4.6. The attractive L-VdW force is calculated as outlined in § 2.4.3. This is adjusted for retardation of the interaction as separation distance increases using the estimation method of Russel, et al. (**3**, p155). The repulsive force that results from the overlap of the DEBL's is calculated using the Derjaguin approximation for constant potential $\Phi = 2\pi\varepsilon_r\varepsilon_o\psi_o^2 a\ln\left(1 + e^{-\kappa h}\right)$. The total interaction energy is then the sum of these two forces.

To obtain an order-of-magnitude estimate of the electric field that would be necessary to bring two particles together, the maximum interparticle repulsion force was divided by the charge on a single average particle to obtain the voltage gradient that would produce an equivalent force on an isolated particle, independent of EHD effects.

Table 4.4 Particle Interaction Properties

	Trial 11	Trial 16	Trial 20
Max. Energy Barrier to Floccing	230 kT	70 kT	3.5 kT
Max. Interparticle Repulsion Force	28.2 pN	15.5 pN	1.42 pN
Electric Field to Produce an Equivalent Force	1,120 V/cm	590 V/cm	60 V/cm
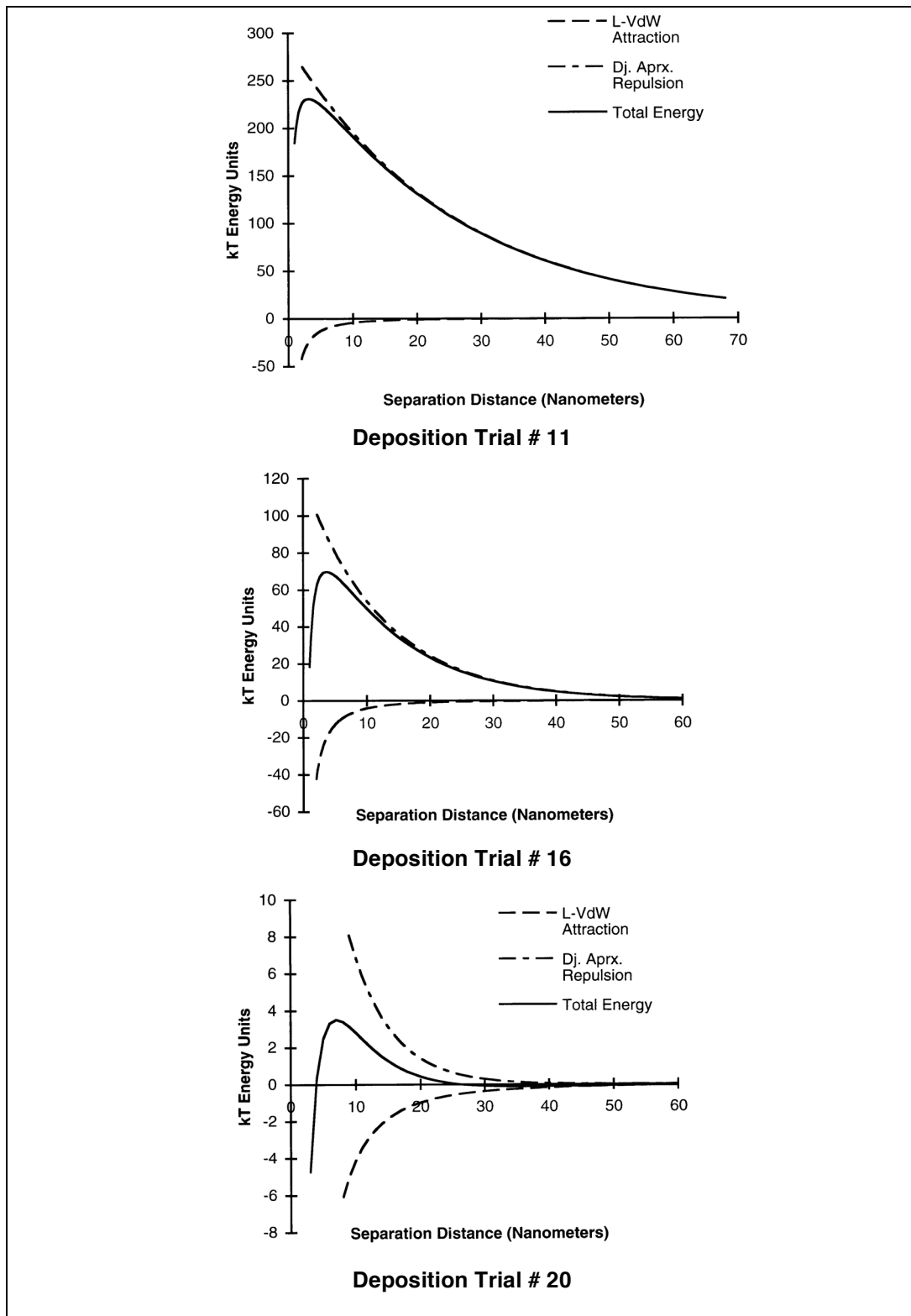
Fig. 4.6 Calculated electrostatic stabilization energies.

4.4.2 Chemistry of Conduction

There are three components to direct current conduction in a solution. Electrochemical reactions at the cathode transfer electrons to the solution to either reduce positive ions from solution or introduce negative ions into solution. At the anode electrons are removed from solution either by removing electrons from negative ions or the oxidation of neutral atoms or molecules to produce positive ions. Between these two electrodes conduction in solution consists of the motion of ions from one electrode to another, with the possibility of these ions participating in chemical reactions along the way. These components for the specific solution here are as follows:

Cathode Reactions — The cathode reaction in this system is fairly simple. Hydrogen ions arriving at the surface in the form of hydronium or ethoxonium ions are neutralized to form hydrogen gas and water or ethanol. In the absence of other positive ions which could form a soluble salt with hydroxide or ethoxide ions there will be no electrolysis of the solvent.

Anode Reactions — The chemistry at the anode is slightly more complex with several possible reactions. The primary reaction is presumably the electrolysis of water to produce hydronium or ethoxonium ions and oxygen gas. Other reactions that could be occurring are: the oxidation of chloride ions to form chlorine gas; the combination of the electrolysis of ethanol with the neutralization of a chloride ion to produce ethylene chloride; a combination of electrolysis reactions to produce ethane gas, and the possible formation of platinum chlorides. Reactions which produce hydronium or ethoxonium are essentially neutral. They generate ions which simply replace ions consumed at the cathode. These reactions are also essentially equivalent as the H_3O^+/H_2EtO^+ ratio will go to equilibrium in solution regardless of which ion is produced more rapidly at the electrode.

Reactions which consume chloride ions, either producing chlorine gas or ethylene chloride, will result in a net decrease in ionic concentration in solution. In an extended conduction test in 99.5% ethanol with added HCl there was a drop in ionic concentration equivalent to $\approx 20\%$ of the total electron flux through the solution. This means that 80% of the current at the anode results in the formation of H_3O^+/H_2EtO^+. Over the time span of the depositions here the molar current flux is not significant in comparison to the total quantity of ions in the suspension.

Conduction Through the Solution — Since no ions or reactive chemical species are produced at the cathode, there are no neutralization reactions in the solution, and, although not in concentration equilibrium, the solution remains in chemical equilibrium during

conduction. Ions are only created and consumed at the electrodes and all conduction in the solution takes place by transport of these ions between the electrodes.

Independent of conduction, in ethanol with HCl the formation of ethylene chloride and water is energetically favorable. There is some indication that at sufficient concentration of HCl this mixture may become explosive.(4) However, at room temperature and at the concentrations used here this reaction is very slow. Stock solutions of HCl in ethanol showed no decrease in ionic concentration over several months.

4.4.3 Conduction in the Solvent - Without Convection

The Quasi Neutral Limit Current — A useful first step is to return to the concept of the quasi-neutral limit current outlined in Ch. 2. This can establish the scale on which the problem should be approached and thereby allows some simplifying assumptions.

In Ch. 2 the problem was analyzed for the maximum current that could be carried by a cell with given dimensions, ionic concentration and ionic mobility. For the deposition solutions considered here, the ionic mobilities, concentrations and current density are known, and the question can be re-framed to ask what is the maximum cell size which can conduct this current without convection. Assuming a simple parallel plate cell in which positive protonated ions are created at the anode and consumed at the cathode, the maximum thickness for a given current density will be a simple transposition of Eq. [2.42]:

$$d_{\lim} = 2\frac{FD_{H^+}}{I}c_{\mathrm{o}} \qquad [4.4]$$

Taking c_{o} as the ionic concentration in the bulk solution and the proton diffusion rate at 0.8×10^{-10} m^2/s, the maximum distance between electrodes is 22, 23, and 21 μm using the bulk concentration and current density figures from deposition trials 11, 16 and 20 respectively. Because of the linear relation between concentration and conductivity these distance are similar for all three solutions. Further calculations show that this gradient will form in a fraction of a second.

Given that this thickness is three orders of magnitude lower than the scale of the deposition cell, it is clear that the applied currents in these depositions far exceed the ability of the solution to conduct without violating the assumptions of no convection and quasi neutrality, and these limits are exceeded in a fraction of a second.

To get a picture of what is going on it is helpful to start with a picture of the hypothetical limit current case. In this hypothetical 22 μm cell the ionic concentration will go from almost zero at the cathode to c_{o} at the anode. This situation is maintained in a steady state by the presence of the anode, which blocks the further migration of the

negative chloride ions. The chloride ion profile then remains stable as electrophoretic migration toward the anode is matched by concentration diffusion back toward the cathode. This is shown in Fig. 4.7 (a).

Ionic Concentration Across
the Cell at the Limit Current

Ionic Concentration Gradient Forms
at Cathode and Moves Away at the
Speed of the Chloride Ions

(a)   (b)
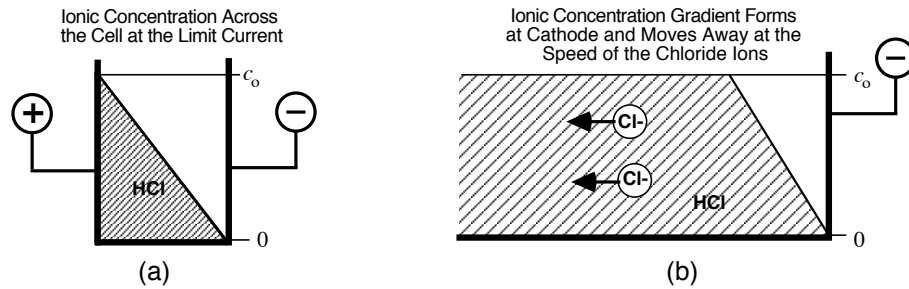
Fig. 4.7 (a) Ionic concentration across the cell at the equilibrium quasi-neutral limit current, (b) anions in the bulk continue to move away from the cathode gradient region.

Beyond the Limit Current- Layers of Conduction — In the actual cell there isn't an anode to block the motion of the chloride ions away from the cathode. At the high side of this concentration gradient, the chloride ions will be moving away from cathode at the same speed as the general migration of chloride ions in the bulk solution. This is shown in Fig. 4.7 (b). Since there is a constant current flux in this system the gradient layer cannot become significantly wider while transmitting the same current without violating quasi neutrality. This means that a moving gradient layer will be formed, slightly less steep than the static gradient layer, that moves away from the cathode at the same speed as the migration of chloride ions in the bulk. This opens up a region between the moving gradient region and the cathode where charge neutrality is completely violated, a very high voltage gradient is created, and conduction is primarily by unaccompanied positive ions. This is illustrated schematically in Fig. 4.8.

Ionic Concentration Gradient Forms at Cathode and Moves
Away at the Speed of the Chloride Ions Opening a Layer
of Unbalanced Charge Conduction at the Cathode

(a)   (b)   (c)
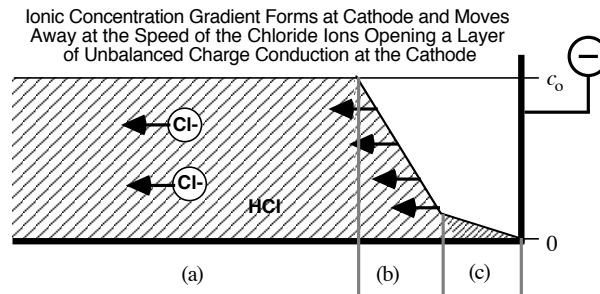
Fig 4.8 Electrochemical boundary region near the cathode without convection is divided into four zones; a) neutral region or bulk solution, b) quasi-neutral or gradient region, c) charged layer or unbalanced charge region, and d) diffuse boundary layer (not shown).

The above treatment shows that the electrochemical boundary layer that is of interest here is on the scale of microns. This justifies ignoring both the anode electrochemical layer and the cathode diffuse electrostatic boundary layer. At the anode chloride ions will be accumulating, the ionic concentration will be going up, and eventually this will cause bulk EHD convection in the cell. However, this is happening two centimeters away from the 20-30 μm cathode electrochemical layer that is analyzed here. The cathode diffuse electrostatic boundary layer (DEBL) will be on the scale of the Debye length prior to the beginning of deposition, 6 to 26 nm. When current begins to flow the ionic concentration outside the DEBL will go down, but this layer will remain well below 1 μm. This boundary layer does have an effect on how the very first layers of particles deposit and adhere to the electrode surface, but this is beyond the scope of the current analysis.

In the following quantitative analysis of the conducting gradient layers in regions A, B & C, the following coordinate system will be used:

- Positive points to cathode.
- A positive current is positive ions moving in a positive direction (toward the cathode) or negative ions moving in a negative direction.
- Concentration and electrostatic potential decline toward the cathode therefore $\dfrac{\partial c}{\partial x}$ and $\dfrac{\partial \phi}{\partial x}$ are negative quantities.

As ionic concentration declines in the gradient layer, ionic mobility will rise toward the limit value at zero concentration. To simplify the analysis, the mobilities and diffusion constants are assumed to be constant at their bulk values in the gradient layer, and are taken at their zero concentration limit values in the unbalanced charge layer.

The following analysis of the quasi neutral gradient region is extended from the work of Levich (**5**). The concept and equations for the unbalanced charge conduction layer are from Chazlaviel (**6**).

Region A - Bulk Conduction & Mobility — To calculate the electric field in the bulk solution near the cathode the specific current is divided by the conductivity to get the electric field gradient:

$$\frac{\partial \phi}{\partial x} = \frac{I}{\kappa} \qquad\qquad [4.5]$$

This gives voltage gradients of 13.9, 13.0 and 14.1 V/cm for the three cases considered here. The velocity of the chloride ions in the bulk is then the mobility times the field gradient:

$$u_{Cl^-} = v_{Cl^-} \frac{\partial \phi}{\partial x} \qquad [4.6]$$

The chloride ion velocities are then 30.3, 27.7 and 28.3 μm/s. Once a stable gradient layer is formed it will move away from the cathode at this velocity.

Region B - The Quasi-Neutral Moving Gradient Layer — The analysis of this layer is based on two assumptions: that of quasi neutrality and that of an equilibrium profile moving gradient layer.

Anywhere there is a concentration gradient in a conducting solution there will also be a change in the voltage gradient. The voltage gradient only changes where there is a net accumulation of positive or negative charge. The assumption of quasi neutrality is only that the difference between the concentration of positive and negative ions at any point is very small compared to the total number of ions present. This does not preclude large changes in voltage gradients, since even a small charge imbalance can create very large voltage gradients.

As the gradient layer moves away from the cathode there are three ways that the gradient profile can evolve. It can: 1) become continually steeper, 2) can achieve an equilibrium profile, or 3) it can grow as it moves with the same total concentration drop spreading over a wider distance. The first case is self limiting. The maximum possible gradient would be a discontinuous step in concentration, however, diffusion would provide a stricter limit on how steep the gradient can become. The gradient is also limited in how flat it can become. Similar to what was shown in the static limit current discussion, the current flux will set a minimum possible gradient through the layer. If the gradient profile is then limited both by how steep and how flat it can become, it must achieve some profile between the two extremes. Since there is no input that would cause it to oscilate, it must approach a steady, equilibrium profile.

Based on the assumption of quasi neutrality, as current flows through the solution there will be no net accumulations of either positive or negative charge. To obey this restriction the net ionic flux must be constant at all points through the gradient layer. This criterion can be expressed by:

$$\frac{I}{F} = J = -D_{H^+} \frac{\partial c_{H^+}}{\partial x} + D_{Cl^-} \frac{\partial c_{Cl^-}}{\partial x} - v_{H^+} \frac{\partial \phi}{\partial x} c_{H^+} - v_{Cl^-} \frac{\partial \phi}{\partial x} c_{Cl^-} \qquad [4.7]$$

The restriction that the profile of the gradient layer be stable implies that the net motion of the Cl^- ions at all points in the gradient layer will be the same as the migration of the Cl^- ions in the bulk. This can be expressed in terms of current by:

$$\frac{v_{Cl^-}}{v_{Cl^-}+v_{H^+}}J\frac{c_{Cl^-}}{c_{Cl_o^-}} = D_{Cl^-}\frac{\partial c_{Cl^-}}{\partial x}-v_{Cl^-}\frac{\partial \phi}{\partial x}c_{Cl^-} \qquad [4.8]$$

The right hand side of this equation is the flux of chloride ions. On the left $\dfrac{v_{Cl^-}}{v_{Cl^-}+v_{H^+}}J$ is the proportion of net ionic flux due to Cl^- ions in the bulk, and $\dfrac{c_{Cl^-}}{c_{Cl_o^-}}$ is the ratio of Cl^- ions at a point in the gradient layer to the concentration of Cl^- ions in the bulk.

Using the assumption of quasi-neutrality:

$$c_{Cl^-} \approx c_{H^+} = c \qquad [4.9]$$

where c is a function of position x, these equations can be simplified to:

$$J = \left(D_{Cl^-}-D_{H^+}\right)\frac{\partial c}{\partial x}-\left(v_{Cl^-}+v_{H^+}\right)c\frac{\partial \phi}{\partial x} \qquad [4.10]$$

$$\frac{v_{Cl^-}}{v_{Cl^-}+v_{H^+}}J\frac{c}{c_o} = D_{Cl^-}\frac{\partial c}{\partial x}-v_{Cl^-}c\frac{\partial \phi}{\partial x} \qquad [4.11]$$

Multiplying Eq.[4.21] by $\dfrac{\left(v_{H^+}+v_{Cl^-}\right)}{v_{Cl^-}}$ gives:

$$\frac{c}{c_o}J = \frac{\left(v_{Cl^-}+v_{H^+}\right)}{v_{Cl^-}}D_{Cl^-}\frac{\partial c}{\partial x}-\left(v_{Cl^-}+v_{H^+}\right)c\frac{\partial \phi}{\partial x} \qquad [4.12]$$

This can be subtracted from Eq. [4.20] to give:

$$\left(1-\frac{c}{c_o}\right)J = \left[\left(D_{Cl^-}-D_{H^+}\right)-\frac{D_{Cl^-}\left(v_{Cl^-}+v_{H^+}\right)}{v_{Cl^-}}\right]\frac{\partial c}{\partial x} \qquad [4.13]$$

The term in square brackets can be simplified as follows:

$$\left(D_{Cl^-}-D_{H^+}\right)-\frac{D_{Cl^-}\left(v_{Cl^-}+v_{H^+}\right)}{v_{Cl^-}} = D_{Cl^-}-D_{H^+}-D_{Cl^-}-\frac{D_{Cl^-}}{v_{Cl^-}}v_{H^+} = -2D_{H^+} \qquad [4.14]$$

Substituting this into Eq. [4.13] and re-arranging gives:

$$\frac{-J}{2c_oD_{H^+}}dx = \frac{1}{c_o-c}dc \qquad [4.15]$$

Integrating both sides gives:

$$\frac{-J}{2c_oD_{H^+}}x+k_1 = -\ln\left(c_o-c\right) \qquad [4.16]$$

where k_1 is a constant of integration. By re-arranging terms, taking the exponential of both sides, and performing one more re-arrangement, a formula for the concentration is obtained:

$$c = c_o - k_1 \exp\left[\frac{J}{2c_o D_{H^+}} x\right] \qquad [4.17]$$

The value for the integration constant k_1 then must be determined by boundary conditions for the problem. Since c will only approach c_o asymptotically, there is no point x where $c=c_o$. On the other end, there is a theoretical point where $c=0$. If x is set equal to zero at this point the equation becomes:

$$c = c_o - c_o \exp\left[\frac{J}{2c_o D_{H^+}} x\right] \qquad [4.18]$$

In this equation J, D_{H^+} and c_o will be positive, therefore for increasing negative values of x, c will approach c_o. The value of $\left[\frac{J}{2c_o D_{H^+}}\right]^{-1}$ for the three cases analyzed here is 21.8, 23.1 and 21.4 μm. This number is a useful index of the thickness of the moving gradient layer. Once again because the current flux is proportional the concentration, the thickness of the moving gradient layers in all three cases is similar.

In a similar manner it is possible to solve for the potential, field and field gradient. The details of this are given in appendix B, the results are listed below.

$$\phi = \frac{-J}{c_o\left(\nu_{Cl^-} + \nu_{H^+}\right)} x + \frac{RT}{F} \ln\left(1 - \exp\left[\frac{J}{2c_o D_{H^+}} x\right]\right) + \phi_o \qquad [B.16]$$

$$\frac{\partial \phi}{\partial x} = \frac{-J}{c_o\left(\nu_{Cl^-} + \nu_{H^+}\right)} + \frac{-J}{2c_o \nu_{H^+}}\left[\left(1 - \exp\left[\frac{J}{2c_o D_{H^+}} x\right]\right)^{-1} - 1\right] \qquad [B.7]$$

$$\frac{\partial^2 \phi}{\partial x^2} = -\left(\frac{J}{c_o}\right)^2 \frac{\exp\left[-\frac{J}{2c_o D_{H^+}} x\right]}{4 D_{H^+} \nu_{H^+}\left(1 - \exp\left[-\frac{J}{2c_o D_{H^+}} x\right]\right)^2} \qquad [B.12]$$
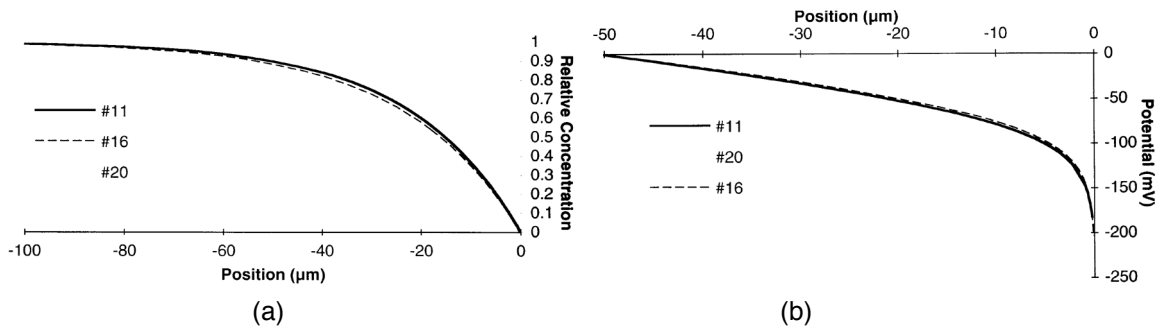
Fig. 4.9 Equilibrium moving concentration gradient in quasi neutral region.

Table 4.5 Moving Gradient Layer Region

	Trial 11	Trial 16	Trial 20
Conductivity	2.31 μS/cm	9.58 μS/cm	35.4 μS/cm
Current density (I)	0.32 A/m^2	1.25 A/m^2	5.0 A/m^2
Limit current thickness	22 μm	23 μm	21 μm
Bulk voltage gradient	13.9 V/cm	13.0 V/cm	14.1 V/cm
Bulk Cl$^-$ ion velocity	30.3 μm/s	27.7 μm/s	28.3 μm/s
$\left[J/2c_o D_{H^+}\right]^{-1}$	21.8 μm	23.1 μm	21.4 μm

This gradient layer will take approximately 1/2 second to form. This estimate is based on the ionic flux, and a full calculation is not made here. However, after this approximately 1/2 second inception time the gradient layer will begin to move away from the cathode at the migration velocity of the chloride ions in the bulk, ≈ 30 μm/s. This opens up a region of unbalanced charge conduction designated here as region C.

Region C - Unbalanced Charge Conduction Layer — The ionic concentration never actually becomes zero, but at some point it becomes so low and the voltage gradient so high that the assumption of quasi-neutrality will no longer be valid. Given the exponential decline in concentration and rise in voltage through the quasi-neutral gradient region, the edge of this region can be considered a point at which conduction changes to conduction purely by cations with a zero concentration of anions. Because of the very high voltage gradient in this region, migration will be so much higher than diffusion that diffusion can be ignored. This allows current flux to be written as a function only of electric field and cation concentration:

$$J = -v_{H^+} c_{H^+} \frac{\partial \phi}{\partial x}$$ [4.19]

The electric field gradient will then be determined by the cation concentration:

$$\frac{\partial^2 \phi}{\partial x^2} = -\frac{F c_{H^+}}{\varepsilon \varepsilon_o}$$ [4.20]

Combining these equations gives:

$$-\frac{F c_{H^+}}{\varepsilon \varepsilon_o} = \frac{\partial^2 \phi}{\partial x^2} = \frac{\partial}{\partial x}\left[-\frac{J}{v_{H^+} c_{H^+}}\right] = \frac{J}{v_{H^+}} \frac{1}{c_{H^+}^2} \frac{\partial c_{H^+}}{\partial x}$$ [4.21]

Separating variables and integrating to determine concentration as a function of position gives:

$$c_{H^+} = \left[\frac{J\varepsilon\varepsilon_o}{2Fv_{H^+}x} \right]^{\frac{1}{2}}$$ [4.22]

The constant of integration is set to zero by taking a boundary condition of $c = \infty$ at $x = 0$.

This expression can be substituted into Eq. 4.40 and both integrated and disintegrated to give the potential, potential gradient, and the rate of change of the potential gradient:

$$\phi = \phi_o - \frac{2}{3} \left[\frac{2JF}{v_{H^+}\varepsilon\varepsilon_o} \right]^{\frac{1}{2}} x^{\frac{3}{2}}$$ [4.23]

$$\frac{\partial \phi}{\partial x} = - \left[\frac{2JF}{v_{H^+}\varepsilon\varepsilon_o} \right]^{\frac{1}{2}} x^{\frac{1}{2}}$$ [4.24]

$$\frac{\partial^2 \phi}{\partial x^2} = - \frac{1}{2} \left[\frac{2JF}{v_{H^+}\varepsilon\varepsilon_o} \right]^{\frac{1}{2}} x^{-\frac{1}{2}}$$ [4.25]
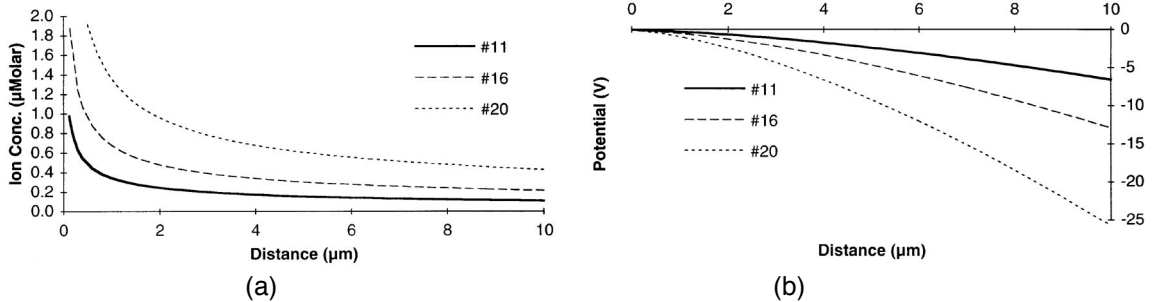
Fig. 4.10 Concentration gradients (a) and potential gradients (b) in an unbalanced charge conduction layer. Note that the potentials here are expressed in Volts.

Table 4.6 Ion Depleted Region

	Trial 11	Trial 16	Trial 20
Current density (I)	0.32 A/m^2	1.25 A/m^2	5.0 A/m^2
Ionic Flux (J)	3.32 μMol/s•m^2	12.9 μMol/s•m^2	51.8 μMol/s•m^2
Hydrogen ion mobility v_{H^+}	3.15x10^{-8} m^2/V•s		
$\left[\dfrac{2JF}{v_{H^+}\varepsilon\varepsilon_o} \right]^{\frac{1}{2}}$	0.31x10^{-9} V•m$^{-3/2}$	0.61x10^{-9} V•m$^{-3/2}$	1.21 V•m$^{-3/2}$

Matching Regions B & C — The assumptions for Region B lead to a zero ionic concentration at $x_B = 0$, in Region C the concentration of positive ions goes to infinity at $x_C = 0$. Clearly both of these cases are non-physical and there must be a transition from one region to the other at reasonable values of the ionic concentration. For the purposes of the analysis here, the two functions are matched where the electric field and electric field gradient are equal. This gives a function which is continuous in electric field but has a discontinuity in ionic concentration. The position of the match points in the coordinates of each region and the voltage gradients at the match points are given in Table 4.6.

An accurate solution would have to solve for electric field and ionic concentration in a transition region where both the concentration of unpaired positive ions and the concentration of negative chloride ions are both too large to ignore. An exact solution for this transition region is beyond the scope of this thesis, however, this region is relatively thin, less than a micron, with a voltage gradient on the order of 1,000 V/cm. An uncertainty of 25% in the voltage drop across this transition would only yield an error of ± 250 mV which does not affect the basic conclusions of this section.

(a) (b)
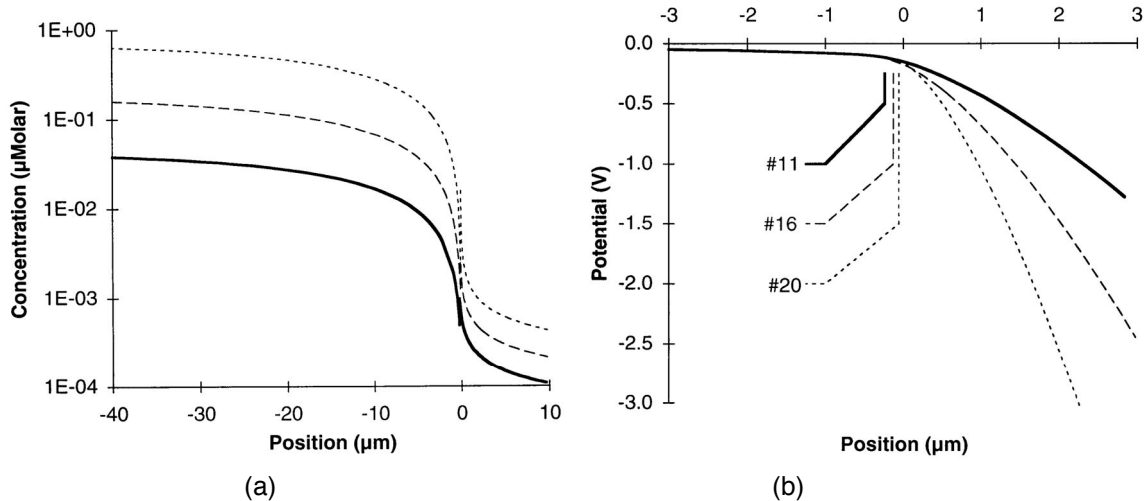
Fig. 4.11 Matching of Regions B & C. Position is indicated in Region B coordinates. Lines indicate position of transition. Note that ionic concentration is shown on a log scale.

Table 4.7 Matching Regions B & C

	Trial 11	Trial 16	Trial 20
Region B Position (x_B)	-0.24 μm	-0.13 μm	-0.06 μm
Region C Position (x_C)	0.12 μm	0.08 μm	0.01μm
Voltage Gradient	-1,080 V/cm	-1,690 V/cm	-1,060 V/cm

Summary of Conduction Without Convection — At constant current in the absence of convection it will take approximately one half second for a gradient layer to form at the cathode. This will cause a rise of 100 to 200 mV due to the increased resistance of the gradient layer. Once the gradient layer has formed it will move away from the cathode at 30 μm/s. After one second a 15 μm thick ion depleted layer will open between the gradient layer and the electrode. To maintain a constant current, the voltage in these three cases will have risen by 12, 24 and 47 V. In the highest current case, the voltage would reach the 1,000 V saturation of the current supply used in these experiments within 5 seconds.

This behavior is, in fact, never seen in a low viscosity electrolyte solution. The reason for this is the rapid transition to convective flow at the electrode. The nature of this transition to convection is the subject of the next section.

4.4.4 Conduction in the Solvent - Convection

Force on the Solvent - Without Convection — The only force available to drive convection on the micron scale of the electrochemical boundary layer is electrostatic force. Fig. 4.12 shows the body force on the fluid next to the cathode for the conductivity and current flux conditions of deposition 16 without convection. The body force on the fluid at any point is simply the product of the net electrostatic charge density per unit of solvent times the electric field at that point.

$$F = qE \qquad\qquad [4.26]$$

The body force is a vector pointing toward the cathode, i.e. the solution is attracted to the cathode.

(a)   (b)
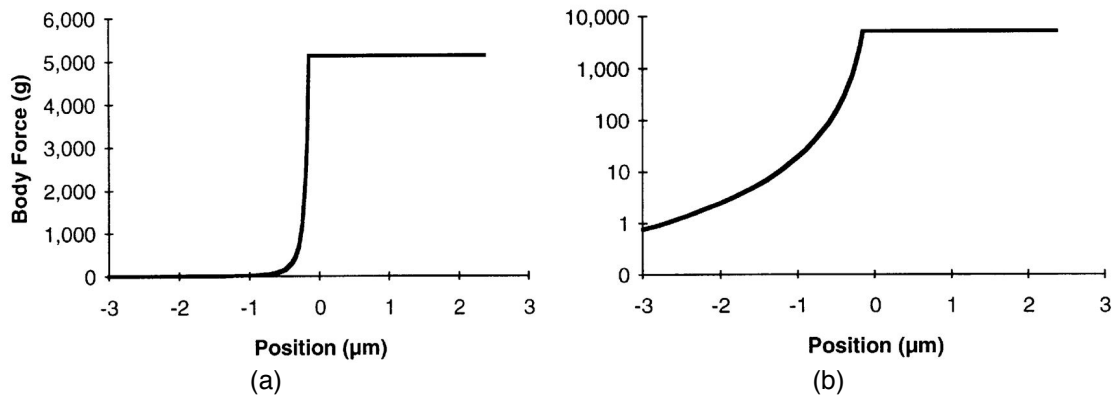
Fig. 4.12 Electrostatic body force on ethanol next to the cathode for current and conductivity conditions of Deposition 16. The force is given in multiples of the gravitational force on ethanol. Position is in reference frame for Region B. (a) linear scale, (b) Log scale.

In the gradient layer the electrostatic charge is calculated from the gradient of the electric field:

$$\frac{\partial^2 \phi}{\partial x^2} = \frac{q}{\varepsilon \varepsilon_o} \qquad\qquad [4.27]$$

in the gradient region the electrostatic charge and electric field both go up exponentially as the total ionic concentration drops. This gives a very rapid rise in the body force over the last few microns of the gradient layer.

In the unbalanced charge layer continuity gives the result that charge and electric field are inversely related, therefore their product, the body force, is constant.

Basis of Convective Instability — With the attractive force on the solvent rising toward the cathode, it is not immediately obvious why this layer should be convectively unstable. If this were a gravity/density gradient, this would be the definition of stability.

The fact that this layer is severely unstable to convection comes from the orders of magnitude difference in the transmission speed of changes in the solvent due to 1) electric field, 2) convection and 3) diffusion/migration, and in the response times of the

corresponding changes of the solvent 1) electrostatic charge/ionic flux, 2) fluid momentum, and 3) ionic concentration differences.

Changes in electric field are effectively transmitted instantaneously through the solvent. This results in a change in the direction and speed of ionic migration and therefore flux in the solvent. For our purposes here this change is also effectively instantaneous. Wherever there is a ionic concentration gradient there will also be a change in electrostatic charge. This only requires a small relative change in the position of positive and negative ions, and occurs on the scale of milliseconds. This charge then feeds back to modify the electric field in the solvent.

Convection can move parcels of solvent with different ionic concentration or chemical composition through the solvent as speeds from millimeters to centimeters per second. The time necessary for convection to begin will depend on the accelerating force per unit volume in the fluid. As shown in Fig. 4.12, the force on the fluid in this case reaches to several thousand times the force of gravity on that same unit of fluid.

Diffusion and migration are the slowest processes in the solution. The maximum diffusion speed in this problem is $\approx$3 mm/s in the highest concentration gradient regions. The maximum migration speed occurs for the positive ion in the charge depleted zone, reaching $\approx$5 cm/s. However, much more typical is the range of speeds in the charge balanced region of 30 μm/s up to 4 mm/s. This means that inhomogeneities in ionic concentration will be very slow to dissipate in comparison to electric field changes and convective motion.

Convective Instability - Example — Convection at the electrode will take the form of a vortex with fluid at one side moving toward the electrode and at the other moving away. To create a very simple conceptual and analytical model of this flow, the two sides of the vortex are replaced by two tubes, Fig. 4.14. One end of the tubes is open to the bulk solution while the other end terminates at the cathode. At the cathode end of the tubes there is a bridge which allows fluid motion from one tube to the other.

(a)   (b)
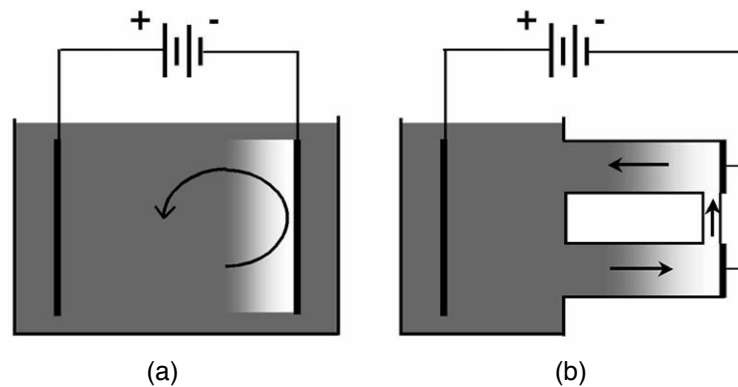
Fig. 4.13 A two dimensional circular vortex at the electrode (a) is modelled by two tubes hydraulically connected at the electrode surface (b).

To illustrate the forces driving convection the case shown in Fig. 4.14 is taken as a baseline case. In each of the tubes the gradient layer is assumed to have formed uniformly and moved away from the electrode by two and one half microns. A finite perturbation is then added. A one half micron layer of fluid from the depleted layer is moved instantaneously from tube B to tube A. Two cases at opposite extremes are then considered, constant current and constant voltage through each of the tubes.

After gradient and charge depleted layer have developed, 0.5 *µ*m of solvent is displaced from Tube B to Tube A ,changing relative positions of gradient layers.

Force and Pressure in Tube A.

Force and Pressure in Tube B
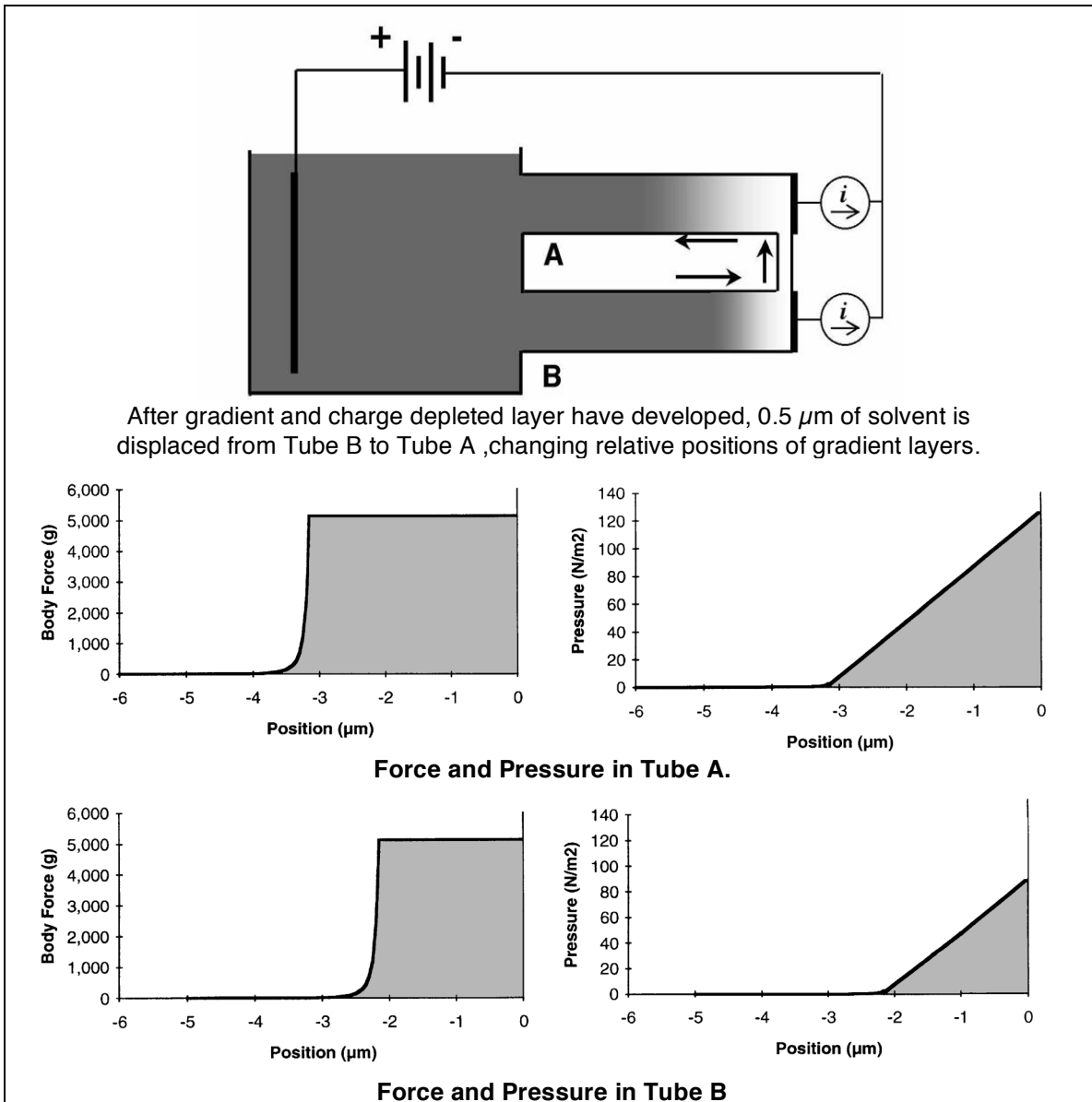
Fig. 4.14 If a constant current is maintained in each of the two tubes leading to the electrode, pressure forces will resist any flow between the tubes. In this case convection will be strongly damped.

The constant current case is the simplest and most intuitive. In this case the electrostatic body force on the solution remains the same, but in tube A the depleted layer is thicker. The integral of the body force from the bulk to the electrode gives the hydrostatic pressure at the electrode. With a thicker depleted layer, an identical body force is integrated over a longer distance, and the pressure at the electrode in tube A is higher than at the electrode in tube B. This would force the displaced fluid back into tube B until the depleted layers are the same thickness again. Thus in the case of a uniform current flux across the electrode surface, this layer would be stabilized against convection.

However, this intuitive case is not representative of the case in the unconstrained solution. The power supply will adjust so that the same total current is conducted through the solution, but there is no requirement that the current flux be uniform across the electrode surface. Given a uniform potential at the electrode and the much higher conductivity of the bulk solution relative to the gradient and depleted layers, these layers are best described as separating two equipotential planes.

Returning to the two tube example, when a portion of the depleted layer moves from tube B to tube A, the effective resistance of tube A increases dramatically while that of tube B drops equally dramatically. Using the hierarchy of effects laid out above, the first change will be in electric field, current flux, and electrostatic charge. The change in electrostatic charge and electric field will translate into an immediate change in body force and therefore hydrostatic pressure. The concentration profile in the gradient layer will initially be assumed constant, and the forces that would drive convection will be assessed.

In the base case when the gradient layer has moved away from the electrode by 2.5 μm, the total voltage drop over the 100 μm next to the electrode is 2.09 V. This is taken as the constant voltage for the following analysis. When one half micron of fluid is displaced from tube B to tube A, the current in tube A will drop by 33% while the current in tube B will increase by 55%. Although the total voltage drops are equal through each of the tubes, the electric fields are higher in tube B. The electric field gradients are also higher in tube B, which indicates higher net electrostatic charge. This higher electrostatic charge acted on by higher electric fields leads to much higher body forces on the solvent in tube B.

This is shown in the graphs in Fig. 4.15. The pressure at the electrode in tube B rises to 140 Pa from 110 Pa while the pressure drops to 80 Pa in tube A. In this case an initial disturbance will lead to a pressure difference that will drive the system further in the direction of the disturbance.

After gradient and charge depleted layer have developed, 0.5 *µ*m of solvent is displaced from Tube B to Tube A ,changing relative positions of gradient layers.

Force and Pressure in Tube A.

Force and Pressure in Tube B
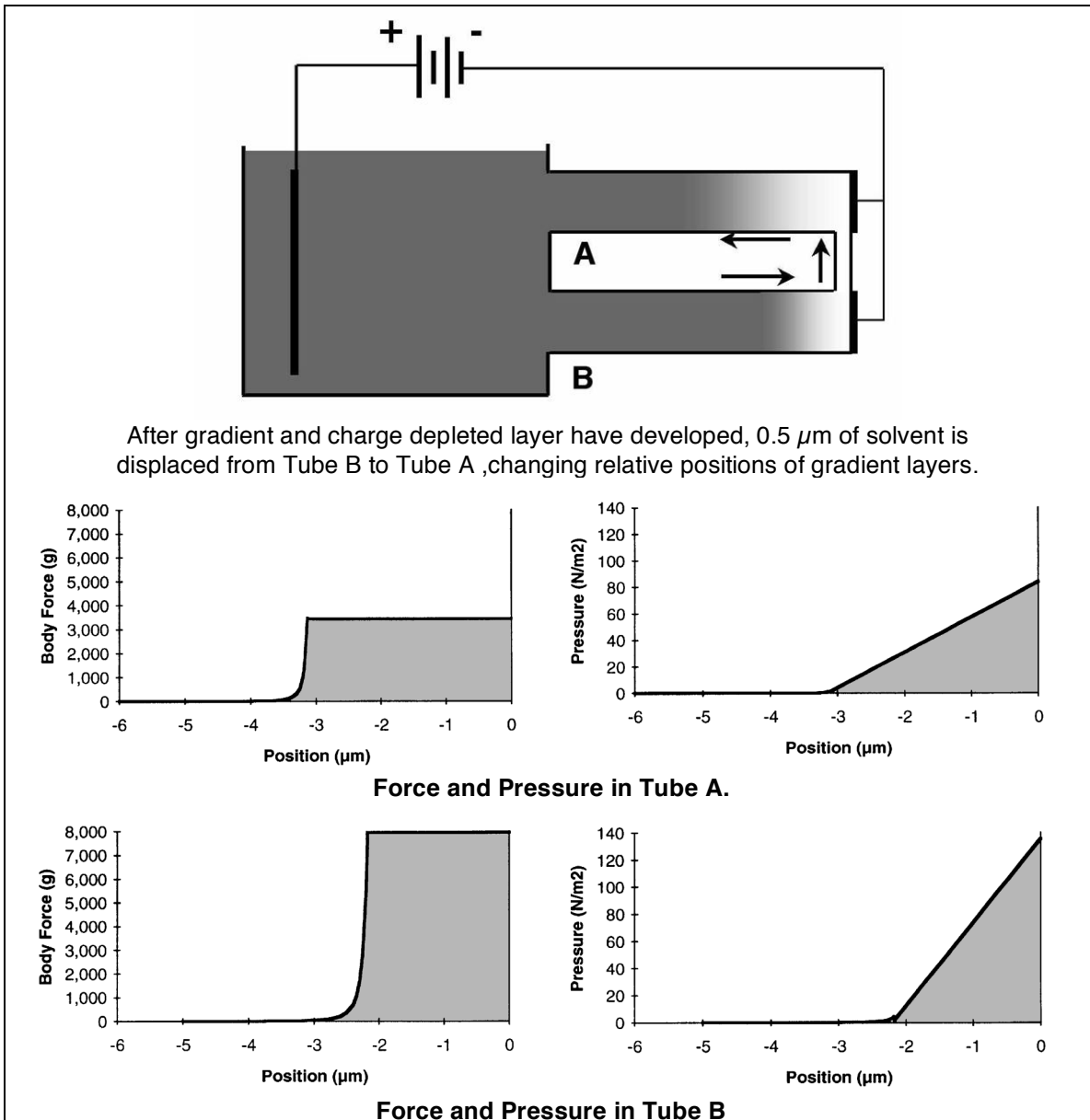
Fig. 4.15 At a constant voltage, a small disturbance will lead to pressure forces which drive the system farther from equilibrium. This system is convectively unstable.

Once this instantaneous electrostatic/electrodynamic analysis is done it is now necessary to look at the slower responding phenomena, convection and diffusion. Convection is driven by pressure differences. In this case the instability of the charge depleted layer drives convection while convection increases the instability of the charge depleted layer. On the other hand, the increased conduction in tube B will cause the gradient layer to become steeper and recede faster from the electrode, with the opposite

occurring in tube A. Thus the change in speed of the gradient layers acts to dampen the instability.

In the two tube example of Fig. 4.15, the gradient layer in tube B would accelerate to 45 μm/s away from the cathode while slowing to 20 μm/s in tube A. This gives a relative speed of 25 μm/s.

To compare this to convection it is necessary to estimate possible convection speeds. This can be done by combining the pressure differential with an estimate of the mass to be accelerated. To get an order of magnitude estimate of the mass, a conservative estimate of an initial vortex size of 30 μm is taken. This would obviously include all of the depleted layer as well as the steepest portions of the gradient layer. This is then roughly approximated by making the two tubes in the above example 30 μm long. The pressure difference between the two tubes is 60 N/m^2 with a mass to be accelerated of 0.048 kg/m2. This gives an acceleration of 1,250 m/s^2. At this acceleration the convection speed would exceed the relative speeds of the gradient layers in 20 ns. If this pressure were stable over a distance of 0.5 μm the solvent would accelerate to 3.5 cm/s, more than one thousand times the speed of the gradient layers.

The example used here is somewhat exaggerated. It is unlikely that in a free solvent a several micron depleted layer would form. Because of the high instability of the these layers, it is far more likely that convection begins even before the gradient layer is fully formed. This is supported by current voltage measurements which show a simple linear resistance behavior when passing the limit current. Determining the actual point where convection begins is beyond the scope of the current discussion, however, this example gives a good example of the forces that develop in the absence of convection. This both serves as an illustration of the necessity of convection in the solvent without particles and background for the next section where the effect of particles is finally introduced.

Returning to the two tube example, convective motion will only proceed until the gradient layer comes up against the electrode in tube B. In this two tube example the system would quickly reach an equilibrium state with solvent flowing through the system at approximately 60 μm/s. Solvent flowing into tube B will exactly match the motion of the gradient layer relative to the solvent so that the gradient layer is stationary relative to the electrode. Virtually all of the current will be carried through this tube, with tube A filing up with ionically depleted solvent. The gradient layer will stabilize at a distance just far enough from the cathode that the electrostatic force on the solvent creates enough pressure to drive the convection.
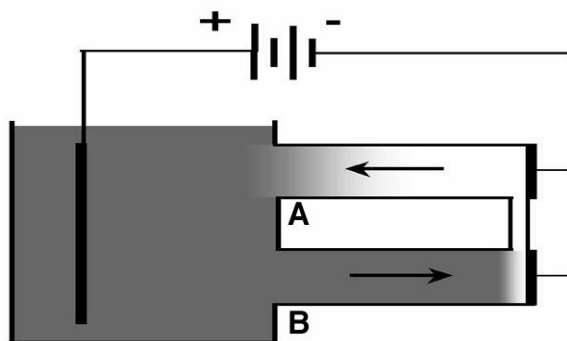
Fig. 4.16 Stable convection in two tube case. Almost all current will be carried by solvent in tube B while tube A fills with ion depleted solvent. The fluid will flow at a speed just sufficient to keep the gradient layer fixed relative to the electrode.

Stable Convection — The two tube example above is a case where geometric constraints on the system allow a stable convection pattern to develop. Having a fixed geometric constraint on the system on the same scale as the vortices is a condition for the formation of a stable vortex or system of vortices. These geometric constraints can be broken into electrode distance and pinning.

If the electrodes are close enough together that a single vortex between the electrodes provides sufficient transport to suppress the formation of additional vortices a stable system of vortices can form. This requires either the current be very low, leading to very slow vortex motion, or the electrodes be very close together. Examples of stable vortices between closely spaced electrodes are given in (**7, 8, 9**).

Fig. 4.17 gives an example from (**7**) of stable vortices forming between closely spaced electrodes. The anode is a transparent sputtered coating of conductive indium/tin oxide on glass. The cathode is platinum. The electrodes are parallel with a spacings of 175 and 120 μm in (a) and (b) respectively. The fluid is an electroluminescent rubrene electrolyte solution. The photographs are taken through the transparent anode looking at the cell perpendicular to the electrodes. The bright areas indicate where positively charged solution flows toward the cathode where electrochemical reduction causes it to luminesce, as shown in the schematic portion of Fig. 4.17. Note that the glowing areas occur at a spacing roughly 2x the interelectrode spacing, indicating a roughly circular crossection to the vortices.
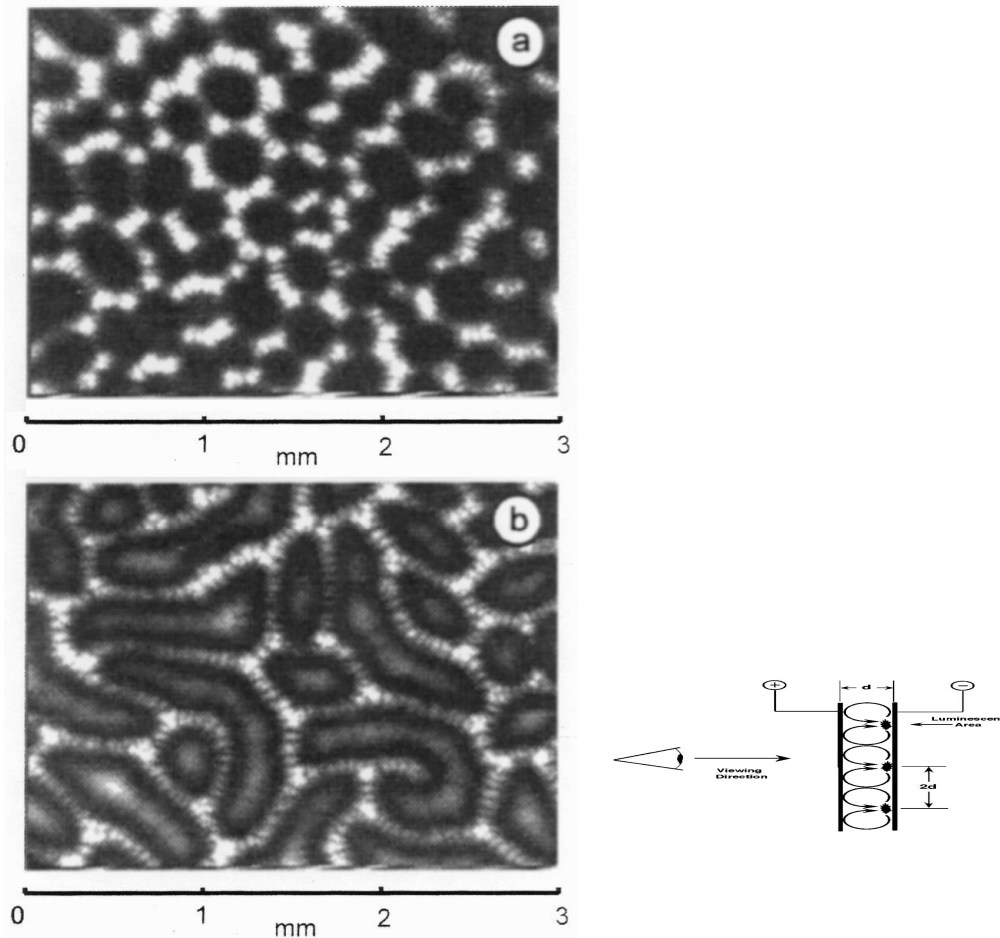
Fig. 4.17 Stable convective cells in DC conduction between closely spaced parallel electrodes, visualized using electroluminescent electrolyte photographed through transparent anode. Luminescent areas indicate flow impingement on the cathode. (a) Quasi-hexagonal arrangement of toroidal vortices, electrode spacing 175 μm, (b) Paired vortex tubes, white areas indicate flow impingement on the cathode, light areas indicate flow impingement on the anode, dark areas indicate flow parallel to the electrodes, electrode spacing 120 μm. From (**7**).

In Fig. 4.17(a) the vortices are essentially toroidal and arranged in a quasi-hexagonal pattern with fluid moving toward the anode in the center of the dark areas. These toroidal vortices represent the highest energy arrangement of vortices between two plates. The vortices in Fig. 4.17(b) show a slightly lower energy arrangement with the vortices arranged as parallel pairs of vortex tubes which connect back to each other at random distances.

Fig. 4.18 shows an entirely different system. This is a nematic liquid crystal between two glass plates being driven in conduction by an alternating current. The arrangement of multiple, parallel, counterrotating vortex tubes is an example of the lowest energy arrangement of stable vortices between two parallel plates.
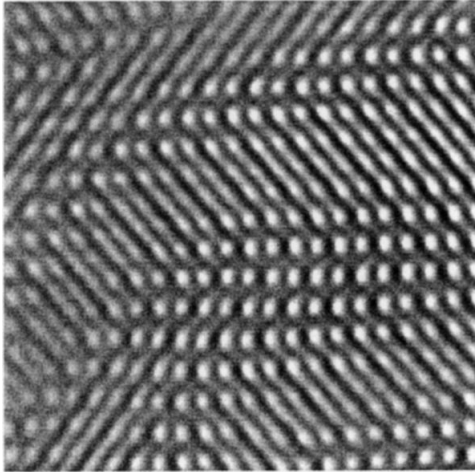
Fig. 4.18 Stable convective cells in AC conduction between closely spaced parallel electrodes, fluid is nematic liquid crystal solution as used for LCD displays, electrode spacing 26 μm, area shown is 497 μm square, the spacing between the parallel vortices is 18 μm. From (**8**).

There is an energy barrier between the quasi-hexagonal, toroidal vortex state and the parallel tubular vortex state, however, if there is sufficient instability in the system, it will evolve toward the parallel tubular arrangement. This transition can also be forced. If there is an overall flow of the fluid in one direction parallel to the electrodes, toroidal vortices will be stretched in the direction of the flow. This can cause the toroids to break and re-link to form long vortex tubes in the direction of flow. This can result in very commonly seen parallel ridge or deposition patterns during EPD where a larger convective flow directs the formation of parallel vortex tubes at the surface. A clear example of this is given in the photograph of the deposition of silver powder in Ch. 5.
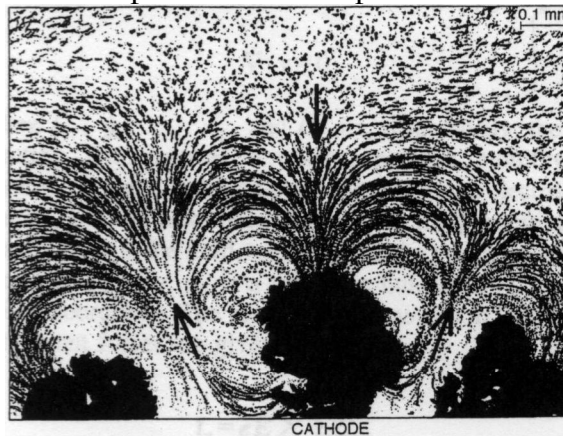
Fig. 4.19 Pinned convective cells From (**7**).

Stable vortices can also form around irregularities on the electrode surface. These can pin either the inflow or outflow of a vortex. An example of this is given in (**9**). Here growing filaments of copper focus electric fields on their tip and focus the inflow of fluid

to a specific point. This sort of pinning can also occur due to non-uniformities in the conductivity of the electrode or non-uniform accumulation of deposit forming on the electrode surface.

Free Convection — In the usual EPD cell the electrode is a uniform conductive surface, there is a large distance between the anode and cathode, and a current is used which is several orders of magnitude higher than the limit current for the cell. In this case circular vortices will form at the surface with the diameter and spacing on the same scale as the ionic concentration gradient layer. These vortices will increase ionic transport, but as the vortices themselves become ionically depleted they will grow out into the bulk solution. The resulting oval crossection of the vortices will not be stable and these vortices will break apart, merge and grow. The larger vortices will then provide more ionic transport to the surface. However, at some point the vortices will become large enough that they do not provide sufficient transport in the layer immediately adjacent to the electrode. Once again a steep ionic concentration gradient layer will form generating a new set of small vortices. In some cases a stable system can form where a large vortex transports ions in from the bulk and a set of small tubular vortices aligned with the larger vortex flow provide enhanced transport at the electrode surface. This is particularly common where the larger vortex is pinned by some inhomogeneity in the system. In other cases, particularly where the cell and electrode are uniform on the scale of the gradient layers, there will be a continuous, chaotic, "boiling" layer of vortices being generated, breaking, merging, growing, and re-generating.

(a)   (b)   (c)   (d)
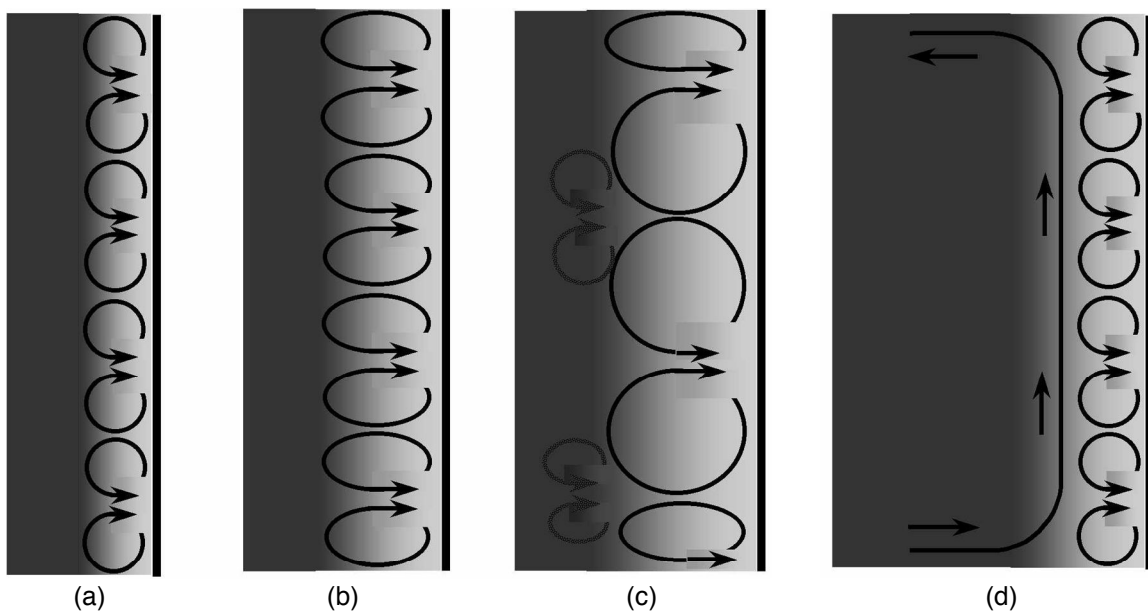
Fig. 4.20 Unstable convective cells.

4.4.5 Conduction in the Solvent - Effect of Particles

Having examined conduction without convection, the forces initiating convection, and the growth of convection, it should be clear the vital importance of ionic transport and ionic concentration changes in determining the behavior of a fluid in D.C. conduction. It is necessary to understand this first because of the somewhat surprising result that the most important effect of the addition of particles to this system is the change of ionic transport and the buffering of ionic concentration changes during D.C. conduction.

This result is counterintuitive because of the negligible effect the particles have on conductivity and conduction. As stated in Ch. 3, the difference in conductivity of a solution with 1 vol.% of particles either suspended or sedimented out was less than the margin of error in the conductivity measurement. Taking the net positive surface charge on the particles and the migration velocity of the particles in a D.C. electric field, the contribution to current flux in the bulk solution for the three cases here is 1.9, 0.4, and 0.06%.

However, when the total reversibly adsorbed HCl on the particle surfaces is considered, the picture is entirely different. The dissolved HCl in solution in these three cases is 0.045, 0.192, and 0.751 Mol/m^3. The available HCl on the surfaces of the suspended alumina is 0.865, 1.11 and 1.28 Mol/m^3. This means that, per unit volume, the amount of HCl which can desorb from the particle surfaces is 20, 6 and 2 times the HCl in solution. This applies to the molar flux of HCl as well. Taking the migration speed and concentration of the alumina particles in the bulk solution, the total flux of HCl carried by the particles is 11.7, 12.3 and 8.47 μMol/s•m^2 toward the cathode. This compares to the flux of dissolved chloride ions away from the cathode of 1.36, 5.32 and 21.3 μMol/s•m^2. Through the following analysis it should become clear how important the adsorption measurements of Ch. 3 are to understanding deposition in this system.

In this section particles that are stopped at the deposition electrode are only referred to as an accumulation of particles. Whether or how these particles form a deposition on the electrode is a subject for the next section. The effects of these particles on ionic gradients depend only on their presence, regardless of whether they have formed a rigid deposition or not.

4.4.5.1 Comparison of Trials #11 & #16

To begin with, the focus will be on deposition trial #'s11 and16. The objective will be to show why there is a stable linear voltage rise accompanied by deposition in trial #16 and no voltage rise or deposition in #11.

Bulk Migration — In the solution without particles, an ionic concentration gradient forms at the cathode as H^+ ions are consumed and Cl^- ions migrate away faster than they are replenished by diffusion from the bulk. With particles present, the migration of Cl^- ions away from the electrode will be countered by the electrophoretic migration toward the electrode of adsorbed Cl^- ions on the particles. In both cases #11 and #16, the flux of adsorbed Cl^- carried by the particles is greater than the migration of dissolved Cl^-. Wherever the particles are free to move by electrophoresis no large ionic concentration gradients would be expected to develop. Up to the front of accumulating particles at the electrode the ionic concentration in solution will be the same as the bulk.
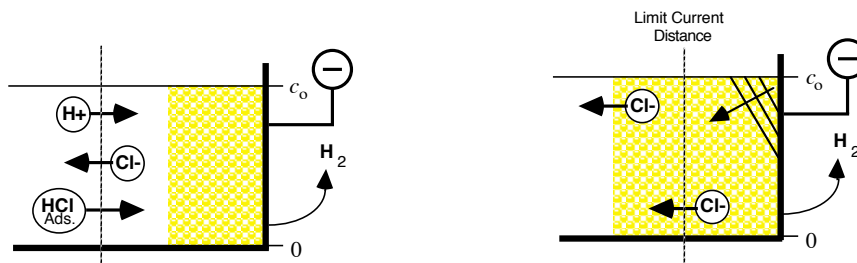
Fig. 4.21 In the bulk solution Cl^- migration is counteracted by electrophoretic motion of adsorbed HCl. At the cathode electrophoretic motion of the particles is stopped, but migration of Cl^- in solution continues.

Accumulated Layer — When they come up against the electrode, the electrophoretic motion of the particles stops. Where the electrophoretic migration is stopped, the flux of adsorbed Cl^- becomes zero while the migration of Cl^- in solution continues. It is in this area concentration gradients can develop.

Because there are no direct measurements of this layer, it is necessary to make some assumptions about the accumulation of particles at the electrode. In the bulk electric field of 13.9 V/cm in trial #11 the alumina particles will migrate at a speed of 13.5 μm/s. At the electrode the particles will accumulate at an estimated density of 20-25 vol. %. This gives an average interparticle separation of 80-90 nm. This estimated density is very approximate, and there will most likely be a density gradient through this accumulated

layer, however, the conclusions reached here will be valid for a wide variation in this density. At an average density of 25% the accumulated particle layer will grow at a rate of 0.375 μm/s, giving a total thickness of 45 μm over the 120 s of the deposition experiment.

In deposition trial #16 an accumulated layer density of 35% will be assumed. The reason for this higher assumed density will be given later. In the bulk electric field of 13.0 V/cm the particles will migrate at a speed of 11.0 μm/s, accumulating a 38 μm layer over the 120 s deposition time.

Assumed Gradient — Accurately modeling the development of these concentration gradients will likely require numerical simulation at some future date. However, by making some simplifying assumptions it is possible to establish a rough numerical criterion for what type of gradients will develop and when deposition of the particles will or will not occur. It is then also possible to qualitatively describe the development and shape of the concentration and potential gradients in this accumulated layer without the simplifying assumptions.

The greatest simplification can be made by replacing the actual non-linear adsorption isotherm with a simple linear adsorption for each of the cases. This is shown in Fig. 4.22.
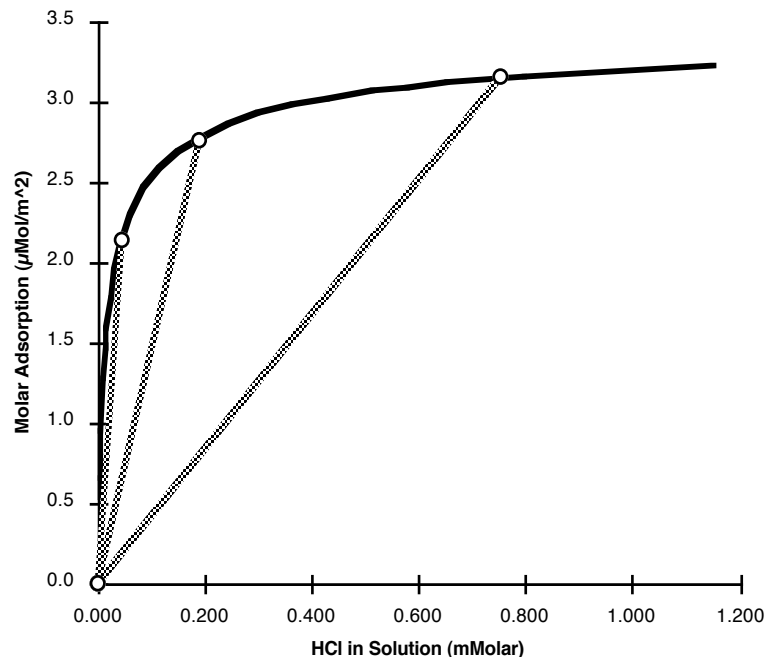
Fig. 4.22 Adsorption isotherm for HCl on alumina. Circles show the total adsorption for cases 11, 16 & 20. Lines show the linear adsorption assumption for each of the three cases.

The second assumption is that ionic concentration in solution is small relative to the adsorbed HCl in the accumulated layer. The implication of this second assumption is that desorption of HCl largely compensates for the consumption of H+ at the cathode and the migration of Cl- away. This means that the overall motion of the gradient layer will be slow relative to the movement of ions within the gradient layer. This then leads to the concept of the quasi-static, quasi-neutral gradient layer. In the Levich limit current case the migration of ions is blocked by the electrode at one end of the electrochemical cell, resulting in a constant ionic concentration at that point. In this case the desorption of HCl does not result in a fixed concentration but one that changes relatively slowly. Because of this slow change in concentration and therefore slow movement of the gradient layer, it approaches the behavior of a stationary gradient layer (quasi-static), and the analysis of Levich, given in section 2.2.8, can be applied. This means that a linear concentration gradient layer will form with a slope equal to the slope in the limit current case, declining from a point where the concentration is equal to the bulk solution to a lower concentration at the electrode.

The ionic concentration gradient in the accumulated layer will then develop as shown in Fig. 4.23(b). A gradient with a constant slope will form at the cathode and will move slowly away as the adsorbed HCl in the layer next to the electrode is desorbed and consumed. Only when the edge of the gradient layer has moved to the limit current distance from the electrode will the concentration at the electrode drop effectively to zero allowing a depleted charge conduction layer to form, and it is only the formation of a charge depleted conduction layer that can account for the large voltage rises seen in the deposition trials.

This analysis is then turned around to define a criterion for the formation of a charge depleted layer. A control volume is defined which is bounded on one side by the electrode and on the other by an imaginary plane at the limit current distance from the electrode. If the net flux of Cl- out of this volume is more than 1/2 of the Cl- within this volume then a charge depleted layer can be expected to form.
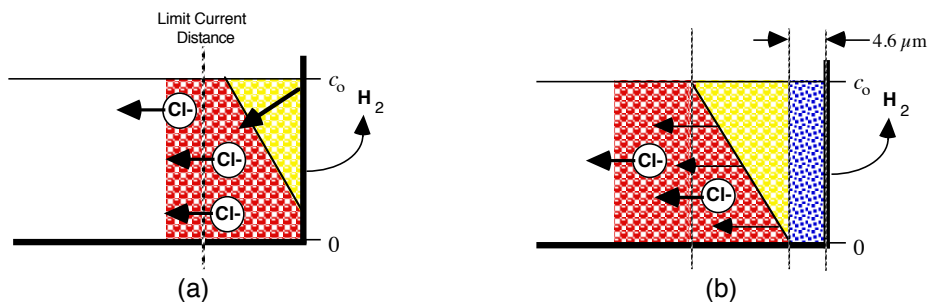
Fig. 4.23 (a) In deposition trial #11 the total Cl- flux out of the control volume is less than 1/2 of the total content. (b) Trial #16 gradient layer moves away from electrode creating ion depleted layer.

Applying this criterion to deposition trials #11 and #16 clearly shows the difference between the two. In #11 the limit current distance is 22 μm. Since electrophoresis of the particles over the course of this trial results in an accumulated layer of approximately

$45 \, \mu$m, the control volume can be assumed to be completely filled by particles at a volume density of 25%. This then gives a total content of HCl, both adsorbed on the particles and in solution of $476 \, \mu$Mol/m^2. The flux of dissolved Cl- out of this volume would be $1.36 \, \mu$Mol/s•m^2, or only $163 \, \mu$Mol/m^2 over the 120s of this trial. This is only 35% of the Cl in the control volume, therefore in this case the presence of reversibly adsorbed HCl on the surface of the particles will suppress the formation of a charge depletion layer. Little or no voltage rise would be expected. This is shown is Fig. 4.23 (a)
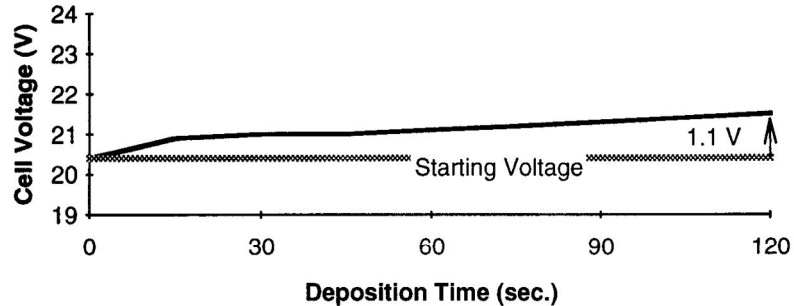
Fig. 4.24 Voltage rise during deposition trial #11 .

In the case of trial #16 the limit current thickness is $23 \, \mu$m. Again this volume will be more than filled by particles due to electrophoresis during the deposition trial. This then gives a total content of HCl in the $23 \, \mu$m control volume of $895 \, \mu$Mol/m^2. The molar flux of Cl- out of this volume is $5.32 \, \mu$Mol/s•m^2, or $628 \, \mu$Mol/m^2 over the course of the trial. This clearly exceeds the criterion set out above of 1/2 the molar contents of the control volume. In this case an ion depleted layer would be expected to develop. This is consistent with the 3.3 V rise actually seen during this deposition trial.

Assuming a constant gradient moves from the cathode, the total outward flux of Cl-ions could be accounted for by desorption from a $23 \, \mu$m gradient layer and a $4.6 \, \mu$m thick charge depleted layer. This $4.6 \, \mu$m is calculated based on the 35 vol. % particle density assumption for the accumulated layer. If this $4.6 \, \mu$m layer is consolidated to 60 vol. % by the high electric field in the depleted layer, the resulting layer would be $2.7 \, \mu$m. This is only 20% less than the actual estimated deposition thickness of $3.3 \, \mu$m.
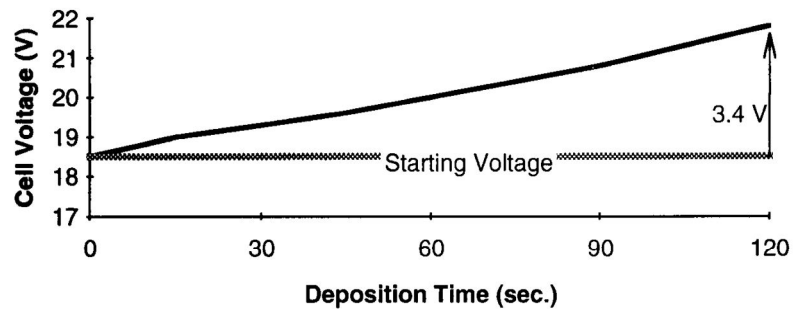
Fig. 4.25 Voltage rise during deposition trial #16 .

Actual Gradients — The one thing that does not fit in this picture is the early onset of the voltage rise in this deposition trial. According to the simple model above, it would take 84 seconds before 1/2 of the Cl- ions have migrated out of the control volume. This means that there should be an 84 sec. delay before the formation of an ion depleted layer with its accompanying anomalous voltage rise. However, as shown in Fig. 4.25, the voltage rise begins almost immediately and continues linearly through the duration of the deposition.

This can be accounted for by returning to the modeling of the adsorption isotherm. It is obvious by inspection that a simple linear model becomes a poorer and poorer representation of the actual adsorption/desorption behavior as the ionic concentration in solution increases. For the conditions of deposition trial #11 it is not unreasonable. However, for the conditions of trial #16 by the linear assumption 50% of the adsorbed HCl particles would desorb if the solution ionic concentration dropped by 50%. Based on the actual isotherm, in reality less than 10% would desorb by this point.

A very simple modification of the linear assumption can slightly improve the fit to the actual isotherm, but more importantly can illustrate one of the most important features of the concentration gradient in the presence of particles. The modification is as shown in Fig 4.26 below. It is assumed that there is zero desorption during the first 50% drop in solution concentration of HCl and the desorption is linear thereafter.
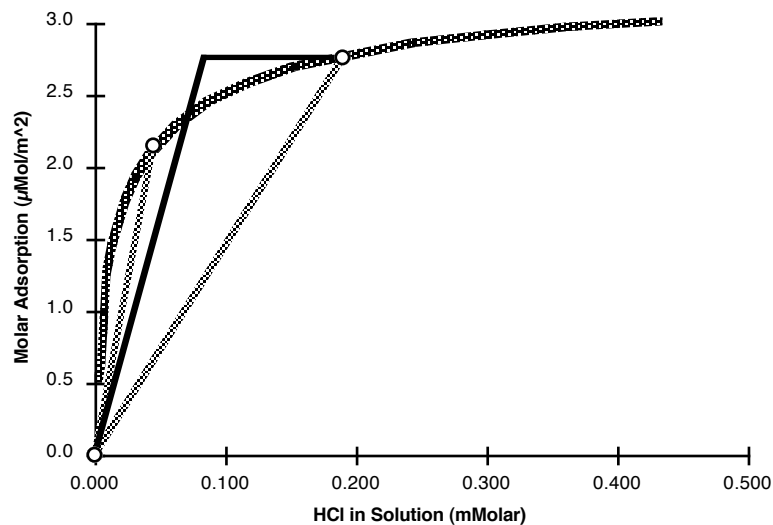
Fig. 4.26 Adsorption isotherm for HCl on alumina. Circles show the total adsorption for cases 11 & 16 Gray lines show the linear adsorption assumption. Black line is modified linear assumption for case 16.

The development of the gradient layers under this modified assumption would proceed as shown schematically in Fig. 4.27. When the current is turned on the concentration at the electrode will drop by 50%, which will be referred to as the 1/2 c_o point. Without buffering by desorption from the particles this will happen very quickly, on the order of a tenth of a second. Once HCl begins to desorb from the particles the 1/2 c_o point will move away from the electrode at a relatively slow rate. Because the current density has not changed the gradient between the 1/2 c_o point and the electrode will once again be the same as the quasi-neutral equilibrium gradient. The limit current distance is now between the 1/2 c_o point and zero at the electrode and is therefore 1/2 the previous distance, or 11.5 μm. One half the adsorbed HCl in this volume is only 112 μMol/m^2. This would be consumed in 21 seconds, after which an ion depletion layer would begin to form. As this quasi-static, quasi-neutral layer is forming, the gradient between the bulk solution and the 1/2 c_o point will flatten and broaden, asymptotically approaching a linear gradient between the 1/2 c_o point and the concentration at the opposite electrode. The development of this gradient can explain the voltage rise over the first few seconds before the voltage begins to rise due to the growth of the ion depletion layer.
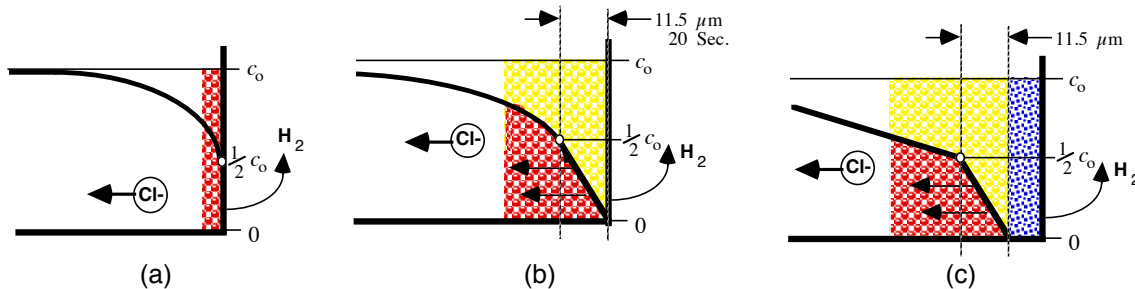
Fig. 4.27 Evolution of the concentration gradient layers under the modified desorption assumption of Fig. 4.x17 (a) the concentration at the electrode will quickly drop to 1/2 c_O (b) an 11.5 μm quasi-static, quasi-neutral gradient layer will slowly form. (c) the gradient layer will migrate opening up an ion depleted zone.

From looking at this modified assumption it is now possible to qualitatively describe the shape of the concentration gradients in the actual system. The key feature of the actual adsorption isotherm is that the desorption rate increases as the solution concentration decreases. At higher concentrations there is relatively little desorption. Most desorption occurs at low solution concentrations. The result is that most desorption coincides with the transition from quasi-neutral to unbalanced charge conduction.

Thus the actual gradients can again be separated into three regions: quasi-neutral, transition and ion depleted.

With particles present, the quasi-neutral region will no longer be characterized by a moving gradient but by an evolving gradient pinned at one end by desorption from the particles in the gradient region. This gradient will evolve in a similar manner to a thermal gradient in a homogeneous solid. The concentration will drop rapidly to a low level at the edge of the transition region and will evolve with time from an exponential drop near the transition layer toward a linear gradient across the cell. The electrostatic forces on the solvent in this region will be orders of magnitude less than the forces in the ion depleted region, but since the layer itself is orders of magnitude thicker it is just as likely to contribute to convection. The convection patterns will just be on a much larger scale - commensurate with the scale of the layer.

The transition layer is now larger and dramatically more important. This layer will be characterized both by unbalanced positive and negative ion concentrations, high voltage gradients and a majority of the desorption of HCl from the particles. The relatively slow motion of this layer is dictated by the desorption rate of HCl within the layer, and it is the motion of this layer which dictates the thickness of the ion depleted layer.

The ion depleted layer is regulated and stabilized by the transition layer. The role of particles in this layer is relatively minor. It appears from voltage measurements that the particles contribute just enough to conduction in this layer to offset the reduction in conductivity due to the physical blocking of the non-conductive particles. This contribution to conductivity could be either by catalyzing the auto-protolysis of the solvent or by promoting EHD convective transport within the pores.

4.4.5.2 Stabilization of Ion Depleted Layer

In discussing convection without particles it was shown that an ion depleted layer is very unstable to convection and no significant voltage rise due to an ion depleted layer is expected nor is found in actual experiments. However, the explanation for the voltage rise in these deposition trials depends on the formation of a stable ion depleted layer, therefore the presence of particles must stabilize the depleted layer. Here the vital role of the transition layer as outlined above becomes apparent.

The difference made by the particles can be illustrated by returning to the two tube example from above but now assuming the tubes to be packed with particles. Again the current is allowed to flow until a 2.5 μm ion depleted layer forms. If 0.5 μm of fluid is now displaced from tube B to tube A there will be virtually no change in the system. Since the quantity of HCl adsorbed to the particles is two orders of magnitude higher than the quantity of H^+ or Cl^- in solution, a motion of the fluid which leaves the particles in place

will have almost no effect. The ionic content of the solvent will be determined almost instantaneously by equilibrium adsorption/desorption in the pores between the particles. As long as the particles remain in place the position of the transition layer relative to the electrode will remain the same. This stabilizes the depleted layer against small, brief fluctuations in fluid motion.

However, it is possible to postulate a preponderate perturbation. Initially the particle density in the tubes is assumed to be 35 vol. %. The current is allowed to flow until a 3 μm depleted layer develops. If then in tube B the electrostatic force causes the particles in the ion depleted zone to suddenly consolidate to 52 vol. %, there will now be a 2 μm ion depleted layer in tube B and a 3 μm layer in tube A, the same situation as shown in Fig. 4.15. The electric field acting on the charged fluid will cause a hydrostatic pressure driving convection from tube B to tube A.

At this point the picture becomes more complicated and requires a combination of analysis, computer modeling and experiment to resolve. While there is an electro-hydrodynamic force driving convection, the viscous drag of the flow through the particle bed retards it. Higher voltage gradients in tube B will lead to a higher current flux. This means a faster migration of the transition region away from the electrode, and vice versa in tube A. Without particles the gradients move with the convecting fluid and can accelerate quickly toward or away from the electrode. With particles present, the location of the gradients are fixed by the particles and only move slowly in response to convective flows. This means that effect of diffusion and migration of ions can be on the same scale as the effects of convection. This also means that electric fields, diffusion and migration in the lateral direction can no longer be ignored.

It is clear from experimental results which show linear voltage rises accompanied by smooth uniform depositions that small perturbations are damped in the growth of these layers. This is direct evidence that within the particle layer viscous drag, adsorption/desorption and very high voltage gradients combine to allow migration and diffusion of ions to dominate over convective instability. Unfortunately, time does not permit the inclusion of a more complete analysis here, and the exact mechanisms and limits of this damping must be reserved for future discussion.

4.4.5.3 Deposition Trials #'s 16& 20

While the picture given above for deposition in trial #16 is complex, the evolution of the deposition process during trial #20 becomes even more so. In deposition trial #11 the accumulation of particles at the electrode suppressed the formation of a high voltage

gradient and no deposition occurred. In deposition trial #16 the flux of Cl- on the particles toward the electrode was higher than the migration of Cl- ions in solution away from the electrode. This means that high voltage gradients could only form within the accumulated particle layer. Adsorption equilibrium within this layer suppresses convective motion, and analysis based only ionic migration can account for the observed behavior. In deposition trial #20, on the other hand, the molar flux of Cl- ions in solution away from the cathode is 21.3 μMol/s•m^2 while the flux of Cl- on the particles toward the electrode is only 8.5 μMol/s•m^2. This means that the particles will neither suppress the formation of an ion depletion region, nor will they contain this region within the layer of accumulated particles at the electrode surface and thereby suppress convection.

Clearly, to account for the 18.9 V rise in cell voltage over the course of this deposition trial the particles must stabilize an ion depleted layer. However, without convection there would be a total flux of Cl- ions away from the electrode of 2500 μMol/m^2. The total Cl- quantity available in the region next to the electrode is only 1000 μMol/m^2. The remaining 1500 μMol/m^2 can only be accounted for by convective flows which wash Cl- ions from the bulk back toward the cathode.

Before entering into a description of the conduction layers in this deposition trial it is useful to review a combination of calculated and experimentally observed quantities. Based on the particle mobility in the bulk electric field of 14.1 V/cm, an accumulation of 31.7 g/m^2 of particles at the electrode would be expected. The weight of deposited particles after rinsing was 26.1 g/m^2 or 80% of the particles that would be expected to accumulate at the electrode. During rinsing, although it was not measured, a substantial overlayer of very loosely deposited material was removed. This appeared to be more than the 20% difference between the expected particle accumulation and the densely deposited layer. The densely deposited layer which could not be removed by rinsing will have a volume density of 50 to 60 %. This gives a thickness of 11 to 13 μm. Over the course of the deposition trial the voltage rose by 18.5 V. For the conditions of this deposition trial an 18.5 V potential difference would correspond to conduction through a stable ion depleted layer of 8 μm without particles present.

Ionic concentrations and concentration gradients will determine conductivity and mechanisms of conduction in the region next to the electrode. This in turn determines voltage gradients in the layer of particles accumulating at the electrode, which, in turn, determines the mechanism of deposition and consolidation of the particles. To describe the nature of the concentration gradients that develop during deposition #20 the following paragraphs will approach the system as a series of layers between the bulk suspension and the electrode.

The first layer is the fluid suspension outside the accumulated particle layer. Because there is a net flux of Cl- ions away from the cathode, the gradient layer will move away from the cathode faster than particles accumulate. This means that the gradient where the solution ionic concentration drops to very low values will continually try to move out of the accumulated particle layer into the fluid suspension. The fluid suspension, however, is convectively unstable in the presence of steep concentration gradients, therefore this layer will be in constant convection. Moreover, because this layer is not bounded nor are there any vortex pinning non-uniformities at the accumulating particle surface, this convection will be random and chaotic with vortices constantly forming, growing, merging, and re-forming. This means that at the surface of the accumulated particle layer the solution ionic concentration will be constantly fluctuating as an ion gradient attempts to migrate out of the accumulated layer and convection washes ions back in from the bulk solution.

At the surface of the accumulated layer is a low density particulate layer that serves as a buffer between the unstable convection of the fluid suspension and stable layers within the accumulated particle layer. When a convective flow moving toward the accumulated layer washes in solvent with a relatively high ionic concentration, the particles in the buffer layer will adsorb most of the extra ions before the flow can penetrate past the buffer layer into the accumulated layer. Where convection brings solvent with a higher ionic content up to the buffer layer there will be higher ionic and voltage gradients between the fluid suspension and the buffer layer. This will cause an increased local hydrostatic pressure which will cause the flow toward the electrode to spread laterally. The increased voltage gradient will also speed the outward migration of Cl- ions, depleting the ions which were adsorbed from the inward flow. Because of the steep slope of the adsorption isotherm at low solution concentrations, the total ionic concentration in this layer can fluctuate significantly while limiting solution ionic concentration to a very narrow range of values.

Behind the buffer layer is a transition layer in which the total concentration drops to the extremely low level that marks the beginning of the ion depleted conduction layer. Where the buffer layer is marked by continually varying ionic concentrations, the transition layer will be marked by a stable and steeply declining total concentration of HCl. In deposition trial #16 this transition layer will move outward at a speed dictated by the depletion of ions adsorbed to the particles in the accumulated layer. In this case, #20, the motion will be blocked by the buffer layer, which itself is tied to the motion of the boundary of the accumulated particle layer. The actual mechanism of this blocking is the backward diffusion of Cl- ions toward the cathode balancing the migration of Cl- away.

This means that the gradient in this case will be much steeper than in the case of deposition #16. Nevertheless, this layer still serves the same function as in deposition #16, which is to stabilize the boundary of the ion depleted conduction layer.

This ion depleted conduction layer is then the final layer. It is also the thickest and accounts for most of the voltage rise in during the deposition. The transition layer will be very thin and therefore there will be a sharp transition from the relatively moderate voltage gradients of quasi-neutral conduction to the extremely high voltage gradients necessary to drive unbalanced charge conduction in the ion depleted layer.

The primary difference between deposition trial #'s 16 and 20 is the mechanism regulating the thickness of the ion depleted layer. In deposition trial #16 the movement of the gradient layer is a function of ionic migration. In deposition trial #20 it is a function of the accumulation of particles. In both cases there will be a strong automatic leveling effect for the ion depleted layer.

In deposition trial #16 the thickness will be regulated by ionic flux. In any areas where the ion depleted layer is relatively thinner there will be a higher voltage gradient leading to faster outward migration of Cl- ions. This causes faster motion of the transition layer until the thickness of the ion depleted layer is evened out. Likewise thicker areas will be evened out by slower growth. In the conditions of this trial the automatic leveling effect only applies to the ion depleted layer. There is no mechanism to regulate the thickness of the accumulated particle layer. The total thickness of the particulate layer will be determined by convection and deposition cell geometry.

Under the conditions of deposition #20 there will be an automatic leveling effect for the entire deposition thickness. Because the motion of the transition layer is limited by the proximity of the surface of the accumulated layer, in areas where the total layer is thinner, the ion depleted layer will be thinner as well. This means that there will be a higher voltage gradient in the suspension attracting more particles to the thinner area.

4.4.5.4 Voltage Rise vs. Deposition Thickness

Throughout the previous discussion it was assumed that the anomalous voltage rise seen in the cases where a deposition formed was due to the formation of an ion depleted conduction layer. If this is correct then some correlation would be expected between an estimated ion depletion layer thickness and the deposition thickness.

The first step is defining what is the anomalous voltage. Deposition trials #5 through 9 had an average voltage rise of 0.4 V. Deposition trials # 10 & 11 showed the deposition of a monolayer of particles accompanied by voltage rises of 1.0 and 1.1V.

Based on these observations it will be assumed that 1 V of the voltage rise during deposition can be attributed to voltage necessary to drive a direct current through the solvent (often referred to as concentration polarization) and to voltage rise due to blocking of the electrode surface by deposited particles. The anomalous voltage is then taken as the voltage rise above one volt over the course of a deposition trial.

An ion depleted layer thickness can then be generated based on this anomalous voltage and the ionic flux density by using the equation for the potential drop across an unbalanced charge conduction layer, Eq. [4.23].

$$\phi = \phi_o - \frac{2}{3}\left[\frac{2JF}{\nu_{H^+}\varepsilon\varepsilon_o}\right]^{\frac{1}{2}} x^{\frac{3}{2}}$$

[4.23]

The calculated thickness for each deposition trial from 12 to 21 is shown in Fig 4.28 as an 'x'. Superimposed on these calculated values are circular spots indicating the actual estimated deposition thickness based on a 60 vol. % density. The correlation is almost perfect for depositions 12 to 19. For depositions 20 & 21 the calculated ion depletion layer is 30% less than the actual estimated thickness.
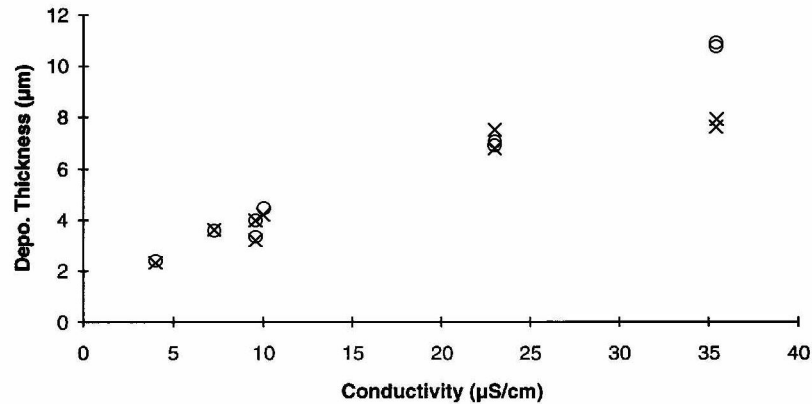
Fig. 4.28 X's are calculated ion depletion layer thicknesses, circles are deposition layer thicknesses based on experiment.

The correlation between the results of this calculation and the actual deposition thickness is actually much better than would be expected even if the theory were perfect. The depleted layer thickness calculation assumes unimpeded motion through pure solvent. In the deposition layer 60% of the volume will be occupied by non-conducting particles, leaving only 40 vol. % open porosity for ionic conduction. This should increase the resistance of the layer, leading to the expectation that the above calculation would give a higher thickness numbers than the actual deposition thicknesses. There are several possible explanations for this excess of accuracy. Determination of which explanation is correct will require further experimentation.

4.4.6 Deposition and Consolidation of Particles

Finally, the above discussion of conduction has provided sufficient background for address the putative subject of this chapter, the formation of a particulate deposition. All of the deposition trials made here began with an electrostatically stabilized suspension of particles. In some cases the repulsion force keeping the particles apart in suspension was overcome to yield rigid depositions of varying density and uniformity. The properties of these depositions can be accounted for by four mechanisms: 1. Electrostatic deposition, 2. Electrosedimentary deposition, 3. Convective deposition, and 4. Electrostatic consolidation.

Electrostatic Deposition —The definition of electrostatic deposition makes it appear to be one of the simplest mechanisms of EPD. In this case the force of the external electric field acting on an undeposited particle is sufficient to overcome the interparticle repulsion causing that particle to come into contact with an already deposited particle, thereby becoming part of the growing deposition.

This would be a simple mechanism if the DEBL around the particle was static. Unfortunately the diffuse layer is dynamic in several modes. It will polarize around the particle, it is pumped around the particle, and as it flows around the particle ions will be diffusing in and out of the layer. A quantitative understanding of how a deposited and undeposited particle come into contact and the electric field necessary to make this happen will most likely require computer simulation. Here there is only time for a very brief, but, hopefully, illuminating qualitative description.
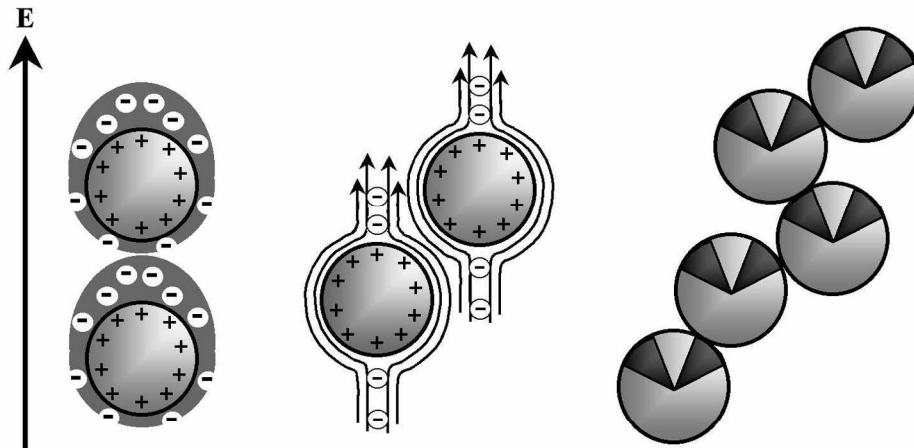
Fig. 4.29 (a) Polarization of a particle /boundary layer, (b) EHD convection make direct linear alignment unstable, (c) .

The first step is to begin with a single fixed particle surrounded by a diffuse electrostatic boundary layer. When an external electric field is applied the mobile ions in the diffuse layer will migrate to one side of the particle, creating an electric dipole. If this were a static dipole then a mobile particle would be expected to line up with the first particle on a line parallel to the electric field. However the ions in solution are mobile. The particle/diffuse layer dipole will attract ions from the solution at one end of the particle, the electric field will drive those ions in a layer of fluid around the particle, and they will diffuse outward on the other side. This creates an outward flow of solvent on the side of the particle away from the electrode. This then makes the position in a direct line with the electric field unstable for an approaching particle. At a position on a line perpendicular to the electric field there is no force to cause deposition. This means that between 0°, parallel to the electric field, and 90°, perpendicular to the electric field, there is a limited angular range where one particle will deposit on another. This type of deposition growth leads to very low density as angular chains and sheets of particles grow, blocking off considerable empty volumes between and below them.

The magnitude and importance of the polarization and EHD forces around a particle can be illustrated by looking at the electrophoresis of particles under the conditions of deposition trial #16. The electrostatic charge on an average sized (270 nm dia.) particle is 2.6×10^{-16} Coulomb. If polarization of the DEBL is ignored, the force on this particle due to the bulk electric field of 13 V/cm would be 3.4×10^{-13} Newton. If this force is balanced by a simple Stokes drag force, $6\pi\mu a u_\infty$, ($\mu = 1.07$ mPa•s; $a = 135$ nm) the particle's migration speed, u_∞, would be 126 μm/s. The actual speed based on the measured mobility is 11 μm/s. Thus the effects of EHD flows around the particle and polarization of the DEBL cause a 90% reduction in the migration velocity of the particle. This clearly shows the need for future work to consider the problem of the deposition of particles as a problem of electrohydrodynamics and not electrostatics.

Electrosedimentary Deposition —Electrostatic deposition becomes even more complicated as multiple particles are involved. The theory itself is very simple. The electric field will pull on a particle which itself will not deposit, however, the repulsive force will push on a particle closer to the electrode. Eventually the force on a large enough stack of particles will cause the particle closest to the electrode to deposit.

Unfortunately there are many problems with this very simple picture. The first is simply that the particles will not arrange themselves in a straight line. The undeposited particles will move relative to each other driven by electrostatic attraction, repulsion and

linking of EHD flows. It is possible that with thin boundary layers and low voltage fields the particles can be brought into a close packed arrangement where their movement is blocked. However, based on observations of various depositions it appears to be far more common that this layer remains low density and continues to behave as a fluid. Because of this, these particles need to be approached as dense colloidal layer rather than as individual particles.

The second complication is that at the same time as the electric field is pulling on the particles it is pushing on their DEBL's. This will cause a dielectric displacement reducing the electric field in this layer. The EHD flow of the DEBL's away from the electrode will also create a viscous drag force pushing the particles away from the electrode. This pushing and pulling points out a third complication with the simple view of the electrosedimentary mechanism. So long as this layer is charge balanced, the net electrostatic force on this layer will be zero. The same force that acts to attract the particles will act to repel the solvent around them. If there is to be a net electrostatic force on this layer it becomes a question of conductivity, conduction and ionic balance as was discussed above.

Although the net electrostatic force on this layer may be zero, this does not necessarily mean that the total force is. The pumping of the solvent in the DEBL's away from the electrode will create a hydrostatic pressure driving solvent the other way outside of the DEBL's to keep the volume constant. If the particles have become closely packed enough that this layer is effectively not fluid, this pressure can cause the innermost particles to deposit. The far more likely case is that the interaction of EHD flows around the particles will keep them from forming a closely packed arrangement. This layer will then still behave as a fluid, and any hydrostatic force that develops will drive convection rather than deposition.

With all of these confounding effects, the question then becomes, does this effect really exist? The answer is that it appears to exist, although the evidence for it is only indirect. Suspensions which have a calculated repulsion force greater than the force of the electric field on a single particle, can be deposited, and this can occur without a significant voltage rise which would indicate that a higher voltage gradient layer has formed. This mechanism appears to work only for suspensions which have a repulsion force only two or three times the force of the electric field and yields only low density depositions. The details of how this mechanism might work will require further experimentation and analysis.

Convective Deposition —This is the case where the hydrodynamic force of moving solvent can force particles into contact. If the solvent motion is perpendicular to the

surface, forcing particles straight into the deposition this can yield a dense, well packed deposition - similar to slip casting. If the flow is tangent to the surface particles will contact and deposit on high points on the surface leading to uneven growth and low density deposition. Unsteady flows will deposit particles in both modes leaving a mostly even but low density deposited layer.

Electrosedimentary Consolidation — Although exactly what happens during electrostatic deposition is unknown, once deposition has occurred and the accumulated particle layer is no longer fluid, this problem is transformed into the more familiar and tractable problem of conduction through a particle bed. Example analyses of this problem in the case of equilibrium conduction can be found in (**10, 11, 12**). The problem here is somewhat different given that fluid motion is blocked at one side of the particle bed, but otherwise the same factors apply to the analysis: electric field, surface charge density, and ionic content. The result is that there is a hydrostatic force on the entire layer as well as an electrostatic force on the particles in the layer, the magnitude of each being determined by the factors mentioned above. This combination of forces can consolidate what may begin as a very low density deposition. Since the sum of these forces will increase with depth into the deposition this can lead to a gradient of increasing density from the deposition surface to the electrode.

Ion Depletion Enhanced Electrostatic Consolidation — Part of the force acting on the particles in the electrosedimentary consolidation mechanism described above is an electrostatic force acting directly on the particles. An important part of the definition of that consolidation mechanism is that it occurs during equilibrium conduction. This is an important distinction because what happens during non-equilibrium conduction, specifically when an ion depleted layer begins to form and grow, is so dramatically different in nature and scale that virtually the only similarity is the application of the fundamental equations of electrostatics.

To appreciate the scale of the forces generated here it is helpful to return to the force calculations for a particle under the conditions of deposition trial #16. As mentioned above the force on the particle in equilibrium translation in the bulk electric field is 3.4×10^{-13} N, which is equivalent to 840 times the force of gravity on the same size particle. The viscous force due to EHD flow in the opposite direction is then approximately 770 G in the opposite direction, giving a net force moving the particle through the solution of 70 G.

This would seem like a fairly substantial force until a comparison is made to the force that can be generated in the ion depleted conduction layer. As a particle moves through the quasi-neutral gradient region into the transition region the HCl on the particle

will desorb, reducing the particle charge. However, as was shown in Ch. 3, in pure solvent the particle still has a significant positive charge of approximately $4x10^{-17}$ coulomb. Fig. 4.30(a) shows the potential gradient next to the electrode after an approximately 3 μm charge depleted layer has developed. This shows the extent to which the potential gradient changes from the 13 V/cm of the bulk suspension. Fig. 4.30(b) then shows the force that this electric field exerts on an average sized particle in this layer. One item to note is that in the charge depleted layer there will be no counter ions, therefore there will be no electrostatic boundary layer or EHD pumping of fluid away from the electrode to counter the direct electrostatic force. 100% of this electrostatic force goes into compacting the particles in this layer. The second item to note is the sharp rise in the force on the particles. Although the actual shape of the voltage gradient in the transition region has not been solved for here, it is clearly much less than a micron and is, in this case, on the same scale as the particles themselves. Despite the uncertainty about the exact shape of the transition region, it is possible to state that over a distance of two to three times the average particle diameter, the force on the particles will go up by an order of magnitude. This means that there can be a very sharply defined edge between a highly compacted deposition layer and an undeposited accumulated particle layer or a loose, low density deposited layer. Add to this the automatic leveling effect mentioned above and this mechanism can account for the thin, densely packed depositions with exceptionally uniform thickness that are frequently observed to be the product of a deposition accompanied by a linear voltage rise.

(a)   (b)
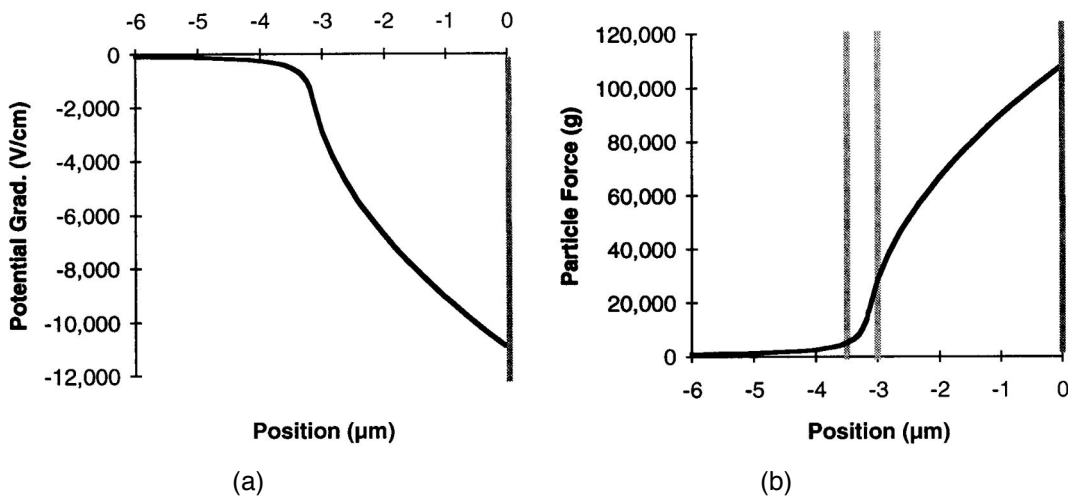
Fig. 4.30 (a) Potential gradient with 3 μm depleted layer for conditions of deposition trial #16, 0 position indicates electrode surface; (b) Electrostatic force on an average size particle in multiples of standard gravitational force on the same particle. Gray bars indicate approximate location of transition layer.

4.4.7 Description of Experiment

Finally it is now possible to return to the description of what results were obtained in this series of deposition trials with the object of offering a description of why these results were obtained. In light of the above discussion, the three categories used to group the depositions as shown in Fig. 4.3 will now be extended to four, with deposition trial #'s 20 and 21 treated as a separate category.

Deposition Trials 1-4 — This set of trials was performed on a suspension with no added acid. As discussed in Ch. 3, the particles develop a positive 60 mV surface potential due to the dissociative adsorption of ethanol molecules and desorption of ethoxide ions. Due to the uncertainty of the actual ionic strength in the solution, the particle interaction force calculations are not shown here. However, knowing that the DEBL is thick and that the surface potential is relatively high allows two conclusions; a high surface potential means the energy barrier to floccing due to random motion is high and the thick boundary layer means that this interaction energy will be spread over a long distance leading to a low repulsive force. This means that the particles are well stabilized against floccing due to random motion in the quiescent solution but there is very little repulsive force resisting floccing by hydrodynamic or electrostatic forces.

When the current is turned on in these suspensions the solvent will rapidly transition to convection at the cathode. With no surface adsorbed ions the particles will have little effect on the development of ionic concentration and voltage gradients in the system. This convection was visible as the ripple patterns in all of the depositions, but is most obvious in the first deposition. Here inflowing suspension in the center of the deposition electrode allows a deposition to form while the balancing outflow of solvent at the edges of the electrode wash particles away leaving those areas bare.

The depositions that occurred in these four trials likely occurred by a combination of all three deposition mechanisms mentioned above. Convective deposition is a likely cause of the ridge patterns seen in the depositions when they are rinsed, but convective deposition cannot occur without some deposition occurring first by some other mechanism. The only other mechanisms available are electrostatic and electrosedimentary.

While convection may account for some deposition it is more likely to result in particles being washed away from the surface. Based on the bulk electric field and mobility of the particles, if the solvent were motionless and 100% of the particles accumulating at the electrode deposited, the expected deposition weight would be 54 g/m^2. This is very close to the actual deposition weight achieved in trial #3 of 53 g/m^2. However, that weight is after rinsing off a weakly deposited overlayer which would have raised the total weight well above expected. In contrast, deposition trial #4 yielded a deposition weight of only 34 g/m^2 even without rinsing. The wide scatter in deposition

results in these four trials indicate the importance of the manner in which convection develops on the final deposition results.

After the particles have deposited on the surface of these depositions they appear to be subject to electrosedimentary consolidation. This would need to be confirmed by more careful future measurements of density gradients, but visual observation suggests that the deposition density increases continuously from the deposition surface to the electrode.

Deposition Trials 5-11 — This set of deposition trials was performed on a series of suspensions where progressively more HCl was added to the solution. In this range the majority of that added acid was adsorbed by the particle surfaces resulting in a large rise in the particle surface potentials. Enough of the HCl remains unadsorbed, however, that the free ionic content goes up and the DEBL thickness goes down. The higher potential creates a higher energy barrier to floccing by random motion, and the thinner diffuse layer means that this energy rise occurs over a shorter distance, meaning a much higher maximum repulsive force exists as well.

Even this dramatically increased stabilizing force could potentially be overcome if it were possible to develop the extreme voltage gradients associated with the transition and unbalanced charge conduction layers. However, under the conditions of these deposition trials the adsorbed HCl on the particles is too high and the current flux too low to allow these gradients to develop. The result is that no anomalous voltage rise occurred in this set of trials and do deposition occurred beyond a monolayer of particles.

(The deposition of a monolayer of particles noted in deposition trials 10 and 11 involves the deposition of positively charged particles onto a negatively charged electrode surface. Despite its simple description this is a surprisingly complex process, the discussion of which must be reserved for a future work.)

Deposition Trials 12-19 — Although total surface charge does not change significantly over this set of trials, because of the increasing ionic concentration of the solution the surface potential declines steadily as the DEBL gets thinner. These two effects lead to a decrease in both the total energy barrier to floccing and the maximum interparticle repulsive force. Nevertheless, in all of these suspensions the energy barriers and repulsive forces remain high and the suspensions will exhibit long term stability.

The most important change here from the previous set of deposition trials is the change in the ratio of conductivity to adsorbed HCl. In deposition trials 5-11 the quantity of HCl adsorbed to the particles rose much faster than the conductivity, so desorption from the particles was able to suppress the formation of an ion depleted layer. In this set of trials the adsorption is reaching saturation and the bulk of the added HCl goes to increasing the conductivity of the solvent. With this increase in conductivity comes an increase in the current flux. The flux of Cl- ions out of the accumulated particle layer is now sufficient to

deplete the adsorbed Cl- on the particles next to the electrode, allowing an unbalanced charge conduction layer to form. Particles within this layer are compacted to almost maximum random packed density by the electrostatic force in this layer. This creates the dense, uniform deposition layer that is not removed by rinsing. That this layer is created by an ion depleted conduction layer is shown by the extraordinary match between estimated ion depletion layer thicknesses based on voltage rise and actual deposition thicknesses over this conductivity range, as shown in Fig. 4.29.

The ratio of conductivity to adsorption has not risen to the point that the flux of Cl- ions in the bulk away from the cathode is greater than the flux of Cl- adsorbed to the particles toward the cathode. This means that the electrophoresis of particles is able to suppress the formation of steep concentration gradient layers in the bulk solution that would drive EHD convection. Once the particles stop moving in the accumulated layer at the electrode they no longer prevent the formation of a gradient layer, but the large quantity of HCl that the particles can adsorb and release provides a vital role in stabilizing the gradient layers against convection within the accumulated particle layer. The high voltage gradients and the ionic buffering action of the particles creates a strong automatic leveling effect for the charge depleted layer. This means that the dense deposited layer can be extremely uniform over a large area regardless of non-uniformities of the electric field in the bulk suspension.

The fact that the net flux of Cl- ions in the bulk solution is toward the cathode means that particles will accumulate at the electrode faster than they are compacted into a dense deposition layer by the growth of the ion depleted layer. In the case of deposition trial #16, based on the particle mobility and bulk electric field the total particle accumulation at the cathode would be expected to be 53 g/m^2. Given the likelihood that convective motion of the suspension is suppressed, this estimate is likely fairly accurate. Of this only 8.1 g/m^2 is converted into a high density deposition. The balance is either not deposited at all or forms a weak, low density deposit which is easily rinsed off.

The ratio of particle accumulation to deposition is a topic for future study, but the fact that a significant overlayer of particles (tens of microns) remains on the surface of the deposition electrode as it is removed from the deposition device and transferred to the rinse solution indicates that a significant portion of the accumulated particle layer does form a rigid deposition. The fact that it then easily rinses off indicates that this deposited layer has a very low density. Since the only two mechanisms for deposition in this layer are either electrostatic or electrosedimentary, it is possible to state that under these conditions, electrostatic stabilization with a DEBL thickness approximately 10% of the average particle radius, these mechanisms will not yield a densely packed deposition in the absence of the ion depletion enhanced electrostatic consolidation.

Deposition Trials 20-21 — Although the estimated stabilizing energy barrier in these suspensions is low, the suspensions appear very stable with no visible sedimentation occurring over eight hours standing after the deposition trials were completed.

The primary difference between these two deposition trials and the previous set is the net Cl- ion flux in the bulk solution. In the previous set of depositions the sum of the Cl- ion migration in solution and Cl- ion migration on the surface of the particles gave a net Cl- ion flux toward the cathode. In these two trials conductivity has outstripped adsorption and the net Cl- flux is now away from the cathode. This means that the particles will no longer contain the formation of steep gradient layers within the layer of accumulated particles at the electrode. The suspension outside of the accumulated particle layer will transition to convection.

The large voltage rises here show that this convection outside the accumulated layer does not prevent the formation and growth of an ion depleted layer. Since an ion depleted layer is extremely unstable in the absence of particles, there must be a layer of particles which acts as a strong buffer between the unstable convection of the fluid suspension and the depleted layer. This is likely due to the high energy of adsorption of the Cl- ion to the particle surface and the resulting difference between Cl- in solution and adsorbed Cl- of several orders of magnitude. This, in combination with high voltage gradients, allows migration to dominate convective transport creating an effective constant current density condition.

The total deposition weight was 26.1 g/m^2. In the absence of convection based on the particle mobility and the bulk electric field, an accumulation of 31.6 g/m^2 of particles would be expected. The weight of particles rinsed off of the deposition was not measured, but the quantity rinsed off appeared to be more than the 20% discrepancy between these two numbers. This would suggest that electroconvective deposition was taking place, with convective flow accounting for the additional particle transport to create a thicker overlayer. This would have to be confirmed by future experimentation.

The most significant discrepancy is shown in Fig. 4.28. Based on the observed voltage rise, the ion depleted conduction layer would be expected to be 8 μm or less, while the depositions are approximately 11 μm thick. If the dense deposition and the depleted layer are the same thickness this would imply a much higher than expected conductivity of this layer. Alternatively, part of the overlayer could be compacted to a sufficient density to resist rinsing. This could occur by electrosedimentary compaction, hydrodynamic compaction due to convective flows, or a high voltage gradient transition region in the buffer layer leading to electrostatic compaction. Determining which of these explanations is correct will require further experimentation and analysis.

4.5 Conclusions

       The objective of this chapter has been to present a detailed analysis of a simple deposition. A system was chosen which is known to produce good deposition results while being simple, stable, robust and reproducible. Alumina/ethanol with HCl has proven to be such a system. As shown in Ch. 3 the surface charge is uniformly positive and determined by a robust equilibrium between the solvent and Cl- in solution. The suspension is stable over an easily measurable range of conductivities and has a window of conductivities where uniform, dense depositions can be reliably reproduced.

       The analysis of conduction made here shows that at constant current without convection or suspended particles, voltage would be expected to shoot up rapidly as an ion depleted conduction layer grows at the cathode. In the absence of some other transport mechanism, ionic migration and diffusion cannot provide sufficient ionic flux to the electrode under the conditions of ionic quasi-equilibrium. To maintain current an unbalanced charge layer must form which can only be created by very high voltage gradients. However, this analysis also shows that this type of layer is highly unstable to convection. The fact that no anomalous voltage rise is seen under constant current conditions in these electrolyte solutions indicates that convection begins almost immediately after the current is turned on and before a fully depleted layer can form.

       The addition of suspended alumina particles dramatically changes this picture of conduction by changing ionic transport in the solution and buffering ionic content changes at the electrode. As HCl is first added to the alumina suspension most will be adsorbed to the particle surfaces with little remaining in solution to increase conductivity. As the particle surfaces become saturated, more and more of the added HCl will remain in solution and conductivity will begin to rise faster than total adsorption. This leads to three conduction regimes in this alumina/ethanol/HCl suspension:

1. *Convection - suppressed; depletion layer - suppressed* — In the low conductivity case ionic flux in solution is small compared to the flux of adsorbed ions carried on the surfaces of the particles. This prevents significant concentration gradients from forming and suppresses EHD convection. The large reservoir of adsorbed Cl- in the accumulated particle layer at the electrode prevents the formation of a depleted layer over the time of this deposition.

2. *Convection - suppressed; depletion layer - stabilized* — In this higher conductivity case the net flux of Cl- ions in the bulk is still in the direction of the cathode suppressing bulk convection, but the higher ionic flux is sufficient to deplete the adsorbed ions in the accumulated layer at the electrode. An ion depleted conduction

layer will form. It will be stabilized by the adsorption/desorption of ions in the transition layer, and a significant linear voltage rise is observed.

3. *Convection -active; depletion layer - stabilized* —In this high conductivity case the flux of dissolved Cl- ions in the bulk away from the cathode is greater that the flux of adsorbed Cl- on the particles moving toward the cathode. This means that steep gradient layers can form in the bulk solution which initiate convection. Convection then provides the additional ionic transport necessary to maintain constant current in the cell. However, the buffering effect of particles in the accumulated layer at the electrode still allows an ion depleted layer to grow. The high response of adsorption to small changes in solution concentration at low concentrations means that the particles can stabilize an ion depleted conduction layer — even in the presence of fluctuating ionic concentrations at the surface of the accumulated particle layer due to unsteady convection in the bulk solution.

Finally, with a picture of ionic concentrations, voltage gradients and convection states, it is possible to address the forming of a particulate deposition. Three mechanisms were presented as ways that particles in suspension could be forced into contact in the accumulated particle layer at the electrode: electrostatic, electrosedimentary, and convective deposition. While these mechanisms alone were able to create a deposition which was rigid enough to be removed from the deposition solution and handled, these depositions were low enough density, and therefore low enough strength, that they could easily be rinsed off. The prerequisite for the formation of a densely packed deposition layer is the presence of an ion depleted conduction layer. It is only the extreme voltage gradients in this layer that exert sufficient force necessary to compact the particles to maximum density.

An additional benefit of this stabilized ion depleted layer is a strong automatic leveling effect. Because the voltage gradients in this layer are several orders of magnitude larger than in the bulk suspension, even a small irregularity in the thickness of this layer can lead to a large deflection of the bulk electric field, ionic flux and particle electrophoresis. All of these effects act to strongly damp any thickness variation in the dense deposited layer.

Since the ultimate objective of EPD is usually to produce just these uniform thickness, densely packed layers of the particulate material, all of the various effects that occur in this type of deposition are collected under the name, "Ion Depletion Enhanced - Automatic Leveling" deposition. Although the depositions made here were from an electrostatically stabilized suspension this is not exclusive. Any set of deposition mechanisms where the primary role of forming the dense deposited layer and defining its

thickness is played by a stabilized ion depleted conduction layer would be included in this category.

Designing a suspension for Ion Depletion Enhanced deposition — There are three basic requirements for a suspension to be suitable for this deposition forming mechanism:

1. Depletion of the electrolyte at one electrode during conduction.
2. Particles which have a surface charge which is uniformly opposite that of the depletion electrode at all electrolyte concentrations down to that of the ion depleted layer.
3. Strong adsorption of the electrolyte by the particle surfaces.

Although these conditions may at first seem onerous, given the wide variety of solvent/electrolyte combinations available there is no reason this deposition forming mechanism could not be applied to a variety of non-conductive particulate materials. Two additional examples of this type of deposition are given in Ch. 5; PZT in acetone and TiO_2 in ethanol, both with iodic acid, HI, as the added electrolyte.

Recognizing Ion Depletion Enhanced deposition — The unmistakable sign that this effect is occurring is a continuous linear voltage rise at constant current over the course of the deposition.

Future Work — Although there are many questions that can still be asked about this deposition forming mechanism, the above analysis highlights two particular research directions that would be of the most value in confirming and extending these results, one experimental and the other analytic. On the experimental side the objective would be to directly observe density gradients and structure of a deposition without either rinsing or drying, and if possible, without even removing from the deposition from the deposition suspension. Some of the options for preserving this as-deposited structure are: freeze drying, supercritical drying, or metal infiltration by electrodeposition. On the analytic side what is needed is a series of finite element models beginning from a simple one dimensional diffusion, migration, desorption gradient model to three dimensional models incorporating convection. These would help to identify the critical points between stability and convection and illustrate more clearly how the particle surfaces act to buffer and stabilize what is normally an extremely unstable ion depleted conduction layer.

Symbols used in Chapter 5

a	Particle radius (m)
c	Molar concentration of dissolved salt (Mol/dm^3)
e	Elementary charge (1.602E-19 C)
$\mathbf{E}$	Reduced electrophoretic mobility (non-dimensional)
h	Surface to surface separation distance
k	Boltzman Constant (1.381E-23 J/K)
q	Surface charge density (C/m^2)
r	Center to center particle separation distance
T	Temperature (K)
u_{E}	Particle electrophoretic mobility (μm·cm/V·s)
z	Ion valence
ε_{o}	Permittivity of free space (8.854E-12 C^2/J·m)
ε_{r}	Relative dielectric constant
ζ	Particle Potential at Shear Layer (mV)
$\tilde{\zeta}$	Reduced particle potential at shear layer (non-dimensional)
η	Solvent Viscosity (Poise)
κ	Inverse Debye length (m^{-1})
ρ_{∞}	Number density of dissociated molecules of a binary salt in bulk solution (m^{-3})

Chapter 5
<u>Example Applications of Electrophoretic Deposition</u>

<u>5.1 Introduction</u>

Chapter 2 was a purely theoretical discussion of the mechanisms of EPD. Chapters 3 & 4 were detailed analyses of an ideal system deliberately chosen for its simplicity. This chapter now leaves simplicity behind to offer specific case studies of the application of EPD to non-ideal materials. These case studies not only cover the deposition of the materials but devote an equal or greater consideration to the processing necessary to turn these depositions into useful structures. This is important firstly because demonstrating useful end products that would be difficult and/or expensive to produce by any other means demonstrates the value of EPD. Secondly, examining what needs to be done to a deposition to turn it into a useful product highlights what is important in the EPD process.

The first demonstration is the deposition of a silver/palladium powder. This includes an extended discussion of the electrostatic stabilization and EPD of the powder. This includes a short mention of two of the most significant problems in obtaining a uniform deposition of a metal powder, gravitational convection and ramified growth.

The second half of this section is then devoted to a discussion/demonstration of how these depositions can be incorporated into multilayer devices. The key point demonstrated here is that the minimum scale for EPD is the size of the individual particles. This means that EPD can take maximum advantage of reduced particulate sizes to produce the minimum thickness and feature sizes possible from a given particulate size starting material. This makes EPD the ideal technology for handling the very fine powders and producing the very thin layers that will be necessary for the fabrication of nano-scale composite devices.

The next section is devoted to the forming of intermediate thickness films of lead zirconate titanate (PZT) a piezoelectric ceramic. This begins with a description of some of the steps taken to find a suspension/deposition solvent system. This includes some experiments that, in hindsight, might lead to better deposition systems for the formation of these films than the one chosen. However, analysis of the chosen system, very low ionic strength glacial acetic acid, shows the mechanism for producing extremely low density depositions. There are many applications where this might be a significant advantage. If the deposition is allowed to dry normally then capillary forces will consolidate the deposition to close to maximum random packing density. The second half of this section is devoted to turning this packed particle coating into a dense continuous film, and evaluating the quality of that film in comparison to bulk samples of the same material.

Finally, the deposition of titania from acidified ethanol is discussed. The main point of this section is to highlight the advantage of the automatic leveling behavior of the ion depletion enhanced deposition mechanism compared to the direct electrostatic deposition mechanism.

5.2 Silver/Palladium Deposition

For nearly fifty years multilayer ceramic structures have been fabricated by casting a continuous ceramic tape, screen printing a patterned electrode layer onto the tape, stacking the tape layers and lamination of these multicomponent tapes. This is followed by de-binding and sintering to form devices such as multilayer ceramic capacitors and multilayer co-fired ceramic (MLCC) substrates and wiring modules. As with all electronic devices, there is continuous pressure to reduce device sizes and increase volumetric efficiency. The state of the art is being pushed fastest in the multilayer capacitor industry where commercial devices currently available have 2 μm dielectric layers separating 0.5 μm electrode layers, with the near term target to reduce these thicknesses to one micron and a few hundred nanometers respectively. Aiding this drive to sub-micron feature sizes is an increasing availability of ceramic and metal powders in the nanometer size range. It is unclear at this point if tape casting and screen printing will be able to take advantage of these nano powders to produce the sub-micron features necessary for future devices. It is therefore important to consider and demonstrate new methods to take particulate processing into the nanoparticle age.

Unlike the deposition in Ch. 4, this is an example of an EPD system with minimal accompanying electrolytic conduction. While this does not eliminate electrochemical effects, analysis of the particles' electrostatic stabilizing force suggest that in this case deposition can be explained by the simple electrostatic force on a charged particle in the applied electric field.

This, arguably the simplest of the EPD mechanisms, allows particles to be brought into the deposition uniformly from their random distribution in the bulk suspension. The random addition of individual particles to the deposition allows the formation of extremely uniform thin particulate layers. As is shown below, layers of particles deposited by EPD only two to three particle diameters thick can be consolidated and sintered to form dense, continuous layers in a multilayer structure.

5.2.1 Materials

Deposited Powder — The powder used is a 70/30 alloyed silver/palladium composition (EGAG07001 from PGP Industries, Inc. Santa Fe Springs, California.) The particles are spherical with an average diameter of 0.3 μm as determined by light scattering (MasterSizer, Malvern Instruments, United Kingdom). The surface area is 1.73 m^2/g as determined by single point BET (Monosorb MS-12, Quantachrome) giving an equivalent surface area diameter of 0.32 μm.

Acetic Acid — J. T. Baker glacial acetic acid, 99.5-100.5%, (J. T. Baker Co., Phillipsburg, New Jersey.) was used as the suspending solvent.

Deposition Substrates — Deposition was conducted onto three types of substrates - Pre-sintered alumina substrates (Superstrate 996, Coors Ceramics Co., Golden, CO), glass, and polyester film. The conductive deposition electrode on all three substrates was created by a sputtered platinum coating of $\approx$ 40 nm thickness. Patterns on glass substrates were created by scribing a continuous coating. Patterns on polyester film substrates were created using an UV-photolithographic mask on the film surface.

Pre-formed Ceramic Tapes — Laminations were carried out on pre-formed ceramic tapes. These include a commercially produced tape, DuPont LTCC tape 951-A, and tapes made in-house by Bi-coating Cabot hydrothermal BaTiO$_3$ powder (BT-8, Cabot Performance Materials, Boyertown, PA), (**1**) and mixing the powder with binder and solvent to form a slip, which was cast into tape by traditional methods.

5.2.2 Experimental Procedure

Suspension— Suspensions were produced by the addition of 1.0 g of powder to approximately 100g glacial acetic acid having a conductivity of less than 0.03μS/cm prior to the addition of the powder. The powder was then dispersed by sonication using a Branson Sonifier 350 at 70% setting for two minutes while stirring.

Mobility — Mobility was measured using a Delsa 440 laser Doppler velocimeter (Beckman Coulter, Inc., Fullerton, California). This instrument measures particle velocity in suspension within a rectangular capillary measuring 0.98 mm high, 3.17 mm wide, and 5.18 mm long. To separate the electro-osmotic flow of the fluid in the capillary from the electrophoretic motion of the particles, particle velocity was measured at nine points across the capillary, the results fitted to a parabola, and the particle velocities at the theoretical stationary levels calculated from the fitted parabola. The theoretical stationary layers at the center of the width of this capillary occur at 16% of the capillary height away from the top and bottom of the capillary. This is similar to the procedure outlined by Pelton et al. (**2**).

The measurement for each point from top to bottom of the capillary consisted of applying a constant voltage in one direction for two seconds, a one second interval, followed by application of the voltage in the opposite direction for two seconds. This is repeated for a total of 30 seconds. This is intended to minimize the voltage drop due to electrochemical polarization at the electrodes.

For a significant signal to be generated by the instrument the laser must be able to propagate across the capillary with only modest scattering. This requires that the sample have a volume density of particles in suspension of approximately 0.01%, one tenth the volume density of the deposition suspensions used here. To prepare these dilutions the suspension was allowed to sediment overnight yielding a clear supernatant. Some of this supernatant was removed, the particles re-suspended, and the suspension and supernatant mixed to yield the appropriate suspension density for measurement.

Conductivity — Conductivity was measured using an open sided, rectangular, parallel plate conductivity cell having a cell constant of 0.107 cm^{-1} (Thermo Orion, Beverly, Massachusetts). The voltage across the conductivity cell was measured using a voltage divider circuit. A 10 Hz sine wave input signal of ≈ 1V rms was provided by an HP 33120A signal generator. The voltage across the conductivity cell was reduced to $\approx$ 0.5 V rms using a resistance decade box. The total input voltage and voltage across the decade box were measured using an HP 54645A oscilloscope and used to calculate the resistance across the conductivity cell. This setup was calibrated over the range from 1 to 60 μS/cm by titration of KCl in water using the equation of Lind et al. (**3**) as standard.

Deposition — The powder was deposited onto a platinum electrode surface sputtered onto either a glass plate, for the overcasting demonstration, or onto 2.54 cm square pieces of uncoated polyester film tape casting carrier for the lamination demonstrations. The suspension was placed in a beaker with a gold foil in the bottom to serve as the anode. The deposition surface is held horizontally one half, one or two centimeters above the anode. The particles are then deposited vertically upward to get a deposition that is only due to electrophoretic effects without sedimentation components.

To deposit the particles an electric field of ≈ 300V/cm was applied. For the thinnest depositions the field was pulsed on and off in three or five second intervals to allow electroconvective circulation to dissipate. This was done to maximize the thickness uniformity of these very thin depositions. After deposition was complete, the substrate was removed from the holder and immediately rinsed by dipping and moving back and forth gently in as-received acetic acid. This is to remove any particles which are not deposited but are carried out of the deposition bath in the wetting film of acetic acid on its surface.
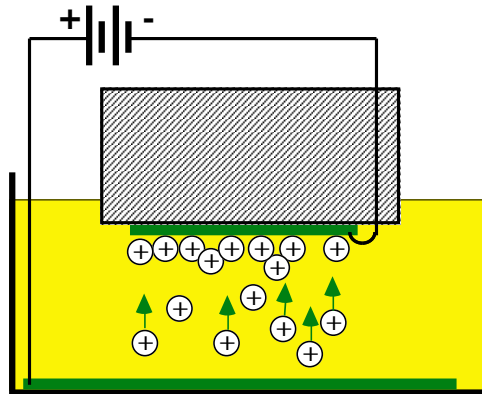
Fig. 5.1 Upward deposition separates EPD from sedimentation.

5.2.3 Dispersion and Deposition Results and Discussion

Electrophoretic Mobility — Several mobility measurements were made at voltage settings of 15, 30, 45, and 60 V. The measured mobility increased linearly by $\approx 20\%$ from 15 to 60 V. This is presumably due to electrode polarization and therefore the mobility at the highest voltage was taken as the most accurate. One measurement at 60 V is shown in fig. 4. The parabola was fitted to the data by least squares. The r^2 fit of the parabola was 0.996. The mobility at the theoretical stationary levels is 0.25 μm·cm/V·s. Reproducibility of measurements was ± 5%. Suspensions with the conductivity reduced by dilution with fresh acetic acid had a mobility $\approx 10\%$ less than the suspensions diluted only with suspension supernatant. Mobilities in the freshly prepared suspension and in the suspension after a series of depositions were estimated at 0.23 and 0.25 μm·cm/V·s respectively.
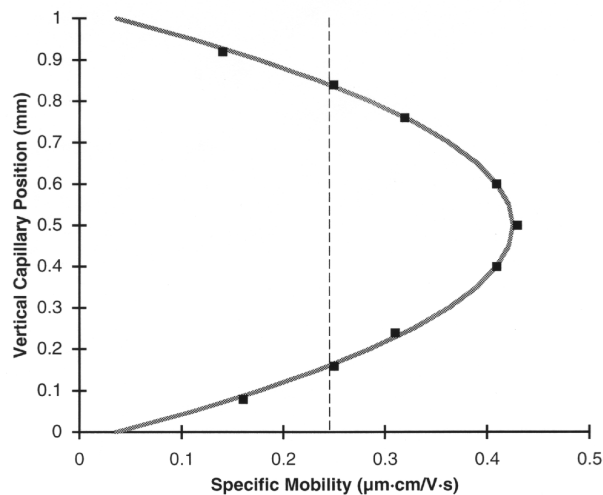
Fig. 5.2 Specific mobility vs. vertical position in measurement capillary. Vertical dashed line intersects parabola at theoretical stationary layers.

Conductivity and Ionic Strength — The conductivity of one typical suspension after sonication was 0.04 μS/cm. This conductivity increased with each deposition, presumably due to the electrolytic formation of ionizable species during conduction. After a total current flux through the suspension of 80 mC over the course of eighteen depositions the conductivity was 0.11 μS/cm. The conductivity measurements were reproducible within ±0.01 μS/cm, however, absent standardization for the range below 1 μS/cm, the absolute conductivity values here should be considered only approximate. Based on prior experience we believe that the measured values will be within a factor of two of the actual values.

In order to estimate the ionic content of the suspension without knowing the specific ionic species leading to conduction, it is necessary to make some assumptions. First, due to the low dielectric constant of acetic acid, it is assumed that any free ions will be univalent. Second, an approximate molar conductivity of 6 μScm^{-1}mMol^{-1} is chosen. This number is based on the work of B. V. Weidner who measured molar limit conductivities of various ammonium and nitrate salts ranging from 5 to 8 in pure acetic acid. [8] Using this value for the ionic molar conductivity it is possible to estimate the ionic content of the suspension as ranging from 6 μMol before deposition, rising to 18 μMol after a series of depositions.

In this series of eighteen depositions averaging twenty seconds each, a total current of 80 mC passed through the suspension. If the conduction does occur by an electrolytic process which produces an ion pair for each electron passing through the solution, this current would result in an increase of ionic content of 9 μMol in the 90 cc of this suspension. This is well within the error limits of the 12 μMol rise in the ionic concentration estimated by conductivity. Therefore, this hypothesis cannot be rejected.

With an estimate for the ionic strength of the solution it is now possible to calculate the inverse Debye length using eq. [5.1] for a solution containing univalent ions. (symbols used are defined in appendix.)

$$\kappa = \left[\frac{2e^2 \rho_\infty}{\varepsilon_o \varepsilon_r kT} \right]^{\frac{1}{2}} \qquad \text{Inverse Debye Length} \qquad [5.1]$$

Ionic concentrations in the bulk solution, c of 6 and 18 μMol will yield Debye lengths, κ^{-1}, of 35 and 20 nm in acetic acid with a relative dielectric constant, ε_r, of 6.2. For the 300 nm particles used here this yields non-dimensional double layer thickness parameters, κa, of 4.3 and 7.5.

Surface potential and Surface Charge — With the particle electrophoretic mobility and the double layer thickness parameter it is possible to estimate the zeta potential of the particle. Unfortunately, the κa values here are within the range of 1 - 10 where the simple

Hückel and Smoluchowski formulae are not valid, and the non-dimensional electrophoretic mobility values, **E**, are 2.6 and 2.8, well outside of the 0 to 1 range for validity of the slightly more complex Henry formulation. (**5**, ch. 3)

$$\mathbf{E} = \frac{3\eta e}{2\varepsilon_r \varepsilon_o kT} u_E \qquad \text{Non-dimensional Electrophoretic Mobility} \qquad [5.2]$$

Therefore to estimate the surface potential, graphic interpolation of the charts published by O'Brien and White was used. (**6**) These calculations include the retardation due to polarization of the diffuse layer around the particle. These charts were calculated on the basis of KCl in water, where the ionic mobility is much higher than in the acetic acid suspension used here. The boundary layer polarization is likely to be higher in the suspension with the lower ionic mobility, leading to an under estimate of the of the actual surface potential. For E = 2.6 and 2.8, and κa's of 4.3 and 7.5, the non-dimensional surface potentials, $\tilde{\zeta}$, are both 3.0. This yields a constant surface potential of 77 mV independent of the solution ionic concentration.

$$\tilde{\zeta} = \frac{e\zeta}{kT} \qquad \text{Non-dimensional Surface Potential} \qquad [5.3]$$

With the surface potential and κa, the surface charge density can be calculated using the empirical formula of Loeb, et al. (**7**) for a 1-1 electrolyte system, eq. [5.4]. This gives a particle surface charge density, q, of 0.20 and 0.32 milliCoulombs/meter^2 for the 6 and 18 μMolar suspensions respectively. For the 300 nm particles here, this gives a total particle charges are 5.5 x 10^{-17} and 9.1 x 10^{-17} Coulombs.

$$q = \frac{\varepsilon_o \varepsilon_r kT}{e} \kappa \left(2\sinh\left(\tfrac{1}{2}\tilde{\zeta}\right) + \frac{4}{\kappa a}\tanh\left(\tfrac{1}{4}\tilde{\zeta}\right) \right) \qquad \text{Surface Charge Density} \qquad [5.4]$$

Stability — To prevent the particles from floccing and sedimenting out of the suspension prior to deposition there must be an adequate force to keep them apart. The force drawing them together is, of course, the London-Van der Waals force and, in this case, the force that must overcome this attraction is the increased osmotic pressure due to the compression/overlap of the particles diffuse counter-ion layers.

The L-VdW attraction between two particles is the product of two terms. The Hamaker Constant, which is a function of the electronic properties of the materials, and a geometric term defined by the arrangement of the materials. This is expressed in eq. [5.5] where A_{131} is the Hamaker constant and the balance is the geometric factor for spheres of radius a at a center to center separation distance of r. (**8** § 5.2)

$$\Phi = -A_{131}\frac{1}{6}\left(\frac{2a^2}{r^2 - 4a^2} + \frac{2a^2}{r^2} + \ln\frac{r^2 - 4a^2}{r^2} \right) \qquad [5.5]$$

L-VdW Interaction Energy for Two Spheres

For the Hamaker constant at zero separation we have used the value calculated by Parsegian and Weiss (**9**) for two masses of silver metal separated by water, $A_{131}(0) = 4.0 \times 10^{-19}$ Joule. Given that silver and palladium form a full solid solution, it is reasonable to expect that the electronic properties of silver palladium will be similar to those of pure silver. Likewise, the close match of the optical frequency refractive indices for water and acetic acid, at 1.333 and 1.372 respectively, indicate that they will likely have a similar dielectric relaxation behavior in the UV range where all of the interaction takes place. These assumptions are supported by the approximation methods of Israelachvilli and their comparison to experimental values. (**10** § 11.4)

The Hamaker constant itself is a function of separation distance. The synchronization of dipole motions that leads to the London electrostatic attraction decays as the separation approaches a significant fraction of the length of the electromagnetic wave mediating this interaction. For the silver palladium particles here the interaction will be in the plasmon frequency range, $\approx 3 \times 10^{15}$ s^{-1}, with a wavelength of 100 nm. This retardation effect leads to a decrease in the effective Hamaker constant by 50% at a separation distance of 10 nm and with the interaction almost completely disappearing at 100 nm. This retardation was calculated here using the method of Russel, et al. (**8** §5.9, 5.10)

The repulsive force was then calculated using the linearized Derjaguin approximation for two spheres at constant surface potential, eq. [5.6]. (**8** §4.10)

$$\Phi = 2\pi\varepsilon_r\varepsilon_o\zeta^2 a \ln\left(1 + e^{-\kappa h}\right) \quad \text{Derjaguin Approx. Repulsion Energy} \quad [5.6]$$
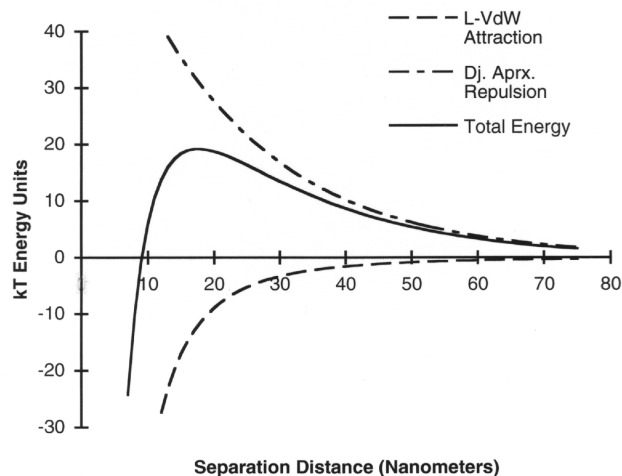
Fig. 5.3 Interaction potential for two 300 nm dia. silver palladium spheres in acetic acid; $c = 18\mu$Mol.; $\psi_0 = 77$ mV.

Summing the L-VdW and electrostatic interaction potentials gives the total interaction energy. This is shown in fig. 5.3 for the particles at the higher ionic strength

condition. The calculated energy barrier to flocculation is 33 and 19 *kT* energy units and the maximum repulsion force is 2.6 x 10^{-12} N and 2.3 x 10^{-12} N for the 6 and 18 μMolar conditions respectively.

For the surface potentials found here, the linearization assumption in the Derjaguin approximation, eq. [5.6] of the electrostatic force will lead to an underestimation of the potential drop near the particle surface and therefore an overestimation of the energy barrier to flocculation and interparticle repulsive force. This may, at least in part, be compensated by a likely underestimation of the surface potential above.

Deposition — With the maximum interparticle force and total particle charge it is possible to calculate the voltage gradient that would produce a force on the particle equal to the maximum interparticle repulsive force. This works out to voltage gradients of 470 V/cm and 250 V/cm for the 6 and 18 μMolar cases respectively. Given the uncertainty in the measurement and calculation of the interparticle potential, this result is in good agreement with the observed voltage gradient necessary for deposition of 300 V/cm. Based on the above analysis it is reasonable to believe that deposition of the particles in this case occurs primarily by electrostatic force on individual particles.

5.2.4 Additional Issues in Ag/Pd Deposition

The deposition of Ag/Pd illustrates two effects that can occur during deposition. The first, ramified growth, is unique to the deposition of metal particles. The second, gravitational convection, is an effect that will occur in any deposition system where the particles are denser than the solvent, except when the deposition is performed straight down.

Ramified Growth — As soon as conductive particles contact the deposition electrode, because of electronic conduction they will take on the electric potential of the deposition electrode. Deposited particles that extend from the deposition electrode will concentrate the electric field at their tip. This will attract other particles to deposit on the highest point, leading the growth of dendrites. This behavior is illustrated diagrammatically in Fig. 5.4.

The actual effect of this growth on a deposition is shown in Fig. 5.5(a) below. Here there are two electroded areas at the top and bottom of the picture. Across the center of the picture is a 25 μm horizontal line of bare glass. The edges of the electroded areas are straight, sharply defined lines. These electroded areas are covered by a deposition of Ag/Pd powder 3 to 4 particle diameters deep. It can be seen that lateral growth of the deposited metal particles has both narrowed the line as well as created a very irregular edge.
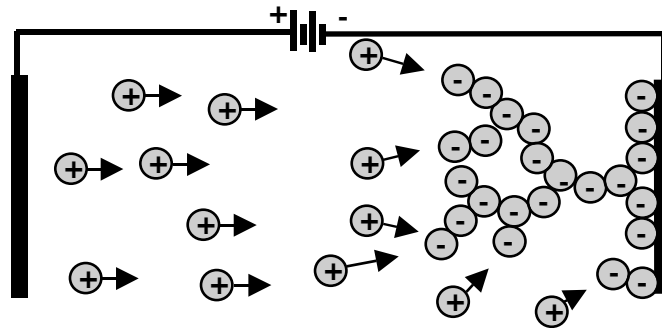
Fig. 5.4 In electrostatic deposition of conductive particles the particles will assume the charge of the deposition electrode.
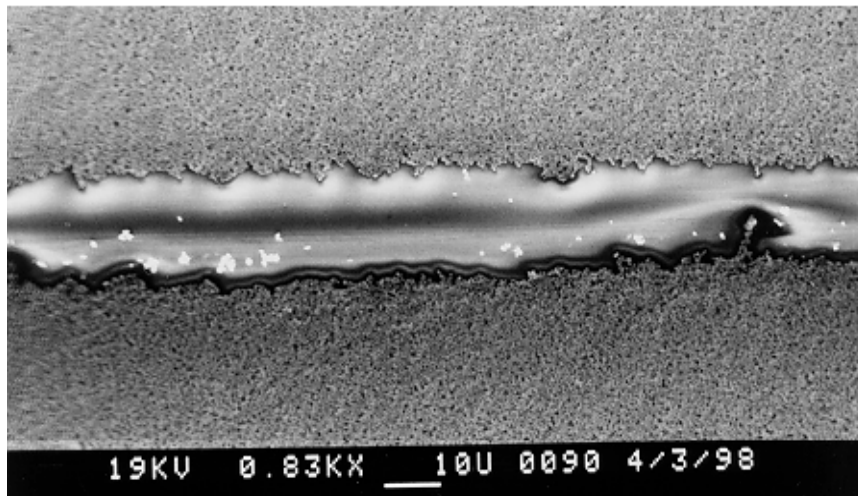
Fig. 5.5(a) Example of the lateral growth of a deposition over an non-electroded line.

At the edge of an electroded area the growth away from the electrode edge will be much more pronounced, as shown in Fig. 5.5(b).
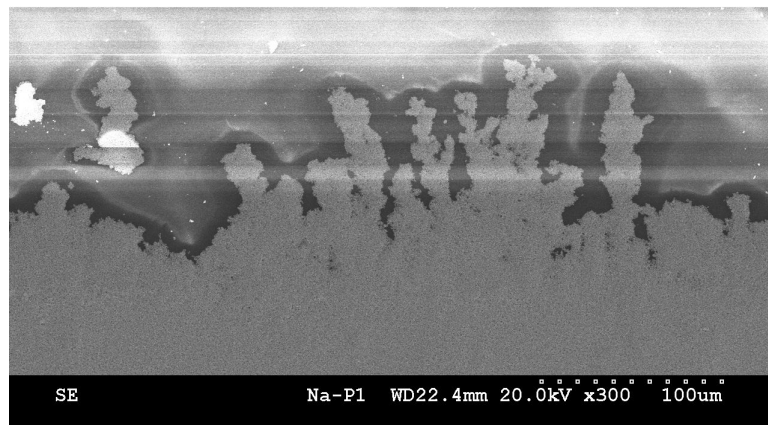
Fig. 5.5(b) Example of the lateral growth of a deposition at the edge of an electroded area.

If deposition is accompanied by EHD convection around the electrode it can drive the particles to deposit in a pattern dictated by the EHD flow. In Fig. 5.5(c) parallel vortices flowing out of the main deposition area cause the extension parallel fingers of deposition instead of fractal trees.
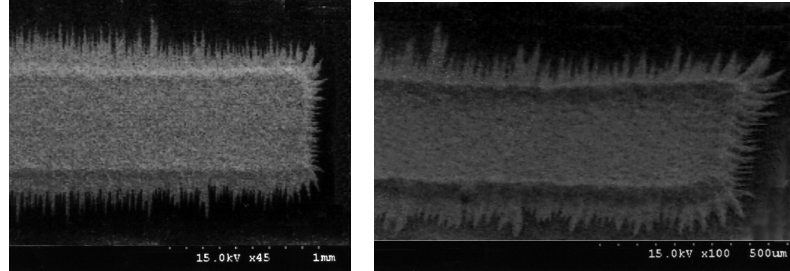
Fig. 5.5(c) Example of the lateral growth of a deposition at the edge of an electroded area influenced by EHD convection.

Gravitational Convection — Another significant complicating effect that commonly occurs in EPD is gravitational convection. As particles are driven away from the counter electrode, the pure fluid layer that forms there will have a lower average density than the fluid containing particles. This fluid will then rise to the top of the cell. This gravitational convection will often dictate the flow direction of EHD convection, with EHD forces adding to the speed of the gravitational convection. In vertical deposition electrode cells this can often lead to a deposition which thickens toward the bottom of the cell. A crossection of this type of convection occurring in a suspension of Ag/Pd is shown in Fig. 5.6. The black areas are dense suspension, light areas are solvent depleted of particles.

10 sec.   **30 sec.**   **60 sec.**
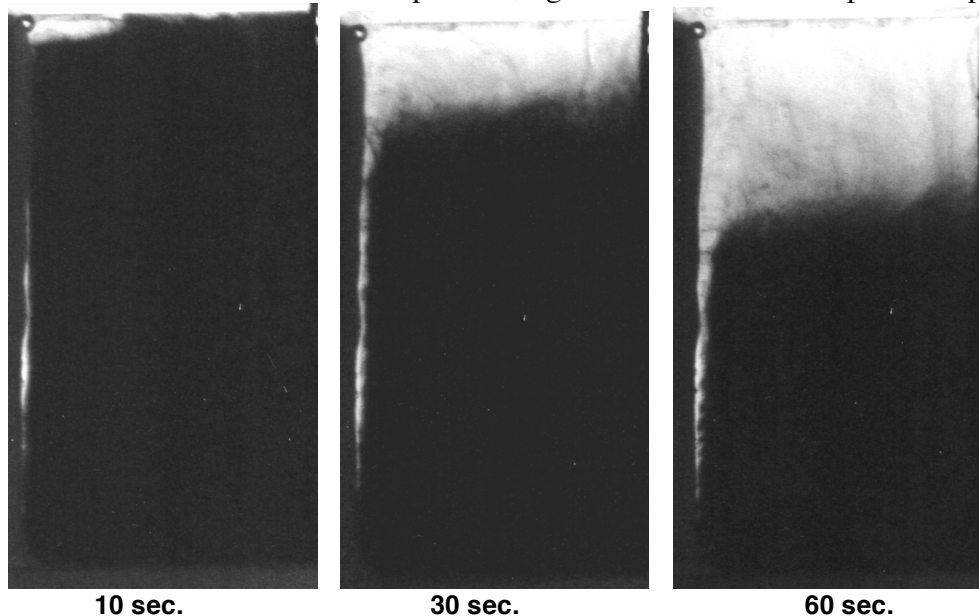
Fig. 5.6 Gravitational convection of Ag/Pd caused by electrophoresis. The particles are driven away from the vertical electrode on the left toward the electrode on the right. Fluid next to the electrode on the left is depleted of particles. With a much lower average density this fluid rises upward, eventually filling the top portion of the cell.

5.2.5 Uniform Coatings on a Rigid Substrate

A very common operation in electronic manufacturing is the formation of a
uniform metallic coating. These are formed by sputtering, screen printing, electroplating
and electroless plating. They are sometimes used as a continuous layer for a ground plane
or electronic shielding. Very frequently these continuous layers are masked and etched to
produce circuit patterns. Here the objective was to produce an electrode which would be
stable and compatible as a bottom electrode for an EPD formed PZT layer to be sintered at
850°C. (**11**)

Demonstration — Shown in Fig. 5.7 below is a one micron layer of
silver/palladium that was formed by EPD onto a standard alumina circuit substrate and
sintering of the deposition. The substrate was prepared by sputtering of a 40 nm platinum
coating to make the surface conductive. The electrode spacing was 2 cm, 500 V was
applied for 45 seconds generating a current of 42 μA/cm^2. After rinsing the dried
deposition weight was 1.0 mg/cm^2. The deposition was densified by heating to 900°C at
15°C/min and allowing to cool at a maximum 15°C/min. The resulting coating was
uniform, adherent and examination by SEM revealed no through thickness pores greater
than 1 μm.

| (a) | (b) |
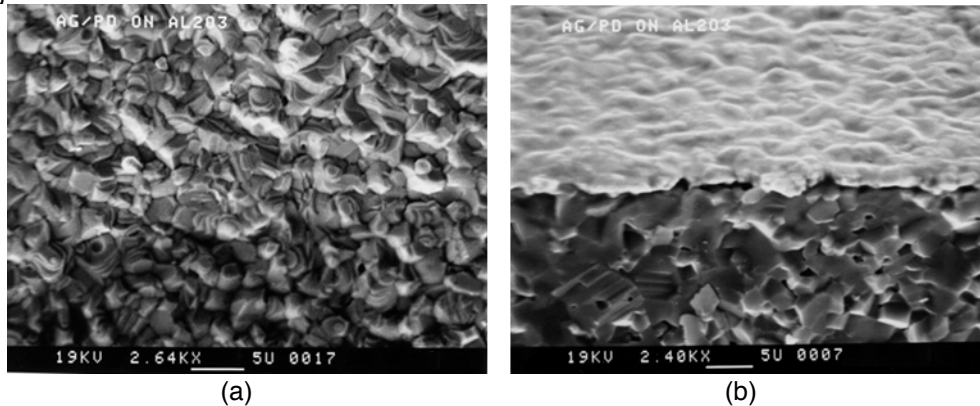
Fig. 5.7 One micron thick Ag/Pd layer on an alumina circuit substrate, (a) top view, (b)
oblique view of fracture edge, Ag/Pd on top, fracture surface of substrate below.

To create a film of this thickness by sputtering would take as much as an hour. To
produce a one micron coating of a single metal such as copper by electrodeposition would
take only a little longer than electrophoretic deposition and would not need a sintering step
to densify the coating, however, forming a coating of an alloyed metal by electrodeposition
is a much more difficult and involved process when it is possible at all. Screen printing
can rapidly create a coating of an alloyed powder, but cannot produce a uniform
continuous coating at this thickness on a rigid substrate. EPD is unique in being able to
produce a controlled stoichiometry alloy layer rapidly and inexpensively in the one micron
thickness range.

5.3 Use of EPD in Multilayer Fabrication

While EPD may have advantages for the production of continuous coatings in certain cases of electronics manufacturing, it is in multilayer electronic device fabrication where EPD has the potential to dramatically improve the state of the art.

The current standard technology for production of multilayer electronic devices consists of: 1) casting of a continuous dielectric particulate tape layer, 2) punching and filling of vias through the continuous tape to provide interconnection between layers, and 3) screen printing patterns of conductor, resistor, inductor and capacitor materials onto the continuous tape. These multicomponent tapes are then stacked, laminated under pressure to fuse the layers together, and sintered to form the final device.

EPD has the potential to reduce the scale of these multicomponent tapes by an order of magnitude over current technology both in thickness and lateral dimensions, improve the uniformity the final device, and remain cost competitive with current high volume production techniques. The demonstrations below cover the forming of continuous layers, forming of a continuous thickness multicomponent tape, creation of micron scale patterns, and a discussion of the forming of multicomponent tapes completely by EPD.

5.3.1 Forming Continuous Layers for Multilayer Devices

The simplest application of EPD is in the creation of uniform thickness tapes, such as are currently produced by doctor blade tape casting. To do this the entire tape carrier is coated with a conductive layer. A voltage is applied to the carrier in a deposition bath and a uniform layer of the particulate material is deposited. Binder can either be dissolved in the solvent for the EPD bath or can be introduced into the tape in a second step.

The advantage of this process is the formation of a tape with more uniform particle packing than can be achieved by traditional tape casting. This in turn should lead to the ability to create uniform tapes that are significantly thinner than is currently possible. This is thinner both in absolute terms and in terms of the number of average particle diameters, i.e. thinner tapes could be created with the same size particles without loss of continuity.

Demonstration

The objective of this experiment was to determine the minimum thickness continuous electrode layer that could be formed using the 0.3μm Ag/Pd powder. Multilayer stacks were built up layer by layer with each layer handled on a polyester film carrier until it was laminated to the stack and the carrier peeled off.

The barium titanate layers were formed by screen printing onto a polyester carrier film. The screen printing ink was prepared using a standard tape casting binder (Ferro B73210) to allow for lamination of the films. The barium titanate powder used was Cabot BT-8 coated with 5 wt.% bismuth oxide to promote sintering in the 700°-800°C range. The BT-8 average particle size is 0.2μm with a generally smooth, equiaxed particle shape. A 2.54 cm square pattern was printed through a 10μm thick screen and was dried at 80°C yielding a 2 to 4μm thick tape layer.

The silver/palladium was deposited onto 2.54 cm square pieces of polyester film with a sputtered platinum layer to make the deposition side conductive. A deposition voltage of 200 V/cm was applied 5 seconds on, 5 seconds off, for a period of 90 seconds (45 seconds on). No binder was added to the silver palladium layers prior to lamination.

Lamination was performed in a heated, uniaxial lamination press at 40 MPa and 70°C. The silver/palladium deposition was placed face down onto a barium titanate layer and pressed. Under these conditions there was enough diffusion of binder from the barium titanate layer into the metal powder to bond it to the stack. The platinum sputtered polyester could be peeled off the stack leaving all of the silver-palladium powder laminated to the layer below. The polyester retained its shiny conductive surface and could be used again for another deposition. A barium titanate layer was then laminated on top of the metal layer and the process repeated.

The results of the first laminate produced are shown in Fig. 5.8 below. The green cross section Fig. 5.8(a) shows the Ag/Pd powder layer that when sintered yields one of the 1.2μm layers shown in Fig. 5.8(b). The polished cross section examined in the SEM was 5 mm wide. The picture in Fig. 5.8(b) is representative of the uniformity of the Ag/Pd layers over the entire width of the specimen. No pores or gaps were seen over the 5 mm examined.

(a)   **(b)**
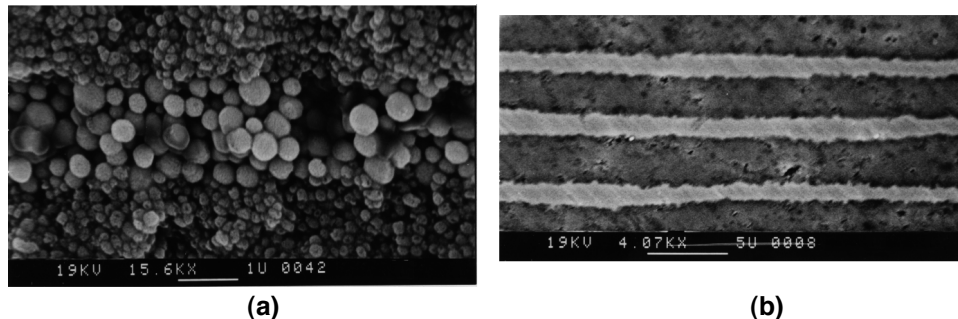
Fig. 5.8 (a) Green cross section showing Ag/Pd powder layer (center) between barium titanate layers (top & bottom); (b) Polished cross section of sintered multilayer showing 1.2 μm thick Ag/Pd electrode layers (light color layers) between 2.5 μm layers of barium titanate.

The continuity and uniformity of these 1.2 μm layers are representative of what would be required of a dielectric layer. An electrode layer can have a significant number of through thickness pores while still maintaining electrical continuity. Based on the multilayer above it appeared that the electrode thickness could be reduced by half without losing continuity. To test this a second multilayer was made using depositions of Ag/Pd powder one half the thickness used in the first example. The depositions were formed using 200 V/cm applied continuously for 15 seconds. The resulting multilayer is shown in Fig. 5.9 below.
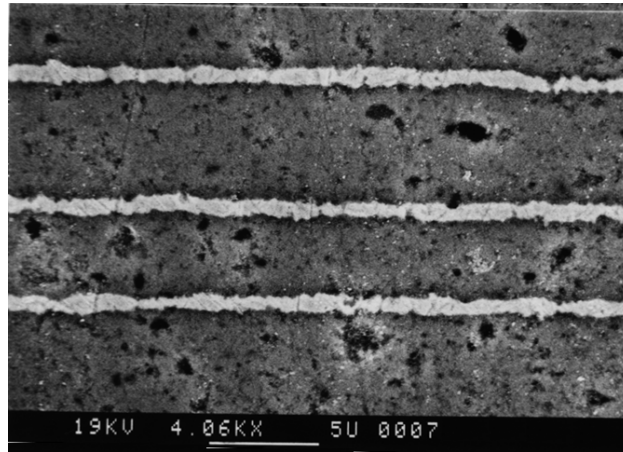
Fig. 5.9 Polished cross section of sintered multilayer showing 0.6 μm thick Ag/Pd electrode layers (light colored layers).

The silver/palladium layers formed averaged 0.6μm thick and were continuous across the width of the 5 mm sample prepared. Examination of the full 5 mm width of the polished cross section in the SEM showed very few pores that extended through the 0.6 μm layer.

What has been demonstrated here are the likely minimum thicknesses possible for two types of layer formed by EPD of equiaxed particles. For dielectric or membrane layers where there should be no through thickness pores or areas of significantly reduced thickness, the minimum thickness will be 4 - 5 times the average particle diameter. This corresponds to the four particle diameter thick layers in Fig. 5.9. For capacitor electrodes, ground planes or shielding layers it is only necessary to maintain connectivity in the plane of the electrode and significant through thickness porosity can be tolerated. Here the minimum thickness will be $\approx$ 2 times the average starting particle diameter. Prior experience in this lab at forming 50 nm thick layers by EPD of 10 nm diameter silver particles (**12**) strongly suggests that this thickness scaling based on average particle diameter will be valid throughout the nanometer region as well. By moving to the EPD of nanoparticles it should be possible to rapidly and inexpensively produce layer thicknesses that have previously only been possible using traditional thin film processes.

5.3.2 Tape Overcasting on EPD Patterns

Another application of EPD is to combine it with traditional doctor blade tape casting to produce a uniform thickness multicomponent particulate tape. By applying a voltage to a conductive pattern on the tape carrier, one type of particulate material can be deposited in that pattern onto the carrier. With multiple patterns more than one material could be deposited. This is followed by normal tape casting of the final material over the deposited components. The solvent containing the binder from the tape casting slip will impregnate the electrophoretically deposited components, incorporating them into the tape. By this means a uniform thickness tape can be produced that incorporates secondary materials for conductors, resistors, capacitors, etc.
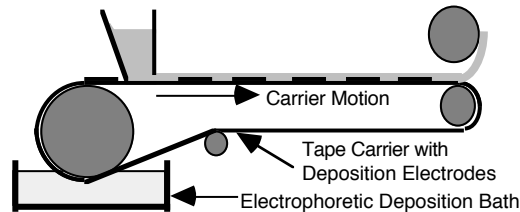
Fig. 5.10 Combining EPD on a tape carrier with tape casting can be used to create a uniform thickness, multicomponent particulate tape.

The advantage of this process is that it creates a uniform thickness multicomponent tape. In the traditional process a uniform thickness tape is cast and secondary components are screen printed onto the surface of this tape, making the thickness of the multicomponent tape uneven. When many of these tapes are stacked, low density areas can be left in the laminate. These cause stress concentrations which can serve will failure origins in sintering or use of the device.

(a)   (b)
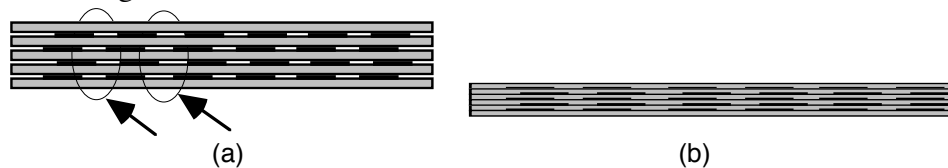
Fig. 5.11 (a) Uneven thickness leads to low density regions; (b) Laminate of even thickness tapes eliminates low density regions in green body

The key to this process is the thickness uniformity of the layers formed by EPD. This would allow a much thinner layer of material to be tape cast over the components already on the carrier than would be possible if the patterned components were screen printed onto the carrier.

Demonstration

There were two particular questions that the tape overcasting experiment was intended to answer. The first was whether a patterned deposition of metal powder, which contains no binder, would retain its pattern during the tape casting operation, or whether

casting the tape over the deposition would wipe out the pattern. The second question was whether the binder from the tape casting slurry would penetrate into the metal powder deposition, incorporating it into the tape, and allowing the two component tape to be peeled cleanly from the glass carrier.

To test this concept, a glass plate was used as a tape casting substrate. An area of the plate was coated with a sputtered platinum electrode and 25μm lines were scribed into the electrode. Depositions of 1.0 to 2.5 μm were made onto the glass surface by continuous application of a 300 V/cm electric field for 30 to 90 seconds. Deposition thickness was determined by weight gain of the glass substrate and later confirmed by direct scanning electron microscopy (SEM) examination of the green tape cross section. A 75 μm thick barium titanate tape was cast over the deposition using a traveling slip hopper with doctor blade.

The results are shown in the pictures below, Fig. 5.12. Fig. 5.12(a) shows the generally rectangular Ag/Pd deposition area on the glass carrier with vertical line pattern at the top edge. Fig. 5.12(b) shows the cast tape as it is peeled off the carrier. The top half of the picture shows the bottom of the cast tape as it is peeled up. The bottom half of the picture is a reflection of the rolled up tape off the glass carrier. The gray is the metal powder deposition incorporated into the white barium titanate tape. The pattern of lines scribed in the deposition electrode is still clearly visible as white barium titanate lines between gray areas of the metal deposition.

(a) (b)
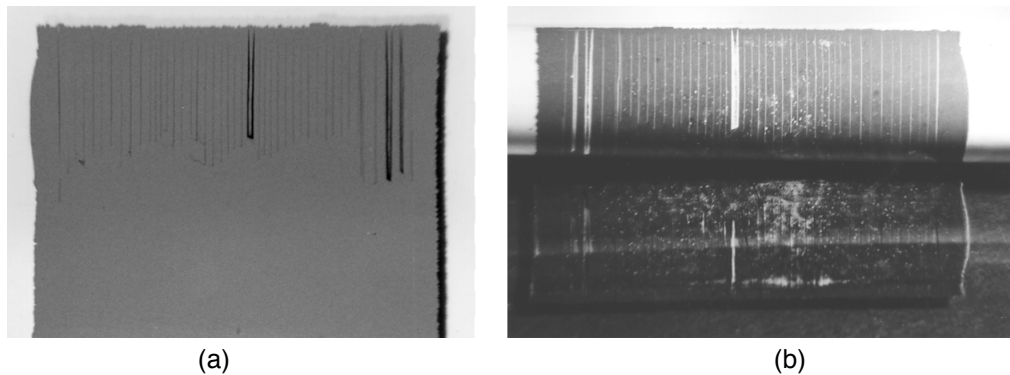
Fig. 5.12 (a) 2.5μm thick patterned deposition of Ag/Pd powder on a glass tape casting substrate; a barium titanate slip was cast over this deposition and in (b) the peel up of this barium titanate cast tape is shown incorporating the patterned Ag/Pd deposition.

5.3.3 Deposition and Lamination of a Conductor Pattern

Patterned components can also be incorporated into a multilayer by direct lamination of a patterned deposition to the stack. A patterned deposition electrode is created on a carrier and a particulate material is deposited on this pattern. Then the carrier is then placed on the laminate stack, heated and pressed to incorporate the patterned deposition into the laminate. After lamination the carrier film with the conductive pattern can be peeled off and reused without needing to recreate the conductive pattern. The layers between the patterned layers formed by EPD can be tapes cast by standard methods. The deposition can either be infiltrated with binder before lamination or can be laminated dry allowing excess binder to flow from the layer below it, bonding the deposited material.

The advantage of using EPD in this process is the incorporation of secondary components into a laminate stack with better particle packing, lower thickness and finer detail sizes than is possible with other printing techniques.

(a)   (b)
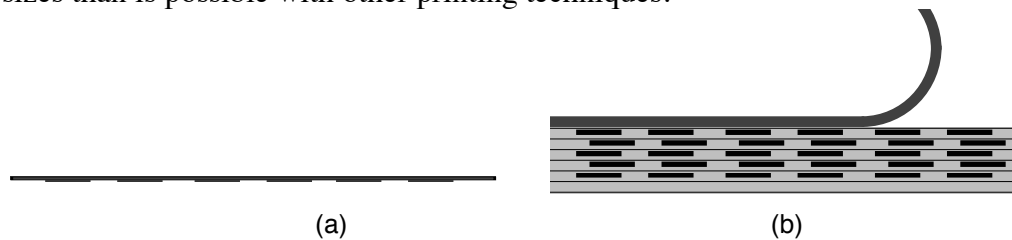
Fig. 5.13 (a) Carrier with patterned deposition of material; (b) Carrier film is peeled off after lamination of the patterned deposition to the stack.

Demonstration

The first step for this demonstration was the preparation of a patterned deposition electrode on a polyester film. A resolution test pattern shadow mask was created by electron beam lithography at the Penn State Nanofabrication Facility. This resolution test pattern includes details from 50 μm down to 1 μm.

Polyester tape casting film was cleaned by wiping with optical quality tissue using alcohol and acetone to remove any coatings or contamination on the surface. The film was spin coated with a UV photopolymer mask and exposed through the shadow mask in contact mode. The unexposed photopolymer was rinsed off exposing a patterned area of bare polyester. The entire surface is then sputter coated with platinum. The photomask and overlying platinum were removed by sonication in alcohol. Well defined conductive lines down to 2 μm were achieved with relatively little effort.

A layer of Ag/Pd powder approximately 1 μm thick was deposited on the pattern by pulsing the voltage field 3 seconds on/ 3 seconds off for 90 seconds at 150 V/cm. The deposition was rinsed in a beaker of as-received acetic acid and allowed to dry. The carrier with the deposited powder was placed face down on to the shiny side of a stack of Dupont

951-A LTCC dielectric tape. This was laminated for 10 minutes at 200 MPa and 70°C. The polyester film carrier was peeled off the tape stack leaving the deposited Ag/Pd pattern as shown in Fig. 5.14

It is worth noting that the sputtered platinum showed remarkably good adhesion to the polyester film. No damage to the deposition electrode pattern was visible due to the initial sonication or in subsequent cleaning following deposition and lamination.
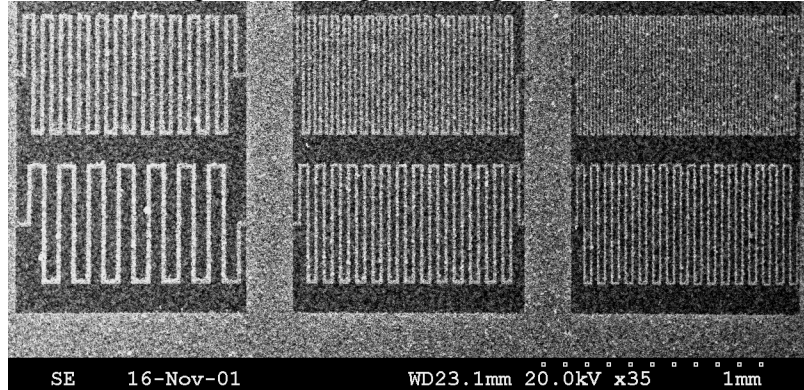
Fig. 5.14 DuPont 951-A LTCC tape with electrophoretically formed pattern laminated to the surface. Deposition electrode pattern line widths are 15, 10 & 5 μm. Powder deposition grows $\approx$ 2 μm beyond edge of deposition electrode edge. Graininess of image is due to porosity of the green tape.

The width of the lines on the deposition electrode pattern are 15, 10 and 5 μm. During deposition the powder deposit grows both laterally as well as in thickness. Here the powder deposit has grown approximately 2 μm beyond the edge of the deposition pattern. Because of this lateral growth, features on the deposition test pattern that had less than a 5 μm spacing between them were not distinguishable. The issues of the growth of the deposition beyond the deposition pattern and its implications for pattern resolution is a matter to be addressed in future publications. However, here we would like to note the primary obstacle to higher line resolution is the tape used for lamination. This tape is typical of a commercially available low loss dielectric tape designed for LTCC processing. Designed for secondary components added at screen printing resolution, the precast tape contains alumina particles ranging in size up to 5 μm. The low uniformity of the 5 μm line shown here is due in large part to the line being the same size as particles in the tape it is being laminated to. Taking advantage of the resolution which is possible using EPD-Lamination will require the development of a new generation of LTCC materials with particle sizes in the sub-micron or preferably nanometer scale range.

5.3.4 Multi-Component Deposition on a Multi-Electrode Substrate

The one aspect of the production of multilayer electronic devices that has not been demonstrated here is the formation of through thickness components. Currently these components are formed in an initially continuous tape by either mechanically punching or laser drilling holes into the tape. These holes are then backfilled with a second component. This process is usually restricted to tapes which are thick and strong enough to be handled off of a carrier. The smallest holes that are routinely formed and filled in this manner are 100 μm.

Multicomponent tapes with through thickness components can be formed by EPD using a carrier with a two part electrode pattern. This is illustrated in Fig. 5.15. The carrier would have a continuous electrode, a photopatterned polymer insulating layer, and a photopatterned top electrode. A voltage is applied to the top electrode in an EPD bath containing a dielectric powder. The deposition is rinsed and placed into a second EPD bath containing metal particles. There the second electrode is energized to produce a deposition with the same thickness as the dielectric material. This two component tape can now be laminated to a multilayer stack. The carrier with the deposition electrode pattern can be peeled off an re-used for another deposition. Because this layer is formed and handled on a carrier until lamination, the only minimum thickness limit is dictated by particle size as discussed in § 5.2.1 above. The minimum lateral dimension of the through thickness components is a subject for future experimentation, however, a lateral dimension two times the thickness of the layer is reasonable attainable.
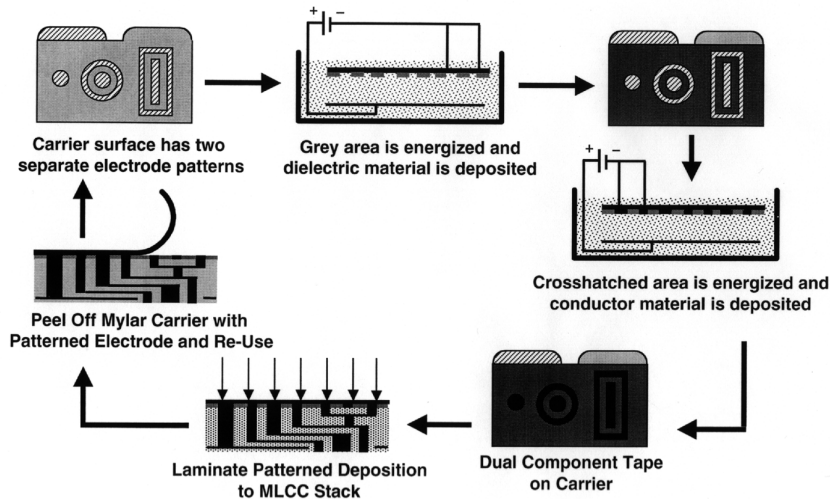
Fig. 5.15 Forming a multicomponent tape for lamination by successive depositions on a carrier with a two part deposition electrode pattern. The pattern illustrates the forming, from left to right, of a standard circular via, a shielded via, and a shielded in-plane conductor line.

In addition to a dramatic reduction in scale of these components, EPD can produce shapes which are not normally possible by punching and filling. The pattern in Fig. 5.15 shows how a coaxial via or a shielded in-plane conductor line could be formed by EPD of multiple components. The current best practice for lateral shielding in LTCC multilayers is the punching and filling of a discontinuous row of vias connected to the ground plane to form what is called a "via fence". (**13**) In contrast, EPD is able to form through thickness components as continuous lines, sharp corners, and, because the multicomponent tape is formed and handled on a carrier, cut out areas. There is no restriction that any single component be continuous to hold the tape together during processing.

5.3.5 Conclusions

This experiment was begun with an example electronic material, a 70/30 Silver Palladium Alloy 0.3 μm dia. powder, designed for co-sintering with a variety of electronic ceramics and in LTCC structures. This powder was dispersed in, and electrophoretically deposited from, a glacial acetic acid solvent. Estimation of the electrostatic stabilizing force indicate that the externally applied field used for EPD is of sufficient magnitude to overcome the interparticle repulsive force. This allows a mobile particle to come into contact with a stationary particle by electrostatic force alone. Thus for this case the growth of the deposition is attributed to the direct electrostatic force acting on each particle individually.

EPD of this Ag/Pd powder was used to demonstrate the formation of continuous electrode layers both sintered on a rigid substrate (constrained sintering) and within a multilayer laminate (free sintering). Based on observations of these layers the following minimum sintered thickness possible by EPD were inferred: for an electrode layer on a rigid substrate - 3 to 4 times the average diameter of the starting powder; for continuous dielectric or membrane layers in a co-fired multilayer - 4 times the average particle diameter; and for electrode layers in a multilayer requiring only in plane connectivity - 2 times the average particle diameter.

Patterned depositions were also produced on a carrier. The minimum line width demonstrated here is 30 times the average particle diameter. The likely minimum line width possible was not determined but will in part depend on matching the particle size of the material being patterned with that of the matrix material around it.

There are several ways to incorporate this patterned deposition into a multilayer device. One method is to cast a tape over the pattern by conventional methods to form a multicomponent tape that can be removed from the carrier. An alternative method is to laminate the pattern directly to a multilayer stack, removing the carrier after lamination. A

multiple component tape can also be produced by multiple depositions on a carrier with two or more electrically isolated deposition patterns. If the resulting tape is continuous then it could be removed from the carrier for stacking or the depositions could be laminated to a multilayer while still on the carrier.

The key technological point here is that by depositing onto a photolithographically produced pattern then transferring the deposition to a multilayer structure, the pattern can be reused. A single photolithographic operation produces a deposition pattern which can be used to electrophoretically deposit multiple parts rapidly and inexpensively. Each of these parts can have details on a dimensional scale which was previously only possible by using lithographic process for each individual part. If a set of nano-scale powders are developed which can be dispersed, electrophoretically deposited and co-sintered, this process would allow the scale of circuitry in LTCC devices to drop by more than two orders of magnitude.

5.4 EPD of a Complex Lead Perovskite Particles

Three features of EPD cited in Ch. 1 as significant advantages over other film techniques are: better stoichiometry control than thin film vapor deposition techniques; better morphology control than sol-gel techniques; and creation of films in the 1 to 20 μm range which are difficult to produce by any of the traditional thin or thick film techniques. This section demonstrates each of these features of EPD.

To demonstrate stoichiometry control a complex lead perovskite was chosen. There are a number of important materials in the lead perovskite family, either solid solutions or compounds. $Pb(B_1,B_2)O_3$ compositions typically have high piezoelectric or electrostrictive activity, important examples of these are $Pb(Ti,Zr)O_3$ and $Pb(Zn_{0.33},Nb_{0.66})O_3$. There is an extensive literature on the compositional modifications of these compounds to optimize their function for specific sensor or actuator applications. Additional information on the application of these materials can be found in the recent reviews by Setter (**14**) and Whatmore (**15**). For the demonstration here a soft, niobium doped, morphotropic phase boundary $Pb(Ti,Zr)O_3$ was chosen. The demonstration of morphology control was not planned, but analysis of the dielectric behavior of the films suggest that grain size in the final film can be controlled by deposition conditions, independent of sintering. Finally, to demonstrate the ability to form films between 1 and 20 μm, films of 5.5, 8.5 and 13.5 μm are reported here.

This work is hardly complete. There are still many improvements in processing that can be made, and there are still significant questions to be answered about the behavior of these films. However, this is a compelling demonstration of the ability of EPD to produce high quality, complex oxide films in a very useful thickness range.

This section takes a narrative form in describing the iterative development of procedures to produce a PZT film with properties comparable to the bulk ceramic. To provide a reference point this section begins with a description of the PZT starting powder and a thorough characterization of its properties in bulk form. This provides a standard for judging the relative quality of the films produced. This is followed by a description of some of the solvent/additive combinations evaluated for dispersion of the PZT powder. The next step after dispersion is deposition, followed by sintering of the deposition to form a dense continuous film. Finally, electrical, electrothermal and electromechanical measurements are made on the film to compare film properties to the bulk.

5.4.1 PZT Powder - Bulk Properties

The PZT powder has a stoichiometry of $Pb(Zr_{0.52}Ti_{0.48})_{0.976}Nb_{0.024}O_3$. It was prepared by reactive calcination of the component powders followed by high energy milling to reduce particle size. High energy milling was conducted for 12 hours in a stirred ball mill with $\approx$ 3 mm dia. spherical zirconia milling media. The calcined powder was dispersed in de-ionized water with Tamol 963 (Rohm and Haas Co., Philadelphia, Pennsylvania), an ammonium salt of a carboxylated polyelectrolyte. pH was adjusted to 10 by the addition of ammonium hydroxide. After drying the dispersant was burned out by heating the powder to 500°C for 8 hours.

Particle size distribution as shown in Fig. 5.16 below was determined by light scattering (Mastersizer S, Malvern Instruments Inc.). Surface area as determined by single point BET adsorption is 3.2 m^2/g. A SEM micrograph of this powder is shown in Fig. 5.17.
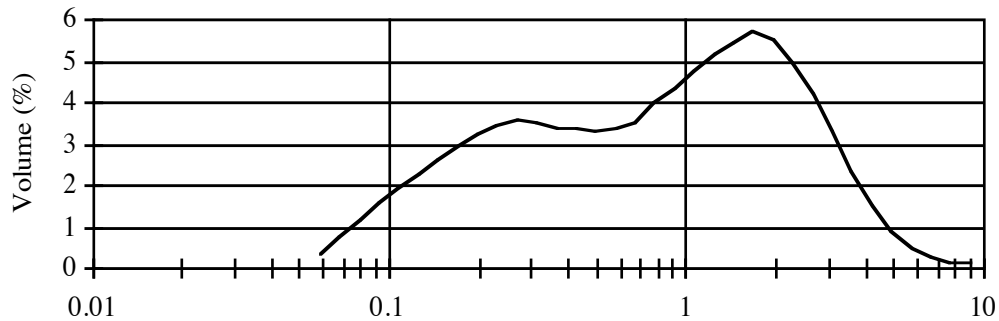
Fig 5.16 PZT particle size distribution , derivative volume percentage in microns diameter.
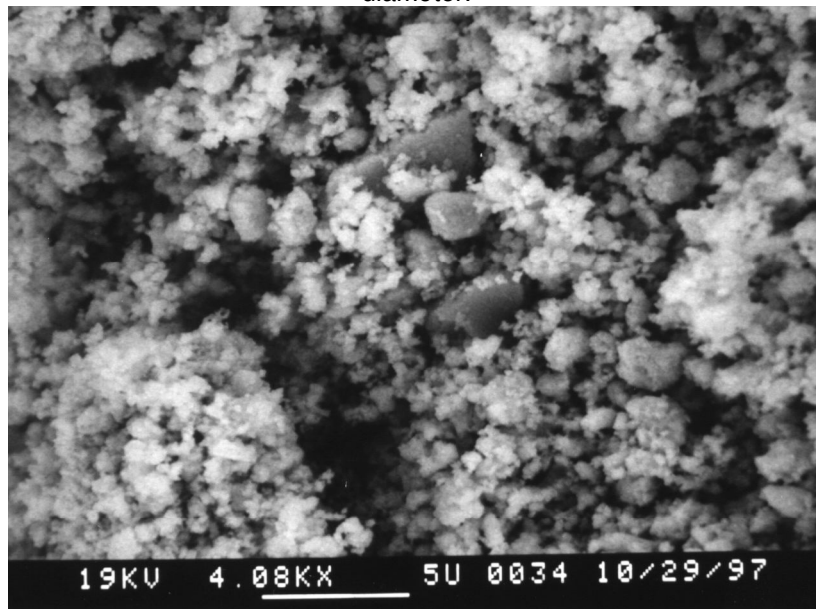
Fig 5.17 SEM photograph of attrition milled PZT powder.

Bulk samples of the sintered ceramic were prepared for property comparison. Six pellets were dry pressed and sintered in a sealed crucible with a lead source at 1,270°C for two hours. The pellets achieved an average final density of 96.2% with a standard deviation of 1.3% based on a theoretical density for PZT of 8.0 g/cc. Approximate dimensions of the samples were 1.4 mm thick x 11.0 mm diameter. The samples were sputter coated with gold top and bottom for electrical tests.

The average dielectric constant measured after sintering was 1,090 with a standard deviation of 70 and an average loss of 1.2%. The samples were poled at several conditions. Poling of three samples at 30 kV/cm and 80°C resulted in an average increase in dielectric constant of 44%. Raising the poling temperature on one sample to 120° C at the same voltage raised the dielectric constant by 58%.
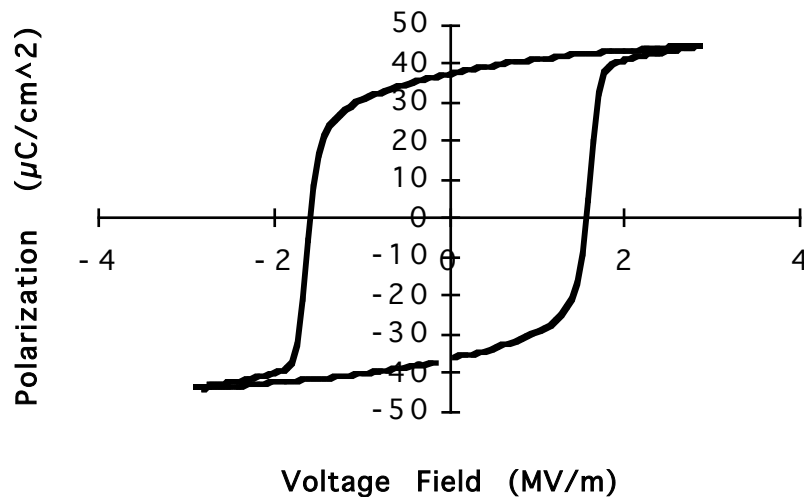
Fig 5.18 Polarization hysteresis on bulk sample, 5 second cycle.
Remnant polarization 36.5 μC/cm^2; coercive field 15.9 kV/cm.

Polarization hysteresis was measured on three samples resulting in symmetric polarization hysteresis loops with an average remnant polarization of 34.1 μC/cm^2 and coercive field of 17.25 kV/cm. An example of these hysteresis loops is given in Fig. 5.18.
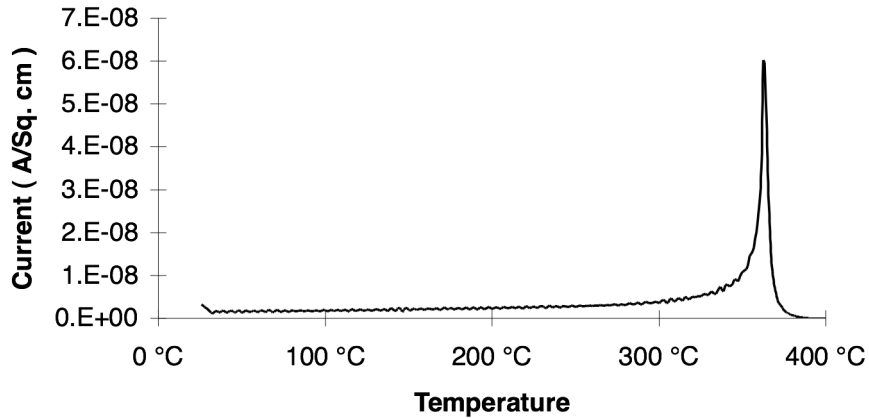
Fig. 5.19 Pyroelectric discharge current for bulk PZT.

A pyroelectric scan at a heating rate of 4°C/min. on one sample poled at 36 kV/cm and 120°C for 5 min. yielded a pyroelectric coefficient at room temperature of 45 nC/cm^2°K. The total discharge current was 41 μC/cm^2. Hysteresis was not measured on the sample used for this measurement, however, the discharge current is comparable to the average polarization measured on other samples. The maximum current occurred at 363°C and dropped below 1 nA/cm^2 at 377°C.
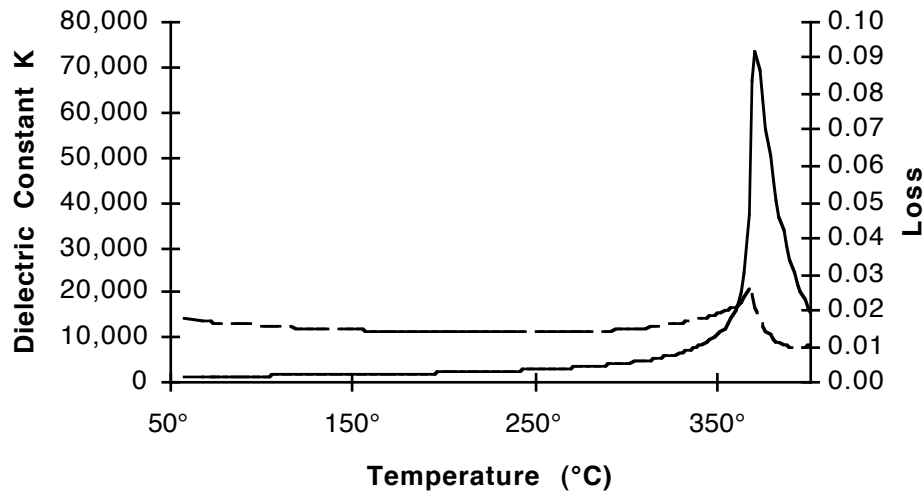
Fig. 5.20 Dielectric constant and loss as a function of temperature at 1 kHz with a 7 V/cm sine wave input.

Dielectric constant as a function of temperature showed a sharp peak at 370°C, with a maximum *K* approximately 50 times the room temperature value. This curve was measured on an unpolarized sample. To compare the relative breadth of peaks, the width in degrees was measured at a dielectric constant halfway between the room temperature and peak values. This yields a value of 19°C for this bulk sample.

5.4.2 Forming a Stable Suspension of PZT Powder

There was no systematic evaluation of dispersion systems for PZT, however, the experiments that were performed lead to a few observations. The first is the polarity of the surface charge that can be developed on the powder. Of the solvent-additive combinations tried, the PZT particles only developed a significant negative charge in water. In methanol, ethanol, iso-propanol, acetone and MEK the particles uniformly exhibited only a positive charge when charge was measured. This includes solvents with the basic additives such as ethanolamine or ammonium hydroxide.

Table 5.1 Solvent-additive combinations showing some dispersion effect on PZT powder.

Solvent	Additive	Dispersion Effect	Comments
Water	—	No	
	Ethanolamine	No	
	NH$_4$OH	No	
	Tamol 963	Yes	Ammonium salt of carboxylated polyelectrolyte (negatively charged adsorbing polyelectrolyte, electrosteric stabilization)
Ethanol	—	No	
	Emphos PS-21a	Yes	Phosphate ester of alcohol ethoxide (weak acid, electrostatic stabilizaton)
	Ethanolamine	No	Insufficient charge for electrostatic stabilization
	Iodine	Yes	Forms iodic acid, creates positively charged electrostatically stabilized suspension
	Lecithin	No	
	NH$_4$OH	No	Insufficient charge for electrostatic stabilization
	OLOA 1200	Yes	Polyisobutene succinimide (Straight chain hydrophobic polymer with negatively charged adsorbing end group, steric stabilization.)
	PEI	Yes	Polyethyleneimine (Amine groups at end of branches adsorb to negative surface sites, electrosteric stabilization)
	Tamol 963	Yes	
	Triethylamine	No	
Acetone	—	Yes	Positive surface charge, very low conductivity, electrostatic stabilization, difficult to reproduce
	I$_2$ in 2-Propanol	Yes	Forms iodic acid, creates positively charged electrostatically stabilized suspension
	Ethanolamine	No	
	NH$_4$OH	No	
2-Propanol	—	No	
	Iodine	No	
Xylene	OLOA 1200	Yes	

This matches the second observation regarding surfactants. Most of the surfactants that showed some improvement of dispersion of PZT were anionic, i.e. negatively charged, polymers. The negative groups on these polymers presumably adsorb to positive sites on the particles. The polymers then provide steric or electrosteric stabilization.

The exception to this is Polyethyleneimine (PEI). This is a highly branched polymer with amine groups at the end of each of the branches. It is possible that the amine groups on the polymer alter the solution chemistry enough that a negative surface charge is formed on the particles, allowing adsorption of the positively charged polymer. However, it is more likely that the amine groups displace another positive adsorbate at negative sites on the particle surface. No deposition attempts were made from polymerically stabilized suspensions, however, Ch. 2 suggests ways this might be attempted.

5.4.3 Deposition

Depositions were successfully accomplished from pure acetone, acetone with added iodine in 2-propanol, and pure acetic acid. Although the most uniform depositions came from the suspensions in acetone, it was easiest to repeatable produce depositions from glacial acetic acid, therefore this was the system that was most extensively studied and produced all of the films studied in section 5.3.4.

5.4.3.1 Acetone

Two depositions were produced from a suspension of PZT in pure acetone. 2.7 g of PZT powder was placed in a 200°C drying oven for one hour to drive off adsorbed water. This was directly quenched into 75.5 g of acetone containing 0.3 wt. % water. The powder was then dispersed by sonication. Deposition was carried out in a 200 ml pyrex beaker between two horizontal stainless steel disks spaced 2 cm apart and filling substantially all of the crossectional area of the beaker. Exposed plate area was 26.8 cm^2.

Deposition was conducted at a constant current of 0.1 mA or 3.7μA/cm^2. The negative pole of the current source was applied to the top plate. The particles in suspension were positively charged and were deposited vertically upward onto the top plate. The initial voltage when current was first applied was 39 V. This indicates a suspension conductivity of $\approx 0.2\,\mu$S/cm. A five minute deposition was accompanied by an accelerating non-linear voltage rise of 171 V. The thickness of the resulting deposition was not measured, however, visual estimation would put the thickness between 5 and 40 μm. The coating was very smooth, even, continuous and complete with no visible indications of convection.
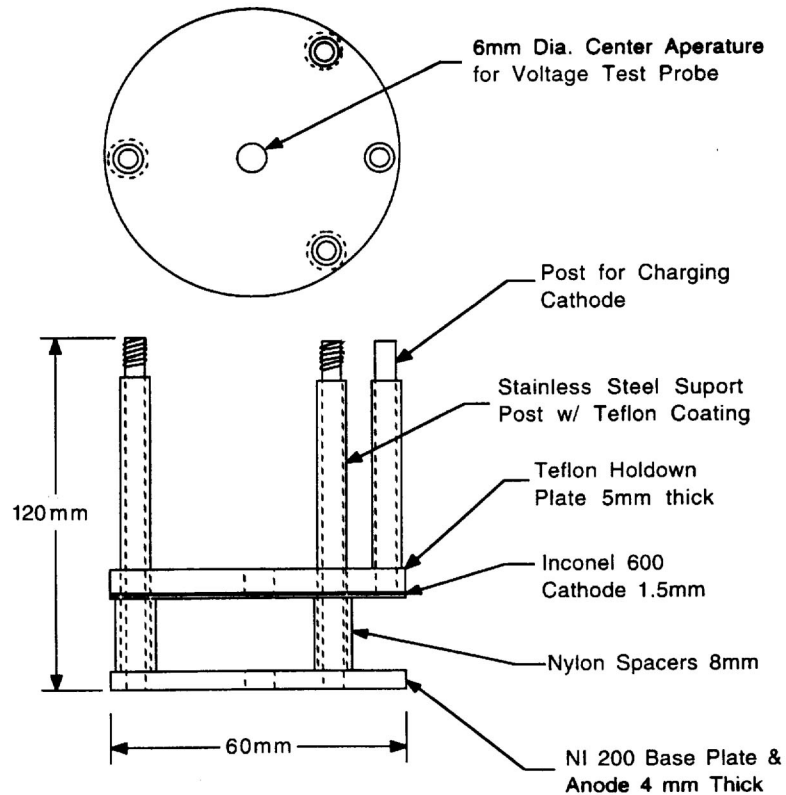
Fig. 5.21 Deposition test device.

Discussion —The powder develops a positive surface charge in pure acetone, although the charging mechanism is not clear. It is possibly due to acetone being very slightly acidic relative to water, thus generating a slight hydronium concentration in the solvent which preferentially adsorbs to the powder surface. Most of the powder sediments out immediately, however the suspension remains dense enough that the sedimentation is not visible. This would indicate that there is a positive electrostatic energy barrier to floccing which is insufficient for long term stability, but sufficient to retard floccing. Sedimentation will therefore initially be fairly rapid and become progressively slower as the volume density in the suspension decreases. In this case the suspension density is decreasing even as the deposition is progressing.

The large voltage rise at constant current indicates that the deposition is consolidated by the ion depletion mechanism in the deposited layer. This conclusion is further supported by the thickness uniformity of the deposition. Because of the low interparticle repulsion it is possible that the particles are initially deposited due to either the density increase or direct electrostatic force. However, there was no evidence of a low

density surface layer, therefore it is likely that the ion depletion layer grows at the same rate as the overall deposition.

One advantage of this deposition is automatic size segregation of particles during deposition. Given that the suspension is only moderately stable, the surface potential of the particles must be between 25 mV, below which it is completely unstable, and 50 mV, above which it would have long term stability. This translates into a mobility somewhere between 0.1 and 0.2 μm·cm/V·s. Taking the midpoint and given an electric field in the bulk suspension of 20 V/cm, the electrophoretic velocity of the particles would be approximately 3 μm/s toward the cathode. The sedimentation rate of a 1 μm PZT particle is $\approx$ 3 μm/s. While an accurate force balance is slightly more complicated, it is clear that, in the absence of convection, the deposition will primarily composed of particles below 1 μm even though more than half of the particles by volume are above 1 μm diameter.

5.4.3.2 Acetone with Iodine in 2-Propanol

A slightly more stable suspension was produced by adding a small amount of a 2-propanol solution containing dissolved iodine. This suspension consisted of 2.3 g PZT, 81.5 g Acetone, and 0.92 g 2-propanol containing 0.5 wt. % dissolved I_2 and 0.06 wt. % water as determined by Fisher titration. The powder was dispersed by sonication while stirring for 2 minutes. This suspension was allowed to sit for $\approx$ 20 minutes before being poured into another beaker for deposition. The sediment remaining in the first beaker weighed 1.32 g indicating that 60% of the PZT powder either was not suspended or had sedimented out in the time it was sitting. The total solution depth in the first beaker was 3 cm.

Deposition was performed on a 2.54 x 2.54 cm alumina substrate with a sputtered platinum electrode on one side. It was suspended horizontally in the deposition beaker by a small clip in the center of one side with the electroded side down 1 cm above a stainless steel anode. The clip also served as electrical contact for the substrate. A constant current of 0.4 mA was applied for two minutes. The initial voltage was 16 V which rose at constantly decreasing rate to 23.6 V at the end of deposition. The total deposition weight was 14 mg. The deposition thickness was not directly measured, however a packing density of 60% in the deposition would give a thickness of 4.5 μm. As in the deposition from acetone alone, the coating was very smooth, even, continuous and complete with no visible indications of convection.

Discussion —Iodine dissolves rapidly in 2-propanol where it reacts to produce a concentration positive and negative ions. This is presumably through the creation of iodic acid, one possible mechanism for which is:

$$C_3H_7OH + H_2O \Leftrightarrow C_3H_7O^- + H_3O^+ \qquad \textit{Protolysis in Propanol/Water}$$
$$C_3H_7O^- + I_2 \Leftrightarrow C_3H_7OI + I^- \qquad \textit{Ionization of Iodine}$$
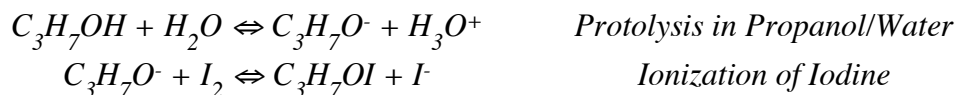
The concentration of iodine in the particulate suspension is 180 μMolar. If this was also the actual ionic concentration in the suspension, the Debye length would be only 6.4 nm, and it is unlikely that the suspension would show any level of stabilization regardless of surface potential. That this is not the actual ionic concentration is also supported by the low estimated conductivity of this suspension, 2 ± 1 μS/cm. Using the molar conductivity of iodic acid in methanol (**16**) as an estimate, this conductivity would translate into an ionic concentration of 10 μMolar. At this ionic concentration the calculated energy barrier to floccing would be 5 kT for two 0.5 μm diameter particles with a surface potential of 40 mV. The difference between the I_2 molar concentration and the ionic concentration is likely the result of both the incomplete ionization of the I_2 and adsorption of ions to the particle surfaces.

It is likely then that the addition of I_2 dissolved in 2-propanol increases the surface potential of the PZT particles in acetone by a slight preferential adsorption of the protonated species over the I⁻ ion. Given the voltage rise during deposition and the visual uniformity of the deposition, it is very likely that the deposition occurs by the ion depletion enhanced electrostatic mechanism. This would occur if the primary positive ion in solution is consumed at the cathode which is consistent with the ionization mechanism proposed above.

The difficulty in estimating the ionic concentration in this system is symptomatic of a larger problem in this system which is the instability of ketone-hydrohalous acid solutions. Tokuoka et. al (**17**) achieved very high ionic concentrations in acetone-I_2 solutions with 0.3 wt. % water. (However, they mention in a footnote that their solutions were not stable for more than one day.) Solutions prepared here, however, showed very low ionization in acetone with this concentration of water. Janz and Danyluk (**16**) reported a very low dissociation constant for hydrogen chloride in pure acetone, unstable conductivity readings, plus a number of possible polymerization or enolization reactions of the acetone catalyzed by the acid.

5.4.3.3 Suspension in Acetic Acid

      The simplest suspension for the EPD of PZT was also the one with the best suspension properties; pure acetic acid. By adding PZT powder at a rate of 3 g per 100 ml glacial acetic acid, a suspension which is stabilized against floccing can be produced with no additives.

      Solvent Chemistry — When the powder is added to the acetic acid, lead oxide on the surface of the powder will react to form lead acetate and water. The acid also reacts with zirconium to a lesser extent, leaving a titania rich surface. After thirty hours, some supernatant was removed for analysis by DC. plasma emission spectroscopy to determine the extent of dissolution/reaction of the particles. The following quantities were determined, expressed in mole percent of each element in the original powder: Pb 2.4%, Zr 0.6%, Ti 0.25%, Nb 0.9%. There was also some sodium remaining from the surfactant used during milling. The dissolved sodium in the supernatant was 0.01% of the total weight of the powder added.

      Conductivity and Ionic Strength — The glacial acetic acid used had an initial conductivity of 0.04 μS/cm. This rose to 0.09 μS/cm after dispersion of the PZT powder. Without specific knowledge of the ionic species present or their mobilities, the same estimated molar conductivity as used in section 5.2.3 above, 6 μS/cm·mM, will be used. This gives an estimated ionic concentration of 15 μMolar which gives a Debye length of 23 nm.

      Electrophoretic Mobility — The electrophoretic mobility of the particles was measured with the Delsa 440 laser Doppler velocimeter using the same process outlined in section 5.2.2 above, with a single potential of 30 V applied to the cell. The data points were fitted to a parabola, giving r^2 fitting parameters of 0.99 and higher. The calculated mobility at the stationary layers was 0.21 μm·cm/V·s. In a suspension not used for EPD, that mobility remained stable for 4 days.

      Surface Potential and Surface Charge — Interpretation of this mobility in terms of surface potential is not straightforward. With a particle size distribution ranging from 60 nm to 6 μm dia. the boundary layer thickness parameter for this suspension, κa, ranges from 1.5 to 150. As shown in Fig. 2.19 this is in the center of the range where mobility changes as a function of relative boundary layer thickness. However, given the sedimentation rate of the PZT particles, the height of capillary in which the mobility is measured, 1.00 mm, and the time it takes to measure the mobilities through the height of the cell, $\approx$ 30 min., it possible to eliminate a large portion of the size range. In 30 minutes any particles larger than 0.35 μm dia. will have sedimented the entire 1.00 mm height of

the measurement channel, while 0.25 μm particles will have sedimented by half the measurement channel height. The measurement procedure is to measure mobilities alternating between the top and bottom of the channel working toward the center, therefore 0.25 μm particles would be included in all measurements. Given that there was no significant difference between measurements between the upper and lower halves of the channel it is not unreasonable to estimate the average measured particle diameter as 0.20±0.05 μm. This gives a *κa* parameter of 9 ± 2. Since the surface potential is well above the ≈ 24 mV validity limit for the Henry formulation, the surface potential was estimated graphically from the results of O'Brien and White, Fig. 2.20 (**6**). This gives a surface potential of 54 mV with an uncertainty due to particle size of ±5%. This is within the error limits of the mobility measurement itself.

Inputting this potential into Eq. [5.4] gives an estimated surface charge density of 0.17 mC/m^2.

Electrostatic Stabilization — With an estimate for the surface potential and ionic strength of the solvent it is possible to make an estimate of the electrostatic stabilizing force. The L-VdW attraction and the electrostatic repulsion energies were calculated using the same estimation formulas as for silver/palladium in section 5.2.3 above. The result is shown in Fig. 5.22 below.
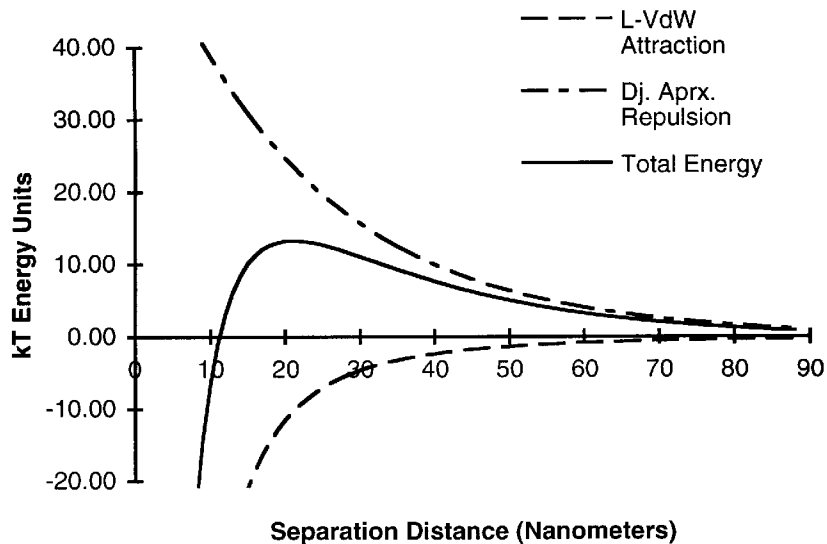
Fig. 5.22 Interaction potential for two 0.5 μm diameter PZT spheres in acetic acid; c = 15 μMolar; ψ_0 = 54 mV.

The total repulsion energy between two surfaces will be a function of the areas of the surfaces that come into proximity. Therefore, the smaller the radius of the particle, the lower the total energy barrier to contact. Even though this stabilizing energy is quite high for larger particles, as can be seen in the picture in Fig. 5.16, these larger particles are

much more angular than spherical. The repulsion at the low radius corners and edges will be much less than for a hypothetical spherical particle of the same size. Thus the stability of the suspension would be less that a straightforward combination of the particle size distribution and Fig. 5.23 would suggest.
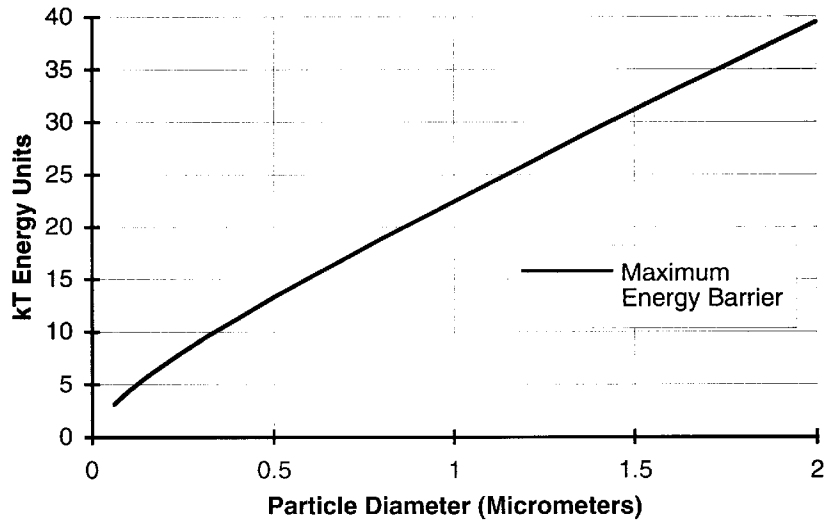
Fig. 5.23 Maximum repulsive interaction potential for two PZT spheres in acetic acid as a function of diameter; c = 15 μMolar; Ψ_0 = 54 mV.

Even if the particles are prevented from floccing sedimentation is a very significant factor in the behavior of these suspensions. The suspensions for EPD are prepared in a beaker with a fluid depth of 3 cm. As can be seen from the sedimentation velocities charted in Fig. 5.24, within five minutes of the end of sonication and stirring all particles above 5.5 μm dia. will have sedimented the full three centimeter depth of the suspension. Within 30 minutes the particles above 2 μm will have completely sedimented out as well. After 24 hours this would include all particles above 0.3 μm.
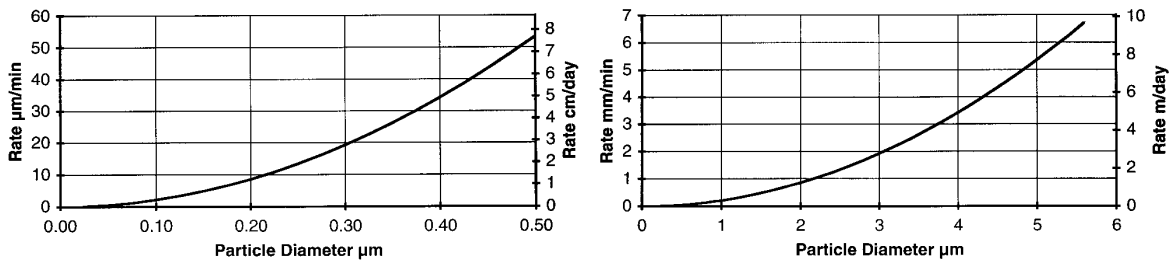
Fig. 5.24 Sedimentation speed for PZT particles in acetic acid at 25°C

Given that the particle size distribution extends down to 60 nm, if the particles were completely stabilized against floccing, after 24 hours particles below 0.3 μm should still be sedimenting out. Particles below 100 nm would show very little sign of sedimentation. As shown by Fig. 2.22, Brownian diffusion would keep a small but significant concentration 60 nm particles suspended indefinitely.

However, after 24 hours the PZT in the actual suspension will have completely settled out, leaving a crystal clear supernatant above a clearly defined sediment layer. This behavior lends considerable support to the measurements and calculations which are the basis of the size-stability chart in Fig. 5.23. Particles above 0.5 μm will have a large enough energy barrier to prevent floccing, but will settle out due to gravity. Particles below 0.3 μm which would stay in suspension longer have an energy barrier which is sufficient to slow, but not stop, floccing. These smaller particles will floc to each other and to larger particles forming masses that will settle out of suspension overnight leaving a completely clear supernatant.

5.4.3.4 Deposition from Acetic Acid

All of the films tested in § 5.4.4 below were deposited using a modified version of the deposition test device shown in Fig. 5.21. In this modification, shown in Fig. 5.25, the top Inconnel deposition disk is replaced with a 0.5 cm thick PTFE disk with a 5.20 cm^2 area square cut out in the center. A cylindrical PTFE holder block is fitted with spring mounted stainless steel wire hooks which both hold a 2.54 cm square alumina substrate to the face of the holder block and provide electrical contact to the face of the substrate. The holder block then mounts on top of the cut out disk so that the cut out masks the edges of the substrate. When a film is deposited the masked off area is not coated and provides an electrical contact point for the film's bottom electrode. The Ni 200 bottom disk then serves as the counter electrode. The cut out disk is held up by 1.5 cm spacers so that the total distance between electrodes is 2.0 cm. With these spacers the electric field gradient near the surface of the substrate is approximately 0.7 cm^{-1} times the applied voltage. For deposition the device is immersed in the particulate suspension in a 6 cm inside diameter Pyrex beaker.
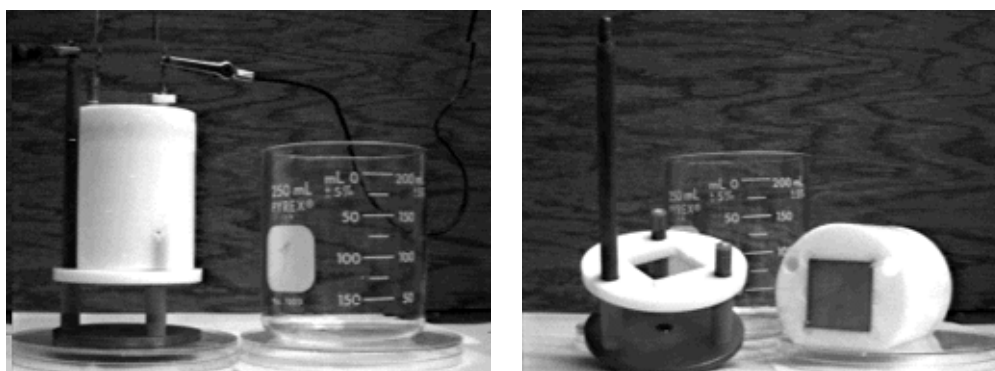
Fig. 5.25 Modified deposition device for deposition onto 2.54 mm square substrate. 5 mm thick PTFE disk masks the edges of the substrate with a 5.20 cm^2 square cut out area for deposition.

Depositions were performed at a constant voltage ranging form 100 to 500 V, which generated current densities from 1 to 100 μA/cm^2. Deposition times ranged from 45 seconds to 4 minutes, and depositions from 3 to 55 μm green thickness were produced. Most depositions were performed at either 250 or 300 V with a targeted final dense film thickness between 10 and 20 μm. During a typical deposition of 2 min. the current would rise by 1 to 2 % in the first 20 sec. followed by a decline over the deposition period also of 1 to 2 %. A subsequent deposition from the same system would then follow the same pattern, but would begin at a significantly higher current. Each successive deposition would then occur at a higher current until deposition was stopped or the suspension became too unstable to deposit. This conductivity rise occurred with both nickel and platinum counter electrodes, as well as during depositions of silver palladium from acetic acid using a gold anode.

Because of the significance of sedimentation, deposition should be started at the same elapsed time from the end of the sonication and stirring in order to insure reproducible results. To evaluate this reproducibility, a series of 16 depositions were made using the deposition device in Fig. 5.25. Before each deposition the beaker with the suspension and deposition device was placed in an ultrasonic bath for one minute while stirring. The beaker was removed from the ultrasonic bath, the holder block with a deposition substrate was placed on the deposition device and deposition was begun exactly 2 minutes after sonication was stopped. There were ten depositions of 90 sec. and six of 60 sec., all at 250 V. The deposition rate was linear with time with an average rate of 0.106 mg/cm^2•s and a standard deviation of 5.5%. The variation in the weight vs. time figure appeared to be random and did not show an up or down trend over the course of the experiment.

One important observation of these depositions was a large consolidation during drying. This was observable as a pronounced thickness change at the edge of the drying front as it moved across a deposition. Prior to drying the deposited powder showed clear pseudoplastic behavior. Using a point probe it is possible to manipulate the deposition like whipped cream or wet plaster and it will set in the rounded shape it is pushed or pulled into.

To evaluate this drying shrinkage, two depositions were made using platinum counter electrodes. Both depositions were made at 250 V for 5 minutes, after which they were removed from the holder block and rinsed by a single dipping in as-received acetic acid. One deposition was allowed to air dry while the other was placed onto a -10°C block of metal causing the acetic acid within the deposition to freeze in less than one half second.

The frozen deposition was freeze dried, impregnated with low viscosity epoxy, cut in crossection, polished and the thickness measured using an electron microscope. This procedure generated a density of only 25% for the freeze dried deposition vs. 60 % for air dried. This would suggest an almost minimum density flocced structure or very possibly some sort of ordered structure induced by EHD flows around the particles. Further work will have to be done to separate what specific structure may have existed in the deposition prior to freezing from structures which may be due to crystallization of the acetic acid.

Mobility measurements made one day later on suspensions that were used for deposition showed a mobility of only 0.14 μm•cm/V•s. This was accompanied by a doubling of the suspension conductivity compared to the initial suspension. Using the same procedures as above this generates a Debye length of 16 nm, and a surface potential of 35 mV. Using the Derjaguin approximation this gives a zero energy barrier to floccing.

This, however, does not always correspond with the observed behavior of the suspension. In some cases the suspension did become unstable after a certain number of depositions and further deposition became impossible. In many other cases, while floccing and sedimentation are slightly higher after 10 - 15 depositions, it is clearly not as rapid as in a completely unstabilized suspension. Furthermore, the fact that the deposition rate does not change, as shown in the reproducibility experiment above, implies that the electrophoretic mobility does not change significantly over the course of several depositions. If the electrophoretic mobility has not changed this would yield a surface potential of 50 mV, giving a energy barrier of 3 to 5 kT. This more closely matches the behavior of the suspension, observably floccing and sedimenting but over the course of 1 to 1 1/2 hours. This would need to be verified by mobility measurements made immediately after a series of depositions.

Conduction at the cathode appears to be by electrodeposition of lead ions and to a lesser extent titanium. Plasma spectroscopy measurements of the concentration of metals in solution in a suspension not used for deposition showed a concentration of lead of 2.0 milliMolar 90 minutes after preparation. Another measurement on the supernatant of a suspension which had been used for deposition showed a significantly lower concentration of dissolved lead. Unfortunately differences in sample preparation do not allow direct comparison of these concentrations. Additional evidence is provided by a substrate used for deposition. The alumina substrate with a polished platinum electrode was sintered at 1,250°C. This substrate was cathodically charged to deposit a coating of PZT. The deposition was later washed off so the substrate could be re-used. When the electroded substrate was heated to 950°C the electrode melted and the surface of the substrate turned

blue. The melting of the platinum electrode can be accounted for by the formation of a low melting point lead-platinum alloy, and the blue color of the substrate can be accounted for by titanium doping of the alumina.

Discussion — Based on the observations above it is possible to begin to assemble a theory for the electrochemical and colloidal behavior of this system during deposition.

When PZT powder is placed in the acetic acid the lead oxide on the surface is rapidly converted to lead acetate in solution, along with a much lower concentration of zirconium and titanium acetate. The lead acetate is then very slightly ionized in solution to form a positive lead single acetate ion and a single negative acetate ion.

$$Pb(C_2H_3O_2)_2 \Leftrightarrow Pb(C_2H_3O_2)^+ + C_2H_3O_2^- \qquad \textit{Ionization of Lead Acetate}$$
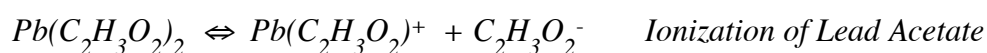
The positive lead acetate ion is then preferentially adsorbed to the zirconate-titanate rich surface leaving a negative acetate ion in solution.

When a voltage is applied to the system, lead and titanium acetates will be reduced on the cathode. Because of the low current and the relatively large reservoir of un-ionized lead acetate in solution, ionic depletion at the cathode is not a significant factor in this case. This is supported by the constancy of the current during deposition.

At the anode nickel will be oxidized to form nickel acetate. If the nickel acetate has a higher ionization constant in solution this would account for the rise in ionic concentration, even though there is a 1 to 1 replacement of lead acetate by nickel acetate. As noted above this rise in conductivity also occurs with gold and platinum anodes. The creation of gold and platinum acetates are possible, but other possible anode reactions should be considered.

There are several mechanisms by which deposition can occur, however, it is useful first to rule out a couple of mechanisms. The first is simple densification. This mechanism requires a very low concentration in the bulk solution and a very low stabilizing force. This would be applicable as the conductivity and stability of the suspension goes down, however at this point deposition becomes more difficult and this would not account for deposition at the initial conditions where there is clearly a significant stabilizing force. The second is ionic depletion at the cathode. Although ions are consumed by electrodeposition at the cathode, if an ionic depletion layer were to form a drop in current would be expected as voltage was concentrated across the ionic depletion layer. Given the constancy of the current this mechanism can be discounted. Finally, there is increased ionic concentration. For this to occur there must be a mechanism for the production of ions at the cathode. However, this requires that there be a soluble cation for

which the free energy of reduction is much larger than the free energy of the ion producing reaction. For this solution this would be the case where the hydrogen ion from an acetic acid molecule is reduced, producing a negatively charged acetate ion, in preference to the reduction of lead, titanium or zirconium ions from solution. This is a possibility, and if further work is done on this system it could be investigated. However, given the evidence of electodeposition of lead and titanium , it is unlikely.

This leaves direct electrostatic force. Given that the force distance profile and surface charge density is essentially the same as for Ag/Pd in section 5.2.3 above, the conclusion here is likewise that the direct electrostatic force is sufficient to overcome the interparticle repulsion. However, in this case the deposited particles will not assume the potential of the electrode. Deposited particles will remain positively charged relative to the solution and will retain a negatively charged boundary layer. This negatively charged boundary layer will flow away from the deposition electrode and will interact with the boundary layer of an approaching particle, which is also flowing away from the deposition electrode. The interaction of these EHD flows between the deposited and depositing particles is very likely to cause some structure to develop in the deposition layer. This structuring would account for the very low density of the deposition prior to drying.

5.4.4 Doping, Sintering & Properties

Having developed a procedure to electrophoretically deposit a thin, uniform, dense layer of PZT powder on a substrate, the next problem is to sinter this deposition to form a dense, continuous, polycrystalline PZT film on that substrate. The following section follows the heuristic as successive processing problems were identified and addressed to improve the quality of the films. While there is room for improvement in the final films produced here, the properties indicate that PZT films with good dielectric and piezoelectric properties can be produced from a particulate precursor down to a thickness of $6\,\mu$m. The successive steps taken here to improve film properties can serve to guide experiments to further develop these films.

The films were deposited and sintered on 25.4 x 25.4 mm alumina electronic circuit substrates (ADS 996, Coors Ceramics Co.). These are unpolished, 99.6 wt. % alumina substrates with the remaining 0.4 wt. % assumed to be a silicate based sintering aid.

5.4.4.1 Sputtered Pt Electrodes

For the first set of films the alumina substrates were made conductive on one side with a sputtered platinum coating ≈ 40 nm thick. The resistance across the substrate from corner to corner was 80 Ω measured using two point probes.

The first attempt at sintering an electrophoretically deposited coating was made by placing the coated substrate into an oven where is was heated to 1,270°C and held for two hours using the same heating and cooling profile as for the bulk samples in § 5.4.1. SEM examination showed a very low density, irregular coating. X-ray diffraction showed that all lead had been lost from the coating leaving only zirconate titanate.

The next series of sintering experiments were conducted in a small platinum metal box 2.6 x 3.0 x 0.5 cm. This box held one substrate and a small amount of lead source. The lead source is a 1:1 molar mixture of $PbCO_3$ and ZrO_2 powders. During sintering the powders will calcine to form $PbZrO_3$. The vapor pressure of PbO from the $PbZrO_3$ is higher than the equilibrium vapor pressure above PZT. PZT in the same environment should retain a stoichiometric lead ratio as lead is lost from the lead zirconate powder above 840°C. The platinum box enclosed the substrate and lead source but was not sealed.

Films were sintered at 100° intervals from 850°C to 1,250°C with a 20 minute hold at temperature. The films showed a progressive increase in grain size and density up to 1,150°. The estimated average grain sizes are 950°C - 0.3 μm; 1,050°C - 1 μm; 1,150°C - 2 μm. Had the progression continued to 1,250°C it may have fully densified, however, again at this temperature all lead was lost and only a very low density zirconate-titanate coating was left.

To address the problem of lead loss it was decided to try to lower the sintering temperatures of the films. Two sintering aids were tested to accomplish this, Li_2O and PbO. To dope the deposition with lithium, lithium carbonate was added to acetic acid where it reacted to form a 0.2 wt% lithium acetate solution. The dried deposition was then re-wetted with the lithium acetate-acetic acid solution, which was dried to leave behind lithium acetate which is burned to lithium oxide during the ramp up to sintering temperature. A weight of lithium acetate solution was added to the deposition sufficient to achieve a 4 mol. % concentration of lithium oxide. The dried weight of the lithium acetate was not detectable. The exact mechanism by which lithium works has not been determined, however samples sintered at 850°C and 950°C showed considerable grain growth and densification. The grain size and density at 850°C with lithium was intermediate between the size and structure of the undoped depositions sintered at 950°C

and 1,050°C. The deposition with lithium sintered at 950°C showed a structure halfway between the undoped depositions sintered at 1,050°C and 1,150°C.

Lead oxide was added to depositions in a similar manner. Lead oxide was added to acetic acid where it reacts to form a lead acetate. A solution was prepared that was 10 wt. % based on lead oxide. A deposition was re-wetted with the lead acetate solution using a pipette. Sufficient solution was added so that after oxidation the lead oxide would be 44 vol. % of the deposited PZT. The excess lead oxide melts at 886°C, provides a transient liquid phase during sintering, and replaces the lead lost to dissolution in the EPD suspension. Since PZT does not form any excess lead oxide phases, PZT and lead oxide should co-exist as separate phases. Then, because of its volatility, the majority of the excess lead oxide evaporates during sintering, leaving stoichiometric or near stoichiometric PZT. This deposition was sintered for 20 min. at 950°C with a 45 minute rise time. This sample showed greater densification and less grain growth than the sample doped with only lithium.

The next step was to combine both lithium and lead oxide. Once again a deposition was re-wetted with lithium acetate to yield a 4 mol. % concentration of lithium oxide. Lead acetate was added to give a 66 vol. % ratio of lead oxide to PZT. The objective was to completely fill the pore structure of the 60 % dense PZT deposition, thereby taking advantage of capillary tension to assist in densifying the deposition as the lead oxide evaporated. This film was sintered at 900°C for two hours with a 45 minute rise time. A fracture crossection of the resulting film is shown in Fig. 5.26. SEM examination of this crossection showed porosity only at the top and bottom surfaces of the film. The top surface showed a grain size of $\approx 0.5\,\mu$m. Grain size in the bulk of the film was not measured.
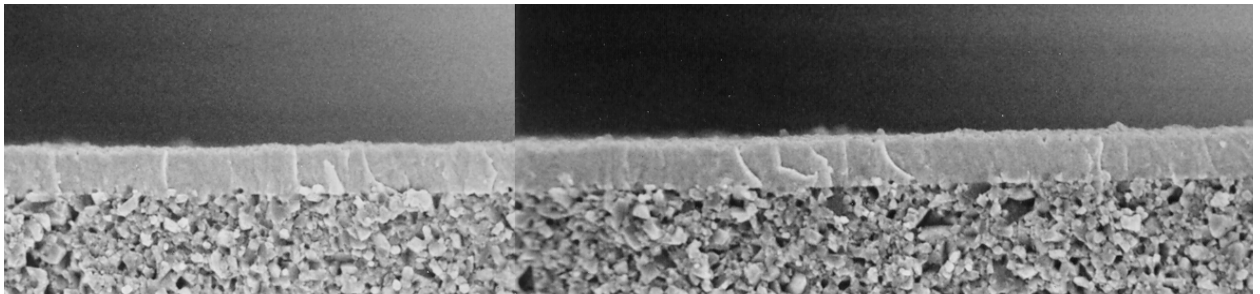
Fig. 5.26 Fracture surface crossection showing a 6 μm PZT film deposited on a dense alumina substrate with a sputtered platinum electrode (not visible) and sintered to full density at 900°C

As shown in Fig. 5.27, the X-Ray diffraction pattern for the film indicates that the film is phase pure PZT with no evidence of remaining crystalline lead oxide or of reaction with the substrate.
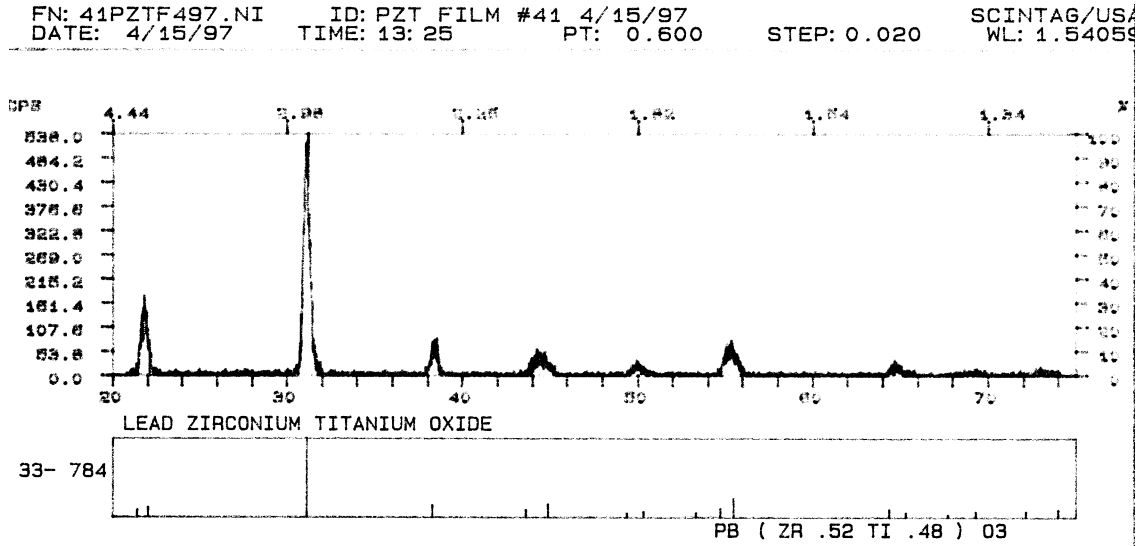
Fig. 5.27 X-ray diffraction pattern shows only PZT phase formed after densification

The weight loss of the substrate and film was equal to 75% of the excess lead oxide added to the film. The balance of the lead oxide appears to have been absorbed by the alumina substrate. There was a distinct yellow band in the alumina extending ≈ 0.3 mm below the PZT coating, as well as yellow staining around the edges of the substrate.

The sintering results for this film were very good, and the density achieved is better that any film produced subsequently. The results of these subsequent experiments strongly suggest that, even though the substrate contains only 0.4 wt. % silicate sintering flux, this flux diffused into the deposition and contributed significantly to sintering.

Unfortunately, during the sintering the thin sputtered platinum electrode de-wetted the interface, remaining only as small spherical inclusions scattered along the PZT-alumina interface. Without a bottom electrode electrical measurements of this film were not possible. The loss of the electrode as a barrier layer also is what allows the substrate's sintering flux to diffuse into the deposited layer.

5.4.4.2 Ag/Pd Screen Print Electrodes

To provide a stable electrode which would remain continuous and planar it was decided that a much thicker metal layer than is practical to produce by sputtering would be necessary. To do this the next set of substrates was electroded by screen printing of a 6/1 silver palladium paste. To minimize the through thickness porosity in the electrode layer, three layers of ink were screen printed and sintered. The surface was then polished to a mirror finish. The substrates were annealed at 950°C for 20 minutes to stabilize the electrode surface. The resulting electrodes were $\sim 10\ \mu$m thick.

The platinum box used for enclosing single substrates during sintering was replaced by a covered zirconia crucible. Three substrates were placed flat, side by side on the flat bottom of the crucible with ≈ 1 gm of lead source in a zirconia boat. This was covered with a dish shaped lid having a volume of 94 cm^3. The edges were sealed with refractory cement which was porous enough to allow gas pressure equalization but prevents convective gas motion and slows gas diffusion in and out of the crucible.

It was found that the amount of lead used for sintering the high density film shown in Fig. 5.26 above was excessive in the presence of a continuous electrode layer. Sets of substrates were sintered with differing levels of added lead acetate. The level of lithium was kept targeted at 4 mol. % with actual levels varying between 2.5 and 4.5 % due to experimental error. The substrates were sintered at 900°C for two hours with a heating and cooling rate of 20°C/min.

The best results were achieved with the addition of lead such that the resulting lead oxide is between 25 and 34 vol. % of the deposited PZT. With less lead oxide the coating did not densify and remained a whitish color. Excess lead oxide causes several types of cracking, exaggerated grain growth and blistering of the electrode.

Re-wetting of the depositions with the lead and lithium acetate solutions was done by dripping the solution from a syringe. Drops frequently had to be placed at several points around the deposition the insure uniform wetting. Frequently, where the drop was added, the solution would wet the interface between the deposition and substrate much faster than the deposition. This would cause many small flakes of the deposition to come off the substrate where the drop was added. During drying the lead acetate did not end up distributed evenly through the deposition. The final areas of the deposition to dry ended up with significantly more lead acetate than the rest of the deposition. This was visible both on the dried deposition and as color and morphology changes over the surface of the substrate. Uniform, dense coatings had a dark brown color. A final sintering experiment did not show any sintering difference between a two hour and a half hour hold at 900°C.

Films that appeared continuous by visual inspection were electroded by masking with adhesive tape and sputtering 2.15 mm diameter gold circular spots on the surface. The resistance between the top and bottom electrodes was measured using steel tipped point probes. Spots with a resistance less than 40 MW were classified as bad. The electrical properties of film with the largest number of good spots are described below.

Film Preparation — The film which is described here, index #81, was deposited at 250 volts applied for 91 seconds with a nickel anode. This converts to an approximate voltage gradient near the deposition substrate surface of 175 V/cm. The deposition suspension was stirred in an ultrasonic bath for one minute and allowed to sit for exactly two minutes prior to the beginning of deposition. This resulted in the deposition of 9.4 mg/cm^2 of PZT. The film was re-wetted with lithium and lead acetate solutions sufficient to yield a 2.5 mol. % lithium concentration and lead oxide 20 vol. % of the deposited PZT. The film was sintered at 900°C for 30 minutes with a 20°C/min. heating and cooling rate. The resulting film had a dark brown area in the center surrounded by a lighter brown halo fading to dark brown again at the edges.

Film Properties — Twenty 2.15 mm diameter gold spots were sputtered onto the top surface of the film in a grid pattern. Of these spots, 13 were good, showing a resistance of more than 40 MΩ. Electronic measurements of these thirteen spots were used to generate the average property values reported in Table 5.2. To allow the direct comparison and correlation of quantities, one particular electroded area, Spot #7, was chosen for which a full set of measurements are reported.
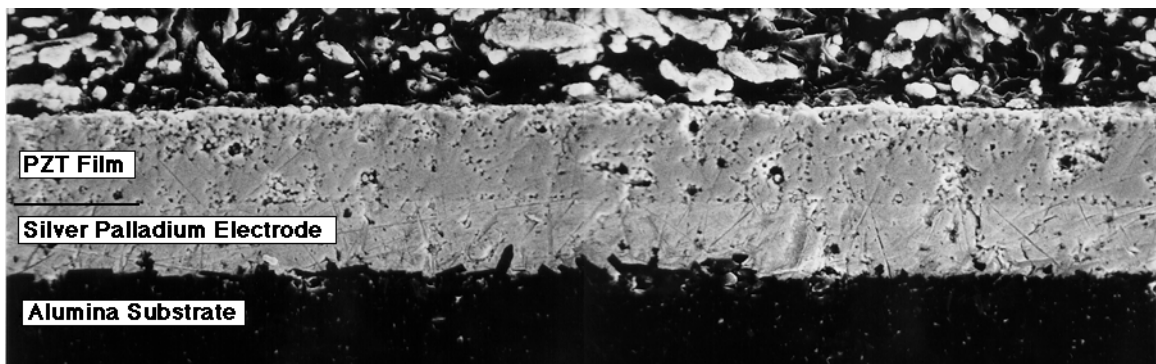
Fig. 5.28 Cut and polished crossection of PZT film. The layers from the top are: conductive silver epoxy; 13.5 μm PZT film; 10 μm Ag/Pd electrode; and alumina substrate.

A polished crossection of the film is shown in Fig. 5.28. This crossection was made through electroded spot #7. The average thickness measured in this crossection is 13.5 μm. Based on the deposition weight and film area, if the film were uniform and fully

dense, the thickness would be 11.7 μm. Given that the apparent density at this point is well above 90%, it is likely that this area is slightly thicker than other areas of the film, and thickness variation will contribute to the variation in capacitance and coercive voltages. All calculated values below, however, were based on the directly measured thickness of 13.5 μm.

Capacitance was measured on an HP 4275A Multifrequency LCR Meter at 100 Hz and 1 Volt. This gives an electric field in the sample of 740 V/cm. This gave an average dielectric constant of 854 with a standard deviation of 8 % and an average loss of 0.049. Two spots which showed a loss of 0.12 and 0.15 were not included in this average. Spot #7 had a dielectric constant of 912 and loss of 0.045. Poling of spot #7 at 60 V (44.4 kV/cm) and 120°C for ten minutes produced an increase in dielectric constant of only 5 % accompanied by an increase in loss of 0.05.

The charge/voltage hysteresis was measured for all 13 electroded spots using a 20 Hz sine wave input with a maximum voltage of 130 Volts, giving a maximum field of 95 kV/cm. Average polarization was 16.5 μC/cm^2 with an average coercive field of 18.7 kV/cm. Many of the hysteresis loops were not symmetric. The average positive polarization was slightly lower than the negative polarization, 16.1 vs. 17.1 μC/cm^2, however the standard deviation of the positive polarization was 30% vs. 15% for the negative polarization. The hysteresis loop for spot #7 is shown in Fig. 5.29 below. The average remnant polarization is 23.4 μC/cm^2 with an average coercive field of 17.0 kV/cm. The positive polarization was measured at 27.5 μC/cm^2 with a negative coercive field of 21.5 kV/cm.
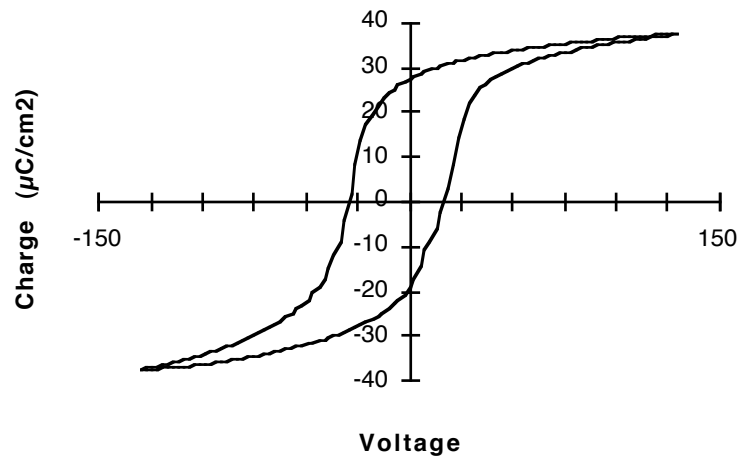
Fig. 5.29 Charge/voltage hysteresis loop for electrode spot #7, film #81.

The d_{33} coefficient was measured in a special test rig designed and built at Penn State (**19**). Spot #7 was positively polarized by the application of 150 V for 5 min. at room temperature. A wire was attached to the spot with silver filled conductive epoxy. In the test rig gas pressure is applied to both sides of the film substrate. The symmetric uniaxial loading is intended to prevent bending modes being induced during testing. The edges of the substrate project out of the pressure chamber between rubber O-rings. Thus the edges of the of the substrate are not exposed to the gas pressure. This means that the pressure on the substrate will be purely uniaxial, orthogonal compression of the substrate and film. The current used for calculating the piezoelectric coefficient was the average of the current in and out of the electrode when pressure is applied and released.
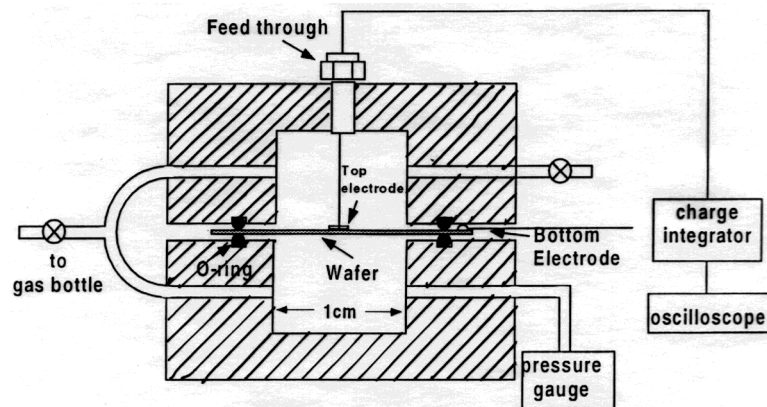
Fig. 5.30 Diagram of pressure cell for testing film d_{33} coefficient.

Applications of pressures of $0.5, 0.75$ and 1.0 MPa gave, respectively, d_{33} values of 155, 151 and 137 pC/N. Because the highest pressure gave both the highest signal and the closest match between positive and negative current (10% difference), it is likely the most accurate measurement therefore an approximate value of $d_{33} \approx 140$ for this film was entered into Table 5.2.

Dielectric constant as a function of temperature was measured on a second film prepared at the same time and in the exact same manner as the above, but which was sintered for two hours at 900°C rather than 30 minutes. The estimated thickness of this film based on deposition weight is 14.2 μm. The dielectric peak is much lower than for the bulk sample, only 11 times the room temperature value and occurs at a temperature of 375°C. The peak is also much broader with a temperature span of 122°C at a level halfway between the room temperature and peak value.
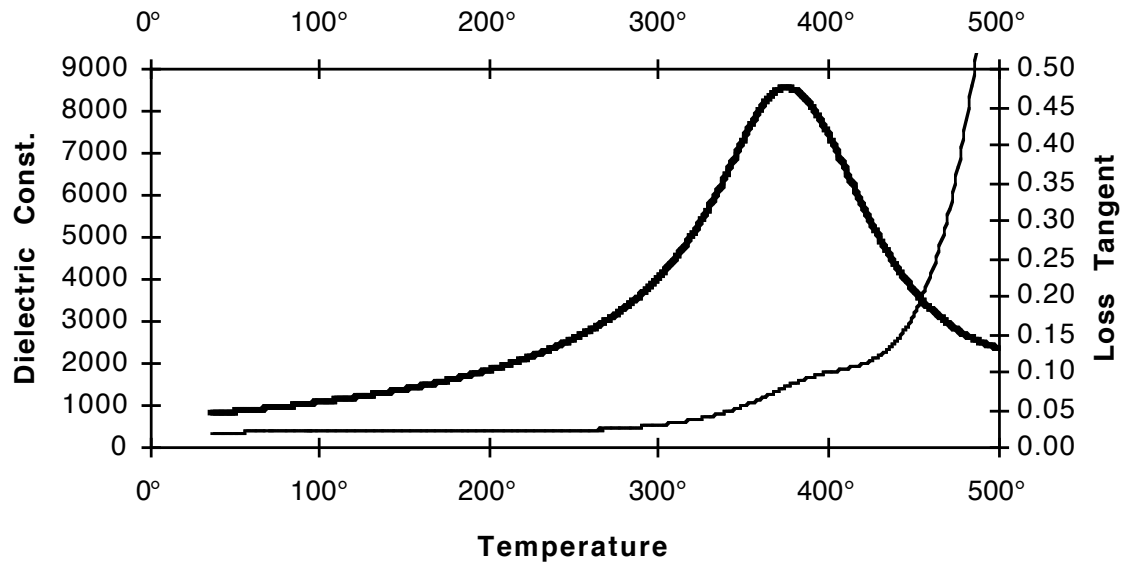
Fig. 5.31 Dielectric constant and loss as a function of temperature at 1 kHz with a 7 V/cm sine wave input.

Pyroelectric current was measured on a third sample which again was deposited at the same time as the first sample and was sintered together with the first sample. This sample had 10% more added lead and 30% more added lithium. Thickness calculated based on deposition weight is 15.0 μm. The first heating run showed a very large positive current, well beyond what could be accounted for by any dielectric polarization. At 335°C the current became negative and increased to -6x10^{-9} A at 400°C. The sample was reheated to 600° in between runs to sinter on a new Ag/Pd electrode contact. During this sintering the gold sputtered electrodes changed from a gold to silver color. It was then positively poled at 120 V for 5 min. at 120°C. The second pyroelectric current measurement did not show the same anomalous positive current but the negative current was even larger, reaching -10x10^{-9} A at 400°. For the final run the film was poled at -150 V for five min., followed by another poling at -120 V for five min. at 120°C.

Discussion — The uneven color of the sintered film likely corresponds to areas of different density in the film, lighter colored areas having lower density. This variation can be traced back to the uneven distribution of the sintering additives when the solution which the deposition is re-wetted dries.
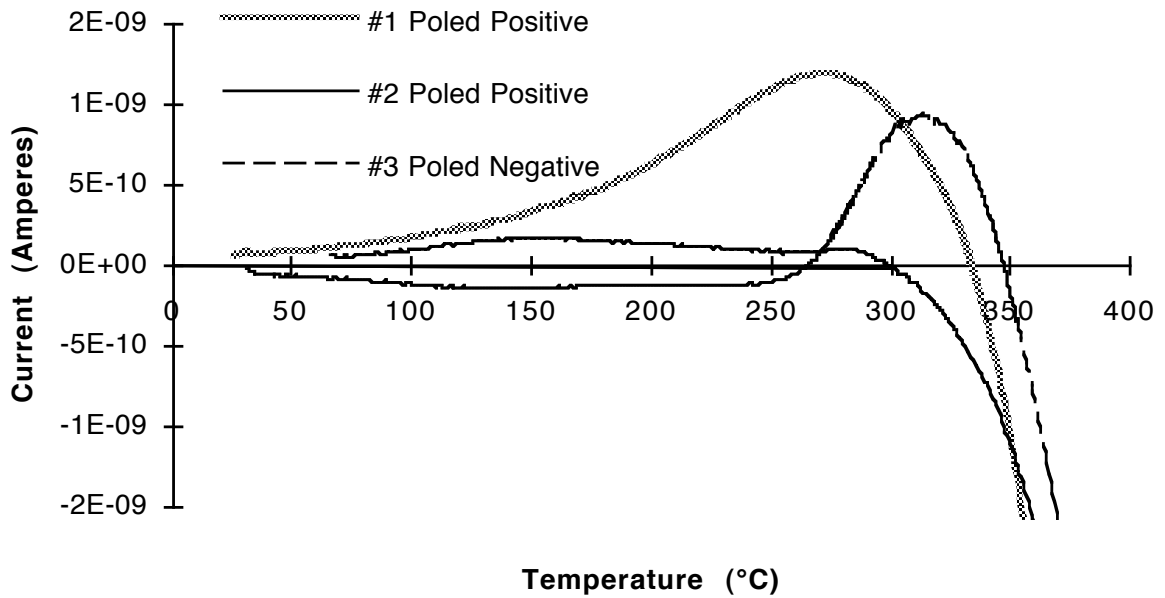
Temperature (°C)

Fig. 5.32 Pyroelectric currents. Heating rate 4°C/min.

The room temperature dielectric and piezoelectric properties of this film compare fairly well the bulk samples. The bulk samples prepared by pressing contain the full range of particle sizes from the starting powder. That combined with the 1,270°C sintering temperature means that the grain size of the bulk sample would be 2 - 3 μm. For the film deposited by EPD the large particles will sediment out and will not be incorporated into the film. This combined with the lower sintering temperature of the film means that the grain size in the film will be < 0.5 μm. This is confirmed by SEM observations of several fracture crossections. The dramatic broadening and height reduction of the dielectric constant peak as a function of temperature is also consistent with a grain size reduction to below a micron, particularly a reduction in the grain to grain boundary volume ratio. These microstructure changes limit extrinsic contributions to dielectric permittivity as reported by Randall et al. (**20**).

The lack of a significant increase in the dielectric constant with poling is also consistent with a strong clamping of the film which prevents domain re-orientation during poling. If this extrinsic effect is clamped out it is possible to describe the piezoelectric effect in terms of intrinsic material properties. Using the intrinsic relationship between the remnant polarization – P_3, dielectric permittivity – ε_{33} and piezoelectric coefficient – d_{33},

$$d_{33} = 2Q_{11}P_3\varepsilon_{33} \qquad \text{Intrinsic Piezoelectric Effect} \qquad [5.7]$$

the electrostrictive coefficient - Q_{11} for the film is 0.037 m^{4}C^{-2}. This value is the same as calculated by Haun (**21**) for a polycrystalline 52/48 PZT using single crystal data and a parallel mixing rule. This result lends support to both the relative accuracy of the d_{33}

measurement and the theory that the lateral clamping of the substrate prevents domain re-orientation even at a thickness of 13 μm.

There were several other phenomena associated with these films on Ag/Pd that were not consistent with the bulk, or accounted for by a simple grain size or clamping effect. The dark brown color of the film is consistent with reduction of lead in the PZT. The asymmetry of the hysteresis loops appears to be due to an asymmetric contact potential.

Because of the possibility that these non-ideal behaviors could be a result of gold-Ag/Pd electrode asymmetry, silver migration into the film, and/or palladium oxidation/reduction, the next step taken was to form films on a platinum bottom electrode which could then have symmetric platinum electrodes sputtered on top.

Table 5.2 PZT Bulk and Film Properties

	Bulk Samples	Film on Silver/ Palladium #81	Film on Platinum #120	Film on Platinum #142
Thickness	1,370 μm	13.5 μm	5.5 μm	8.5 μm
Dielectric Constant. Maximum -Unpoled	1,227	920	980	800
Dielectric Constant, Average - Unpoled	1,157	854	815	712
Standard Deviation	*7%*	*8%*	*12%*	*9%*
Increase in Dielectric Constant with Poling, Max	61%	5%	-3.5%	-5.6%
Ave. Dielectric Loss, Tan δ	0.015	0.049	0.038	0.035
Remnant Polarization Maximum	36.5 μC/cm^2	27.5 μC/cm^2	32.2 μC/cm^2	33.1μC/cm^2
Remnant Polarization Average	35.3 μC/cm^2	16.6 μC/cm^2	24.7 μC/cm^2	28.3 μC/cm^2
Standard Deviation	*N/A*	*24%*	*11%*	*8%*
Coercive Field, Average	17 kV/cm	18.7 kV/cm	17.4 kV/cm	26.1 kV/cm
Standard Deviation	*N/A*	*23%*	*8.5%*	*11%*
Piezoelectric Coefficient, d_{33} Maximum	406 pC/N	140 pC/N		128 pC/N
Pyroelectric Coefficient, p @ 25°C	45 nC/cm^2°K			25 nC/cm^2°K
Electrostrictive Constants, Q_{11}	0.037 m^4/C^2	0.037 m^4/C^2		0.043 m^4/C^2
Dielectric Peak Height/Width	50/19°	11.5/122°	14/93°	8/110°
Sintering - Rise Time/Peak Temperature/Hold Time (min./°C/min.)	300/1,270°/ 120	45/900°/30	64/900°/12	45/950°/5

5.4.4.3 Platinum Screen Print Electrodes

Platinum Electrode Preparation — A single screen printed layer of platinum after sintering had a visually rough surface and when examined by SEM showed many through thickness pores from 1 to 10 μm. To produce a smooth, continuous electrode the platinum was screen printed, sintered, and polished, and the process repeated three times to assure a continuous, pore-free surface. The electrodes were sintered at 1,250° for 30 min. with a 40 min. rise time. The final polishing then brought the surface to a mirror finish. The resulting electrodes were 5 to 10 μm thick.

The electrical properties of two films on Pt electrodes are summarized in Table 5.2. The first, # 120 with a calculated thickness of 5.5 μm was characterized only for dielectric and polarization properties. The second, # 142 with a measured thickness of 8.5 μm, showed a slightly higher average density and was characterized for piezo and pyroelectric properties as well.

Sintering on Pt Electrodes — The first set of depositions on Pt electrodes was sintered with and without added lithium and a target of 20 vol. % lead oxide. The films were then sintered at 900°C for 20 min.

The resulting films showed very uneven sintering behavior. A large part of this appeared to be due to the uneven distribution of the excess lead oxide. When the lead acetate solution dries the lead acetate appears to migrate with the drying front. The areas that dry first end up with very little lead acetate while the final areas to dry end up with an excess. The film with the highest density also had the highest addition of lithium. The films without lithium showed areas with almost no sintering and were still the yellow color of the deposited powder. At the uncoated edges of the substrate there were rough, colored spots which were assumed to be due to interaction between the excess lead oxide and the platinum electrode.

Preparation of Film #120 — A second set of eight films was deposited from a suspension consisting of 2.03 g PZT in 91.1 g of acetic acid. The suspension was prepared one day, used to deposit one substrate at that time, and then used for deposition of the rest twenty four hours later. The suspension was both dispersed and re-dispersed the next day by sonication while stirring for two minutes. Twelve depositions were made with four rejected due to non-uniformity or non-adherence of the deposition to the substrate. Of the good depositions, four were deposited at 250 V and four at 500 V. The suspension was stirred between depositions but was not re-sonified.

Film #120 was deposited one hour after sonication. It was deposited at 500 V for 80 sec. which gave a current density of 60 μA/cm^2 and yielded a deposition of 3.9 mg/cm^2.

The film was doped with lithium by re-wetting the deposition with lithium acetate solution to yield 4.3 mol. % lithium oxide. To obtain a better distribution of lead oxide in the deposition, a spray atomiser was used to spray the lead acetate solution onto the deposition. The amount of lead acetate added was determined by weight after drying of the solution, and after oxidation would yield a 10 vol. % lead oxide in the deposition. This was the highest lead addition in this set of depositions. The film was sintered at 900°C for 12 min. with a rise time of 64 min.

The resulting film was generally a light sea green in color with two irregular patches of darker green near the top and bottom edges. The uncoated edges of the substrate showed no deterioration of the platinum electrode.

Properties of Film #120 — This film showed the best uniformity and continuity of the films produced here. The top surface was sputtered with 37 2.15 mm dia. circular platinum electrodes in seven rows. All of the electrodes were good and showed a dielectric loss of less than 0.06. It was also possible to test the polarization hysteresis with a peak voltage 40 V on all of these electrodes without breakdown of the film. This indicates a very low density of pinholes and cracks in the sintered film.

Based on the weight/area of the deposition, the thickness of the film at 100 % density would be 4.9 μm. An arbitrary density of 90 % was applied, giving an estimated thickness of the film of 5.5 μm. This was used for calculating the dielectric constant and electric field figures.

The values for this film are listed in Table 5.2. The dielectric constant was measured with a 1 kHz sine wave input with a 10 mV peak voltage. This gives a maximum voltage field of 18 V/cm. Hysteresis was measured with a 15 Hz sine wave input with a 40 V peak. Hysteresis loops were symmetric and there was no difference between positive and negative polarizations or coercive fields beyond the limits of experimental error. With the film polarized by the polarization measurements the dielectric constant was re-measured. This showed an average decline of 3.5% while the dielectric loss declined from 0.038 to 0.026.

The temperature/capacitance curve showed a higher peak than the film on silver/palladium with a peak 14 times the 25°C value occurring at 374°C. The half height width is slightly lower at 93°C.

The darker areas of the film corresponded to the electroded areas with the highest capacitance and polarization. This is consistent with these areas having the highest density.

Preparation of Film #142 — This film was one of a set of ten deposited from a suspension of 3.0 g PZT in 142 g acetic acid. The film was deposited 11 hours after the suspension was first prepared and was the seventh film deposited from this suspension. The suspension was stirred while sonicating for 2 min., then allowed to settle for 7 min. prior to the beginning of deposition. The film was deposited at 250 V for 2.5 min. giving a current density of 34 μA/cm^2, and a final deposition weight of 6.6 mg/cm^2.

In an attempt to improve the distribution of the sintering additives a solution was prepared in which both lithium and excess lead could be added to the deposition by spraying. A solution of 25 wt. % lead ethylhexanoate in methyl ethyl ketone was prepared. Dry lithium acetate added to this solution did not dissolve. To dissolve the lithium acetate a few drops of methanol were added to the solution. This resulted in the immediate formation of a substantial quantity of a white precipitate. These precipitates then re-dissolved with sonication. This solution was stable for long enough to spray onto the depositions, but formed another precipitate one day later which did not redissolve.

This solution was sprayed onto the deposition in several coats that were allowed to dry between sprayings. The amount added to the deposition was controlled by weighing after each coat had dried. This procedure was not entirely successful. It appeared that later sprayings would re-dissolve the earlier coats causing migration of the lead organic to areas of higher concentration during drying.

Prior to sintering, the depositions were heated to 450°C at 1°/min. in air to burn out the organic compounds. The lead component burned to red lead oxide, giving the deposition a reddish color. This was visibly non-uniform across the deposition confirming the uneven distribution of the lead organic after spraying.

The final quantity of added lead oxide was 12 vol. % and lithium 5 mol. % of the deposition. This was determined by the weight of lead oxide after burnout and the lead/lithium ratio in the spray solution.

The film was sintered in a sealed crucible at 950°C for 5 min. with a 45 min. rise time. A temperature check ring placed underneath the crucible showed a peak temperature of 890°C, therefore the actual peak temperature experienced by the film will be between this and the 950°C measured by the furnace thermocouple.

Properties of Film #142 — Five electrodes were initially sputtered onto the film surface, and initial tests of polarization and capacitance were made. The surface was then polished with 1 μm diamond paste to remove the first electrodes. The film was then sputtered with a new set of 49 electrodes in 7 rows. 13 electrodes were bad, showing either a short circuit or a dielectric loss of more than 0.10.

Fig 5.33 below shows a polished crossection of the film with a thickness of 8.5 μm. This thickness was used for all electric field and dielectric constant calculations below. The theoretical uniform 100% dense thickness based on deposition weight is 8.3 μm. The density of the film at this point determined by graphical analysis of the SEM image is 87%.
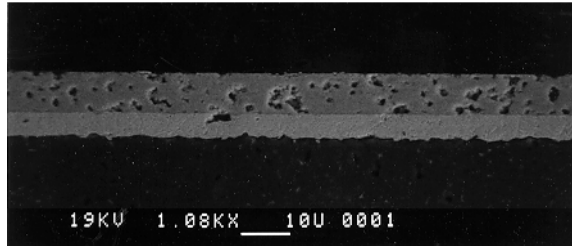
Fig. 5.33 Cut and polished crossection of PZT film. The layers from the top are: 8.5 μm PZT film; 5 μm Pt electrode; and alumina substrate.

Capacitance was measured with a sine wave input at 1 kHz with a 10 mV peak voltage. This gives a electric field of 12 V/cm. The average dielectric constant is 712 with an average loss of 0.035 and a peak dielectric constant of 800 measured at three electrodes. After the film was polarized by hysteresis measurements below, the average dielectric constant declined by 5.6% while the average loss dropped to 0.027. The changes in dielectric constant with polarization ranged from +3% to -7%.

The temperature/capacitance curve, Fig. 5.34, showed a lower peak than the film on silver/palladium with a peak 8 times the 25°C value occurring at 387°C. The half height width is also slightly lower at 110°C. The location of this peak is likely shifted to a higher temperature by the rapid rise in loss in this temperature range.
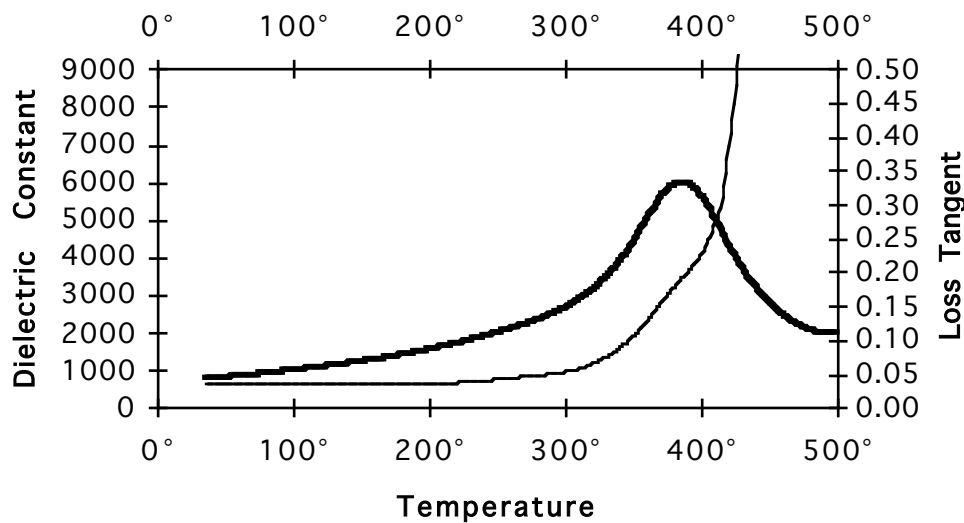
Fig. 5.34 Capacitance as a function of temperature for film #142 at 1 kHz 12 V/cm. Dielectric peak occurs at 387°C.

Polarization hysteresis was measured with a 60 Hz sine wave input with a 100 V peak voltage which results in a field of 118 kV/cm. The average remnant polarization was 28.3 μC/cm^2, with an average coercive field of 26.5 kV/cm. The highest measured was 33.6 μC/cm^2. This hysteresis loop is shown in Fig. 5.35. The hysteresis loops were symmetric with no significant or systematic differences between positive and negative polarization and coercive field. Raising the maximum voltage to 150 V, 177 kV/cm, increased the measured average remnant polarization to 30.7 μC/cm^2 and average coercive field to 29.4 kV/cm. Remnant polarization declined with cycling. Seven electrodes were taken through thirty polarization cycles with a 150 V peak. They showed an average decrease in P_r of 8.6%, with a maximum reduction of 15% and minimum of 1.1%. Three electroded areas were taken through 300 polarization cycles resulting in decreases in polarization of 13, 20, and 4.4%. This polarization fatigue was accompanied by an increase in coercive field of 9, 8, and 11%, respectively.
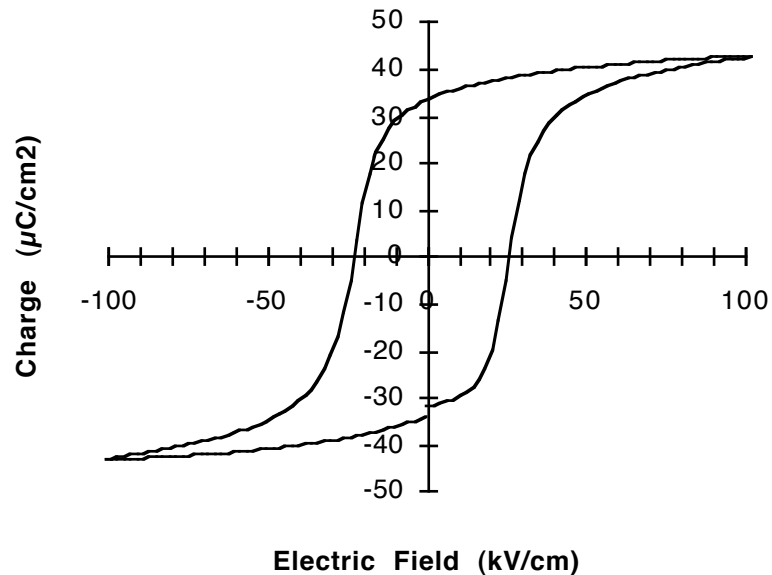
Fig. 5.35 Polarization hysteresis with P_r of 33.6 μC/cm2 and an E_c of 24 kV/cm.

The pyroelectric coefficient of 25 nC/cm^2°K at 25°C was determined by cooling and re-heating a portion of the sample over a range of ±125°C at a rate of 4°C/min. Prior to measurement the film was poled by the application of a 100V potential for one minute at room temperature. Remnant polarization measured on this portion of the sample was 30 μC/cm^2.

When attempting to measure the pyroelectric discharge of this sample it exhibited an anomalous discharge behavior similar to that seen with the film on a silver/palladium electrode above. The film was heated 425°C at 6°C/min. Between 250 and 400°C the positive current from the sample was approximately 30 times the measured remnant polarization.

Temperature (°C)
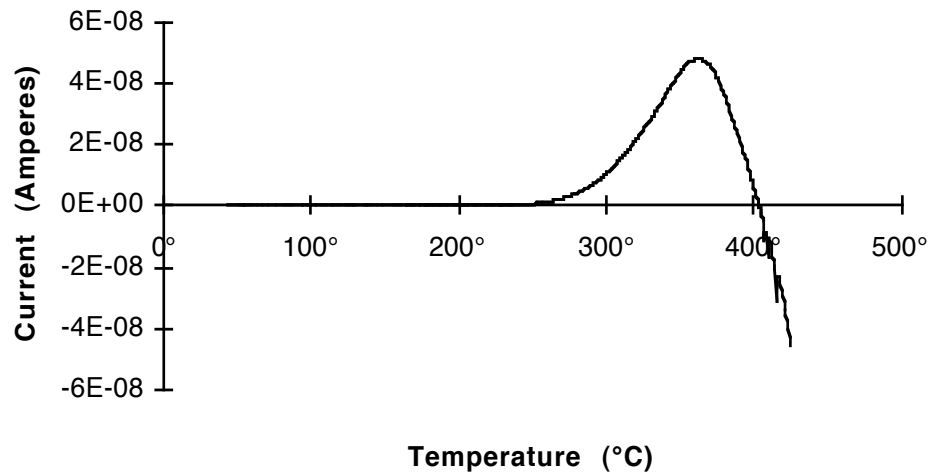
Fig. 5.36 Pyroelectric discharge.

When measuring the d_{33} coefficient of these films it is essential to eliminate bending modes in the substrate. Bending can easily generate much higher in-plane strains in a film on a substrate than are possible to produce orthogonally even with great effort. When placing the electroded substrate into a standard Berlincort meter, it is possible to generate wildly varying readings from negative to positive. Bending mode vibration of the substrate will produce a current due to the d_{31} in-plane compression of the film that will completely swamp any d_{33} current from orthogonal compression of the film.

To eliminate these bending modes a 4.14 mm disk was cut from the film and substrate with a single electrode in the center. 1.65 mm disks cut from an alumina substrate were then attached to the top and bottom of the film disk with crystal bond adhesive. When properly electroded this assembly could be mounted directly in a Berlincourt meter. Because of the low aspect ratios and flat polished surfaces of the elements of this stack bending should be minimized. Because of the small size and mass of the center disk, vibrational bending modes should be eliminated at the frequency of the Berlincourt meter. A crossection view of this stack is shown in Fig. 5.37 with aspect ratios drawn to scale.
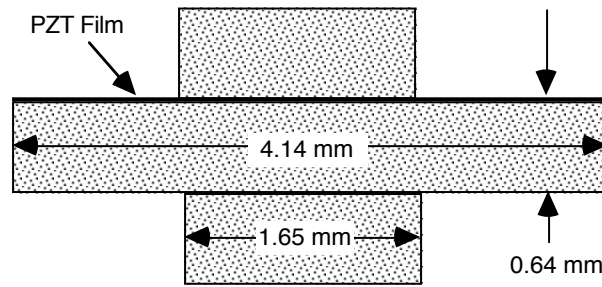
Fig. 5.37 Low aspect ratio stack to minimize bending modes in measuring d$_{33}$.

Using this assembly a series of polarizing voltages were applied to the film and the piezoelectric coefficient measured. The voltages in 10 V increments from 5 V to 75 V were applied for one minute to the film. The resulting d$_{33}$ hysteresis loop is shown in Fig. 5.38.

During poling at 55 V and above there was a measurable current which rose for the first 20 to 30 sec. and then stabilized. The current was not linearly related to voltage, appeared to be time dependent and was slightly higher when the top electrode was positively polarized. In the final polarization reversal performed on this sample, voltages of -65 and -75 V induced steady currents of -3 and -10 μA, and voltages of +55, +65 and +75 V induced currents of +2, +6 and +10 μA, respectively. Polarization hysteresis measured at this electrode prior to preparing it for the d$_{33}$ measurement was symmetric with a P$_r$ of 30 μC/cm^2 with a coercive field of 27 kV/cm. After testing, the polarization hysteresis showed a 40% difference between positive and negative coercive fields, having P$_r$'s of -25.0 and +26.2 with coercive fields of -28 and +20 kV/cm.

Coercive Field (MV/m)
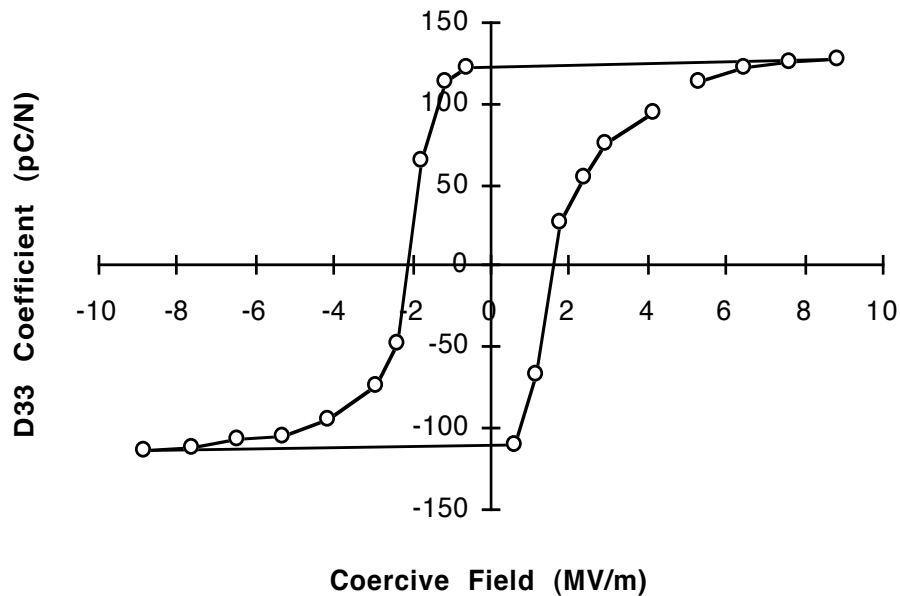
Fig. 5.38 Piezoelectric coefficient hysteresis.

Discussion — The uniformity of both the deposition and addition of sintering aids still needs to be significantly improved. Non-uniformity in deposition and drying is the likely cause of cracks and pinholes in the sintered film which caused 11 of the 49 electrodes to show a short circuit when tested. Non-uniform thickness of the deposition and distribution of sintering aids are likely causes for the relatively high standard deviation of dielectric properties of 9%.

A temperature check ring placed underneath the sintering crucible showed a significantly lower temperature than the programmed peak temperature for the furnace. In the sintering of film #120, a different furnace was programmed for 30 min. at 900°C, but an actual recording of the temperature showed a significant lag in the furnace temperature so that it was only at 900°C for 12 min. Placing a thermocouple inside the sintering crucible would significantly improve control of the sintering process.

The electrostrictive coefficient Q_{11}, calculated from eq. [5.7], is 0.043 m^4/C, which is within the predicted range in (**21**). This, along with the very simple method of measurement, supports the reasonableness of the d_{33} values.

In comparison to the film on silver/palladium, #81, this film showed a lower dielectric constant, dielectric loss, d_{33} coefficient, and dielectric temperature peak, with a higher remnant polarization and coercive field. This set of differences could be accounted for if film #142 had a slightly higher density and a significantly smaller average grain size than film #81.

There are several ways that this could occur. There are different sintering conditions, different sintering additive levels, the electrode material and deposition conditions. Film #81 was held at temperature longer than film #142 which may have allowed for more grain growth. However, previous sintering comparisons on this system showed grain size was only related to the maximum sintering temperature, and there was very little effect of sintering time up to two hours. Film #81 had twice as much lead oxide and half the lithium added for sintering than was added to film #142. Experiments have shown that lithium strongly promotes grain growth while excess lead oxide primarily aids consolidation with significantly less grain growth. Given this, the expectation would be that #81 would have a smaller average grain size than #142. The unknown component in this comparison is the electrode material. Silver/palladium has been shown to affect the sintering of PZT. Clearly, the dramatic difference in film color between the film on Ag/Pd and Pt show that there is some interaction with the Ag/Pd electrode material, however, whether this significantly affects grain size at this sintering temperature is unknown. Finally, there are the deposition conditions. Prior to deposition both suspensions were

stirred while sonicating to redisperse the PZT powder. The deposition conditions were very similar, 250 V for 90 sec. for film #81 and 300 V for 150 sec. for film #142. The key difference is the settling time between the end of stirring and the beginning of deposition. This was exactly 2 min. for film #81 and 7 min. for film #142. In both cases the sedimentation speed of 3 μm particles and larger would be higher than their electrophoretic mobility in the applied field and these particles would not be incorporated into the deposition. The difference is the extra sedimentation time would virtually eliminate any particles in the 1.5 to 2.5 μm range that might be incorporated into the deposition with a shorter sedimentation time. Given previous observations of the equilibrium grain size for lithium and lead fluxed sintering in this temperature range, the incorporation of particles in the 2 μm size range could significantly raise the average grain size in the sintered deposition.

There are a number of factors that point to some sort of electrochemical polarization of the film under high voltage. These are: the anomalous pyroelectric discharge, the non-ohmic current at high voltage fields, imprint, polarization fatigue, and the increase in coercive field with repeated polarization reversals. The presence of this anomalous pyroelectric discharge in films on both types of electrode indicates that at least one component of this effect is unrelated to interactions with the silver/palladium electrode.

The pyroelectric coefficient, p, is the change in polarization, $\boldsymbol{P}$, with temperature:

$$p = \frac{\partial \boldsymbol{P}}{\partial T} \qquad \text{Pyroelectric coefficient} \qquad [5.8]$$

The pyroelectric coefficient of the film is only 60% of that of the bulk sample, even though the polarization is 86% of the value for the bulk sample. This is counterintuitive given that the thermal expansion of the alumina substrate is much higher than that of the PZT film. The expansion of the substrate should cause a larger lateral expansion in the film that in the bulk sample. This expansion would add a piezoelectric component to the pyroelectric current. However, given the much lower permittivity of the film compared to the bulk, the average internal electric field of the film is 2.2 x that of the bulk. Based on the measured thermal coefficients of polarization and capacitance, the ratio of the thermal coefficients of internal electric field is 2.9, and the ratio of absolute change in internal field in the film compared to the bulk is 6.3. The much larger reduction in internal field in the film leads to a reduction in the electrostrictive stress on the film. This causes an expansion of the material in the polarization direction which, through the piezoelectric interaction, reduces the measured pyroelectric current.

5.4.5 Conclusions on the EPD of Complex Lead Perovskites

The conclusions in this section are broken down into three sections from most specific to most general. The first is a description of the nature of the PZT films formed so far, how they could be improved, and what resulting improvements in properties might be expected. This is followed by recommendations for how the EPD and sintering of these films could be changed to achieve these film quality improvements. Finally are general conclusions about the EPD of complex compounds.

Intermediate thickness PZT films — Because of the mismatch in thermal expansion coefficients between PZT and the alumina substrate, these films are highly compressed in the plane of the film. An unconstrained, unpoled, niobium doped PZT has an isotropic thermal contraction of less than 0.05% from the curie temperature to room temperature (≈350°C). Over the same temperature range the alumina substrate will contract by 0.29%. This imposes an excess in-plane strain on the film of -0.25%. This compression forces the ferroelectric domains to align perpendicular to the film. This mechanical domain orientation allows the relatively high polarizations achieved here. Because the domains are aligned almost entirely by the clamping of the substrate, poling does not induce any additional domain alignment and there is no significant change in the dielectric constant.

The most significant difference between these films and the bulk ceramic is the dielectric constant, with a poled dielectric constant of 1,850 for the bulk sample and film constants mostly in the 700 to 900 range. There are three primary sources for this difference, porosity, clamping of extrinsic contributions and low dielectric constant grain boundary phases. Porosity alone can only explain part of the difference. Using the dielectric mixing law, eq. [5.9] where ϕ_p is the volume fraction of randomly dispersed pores, and ε_m is the measured dielectric constant, the dielectric constant of the fully dense material, ε_d, can be calculated.

$$\varepsilon_d = \varepsilon_m \left(1 - \frac{3\phi_p}{(2 + \phi_p)}\right)^{-1} \qquad \text{Dielectric Mixing for Randomly Dispersed Pores} \quad [5.9]$$

For the bulk sample with a measured dielectric constant after poling of 1,850 and a density of 97%, the fully dense dielectric constant would be 1,930. For film #142 with a density of 86% and a measured ε of 700, ε_d, is 870, still only 45% of the bulk sample. Given the similarity of polarization, coercive field and dielectric constant maximum temperature, there is undoubtedly a large component of the film which retains the properties of the Nb-doped PZT starting material. This means that either the dielectric response of the intragranular material is suppressed by the strong lateral compression, or there is a

significant amount of very low permittivity grain boundary phase. Most likely it is some combination of the two.

To the extent that this reduction in permittivity is due to suppression of extrinsic contributions caused by clamping and compression of the film by the substrate, there is little that can be done other than to change or remove the substrate. This is discussed further below.

The issue of grain boundary phases ties in with one of the other significant differences between these films and the bulk ceramic, the relatively high conductivity of the films. There are several issues that could have a bearing on the nature of both conduction and grain boundary phases in these films. The niobium doping of the PZT is, in part, intended to compensate for A-site vacancies that occur during the high temperature sintering of the bulk ceramic and in that case yields a very low conductivity material. In contrast the films are sintered at low temperature in the presence of large amounts of excess lead oxide, which raises questions about the density of lead vacancies to be compensated. The excess lead oxide presumably aids the sintering of the film by allowing the dissolution/precipitation of titania and zirconia from small grains to larger grains. However, zirconia has a lower solubility in lead oxide than titania. This raises the possibility that grains in these films are surrounded by a double shell. The inside shell zirconia rich and the outer shell titania rich, both having much lower dielectric properties than the stoichiometric composition. Finally, there is the added lithium. Based on observed morphology changes in sintering it appears that the primary effect of lithium during sintering is to speed surface diffusion. However, whether lithium ends up concentrated in the grain boundaries or diffused throughout the sample is not known. The low oxidation-reduction potential and small size of the lithium ion does make it one of the first factors to investigate in relation to the conductivity and electrochemical polarization of the films.

The issue of grain boundary phases, conductivity, electrochemical polarization and fatigue in these films all have the potential to be addressed by changes in doping and sintering conditions. To the extent that the relatively low permittivity of these films is due to grain boundary phases, better understanding of these phases can allow them to be minimized, giving a proportionate rise in permittivity. If it is these phases which are the primary cause of the difference in dielectric constant between the film and the bulk, and not the clamping effect of the substrate, permittivities approaching that of the bulk ceramic should be possible.

With polarizations and electrostrictive coefficients similar to those of the bulk ceramic, if the permittivity of the film could also be raised to a value similar to that of the bulk, the piezoelectric and pyroelectric coefficients should follow suit. It is not unreasonable to predict piezoelectric d_{33} coefficients of 300 pC/N or higher. Because of the higher thermal expansion of the alumina substrate, pyroelectric coefficients for the film on the substrate may actually be higher than that of the bulk.

However, for many uses these films will need to be separated from the substrate. The in-plane strain in the film due to the larger thermal contraction of the substrate is -0.25%, while the residual strain in a bulk ceramic due to the alignment of domains during poling is -0.12%, perpendicular to the poling direction. This leaves an additional -0.13% strain in the clamped film. How this additional strain manifests itself in the film will have a dramatic effect on the properties of the film when it is removed from the substrate. This excess strain could result in a greater domain orientation than is possible with only electrical poling. In this case, when the film is released from the substrate, the remnant polarization may drop dramatically, possibly with a further drop in dielectric constant. This would result in a film with very poor piezoelectric properties. On the other hand, if this excess strain results primarily in elastic deformation of the film and not domain orientation beyond what would occur during poling, the release of this film could result primarily in unfreezing domain wall motion. This could result in a substantial increase in the dielectric properties without a substantial loss in polarization. In this case the released film could have properties approaching those of the bulk ceramic. Determining which of these is the actual case is one of the most immediate and interesting tasks to undertake from the rather long future work section of this thesis.

EPD and Sintering of PZT — The following are comments and suggestions further improve the reproducibility, uniformity and properties of these films

• Suspension/deposition — The possibility of depositing this material using the Ion Depletion Enhanced Electrostatic deposition method was shown in §5.4.3.2. If it is possible to do this from a colloidally and chemically stable suspension this would likely lead to a major improvement in uniformity of film thickness and homogeneity of particle packing. The electrostatic deposition method used here has no compensating mechanism for thickness variation, therefore any non-uniformities in cell geometry or convective flows will lead to thickness non-uniformities in the film. Ion depletion enhanced deposition will also consolidate the particles to almost full random packed

density prior to drying. This should lead to more uniform particle particle packing and lessened incidence of cracking during sintering.

• Electrode — Forming the bottom electrode by screen printing and polishing is both time consuming and expensive. As was shown in §5.2.4, this type of electrode could be produced by EPD and sintering. However, this two step process may only have an advantage for alloy or composite electrodes. For single metals, such as platinum, simple electrodeposition is a well known commercially available process which produces a dense electrode without further processing.

• Doping/sintering additives — The largest problem in forming these films is the uniform and accurate distribution of the sintering additives. While better spraying solutions and procedures may help this in the short run, the ultimate solution to this mixture problem will be to precipitate the desired sintering additives onto the surface of the particles prior to deposition. It is not an unreasonable goal to develop a coating which contains sintering additives and dopants, prevents dissolution of the particles and provides surface charge for stabilization and electrophoresis.

• Pyroelectric Measurements — The anomalous pyroelectric discharge in these samples is both interesting and unexplained. It is very likely that the mechanisms involved in this will be related to the mechanism of fatigue and aging in these films.

EPD of Complex Compounds — Based on the objectives outlined in the beginning of this section this demonstration has to be considered an unqualified success. When adjusted for grain size and the clamping of the substrate, the films showed a full set of properties that match properties of bulk samples prepared from the same starting powder.

5.5 Deposition of Titania

The deposition of titania is included here to demonstrate another system in which IDE deposition is achieved and to provide a graphic demonstration of the automatic leveling effect inherent in IDE deposition. There are two parts to this section. The first part is a demonstration to show that deposition of titania from this system is occurring by the IDE mechanism. The second part compares the electrostatic deposition of PZT with no inherent leveling effect with the automatic leveling effect inherent in the IDE deposition of titania.

5.5.1 Materials

TiO_2 — The titania powder used in these experiments is High Purity grade from Ishihara chemical company. The powder particles are close to equiaxed with an aspect ratio of less than 2, as shown in the accompanying photograph.
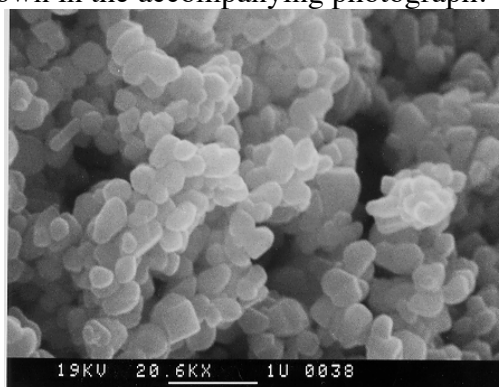
Fig. 5.39 Titania powder.

The powder was determined to be phase pure rutile by powder X-ray diffraction. The BET surface area was 7.4 m^2/g, giving an equivalent spherical diameter of 0.2μm. An average particle diameter of 0.3μm was determined by centrifugal sedimentation light scattering (Horiba CAPA-700 Particle Analyzer). The powder was washed in de-ionized water until 100g of powder mixed with 400g of de-ionized water at room temperature produced a conductivity increase of less than 0.05 μS/cm in the wash water. The powder was dried at 78°C, and equilibrated at 28°C, 30% relative humidity.

Ethanol — The suspensions were made using USP Grade Ethyl Alcohol from Pharmco Inc., Brookfield, Massachusetts, USA. Water content was determined to be 0.07 wt.% by Fisher titration.

Iodine — Iodine used was 99.8% ACS resublimed flakes. A stock solution of 0.5 wt.% iodine in ethanol was prepared and kept on the shelf for preparation of the deposition suspensions.

Substrates — Substrates used were Coors Ceramics alumina electronic thin film substrates, ADS 995 or better. These are 99.5% Al_2O_3 with a grain size of $\approx 1\ \mu$m. The substrates were electroded by sputtering with copper for three minutes followed by platinum for six minutes. The electrodes were then annealed at 850°C for ten minutes. The final thickness was 300 to 500 nm.

5.5.2 Suspension, Deposition and Sintering

The deposition conditions for the 10 micron film shown below were as follows:

Suspension — The suspension was mixed as follows: As-recieved ethanol; 0.34 vol. % TiO_2 powder; Iodine: 0.031 wt.%. The powder was dispersed using a Branson Sonifier 350 at 70% setting for four minutes while stirring. Two hours later, the suspension was re-sonified for two minutes. Final conductivity was measured as 13.5 μS/cm.

Deposition Conditions — A constant current of 0.64 mA/cm^2 was applied for 60 seconds between two electrodes spaced 2 cm apart.

Sintering — The deposited film was sintered at 1,250°C in air. The firing schedule was: heating at 10°C/min. to 1,250°C, 5 minute hold at 1,250°C, and cool down at 20°C/min.

5.5.3 Results

During the constant current deposition the voltage showed a linear voltage rise of 27V over the 60 sec. deposition time. This is shown in Fig. 5.40. The green thickness was not measured for this deposition, however, based on similar depositions the estimated green thickness is expected to be 17 to 19 μm.
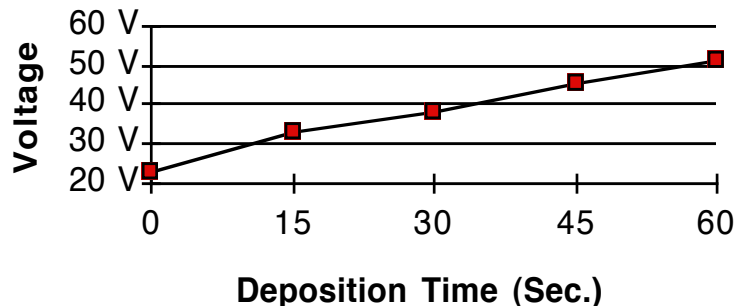
Fig. 5.40 Voltage rise during constant current deposition of titania.

Fig. 5.41 (a) shows a fracture surface crossection of the film formed by the process above. The TiO_2 grainsize is $\approx 10\mu$m. The film is highly adherent, smooth and optically transparent.

Fig. 5.41 (b) shows a fracture surface crossection of a deposition formed by the same process as above. In this case the suspension used above was allowed to stand overnight. The conductivity was elevated by approximately 30%, possibly due to metal ion contamination. This lead to a slightly lower voltage rise of 17 V over the course of the deposition at the same current density, but is otherwise identical to the deposition above. This picture is included to illustrate the uniformity of the unsintered deposition achieved using this method.

(a) (b)
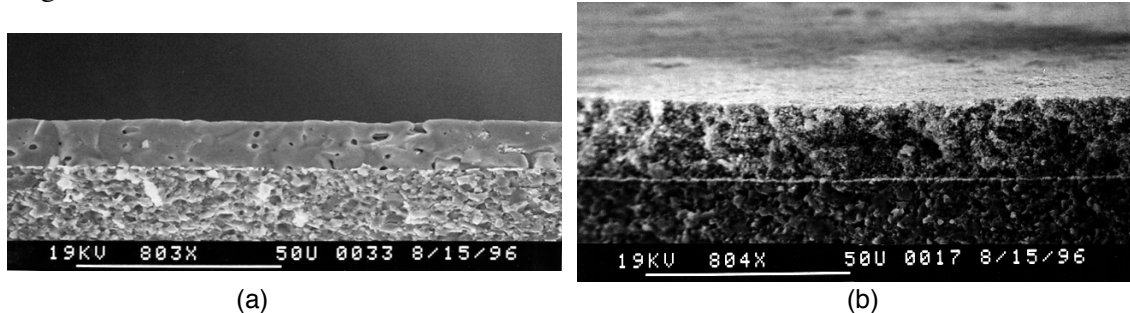
Fig. 5.41 (a) 10 μm TiO$_2$ film with no through thickness porosity on an Al$_2$O$_3$ substrate sintered @ 1,250°C. Deposition Time: 60 sec.@ 0.64mA/cm^2 (b)18 μm unfired deposition of TiO$_2$ particles on an Al$_2$O$_3$ Substrate.

5.5.4 Deposition Conclusion

The observations above can be considered proof of deposition by the ion depletion enhanced electrostatic deposition mechanism. The stability and conductivity of the suspension is improved by the addition of iodine. This is likely due to the iodine reacting in the ethanol to form iodic acid (HI) in a similar manner to what was proposed in §5.4.3.2. This acid then increases the positive surface charge on the particles in the same manner as HCl was shown to increase the surface charge on alumina in Ch. 3. With no change in the bulk suspension conductivity, the voltage rise in the system must be concentrated across the depositing layer. The voltage rise of 27 V across an 18 μm deposited layer gives an average voltage gradient across the layer of 1.5 x 10^6 V/m. This can best be accounted for by positive ions in solution being consumed at the cathode creating an ion depleted layer which is stabilized by the depositing layer of particles.

5.5.2 Deposition Comparison

To test the automatic levelling effect inherent in ion depletion enhanced deposition two depositions were made in systems having distinctly non-uniform bulk electric fields, one using simple electrostatic deposition, the second using the IDE effect.

To create the non-uniform electric field a short conductive post was attached to the center of the same flat substrates used for other depositions made above. In a uniformly

conductive medium the electric field lines will tend to concentrate on the corners of the post, as shown in Fig. 5.42. If particles simply follow these field lines they will accumulate at the corners of the conductive post.

(Note: These depositions were performed vertically upward with positive particles depositing on the cathode at the top of the cell and the post pointing down. Fig.s 5.42-5.44 are shown inverted for clarity.)
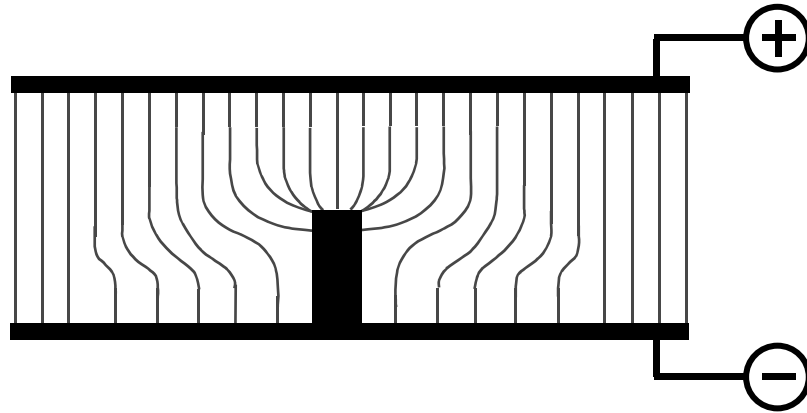
Fig. 5.42 A conductive post in an uniformly conductively medium will concentrate electric field lines at the corners of the post

A deposition of PZT on a post illustrates the non-uniform field effect on deposition in the absence of the automatic levelling effect. The post is a polymer/graphite rod attached to a substrate by a drop of epoxy. The assembly is sputtered with platinum from two angles to assure uniform conductivity over the surface of the post. The PZT powder was deposited from acetic acid as detailed in §5.4.3.4. A constant voltage of 300 V was applied with an average 2 cm electrode spacing. The resulting deposition was removed from the deposition bath and allowed to dry in air. The resulting deposition is shown in Fig. 5.43. This clearly shows the formation of a 'crown' deposition around the edges of the post. The deposition also thins along the length of the post with almost no deposition occuring around the base of the post where the electric field will be the lowest.

This 'crowning' behavior is shown to be dramatically reduced in the case of the IDE depositon of titania. In this case the post is a copper wire also attached to a substrate with epoxy and sputtered with platinum to provide an electrical connection from the surface of the substrate across the epoxy to the copper post. The exact deposition conditions were not recorded, however the titania was deposited from an ethanol/iodine suspension with an

initial voltage of ≈ 20 V which showed a linear rise during deposition. This linear voltage rise being characteristic of IDE depostion. The resulting deposition is shown in Fig. 5.44.

(a)   (b)
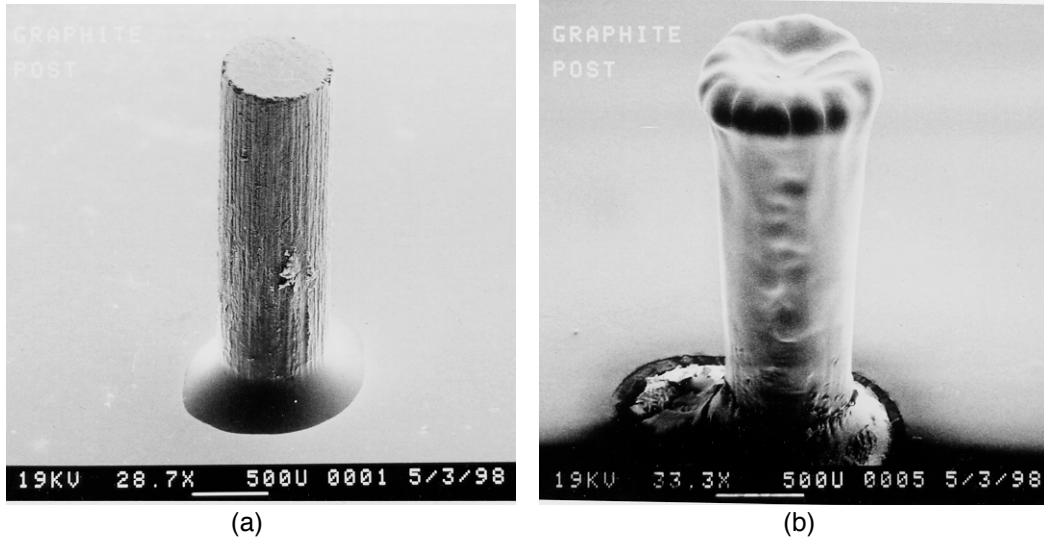
Fig. 5.43 (a) Graphite post on an alumina substrate sputter coated with platinum to provide uniform conductivity. (b) Graphite post after direct electrostatic deposition of PZT.

(a)   (b)
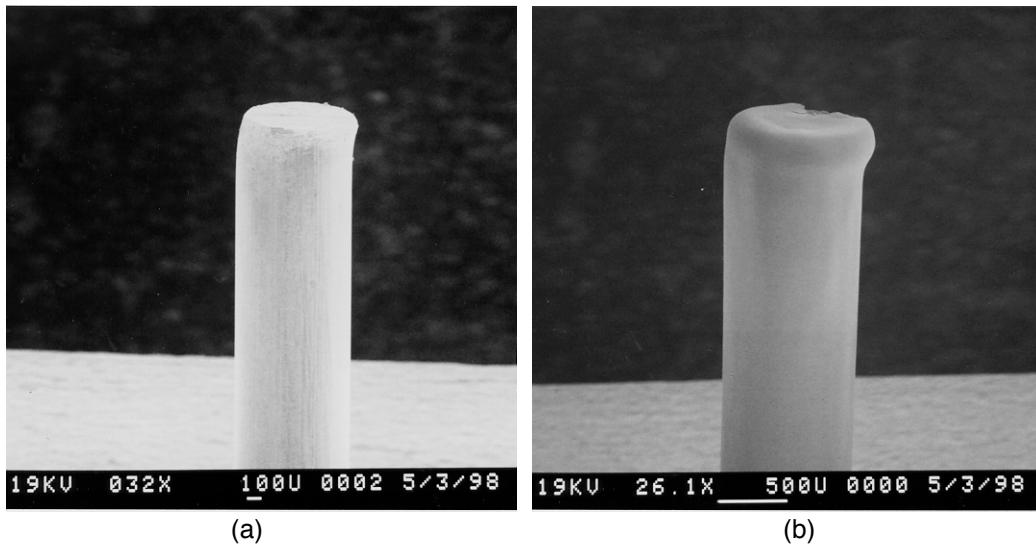
Fig. 5.44 (a) Copper post. (b) Copper post after deposition of TiO_2.

It can be seen that while there is some thickening of the deposited layer around the corners of the post, the coating is generally uniform. With a voltage gradient in the range of 1 V/μm in the deposited layer, a slight thickening of the deposition can lead to a large reduction in the voltage at the surface. This regulation of potential around a surface can compensate for very large initial inhomogeneities in the bulk electric field.

5.6 Conclusion

         In the first chapter several possible advantages for processing by EPD were listed. An important objective of this chapter has been to demonstrate some of these advantages, and what has been demonstrated is the ability of EPD to form thin layers and narrow lines of materials with controlled stoichiometry. However, there is much that can still be done in this area to present a convincing case for the industrial application of EPD.

         A second major objective of this section has been to give examples of the full process of EPD including suspension development and post deposition processing. This allows the presentation several processes that can occur during the EPD of a powder material. These effects include: gravitational convection, ramified growth of metal deposits, density gradients in a deposition, very low density of deposits of non-conductive material by the direct electrostatic deposition, and the large compaction that can occur during drying. This section also highlights the importance of post deposition processing. Either by removing the deposition from the deposition electrode or by constrained sintering of the deposition on the substrate. This full cycle of pre-deposition processing, deposition, and post-deposition processing must be managed in the presence of various ancillary effects to begin to exploit the very real advantages of EPD for specific manufacturing tasks.

Chapter 6

Opportunities for Education, Research and Development in EPD

6.1 Review

This thesis represents an attempt to organize a wide variety of observations of EPD behavior; good, bad, and non-existent. This includes the experience accumulated from observing hundreds of successful depositions as well as a much greater number of deposition attempts that failed in one way or another. Also included in this experience are many experiments in solution and suspension chemistry performed with varying degrees of success. There is neither time, space, nor in most cases any merit in analyzing here the vast majority of the experiments performed over the years leading up to this thesis. However, it was by puzzling over many seemingly illogical results, irreproducible or capriciously reproducible results, tantalizingly incomplete results reported in the literature, and no few surprises, it became clear that not only do a lot of things begin happening as soon as the deposition current is turned on, but that almost none of them can be ignored.

Ch. 1 begins with one of the simplest, but most essential, part of this thesis, which is a clear definition of what is and what is not electrophoretic deposition. EPD is defined as an electrodynamic particulate forming process which begins with a stable suspension of electrostatically charged particles. An electric field is applied to attract those particles to an electrode. At the electrode they are de-stabilized, come into contact with each other, and form a rigid deposition. Importantly, similar but unrelated processes such as electrodeposition, anodization, and electrostatic deposition are excluded.

With a clear definition of EPD, Ch. 2 then launches into an item by item analysis of the component interactions in an EPD system. A great deal of time was spent on developing the information and arguments presented here, since this requires bringing together a wide variety of information from colloidal chemistry, electrochemistry and the relatively little studied subject of electrohydrodynamics in electrochemical cells. Finally, what is left are two lists: one - of effects which can be induced at an electrode by a flowing current, and the other - of mechanisms by which particles can be stabilized in a bulk suspension. By comparing each of the near electrode effects with each of the stabilization mechanisms, a list can be prepared of what effect will cause which type of suspension to become unstable at the electrode surface, allowing particles to come into contact and form a rigid deposition. This then forms the first complete list of mechanisms of EPD and is one of the central contributions of this thesis to advancing the scientific understanding of EPD. This list is repeated below. Some of the mechanisms listed here have been

demonstrated conclusively either here or in the literature. Other mechanisms have not, as yet, been clearly demonstrated and remain hypothetical.

Table 2.4 Mechanisms of Electrophoretic Deposition

Stabilization Type	Deposition Mechanism	Examples
Kinetic/Density	Densification	R. Bagwell - BaTiO$_3$ (Unpublished)
Electrostatic	Electrostatic Force	Here - PZT, Ag/Pd
"	Electrosedimentary	Here - Alumina
"	Ion Depletion Augmented Electrostatic	Here- Alumina Sarkar and Nicholson - Alumina
"	Salting Out	Overbeek - MgO
"	Charge Reduction/ Neutralization	*Unknown*
Polymer Depletion	Squeezing Out	Bouyer & Foissy - SiC
Homopolymer	Squeezing Out	*Unknown*
Terminally Anchored at less than full coverage	Squeezing Out	*Unknown*
Block Co-Polymer at less than full coverage	Bridging Flocculation	*Unknown*
Homo-, Terminal-, or Block Polymer	Desorption of Neutral Polymer	*Unknown*
Terminal polymer, Block or Simple Polyelectrolyte	Desorption of Charged Polymer	H. Saita, (Unpublished) Polyethyleneimine (PEI)
Polyelectrolyte Electrosteric	Polymer Neutralization	PEI

Ch. 2 then concludes with a brief treatment of some of the other effects that can occur when creating an object or coating by EPD, but are not necessarily related to the deposition process. Of particular importance here are EHD convection and drying of the deposition. EHD convection can cause lumping, pitting and flaking of a deposition which may begin by developing perfectly. When a deposition is removed from the deposition bath, the capillary forces in drying will usually be at least an order of magnitude higher than the highest compaction forces in EPD. This can lead to very effective consolidation of some depositions, but cracking and curling in others.

Having developed a list of possible mechanisms of EPD, the next step is to examine one of them in detail. The mechanism chosen for this analysis is one of the most

interesting, and possibly most useful, mechanisms - Ion Depletion Enhanced Electrostatic deposition. It is clear in this type of deposition that electrochemical reactions and the migration/diffusion of ions can dramatically change the chemistry in the solvent near the deposition electrode. Since direct measurement of the effect of either solution chemistry on the particles or the particles' effect on solution chemistry is not practical in this very thin layer, a careful analysis of surface chemistry and surface charge formation was conducted for a well controlled suspension. This is detailed in Ch. 3.

Careful analysis of the data on surface adsorption and charge revealed a very surprising result. Normally when an acid is added to a suspension accompanied by an increase in the positive surface charge on the particles, it is assumed that the increase in the concentration of protonated ions in solution leads to an increased adsorption of protons to the surface, giving a higher positive surface charge. The positive ion is than referred to as being the 'potential determining ion', and the attempt is made to relate surface charge to the solution pH. However, for alumina in ethanol it turns out that the role of the proton is only indirect and the level of surface charge is determined primarily by the concentration and concentration ratio of negative ions at the surface. Surface charge initially develops as ethanol is dissociatively adsorbed at the surface, saturating negative and positive surface sites with positive and negative ions. A positive surface charge then develops due to the more rapid desorption of negative ethoxide ions from the surface. This positive charge is enhanced by the addition of hydrochloric acid. This does not occur by the increased adsorption of positive ions, but by the reduction of ethoxide ion concentration in solution and the replacement of ethoxide ions adsorbed to the surface by chloride ions. This is a radically different model for surface charge formation and regulation than is usually presented.

Although the analysis of Ch. 3 is significant for understanding the development of surface charge, there are two much simpler points which are essential to the development of the ideas presented in Ch. 4. The first is that the number of ions reversibly adsorbed to the particle surface is two orders of magnitude larger than the charge density on the surface. This makes the particles both a substantial source re-dissolvable ions and a strong buffer against ionic changes in the solution around the particles. The second is that the surface charge develops by catalytic decomposition of the solvent. This means that the particles will maintain a significant positive charge even in the complete absence of dissolved ions in the solution.

Ch. 4 then looks at deposition as a case of direct current conduction at constant current with and without the presence of particles. This first step is to show that in the

absence of convection a very high voltage gradient unbalanced charge conduction layer will develop, necessitating a very rapid and extreme rise in total voltage to maintain constant current in the cell. The fact that this sort of voltage rise is almost never seen is explained by the rapid onset of electrically driven convection in the solvent. The presence of particles is then shown to fundamentally change this near electrode behavior in several ways. In the cases of most interest here it is shown that the ionic adsorption equilibrium on the particle surfaces can stabilize the solution against convection and allows the slow growth of an unbalanced charge conduction layer. This behavior is seen as a characteristic linear voltage rise during deposition. Most importantly for EPD it creates an extreme voltage gradient layer that packs the particulate deposition to very high density regardless of how the particles are initially deposited. This compaction effect also occurs in a layer which has an inherently self leveling thickness. Deposition systems exhibiting this effect are referred to here as Ion Depletion Enhanced - Automatic Leveling deposition.

Having broadly covered the science of EPD in Ch. 2, and then done an in-depth scientific analysis of one specific EPD mechanism in Ch.s 3 & 4, Ch. 5 then turns to a technological demonstration of some of the features of EPD. These demonstrations were meant to illustrate the usefulness of EPD in: forming very thin layers and small patterns; depositing materials with a complex composition; and illustrating the difference between two mechanisms of deposition.

6.2 Opportunities

Research for this thesis, in both the lab and library, has generated a wealth of ideas for useful and productive projects that could be undertaken to further the work begun here. These opportunities are divided here into three categories. The first is educational. There has already been a great deal of excellent research and analysis done on the subject of EPD under the guise of hydrodynamics, physics, and colloid, surface, and electro- chemistry. This work needs to be brought together in a form that makes it understandable and applicable for people working with EPD. The second set of topics are scientific. This list could, in fact, be endless, but listed here are just a few topics where this thesis has uncovered particular gaps in available knowledge and understanding. Finally, there are set of technological demonstrations that could raise interest in the application of EPD for manufacturing.

6.2.1 Educational Work

A great deal of time is being wasted in laboratories around the world in repetitious replication of redundant results in randomly regulated research. This picture would be greatly improved if there were resources available that would let interested persons quickly learn and apply what is already known, so researchers can direct their efforts toward advancing understanding and technologists can apply knowledge that already exists. The following two items are represent the most immediate and effective actions that could be taken to ameliorate this situation.

Write Book — There is no book on electrophoretic deposition. Chapter. 2 presents, in brief, most of the scientific topics that are needed to understand the various processes by which EPD can occur. This chapter is a distillation of the information that this author wishes he had know before beginning this research. With further elaboration this could serve as the core of a much needed book on this subject.

Create Colloid Calculation Website — A large number of the calculations in this thesis are based on approximations having varying accuracies and ranges of validity. Analyzing the data in this thesis with even these simple formulas has represented a substantial amount of time invested in programming, analysis to assure the use of consistent units, verification and correction. Currently this work must be repeated by each research group working on these subjects. This results in many calculations not being done, inappropriate application of formulae, and simple mistakes. Creating a web site that makes accurate numerical solutions readily available to anyone working in this field would substantially improve both the productivity of researchers as well as the quality of their output.

6.2.2 Scientific Work

The scientific topics listed here fall into three categories. The first two are made up of research topics with scientific interest beyond just the topic of EPD. These fall into the categories of colloid and surface chemistry and electrode electrochemical boundary layers. The final set of topics are then more directly related to EPD. Some of these topics are direct extensions of the work done in developing this thesis, while others address specific knowledge gaps or pursue topics of particular scientific interest.

Surface Chemistry and Dispersion — In most colloid processes the objective is to disperse particles for as long as possible or to coagulate them as quickly as possible. Since in EPD the objective is to do both, a better quantitative understanding is needed of the zone between stability and coagulation/flocculation, the electrochemical changes needed to move from one state to the other, and the rates at which floccing occurs as the system moves from one state to the other. Several research suggestions for improving this understanding are listed below.

Surface Charge Development — The analysis of Chapter. 3 on surface adsorption and surface charge development for alumina in ethanol presents a significantly different model of surface charge formation than the simple pH model frequently used. The measurement techniques developed here should be applied to other materials in other solvents, most importantly, to insoluble ceramics in water. If this model of surface catalyzed autoprotolysis and competitive adsorption is valid in water as well as in ethanol/water, it could solve a significant problem in the understanding of surface charge formation. This would, for the first time, make surface potential and charge predictable by thermodynamic equilibrium calculations.

pH Measurement in Alcohols/Water — Although there is interest in using standard glass electrode pH probes to make measurements in non-aqueous solvents, there has been relatively little work done to determine the validity of these measurements, to analyze their meaning, and to develop procedures to allow them to be independently reproduced. The chart for measured pH in §3.3.6 is the first time that voltage readings from a glass electrode standardized in an aqueous buffer has been correlated to an independent measure of protonated ion activity. This is also the first measurement that has shown a linear response of a glass electrode in a basic ethanol/water solvent. This work could be extended to other alcohol/water compositions and measured against different standard aqueous reference electrodes. This should lead to the creation of tables which would allow quantitative

interpretation of pH readings in alcohol solvents in the same manner as has long been possible in water.

If the topic of surface charge above is pursued successfully for silica in water, it may also be possible for the first time to develop a theoretical and quantitative model of the functioning of a glass membrane pH probe.

Viscous Retardation of Floccing — Floccing of particles is a dynamic process that has principally been analyzed in terms of static interaction energies. As two particles approach each other fluid must squeezed out from between the particles. This means that Brownian motion is more strongly damped for motion of one particle toward another than motion in other directions. This does not provide a mechanism for stabilization, but can slow the rate of flocculation. This will be most significant for high viscosity suspensions such as in the case of depletion stabilization. Combining an analytical model for viscous damping with the static forces of depletion stabilization may lead to interesting results.

Hamaker constant of Dielectric Materials — Enough is known about the dielectric spectra of many significant dielectric materials that an accurate calculation of the Hamaker constant is possible. Developing the knowledge base necessary to routinely calculate VdW forces from fundamental properties will allow several important questions to be addressed. For example: Is it valid to use bulk dielectric data to calculate the Hamaker constant for nano-particles? What are the VdW asymmetries of asymmetric nano-particles? This is important for both particles with morphologically asymmetry, platelets or rods, as well as with asymmetric dielectric properties. This also raises the possibility of manipulating the VdW forces through the use of high refractive index solvents, particle coatings, and particle size and morphology.

Electrode Electrochemical Layers — In EPD there are two types of deposition that occur. The one that has been featured in this thesis is the particle-particle deposition which must occur to form deposition layers many particles thick. However, equally important is particle-electrode deposition. This is important both for the adhesion of thick depositions and as well as for the forming of single particle or single layer depositions. To understand this type of deposition will require understanding the complex and non-equilibrium electrochemical boundary layers on an electrode while the electrochemical reactions necessary for a current to flow are occurring.

Measure Electrode Rational Potential — The rational potential of an electrode is the potential of the electrode relative to the solvent. Most electrochemistry textbooks say that it is not possible to measure this, that electrode potential can only be measured relative to another electrode. However, while difficult, this is not impossible. Certainly, the potential across the diffuse electrostatic boundary layer is accessible through electrokinetic measurements. Dipping electrodes can give charge per unit area, and impedance measurements can determine the capacitance of the surface layer. This gives enough information to generate the total potential between the bulk metal and solvent.

Model Diffuse Layer on Conducting Electrode — Once the rational potential for an electrode surface in equilibrium with a solvent is established, the next step is to examine how the diffuse layer on the electrode changes as the electrode voltage is changed and ions are forced through the diffuse layer. The nature of the diffuse layer during conduction will determine whether there is an attraction or repulsion between particles in suspension and the electrode surface.

Surface Layer and Transfer Coefficient — One of the significant unknowns in the analysis of surface layers on electrodes during conduction is the nature of the transfer coefficient (§2.2.5). This coefficient, which frequently has a value of 1/2, is often explained using a non-thermodynamic theory involving shifting energy wells and barriers. This theory, unfortunately, has no quantitative or predictive value. Careful analysis of adsorption data in Ch. 3 also showed an unexplained coefficient of 1/2. After considerable reflection, this led to a theory which is both thermodynamic and quantitative to account for this coefficient. With accurate estimations of the ionic activity profiles through the diffuse layer at a conducting electrode from the analysis above, the author believes that a thermodynamic explanation of the meaning of the transfer coefficient based on ion activities will become clear.

Electrohydrodynamic Convection — As was shown in Ch. 4, even at moderate currents the fluid at an electrode must break into convective motion to provide sufficient ionic transport to prevent the formation of an unbalanced charge conduction layer. Analytic expressions for energy dissipation in vortex flow already exist. If expressions for the energy released by vortex flow in a conducting fluid can be derived, these can be combined to give criteria for the stability of a conducting layer without convection, the point of transition to convection, and the scale of

convection. Finite element modeling combined with experimental measurements can then be used to define zones of either stable or unstable/chaotic convection.

Deposition — There are many possible research topics that relate directly to improving the understanding of EPD. The list below merely highlights some of the most interesting of these.

Electrochemical Diffusion Modeling of Deposition Cell — This is a direct extension of the analysis of Ch. 4. Full modeling of the EPD cell will lead to a better understanding of the mechanisms by which the ion depleted layer is stabilized. This will help both to design systems to induce this ion depletion effect as well as to regulate it to control the voltage gradients developed.

Test Theories of Polymer Stabilized EPD — In Table 2.4 there are several mechanisms of deposition that are postulated but have never been proven. Experiments and analysis should be undertaken to perform EPD using these mechanisms to see if they are possible and/or potentially useful.

Combine Brownian Motion with Deposition Forces — As particles are brought together and de-stabilized by any one of the various mechanisms of EPD, the final push that brings the particles together will be provided by Brownian motion. How this final jump occurs will determine the as-deposited density and structure of the deposition. This structure, and specifically the average number of interparticle contacts, will determine the green strength and sintering behavior of the deposition.

Multi-Particle Electrohydrodynamics — How one particle approaches another will be determined by the interaction of their EHD flow fields. These interactions are also likely to affect the motion of groups of particles. (Chaining, circulation, etc.)

Calculate Forces in Electrosedimentation — As particle density rises the calculation of force has to change from a calculation on an individual particle to calculation for a continuous medium.

Complex Control Voltage Wave Forms- Particle Orientation by Di-EPD — Alternating or pulsed current/voltage offer another means for control of the electrode electrochemical boundary layer. An alternating electric field superimposed on the DC electric field used for deposition may allow the orientation of acicular or plate-like particles.

6.2.3 Engineering Demonstration

Pure science, science undertaken solely for the sake of understanding a phenomenon, is a wonderful thing. The articles that were the most helpful in developing this thesis were invariably works of pure science, written with at most vague references to

application. On the other hand, there are many, many articles that have been published on specific applications of EPD, yet very few of these are referenced here because they actually contribute very little to the understanding of the mechanisms of EPD.

However, while scientists may extol the virtues of "pure" science, the people who pay the bills will ask the perfectly reasonable question, "What good is it?" Chapter 5 begins to answer that question with demonstrations of the utility of EPD in manufacturing for microelectronics and micro-electro-mechanical systems (MEMS). This is where EPD is likely to have the greatest competitive advantage compared to other manufacturing techniques. The following engineering demonstrations are then mainly aimed at following up on these topics.

Manufacturing Tests — This is simply a continuation of the experiments begun in § 5.3. This includes forming better multilayers, including the forming and lamination of multi-component tapes incorporating vias and other through thickness components.

Binder Infiltration for Lamination — To make the particulate multilayer laminates envisioned in § 5.3 there must be some sort of binder material to allow each layer to adhere to the laminate stack and peel away from the deposition carrier. Since this binder is not incorporated in the EPD process, it needs to be demonstrated that a binder can accurately and uniformly be incorporated into a thin particulate deposition layer.

Coating of Particles to Control Colloidal and Sintering Behavior — While some materials can be interesting by themselves, devices made up a variety of materials are far more interesting and valuable. As was presented in § 5.3, EPD can be used to form devices using multiple materials. However, EPD can only move particles to a desired arrangement. To make a useful device these particles will usually need to be sintered to form a dense material. Using simple single component particles, the problem of co-sintering different materials will be compounded by the problem of developing suspensions for the EPD of different materials.

Both of these problems could be addressed at one time by developing a universal particle coating procedure. The objective would be to develop a coating with enough versatility that a range of sintering additives or fluxes could be incorporated into the coating but with a similar enough basic composition that the same type of suspension could be used for the EPD of widely different materials.

Deposition of Sinterable Polymers — There is no reason that EPD should be confined to metals and ceramics. There are polymers that can be sintered or sinter-cured at

the same temperature as nano-particulate metals such as copper and silver. Being able to co-sinter high conductivity metals with low loss polymers to form micron scale patterns without photolithography could be very attractive for electronic packaging and interconnect manufacturing.

Create Compound Colloid Crystals — Simple hexagonal close-packed colloidal crystals of mono-sized spheres have long been produced by drying, sedimentation, and, recently, by EPD (ref). If the above scientific recommendations are followed and a sufficient knowledge base is constructed, then it should be possible to mix two suspensions of mono-sized particles of different materials and deposit them together by EPD so that they form complex crystal structures.

This is the one topic listed here that is not directly related to a practical application, however, if the ability to create complex compound crystal structures is demonstrated and publicized, ideas for its potential application are likely to materialize.

6.3 Final Words

This thesis has attacked EPD on three levels. A clear definition of what is and is not EPD leads into a broad overview of the science needed to understand EPD which itself leads to a categorization of the mechanisms by which EPD can occur. A microscope is then turned onto one select mechanism This intense observation then generates unexpected conclusions about the interactions between the particles and the solvent, and between the particles and the electrochemical boundary layer at the deposition electrode. Finally, EPD is looked at on a practical level, with several demonstrations of how EPD can be applied to real manufacturing problems in microelectronics.

Each and every chapter of this thesis has presented either novel ideas, novel juxtapositions of old ideas, or some combination of the two. This thesis is only the first step in presenting these ideas to a wider audience. Some of these concepts may be useful and gain wide acceptance, others may be quickly forgotten. Only the passage of time will determine the ultimate value of the ideas elaborated here.

Appendix A

Fuoss Onsager Conductance Equation

The Fuoss-Onsager conductance equation is the summation of all of the effects on spherical ions moving by electrophoresis in an applied electric field. These effects are:

Electrophoresis — An ion will move in one direction due the applied electric field, but this motion will be retarded by the viscous force of oppositely charged ions moving in the opposite direction.

Dielectric Relaxation — The application of an electric field will cause positive and negative ions to move relative to one another, creating a polarization which reduces the effective electric field in solution.

Osmotic Pressure — Polarization of an ion relative to the counter ions around it will change the distribution of osmotic pressure experienced by that ion.

Viscosity — Oppositely charged ions will strike each other more often than would occur by random motion of uncharged ions. This leads to an increase in the effective viscosity experienced by an ion.

The Fuoss-Onsager equation gets its particular form the integration of the first three terms of the power series expansion of the Boltzman factor e^{ξ}. This leads to a form $const. - \ln(x) + x + ...$ The terms in $c^{\frac{1}{2}}$ are a result of the analysis of relaxation and electrophoresis.

The analysis of completely dissociated electrolytes in high dielectric constant solvents yielded the 1955 Fuoss-Onsager equation (**1**):

$$\Lambda = \Lambda_o - Sc^{\frac{1}{2}} + Ec\ln(_1c) + J(a)c$$

The variables in this equation are Λ_o, the molar limit conductivity, c, the ionic concentration, and a, the radius of closest approach of the ion pair. *S*, *E*, and *J* are all determined by fundamental constants along with the solvent viscosity and dielectric constant.

In 1965 Fuoss, Onsager and Skinner (**2**) made a full theoretical treatment to extend the formula to solutions of ionogens which are not fully dissociated into ions and low dielectric constant solutions where ions can associate into non-conducting pairs by electrostatic attraction. The primary additional term in this equation is γ, the fraction of dissociated ions. This is related to the association constant K_A by the mass action equation: $1 - \gamma = K_A c \gamma^2 f^2 \Lambda$. This then gives the form of the equation used in this thesis:

$$\Lambda = \Lambda_o - S(c\gamma)^{\frac{1}{2}} + E'c\gamma\ln(6E_1'c\gamma) + Lc\gamma - K_A c\gamma f^2 \Lambda$$

Following is a presentation of the components of this equation as presented in (**2**). The use of this formula is then illustrated by the analysis of conductivity measurements made for HCl in 99.43% ethanol used in Ch. 3.

Molar Limit Conductivity Λ_o

This is the theoretical molar conductivity of the electrolyte at infinite dilution.

Onsager Limit Slope $-S(c\gamma)^{\frac{1}{2}}$

This is the tangent slope of the molar conductivity function at zero concentration.

$S = \alpha\Lambda_o + \beta$

$$\alpha = \frac{8.204 \times 10^5}{(\varepsilon_r T)^{\frac{2}{3}}} \qquad \beta = \frac{82.5}{\eta(\varepsilon_r T)^{\frac{1}{3}}}$$

Third Order Terms $E'c\gamma \ln(6E_1' c\gamma)$

$$E' = E_1'\Lambda_o - E_2'$$

$$E_1' = \frac{2.942 \times 10^{12}}{(\varepsilon_r T)^3} \qquad E_2' = \frac{0.433 \times 10^8}{\eta(\varepsilon_r T)^2}$$

Fourth order terms $Lc\gamma$

$$L = L_1 + L_2(b)$$

$$L_1 = 3.202 E_1'\Lambda_0 - 3.420 E_2' + \alpha\beta$$

$$L_2(b) = 2E_1'\Lambda_0 h(b) + 44 E_2'/3b - 2E'\ln(b)$$

$$h(b) = \frac{2b^2 + 2b - 1}{b^3}$$

$$ab = \frac{1.671 \times 10^{-3} \dfrac{esu^2 \cdot cm \cdot {}^\circ K}{erg}}{\varepsilon_r T} \qquad \text{Bjerrum parameter} \quad b \frac{esu^2}{erg} = \frac{e^2}{a\varepsilon_r kT}$$

Adjustment for Ionic Association $-K_A c\gamma f^2 \Lambda$

$$f_\pm = \exp\left[\frac{-\kappa e^2}{8\pi\varepsilon_o\varepsilon_r kT(1 + \kappa a_o)}\right] \quad \text{Ionic activity correction factor.}$$

$$\kappa = \left[\frac{2e^2 cz^2}{\varepsilon_o\varepsilon_r kT}\right]^{\frac{1}{2}} \quad \text{Debye parameter.}$$

Variables

Fuoss and Onsager consolidated many constants into single numbers in their listing of formulas in (**2**). Unfortunately, even though these numbers are not unitless, they did not include units for these numbers. This makes the use of these formulas less than intuitive for the first time user. To help clarify this, the units that need to be used for the variables in this equation are listed here, based on information from the book by Fuoss and Accascina (**3**).

T	Temperature in °K
η	Viscosity in Poise (0.1 N•s/m^2)
Λ_o	Molar Limit Conductivity μS•Liter/Mol•cm
a	Radius of closest approach in Centimeters
e	Unit Charge 4.802x10^{-10} esu
c	Ionic Concentration in Moles/Liter

Example

Fig. A.1 below shows calibration data for the conductivity of HCl in ethanol with 0.57 wt.% water collected during the preparation of Ch. 3. Superimposed on the data points is a plot of the Fuoss and Onsager 1965 equation calculated using the data below. Plus and minus 1% boundary lines show the measurement accuracy as compared to theory.

η	0.01101 Poise
ε_r	24.3
Λ_o	52.4 μS•Liter/Mol•cm
a	3.58x10^{-8} cm
K_A	Unit Charge 4.802x10^{-10} esu
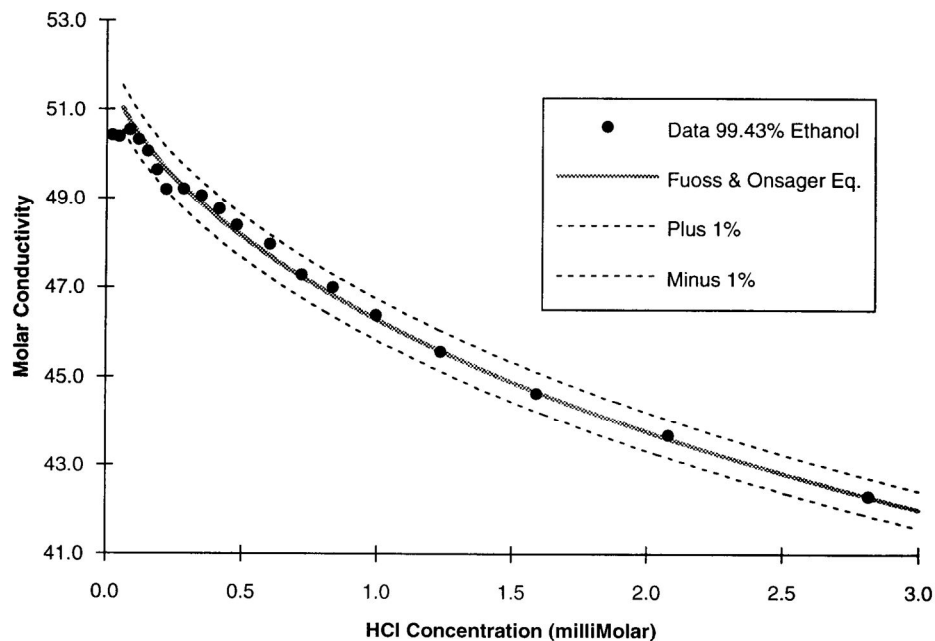
Fig. A.1 Fuoss-Onsager conductivity equation fit to data for the molar conductivity of HCl in 99.43 wt. % ethanol.

Appendix B

Determining potential in the quasi-equilibrium moving gradient layer.

This begins with the formula for total ion flux at any point and for the flux of chloride ions at any point in the gradient layer.

$$J = \left(D_{Cl^-} - D_{H^+}\right)\frac{\partial c}{\partial x} - \left(v_{Cl^-} + v_{H^+}\right)c\frac{\partial \phi}{\partial x} \qquad [4.10]$$

$$\frac{v_{Cl^-}}{v_{Cl^-} + v_{H^+}}J\frac{c}{c_o} = D_{Cl^-}\frac{\partial c}{\partial x} - v_{Cl^-}c\frac{\partial \phi}{\partial x} \qquad [4.11]$$

These were used in Ch. 4 to determine the following value for the concentration as a function of position in the gradient layer:

$$c = c_o - c_o \exp\left[\frac{J}{2c_oD_{H^+}}x\right] \qquad [4.18]$$

The first step in solving these equations for the potential gradient is to multiply

Eq. 4.21 by $\dfrac{\left(D_{Cl^-} - D_{H^+}\right)}{D_{Cl^-}}$ to give:

$$\frac{\left(D_{Cl^-} - D_{H^+}\right)}{D_{Cl^-}}\frac{v_{Cl^-}}{\left(v_{Cl^-} + v_{H^+}\right)}J\frac{c}{c_o} = \left(D_{Cl^-} - D_{H^+}\right)\frac{\partial c}{\partial x} - \frac{\left(D_{Cl^-} - D_{H^+}\right)}{D_{Cl^-}}v_{Cl^-}c\frac{\partial \phi}{\partial x} \qquad [B.1]$$

This is then subtracted from Eq. 4.20:

$$\left[1 - \frac{v_{Cl^-}}{D_{Cl^-}}\left(\frac{D_{Cl^-} - D_{H^+}}{v_{Cl^-} + v_{H^+}}\right)\frac{c}{c_o}\right]J = \left[\frac{\left(D_{Cl^-} - D_{H^+}\right)}{D_{Cl^-}}v_{Cl^-} - \left(v_{Cl^-} + v_{H^+}\right)\right]c\frac{\partial \phi}{\partial x} \qquad [B.2]$$

The first diffusion/migration coefficient in the above equation can be simplified:

$$\frac{v_{Cl^-}}{D_{Cl^-}}\left(\frac{D_{Cl^-} - D_{H^+}}{v_{Cl^-} + v_{H^+}}\right) = \frac{v_{Cl^-} - \frac{v_{Cl^-}}{D_{Cl^-}}D_{H^+}}{v_{Cl^-} + v_{H^+}} = \frac{v_{Cl^-} - v_{H^+}}{v_{Cl^-} + v_{H^+}}$$

The second diffusion/migration coefficient term in square brackets in Eq. B.2 can also be simplified:

$$\frac{\left(D_{Cl^-} - D_{H^+}\right)}{D_{Cl^-}}v_{Cl^-} - \left(v_{Cl^-} + v_{H^+}\right) = v_{Cl^-} - \frac{v_{Cl^-}}{D_{Cl^-}}D_{H^+} - v_{Cl^-} - v_{H^+} = -2v_{H^+}$$

These can be substituted back into Eq. B.2 to give:

$$\left[1 - \frac{v_{Cl^-} - v_{H^+}}{v_{Cl^-} + v_{H^+}}\frac{c}{c_o}\right]J = -2v_{H^+}c\frac{\partial \phi}{\partial x} \qquad [B.4]$$

Re-arranging gives:

$$\frac{\partial \phi}{\partial x} = \frac{J}{-2v_{H^+}c}\left[1 - \frac{v_{Cl^-} - v_{H^+}}{v_{Cl^-} + v_{H^+}}\frac{c}{c_o}\right] = \frac{-J}{2v_{H^+}c_o}\left[\frac{c_o}{c} - \frac{v_{Cl^-} - v_{H^+}}{v_{Cl^-} + v_{H^+}}\right] \qquad \text{[B.5]}$$

Substituting in the previously determined value for c then gives the electric field as:

$$\frac{\partial \phi}{\partial x} = \frac{-J}{2c_o v_{H^+}}\left[\left(1 - \exp\left[\frac{J}{2c_o D_{H^+}}x\right]\right)^{-1} - \left(\frac{v_{Cl^-} - v_{H^+}}{v_{Cl^-} + v_{H^+}}\right)\right] \qquad \text{[B.6]}$$

Noting that the expression $-\left(\dfrac{v_{Cl^-} - v_{H^+}}{v_{Cl^-} + v_{H^+}}\right)$ can also be written as $\dfrac{2v_{H^+}}{v_{Cl^-} + v_{H^+}} - 1$, it is possible

to separate Eq. B.6 into two terms:

$$\frac{\partial \phi}{\partial x} = \frac{-J}{c_o\left(v_{Cl^-} + v_{H^+}\right)} + \frac{-J}{2c_o v_{H^+}}\left[\left(1 - \exp\left[\frac{J}{2c_o D_{H^+}}x\right]\right)^{-1} - 1\right] \qquad \text{[B.7]}$$

This shows clearly that for large negative values of x the electric field will approach a constant number which is equal to the current flux divided by the conductivity of the solution, while the field rapidly approaches $-\infty$ as $x \to 0$.

The electric field gradient can then be expressed using the chain rule as:

$$\frac{\partial^2 \phi}{\partial x^2} = \frac{\partial}{\partial c}\left[\frac{-J}{c_o\left(v_{Cl^-} + v_{H^+}\right)} + \frac{-J}{2c_o v_{H^+}}\left[\frac{c_o}{c} - 1\right]\right]\frac{\partial c}{\partial x} \qquad \text{[B.8]}$$

Taking the derivative with respect to c :

$$\frac{\partial^2 \phi}{\partial x^2} = \frac{J}{2v_{H^+}}\left(\frac{1}{c^2}\right)\frac{\partial c}{\partial x} \qquad \text{[B.9]}$$

The derivative of c as a function of x is then:

$$\frac{\partial c}{\partial x} = \frac{\partial}{\partial x}\left[c_o - c_o \exp\left[\frac{J}{2c_o D_{H^+}}x\right]\right] = -\frac{J}{2D_{H^+}}\exp\left[\frac{J}{2c_o D_{H^+}}x\right] \qquad \text{[B.10]}$$

Substuting this back into Eq. B.9 gives:

$$\frac{\partial^2 \phi}{\partial x^2} = \frac{J^2}{4D_{H^+}v_{H^+}\left(c_o - c_o \exp\left[-\frac{J}{2c_o D_{H^+}}x\right]\right)^2}\exp\left[-\frac{J}{2c_o D_{H^+}}x\right] \qquad \text{[B.11]}$$

A slight re-arrangement yields the final form of the equation:

$$\frac{\partial^2 \phi}{\partial x^2} = -\left(\frac{J}{c_o}\right)^2 \frac{\exp\left[-\frac{J}{2c_o D_{H^+}}x\right]}{4D_{H^+}v_{H^+}\left(1 - \exp\left[-\frac{J}{2c_o D_{H^+}}x\right]\right)^2} \qquad \text{[B.12]}$$

The value of the potential as a function of position can then be determined by integrating Eq. B.7 :

$$\partial\phi = \left[\frac{-J}{c_o\left(v_{Cl^-}+v_{H^+}\right)} + \frac{-J}{2c_ov_{H^+}}\left[\left(1-\exp\left[\frac{J}{2c_oD_{H^+}}x\right]\right)^{-1}-1\right]\right]\partial x \qquad [B.7]$$

Using the following formula for the integration of the inverse exponential term:

$$\int\frac{dx}{1-\exp[kx]} = x - \frac{1}{k}\ln\left(1-\exp[kx]\right) \qquad [B.13]$$

gives an expression for the potential across the cell to the edge of the gradient layer;

$$\phi = \frac{-J}{2c_ov_{H^+}}\left[x - \frac{2c_oD_{H^+}}{J}\ln\left(1-\exp\left[\frac{J}{2c_oD_{H^+}}x\right]\right)-\left(\frac{v_{Cl^-}-v_{H^+}}{v_{Cl^-}+v_{H^+}}\right)x\right]+\phi_o \qquad [B.14]$$

By consolidating terms this becomes:

$$\phi = \frac{-J}{2c_ov_{H^+}}x\left[1-\left(\frac{v_{Cl^-}-v_{H^+}}{v_{Cl^-}+v_{H^+}}\right)\right]+\frac{D_{H^+}}{v_{H^+}}\ln\left(1-\exp\left[\frac{J}{2c_oD_{H^+}}x\right]\right)+\phi_o \qquad [B.15]$$

Using the Einstein relation for the ratio between difusion and migration (Eq. 4.3) brings this to the final expression:

$$\phi = -\frac{J}{c_o\left(v_{Cl^-}+v_{H^+}\right)}x+\frac{RT}{F}\ln\left(1-\exp\left[\frac{J}{2c_oD_{H^+}}x\right]\right)+\phi_o \qquad [B.16]$$

Here it becomes obvious that the first term is the linear voltage gradient driving conduction in the bulk solution with the second term being the additional voltage gradient necessary to drive the same ionic flux in the gradient region.

References

Chapter 1

1. Trau, M., Saville, D.A. and Aksay, I.A., "Assembly of Colloidal Crystals at Electrode Interfaces", *Langmuir,* **13** (1997) 6375-6381

2. Böhmer, M., "In Situ Observation of 2-Dimensional Clustering during Electrophoretic Deposition", *Langmuir*, **12**[24] (1996) 5747-5750

3. Olenick, J.A., Joseph, W. and Hoffman, Hans, "Electrophoretic Enameling-An Area of Steady Advancement",4-290

4. Rogach, A.L., Kotov, N.A., Koktysh, D.S., Ostrander J.W., and Ragoisha, G.A., "Electrophoretic deposition of latex-based 3D colloidal photonic crystals: A technique for rapid production of high-quality opals", *Chemistry of Materials*,**12** [9] (2000) 2721-2726

5. Andrews, J.M., Collins, A.H., Cornish, D.C., and Drecass, J., "The forming of ceramic bodies by electrophoretic deposition", *Proc. Br. Ceram. Soc.*, **12** (1969) 211-29

6. Powers, R.W., "The Electrophoretic Forming of Beta-Alumina Ceramic", *J. Electrochemical Soc.*, Vol. 122, No. 4 (1975) 490-500

7. Dini, J.W., *Electrodeposition: The Materials Science of Coatings and Substrates,* Noyes Publications, Park Ridge, New Jersey, 1993

8. Beck, Fritz, "Fundamental Aspects of Electrodeposition of Paint", *Progress in Organic Coatings,* **4** (1976) 1-60

9. Wu, Souheng, "Electrostatic Charging and Deposition of Powder Coatings", *Polym.-Plast. Tecnol. Eng.*, **7**[2] (1976) 119-220

10. Giersig, M. and Mulvaney, P., "Formation of Ordered Two-Dimensional Gold Colloid Lattices by Electrophoretic Deposition", *J. Phys. Chem.*, **97** (1993) 6334-6336

11. Ryan, W., Massoud, E., and Perera, C.T.S.B., "Electrophoretic Deposition Could Speed Up Ceramic Casting", *Interceram*, **2** (1979) 117-119.

12. Sarkar, P. and Nicholson, P. S., "Electrophoretic Deposition (EPD): Mechanisms, Kinetics, and Application to Ceramics", *J. Am. Ceram. Soc.*, **79**(8) (1996) 1987

13. Gani, M.S.J., "Electrophortic Deposition - A Review", *Industrial Ceramics*, **14**(4)(1994) 163-174

14. Boccaccini, A. and Zhitomirsky, I., *Current Opinion in Solid State and Materials Science*, **6** (2002) 251

15. Hunter, R. J., *Zeta Potential in Colloid Science, Principles and Applications*, Academic Press, New York, 1981

16. Solomentsev, Y., Guelcher, S.A., Bevan, M., and Anderson, J.L., "Aggregation Dynamics for Two Particles during Electrophoretic Deposition under Steady Fields", *Langmuir,* **16** (2000), 9208-9216

Chapter 2

1. Russel, W.B., Saville, D.A. and Schowalter, W.R. , *Colloidal Dispersions,* Cambridge University Press, Cambridge, (1989)

2. Hunter, R. J., *Zeta Potential in Colloid Science, Principles and Applications*, Academic Press, New York, (1981)

3. Israelachvilli, J.N., *Intermolecular and Surface Forces*, Academic Press, New York (1992)

4. Heisinger, Karl, "Molecular Dynamics of Water at Interfaces", in *Structure of Electrified Interfaces* (eds. Lipkovski, Jacek and Ross, P.N.) VCH Publishers, New York (1993) 239-276

5. Frumkin, A.N., "2. Hydrogen Overvoltage and Adsorption Phenomena: Part I. Mercury", In *Advances in Electrochemistry and Electrochemical Engineering,* Vol. 1 (ed. Delahay, Paul) Interscience, New York (1961) 65-138

6. Newmann, John S., *Electrochemical Systems*, 2nd Ed. Prentice Hall, Englewood Cliffs, NJ, (1991)

7. Wang, Joseph, *Analytical electrochemistry*, 2nd ed.,Wiley, New York , (2000).

8. Hogg, R., Healy, T.W. and Fuerstenau, "Mutual Coagulation of Colloidal Dispersions", *Far. Soc. Trans*. **62**, (1966) 1638-1651

9. Levich, Veniamin G., *Physicochemical Hydrodynamics*, Prentice-Hall, Englewood Cliffs, NJ (1962)

10. Chazviel, J.-N., "Electrochemical Aspects of the Generation of Ramified Metallic Electrodeposits", *Phys. Rev. A,* **42**[12], (1990) 7355-7367

11. Van Tassel, J. and Randall, C.A., "Surface Chemistry and Surface Charge Formation for an Alumina Powder in Ethanol with the Addition of HCl and KOH", *J. Colloid and Interface Sci*., **241** (2001) 302-316

12. Hooton, John A. and Merz, Walter J., "Etch Patterns and Ferroelectric Domains in BaTiO3 Single Crystals", *Phys. Rev*., **98**[2], (1955) 409-413

13. Smoluchowsky, M. von, "Contribution à la théorie de l'endosmose électrique at de quelques phenomènes corrélatifs", Bulletin International de l'Académie des Sciences de Cracovie, 8 (1903) 182-200

14. Henry, D.C., "Cataphoresis of Suspended Particles", *Proc. Roy. Soc. A*. **133,** (1931) 106-129

15. O'Brien, R. W., and White, L. R., "Electrophoretic Mobility of a Spherical Colloidal Particle", *J. Chem. Soc. Faraday II*, **74,** (1978) 1607

16. Auzerais, F.M., Jackson, R., and Russel, W.B., "The Resolution of Shocks and the Effects of Compressible Sediments in Transient Settling", *J. Fluid Mech., */ **195** (1988) 437-462

17. Napper, D. H., *Polymeric Stabilization of Colloiday Suspensions,* Academic Press, London (1983)

18. Weitz, D.A. and Huang, J.S., Self-similar structures and the kinetics of aggregation of gold colloids. In *Kinetics of Aggregation and Gelation* (eds. Family, p. and Landau, D.P.), Elsevier 1984

19. Smoluchowski, M. von, "Versuch einer mathematischen Theorie der Koagulationskinetik kolloider Lösungen", *Z. Phys. Chem.* **92**, 129-68 (1917)

20. Glendinning, A.B. and Russel, W.B., "The Electrostatic Repulsion between Charged Spheres from Exact Solutions to the Linearized Poisson-Boltzmann Equation", *J. Colliod and Interface Sci.*, **93** [1], (1983) 95-104

21. Feigin, R.I. and Napper, D.H., "Depletion Stabilization and Depletion Flocculation", *J. Colloid and Interface Sci.*, **75** (2), 525-42 (1980)

22. Solomentsev, Y., Böhmer,M. and Anderson, J.L., "Particle Clustering and Pattern Formation during Electrophoretic Deposition: A Hydrodynamic Model", *Langmuir,* **13** (1997) 6058-6068

23. Solomentsev, Y., Guelcher, S.A., Bevan, M., and Anderson, J.L., "Aggregation Dynamics for Two Particles during Electrophoretic Deposition under Steady Fields", *Langmuir,* **16** (2000), 9208-9216

24. Verwey, E.J.W. and Overbeek, J.Th.G., *Theory of the Stability of Lyophobic Colloids,* Elsevier Publishing Company, New York (1948)

25. Hamaker, H.C., and Verwey, E.J.W., "The Role of the Forces Between the Particles in Electrodeposition and Other Phenomena", *Trans. Faraday Soc.*, **36,** (1940) 180-185

26. Bouyer, F. and Foissy, A., "Electrophoretic Deposition of Silicon Carbide", *J. Am. Ceram. Soc.*, **82**[8], (1999) 2001-10

27. Koelmans, H. and Overbeek, J.Th.G., "Stability and Electrophoretic Deposition of Suspensions in Non-Aqueous Media", *Disc. Faraday Soc.*, **18** (1954) 52-63

28. Buscall, R., and White, L.R., "The Consolidation of Concentrated Suspensions, Part 1. The Theory of Sedimentation", *J. Chem. Soc., Faraday Trans. 1*, **83** (1987) 873-891

29. Bordia, R.K. and Jagota, A., "Crack Growth and Damage in Constrained Sintering Films", J. Am. Ceram. Soc., 76[10], (1993) 2475-2485

30. Hackley, V. A., and Ferraris, C.F., *The Use of Nomenclature in Dispersion Science and Technology*, NIST Recommended Practice Guide, Special Publication 960-3, U.S. Goverment Printing Office, Washington, D.C., August 2001

31. Healy, T.W., and White, L.R., "Ionizable surface Group Models of Aqueous Interfaces", *Adv. Colloid and Interface Sci.*, **9** (1978) 303-345

32. Scherer, G.W., "Theory of Drying", *J. Am. Ceram. Soc.*, **73**[1] (1990) 3-14

33. Scherer, G.W., "Physics of Drying", in *Ceramic Powder Science III,* Eds.: Messing, G.L., and Hirano, S., American Ceramic Society, Westerville, Ohio (1990)

Chapter 3

1. Hamaker, H.C., and Verwey, E.J.W., "The Role of the Forces Between the Particles in Electrodeposition and Other Phenomena", *Trans. Faraday Soc.*, **36,** (1940) 180-185

2. H. Koelmans, and J.Th.G. Overbeek, "Stability and Electrophoretic Deposition of Suspensions in Non-Aqueous Media", *Disc. Faraday Soc.*, **18** (1954) 52-63

3. Malkin, E.S., and Dukhin, A.S., "Deposition of Colloidal Particles on an Electrode in an Alternating Electric Field", *Kolloid. Zh.*, **42,** (1980) 396

4. Sarkar, P., and Nicholson, P. S., "Electrophoretic Deposition (EPD): Mechanisms, Kinetics, and Application to Ceramics", *J. Am. Ceram. Soc.*, **79,** (1996) 1987-2002

5. Parks, G. A., *Chem. Rev.*, "The Isoelectric Points of Solid Oxides, Solid hydroxides, and Aqueous Hydroxo Complex Systems", **65,** (1965) 177-198

6. Romo, L. A., "Effect of C3, C4 and C5 Alcohols and Water on the Stability of Dispersions with Alumina and Aluminum Hydroxide", *Discuss. Faraday Soc.* **42,** (1966) 232-237

7. Lind, J.E. Jr., Zwolenik, J. J., and Fuoss, R. M., "Calibration of Conductance Cells at 25° with Aqueous Solutions of Potassium Chloride", *J. Am. Chem. Soc.* **81,** (1959) 1557-1559

8. Graham, J. R., Kell, G. S., and Gordon, A. R., "Equivalent and Ionic Conductances for Lithium, Sodium and Potassium Chlorides in Anhydrous Ethanol at 25°", *J. Am. Chem. Soc.*, **79,** (1957) 2352

9. Kay, R. L., "An Application of the Fuoss-Onsager Conductance Theory to the Alkali Halides in Several Solvents", *J. Am. Chem. Soc.*, **82,** (1960) 2099-2105

10. De Lisi, R., Goffredi, M., and Liveri, V. T., "Effect of Water on Proton Migration in Alcoholic Solvents, Part 4.—Conductance of Hydrogen Chloride in Butan-2-ol and in Ethanol at 25°C", *J. C. S. Faraday I*, **72,** (1976) 436-447

11. Fuoss, R. M., Onsager, L., and Skinner, J. F., "The Conductance of Symmetrical Electrolytes. V. The Conductance Equation", *J. Phys. Chem.*, **69,** (1965) 2581-2594

12. O'Brien, R. W., and White, L. R., "Electrophoretic Mobility of a Spherical Colloidal Particle", *J. Chem. Soc. Faraday II*, **74,** (1978) 1607

13. Dukhin, A.S., Goetz, P.J., Wines, T.H., and Somasundaran, P., "Acoustic and Electroacoustic Spectroscopy", *Colloids and Surfaces A*, **173,** (2000) 127-158

14. Sawatzky, R. P., and Babchin, A. J., "Hydrodynamics of Electrophoretic Motion in an Alternating Electric Field", *J. Fluid Mech.*, **246,** (1993) 321-334

15. Henry, D. C., "Cataphoresis of Suspended Particles", *Proc. Roy. Soc. Lond. A,* **133,** (1931) 106

16. Loeb, A. L., Overbeek, J. Th. G., and Wiersma, P. H., *The Electrical Double Layer Around a Spherical Colloidal Particle*. MIT Press: Cambridge, Massachusetts, 1961

17. O. Popovych, and R.P.T. Tomkins, *Nonaqueous Solution Chemistry*. Wiley Interscience Publications, New York, 1981

18. Caldin, E. F., and Long, G., "The Equilibrium between Ethoxide and Hydroxide Ions in Ethanol and in Ethanol Water Mixtures", *J. Chem. Soc.*, 3737 (1954)

19. Hunter, R. J., *Zeta Potential in Colloid Science, Principles and Applications*, Academic Press, New York, 1981

20. Isrealachvilli, J., *Intermolecular and Surface Forces, 2nd Edition*, Academic Press, New York 1992

Chapter 4

1. Sarkar, P., Huang, X. and Nicholson, P.S., "Electrophoretic Deposition and Its use to Synthesize YSZ/Al2O3 Micro-Laminate Ceramic/Ceramic Composites", *Ceram. Eng. Sci. Proc.*, **14** (1993) 707-726

2. Graham, J. R., Kell, G. S., and Gordon, A. R., "Equivalent and Ionic Conductances for Lithium, Sodium and Potassium Chlorides in Anhydrous Ethanol at 25°", *J. Am. Chem. Soc.*, **79,** (1957) 2352

3. Russel, W.B., Saville, D.A. and Schowalter, W.R. , *Colloidal Dispersions,* Cambridge University Press, Cambridge, (1989)

4. Laboratory Safety Manual, Department of Environmental Health and Safety, Penn State University.

5. Levich, Veniamin G., *Physicochemical Hydrodynamics,* Prentice-Hall, Englewood Cliffs, NJ (1962)

6. Chazviel, J.-N., "Electrochemical Aspects of the Generation of Ramified Metallic Electrodeposits", *Phys. Rev. A,* **42**[12], (1990) 7355-7367

7. Orlik, M., Rosenmund, J., Doblhofer, K., and Ertl, G., "Electrochemical Formation of Luminescent Convective Patterns in Thin Layer Cells", *J. Phys. Chem. B*, **102**[8], (1998)

8. Bisang, U., and Ahlers, G., "Bifurcation to Worms in Electroconvection," *Phys. Rev. E,* **60**[4], (1999)

9. Marshall, G., Mocskos, P., Swinney, H. L., and Huth, J. M., "Buoyancy and Electrically Driven Convection Models in Thin-Layer Electrodeposition", *Phys. Rev. E*, **59**[2], (1999)

10. Rice, C.L., and Whitehead, R., "Electrokinetic Flow in a Narrow Cylindrical Capillary", *J. Phys. Chem.*, **69**[11], (1965) 4017-4024

11. Tavares, M.F.M., and McGuffin, V.L., "Theoretical Model of Electroosmotic Flow for Capillary Zone Electrophoresis", *Anal. Chem.,* **67**, (1995) 3687-3696

12. Wan, Q-H., "Effect of Electrical Double Layer Overlap on the Electroosmotic Flow in Packed Capillary Columns", *Anal. Chem.*, **69**, (1997) 361-363

Chapter 5

1. Kumar, U., Wang, S.F., Selvaraj, U., and Dougherty, J.P., "Densification and Dielectric Properties of Hydrothermal BaTiO$_3$ with Different Sources of Bi$_2$O$_3$" *Ferroelectrics*, **154** (1994) 283-288

2. Pelton, R., Miller, P., McPhee, W., and Rajaram, S., "Strategies for Improving Electrophoresis Data from the Coulter DELSA", *Colloids and Surfaces A,* **80** (1993) 181-189

3. Lind, J.E. Jr., Zwolenik, J. J., and Fuoss, R. M., "Calibration of Conductance Cells at 25° with Aqueous Solutions of Potassium Chloride", *J. Am. Chem. Soc.* **81,** (1959) 1557-1559

4. Weidner, B. V., "The Conductivity of Electrolytes in Anhydrous Acetic Acid", Ph. D. Thesis, The Pennsylvania State University (1935)

5. Hunter, R. J., *Zeta Potential in Colloid Science, Principles and Applications*, Academic Press, New York, 1981

6. O'Brien, R. W., and White, L. R., "Electrophoretic Mobility of a Spherical Colloidal Particle", *J. Chem. Soc. Faraday II*, **74,** (1978) 1607

7. Loeb, A. L., Overbeek, J. Th. G., and Wiersma, P. H., *The Electrical Double Layer Around a Spherical Colloidal Particle*. MIT Press: Cambridge, Massachusetts, 1961

8. Russel, W.B., Saville, D.A. and Schowalter, W.R. , *Colloidal Dispersions,* Cambridge University Press, Cambridge, (1989)

9. Parsegian, V.A. and Weiss, G.H. "Spectroscopic Parameters for Computation of van der Waals Forces", *J. Colloid Interface Sci.* **81,** (1981) 285-289

10. Israelachvilli, J.N., *Intermolecular and Surface Forces*, Academic Press, New York (1992)

11. Van Tassel, J; Randall, CA, "Electrophoretic deposition and sintering of thin/thick PZT films" *J. Euro. Ceram. Soc.*, **19**[6-7] (1999) 955-958

12. Ogata, N; Van Tassel, J; Randall, CA, "Electrode formation by electrophoretic deposition of nanopowders" *Materials Letters,* **49**[1] (2001) 7-14

13. D. Stevens, and J. Gipprich, "Microwave Characterization and Modeling of Multilayered Cofired Ceramic Waveguides", *Intl. J. Microcircuits & Electronic Packaging*, **22**(1) (1999) 43

14. Setter, N.,"Electroceramics: looking ahead" *J. Euro. Ceram. Soc.*, **21**[10-11] (2001) 1279-1293

15. Whatmore, R.W., "Ferroelectrics, microsystems and nanotechnology", *Ferroelectrics*, **225**[1-4], (1999) 985-998

16. Janz, G.J., and Danyluk, S.S., "Conductances of Hydrogen Halides in Anhydrous Polar Organic Solvents", Chem. Rev., 60 (1960) 209-234

17. Tokuoka, Y., Kishi, T., and Nagai, T., "Electrophoretic Deposition of Nickel Ferrite Particles Dispersed in Acetone", *Denki Kagaku*, **42** (1974) 80-84

18. Northrip, J. W., "High Temperature Discharges in Ferroelectric Ceramics" *Journal of Applied Physics,* **31**[12] (1960) 2293-2296

19. F. Xu, F. Chu, and S. Trolier-McKinstry, "Longitudinal Piezoelectric Coefficient Measurement for Bulk Ceramics and Thin Films Using Pneumatic Pressure Rig," *J. Appl. Phys.*, **86**[1], (1999) 588 -594.

20. Randall C.A., Kim N., Kucera J.P., Cao W.W., Shrout T.R., "Intrinsic and extrinsic size effects in fine-grained morphotropic-phase-boundary lead zirconate titanate ceramics", *J. Am. Ceram. Soc.*, **81**[3] (1998) 677-688

21. M. J. Haun, Z. Q. Zhuang, E. Furman, Sei-Joo Jang, and L. E. Cross, "Electrostrictive Properties of the Lead Zirconate Titanate Solid Solution System", *J. Am. Ceram. Soc.*, **72**[2], (1989) 1140-1144

Appendix A

1. Fuoss, R.M., and Onsager, L.,"Conductance of Unassociated Electrolytes", *J. Phys. Chem.*, **61** (1957) 668-682

2. Fuoss, R. M., Onsager, L., and Skinner, J. F., "The Conductance of Symmetrical Electrolytes. V. The Conductance Equation", *J. Phys. Chem.*, **69,** (1965) 2581-2594

3. Fuoss, R.M., and Accascina, F., *Electrolytic Conductance*, Interscience Publishers, New York, 1959

VITA

Jonathan Van Tassel

I was born quite a while ago in Austin, Texas; a very nice town by most accounts; but I mostly grew up in Cleveland, Ohio. I went back to Austin in the mid-eighties to take a few classes in Economics at the University of Texas and generally see how I liked the place. While I was there they tore down the hospital I was born in. I took the hint and headed back to Cleveland. In a similar vein, in the summer of '81 I went to the Soviet Union for several weeks. It took them about ten years, it was a big place after all, but they tore that down too. I took the hint and haven't been back to the Soviet Union since. Although I have visited Russia a couple of times recently. I got a BA degree in Russian language and culture from Case Western Reserve University in Cleveland in 1982, which in large part explains why I speak French so well. After that I got a job in a financial management company and after that in a demolition company. It has only recently come to light how well this would have qualified me for a top executive post at Enron. Unfortunately, I was not aware of that opportunity at the time, so, through a chain of hapstance and misadventure, I found myself in '91, once again in Ohio, broker than broke and back in school, at Ohio State this time. Surprisingly, not only did they not tear anything down, but they actually built a few new buildings while I was there. The result was that after scrambling, scrabbling, odd-jobbing, selling a pondfull of plasma, and replacing it all with 3 am coffee at the library, I graduated with a BS in Aerospace Engineering in '95. I was rejected for graduate school here at Penn State, so I have stayed here in graduate school for a few more years than absolutely necessary just out of pure natural cussedness.